POLITECNICO DI MILANO

Scuola di Ingegneria Industriale e dell'Informazione

Master Thesis in Nuclear Engineering

POLITECNICO
MILANO 1863

Single Janus particles in a complex plasma environment

Internal Advisor: Prof. Roberto **PIAZZA**

External Advisor: Dott. Volodymyr **NOSENKO**

Francesca **LUONI** Matr. 854997

A.A. 2017 - 2018

To all the people who have believed in me and supported me,
even if they have been missing me every day

Abstract

In the present work, the new field of active particles in a plasma environment is explored experimentally. The particles used were the so-called Janus particles, named so after the two-faced Roman god. With two halves of them having different properties, the Janus particles are known to be active (display self-propulsion) in certain aqueous solutions. The aim of the present work is to investigate whether they are also active when suspended in a low-temperature weakly ionized plasma. The Janus particles used are melamine-formaldehyde microspheres with a diameter of 9,27(10) μm; one half of them was coated with a 10,0(1) nm layer of platinum. The chief result of the present work is that they are active in a plasma environment. The forces which can potentially act as propulsion mechanisms in a plasma environment are investigated both theoretically and experimentally. These forces include the "photophoresis" due to different accommodation coefficients on the particle sides and, when a stronger laser light is used to illuminate the particle, also photophoresis due to a temperature gradient on the particle surface and the radiation pressure force.

Sommario

Nel presente lavoro viene investigato dal punto di vista sperimentale un campo mai esplorato prima: particelle attive in ambiente di plasma complesso. Le particelle Giano, una speciale categoria di particelle attive in soluzione acquosa grazie a particolari proprietá di anisotropia spaziale, sono sospese in un plasma freddo debolmente ionizzato con l'obiettivo di scoprire se esse siano attive anche in questo ambiente. Le possibili forze agenti come meccanismi di propulsione nel plasma sono investigate prima teoricamente e poi sperimentalmente. Le particelle Giano utilizzate sono sfere di melamina-formaldeide dal diamentro di 9,27(10) μm, ricoperte per metá da uno strato di 10,0(1) nm di platino. Il risultato del presente lavoro é che esse sono attive nel plasma e che i meccanismi di propulsione sono, in caso di assenza di forti sorgenti di luce, "fotoforesi" legata ai diversi coefficienti di accomodamento di melamina e platino, e, nel caso in cui un laser di illuminazione venga usato, una combinazione del meccanismo "fotoforetico" con pressione di radiazione alternata e fotoforesi legata a un gradiente di temperatura sulla particella.

Estratto

Questo lavoro di tesi, svolto presso il gruppo di ricerca sulla fisica dei plasmi complessi della DLR (Centro Aerospaziale Tedesco) di Oberpfaffenhofen, Monaco di Baviera, ha avuto come obiettivo quello di studiare il comportamento di particelle micrometriche con particolari proprietá di anisotropia spaziale disperse in un plasma, di evidenziare la presenza di fenomeni di "moto attivo" delle particelle stesse, di analizzarne le traiettorie, ed infine di indagare l'origine fisica di tali effetti.

Per plasma "sporco" (*dusty plasma*) si intende un plasma a bassa temperatura in cui siano disperse particelle solide di dimensioni generalmente micrometriche. Le particelle disperse presentano una carica elettrica che è generalmente negativa in quanto il flusso degli elettroni sulla particella risulta dominante rispetto a quello deglio ioni positivi, che hanno velocitá termiche molto minori. Tale carica cresce in valore assoluto finchè il potenziale superficiale da essa generato, che tende a respingere gli elettroni, cresce a sufficienza da rendere confrontabili i flussi di ioni ed elettroni, raggiungendo cosí una situazione di equilibrio. I plasmi "sporchi" giocano un ruolo molto importante in molte situazioni d'interesse per l'astrofisica (anelli planetari, code delle comete, nubi interplanetarie ed interstellari) e per l'esplorazione spaziale (ad esempio in prossimitá di sonde spaziali, satelliti artificiali, o della stessa Stazione Spaziale Internazionale). Con l'espressione "plasmi complessi" si intendono piú specificamente plasmi sporchi "modello" creati artificialmente in laboratorio per scopi di ricerca. Il gas utilizzato negli esperimenti svolti nel corso di questa tesi é argon, ionizzato attraverso una radio-frequenza di 13,6 MHz in una camera GEC (*Gaseous Electronics Conference RF Reference Cell*) modificata. Le particelle finora studiate nei plasmi complessi, dette "passive", si muovono di moto semplice Browniano dovuto alle collisioni con gli elettroni, gli ioni e le molecole neutre presenti nel plasma.

Di recente tuttavia l'attenzione della comunitá scientifica che si occupa di sistemi dispersi in un fluido si é focalizzata sulle cosiddette particelle "attive", ossia particelle che mostrano una sensibile "amplificazione" del moto Browniano dovuta o ad effetti autonomi di propulsione interna (come quelli che danno origine al moto dei batteri), o alla natura peculiare della loro superficie, che le rende anisotrope (anche quando abbiano geometria sferica) rispetto alla risposta a situazioni di nonequilibrio, come ad esempio la presenza

di gradienti termici o chimici, il che privilegia una specifica direzione del moto. Un importante esempio di quest'ultime é quello delle cosiddette particelle "Giano" (*Janus particles*), denominazione che trae origine dal dio romano dalla doppia faccia, che sono in genere particelle sferoidali di materiale dielettrico sulla cui superficie é depositato un sottile strato emisferico di un metallo quale platino o palladio. Specificamente, le particelle Giano utilizzate in questo lavoro sono sfere di melamina-formaldeide dal diametro di 9,27(10) μm ricoperte per metà da uno strato di 10,0(1) nm di platino. Quando sospese in acqua, queste particelle presentano un moto attivo per effetto delle reazioni chimiche catalizzate dal metallo, che é oggetto di intensa analisi sperimentale. Finora, tuttavia, non erano presenti in letteratura studi del comportamento di particelle attive in un gas ionizzato. La domanda principale che ci si é posti in questa tesi é se l'anisotropia superficiale delle particelle Giano abbia conseguenze anche sulle interazioni con elettroni, ioni e molecole neutrali presenti nel plasma, promuovendo anche in questo caso sensibili deviazioni dal semplice comportamento Browniano. Inoltre, scopo della tesi é stato anche quello di evidenziare e quantificare, almeno in prima approssimazione, quali siano le forze che in un plasma possano dare origine a questi effetti.

Per quanto non sia al momento facile stabilire quanto lo studio del comportamento di particelle Giano possa avere interesse applicativo per i plasmi "sporchi", *in primis* lo studio che é stato svolto, di fatto il primo in cui vengano utilizzate particelle potenzialmente attive, è sicuramente di interesse generale nello studio della dinamica di particelle sospese in un plasma, inoltre il sistema considerato rappresenta in qualche modo un caso limite, perché "estremizza" situazioni di fatto presenti per particelle omogenee di melamina–formaldeide, ampiamente utilizzate come sistemi modello, che spesso, a dispetto della loro presunta uniformità, presentano imperfezioni e disomogeneità della composizione superficiale non trascurabili e difficilmente quantificabili. Alcuni esempi di meccanismi capaci di generare su particelle passive meccanismi di "simil–attivitá" sono: la cosiddetta "fotoforesi negativa" nel caso di particelle caratterizzate da imperfezioni e difetti sulla loro superficie (una cosiddetta "macchia calda" si genera per via di fenomeni di riflessione e rifrazione sulla faccia della particella non rivolta verso il fascio laser e il momento trasferito alla particella dagli urti con ioni, elettroni e molecole neutre del plasma genera un moto direzionato verso la sorgemte di luce), la cosiddetta *rocket force* dovuta a danni generati sulla superficie della particella con un potente laser di manipolazione, e il cosiddetto "effetto scia" (*wake effect*), dovuto ad una "scia" di carica positiva che si crea nella regione di guiana sotto le particelle cariche negativamente per via della deviazione del flusso di ioni diretto verso il basso. L'attrazione di questa cosiddetta scia agisce su particelle di massa leggermente superiore alle altre che levitano quindi leggermente al di sotto delle altre, e dà vita al fenomeno cosiddetto di "canalizzazione" del moto di queste ultime. Studiare particelle attive nei plasmi ha inoltre come applicazione la migliore comprensione di fenomeni legati a particelle che si muovono violentemente nei plasmi di dispositivi per la fusione nucleare.

In generale, sulle particelle disperse in un plasma complesso agiscono molteplici forze,

anche quando queste particelle siano omogene ed isotrope. In primo luogo, su di esse agisce la forza peso, a meno che gli esperimenti non vengano svolti in condizioni di microgravità (campagne di volo parabolico o sulla stazione spaziale internazionale). Per contrastare gli effetti della forza peso, la quale farebbe sedimentare rapidamente le particelle sul fondo della camera in cui viene generato il plasma, si applica in generale un campo elettrico diretto in senso opposto generato da un elettrodo. Ció dá origine ad una cosiddetta regione "di guaina" (*sheath*) fra l'elettrodo e il *bulk* del plasma, che è invece caratterizzato da quasi-neutralità di carica, all'interno della quale levitano le particelle stesse. A queste due forze che si bilanciano lungo la verticale si aggiunge un'ulteriore forza di trascinamento degli ioni (*ion drag*), molto piú debole delle prime due, dovuta ad un flusso di ioni diretto verso il basso nella zona di guaina causato dallo stesso campo elettrico che permette alle particelle disperse di levitare. Questa forza è dovuta al momento trasferito dagli ioni alla particella quando essi vengono da essa adsorbiti o semplicemente diffusi. Queste tre forze confinano verticalmente la particella, la quale si puó solo muovere dunque nel piano orizzontale. Si possono infine avere anche forze agenti lungo la direzione orizzontale, dovute al trascinamento di molecole neutre del plasma (*neutral drag*) e che sono di fatto le forze di frenamento viscoso delle molecole neutre del gas che si oppone al moto delle particelle disperse. È opportuno notare che tali molecole neutre, nei plasmi debolmente ionizzati utilizzati in questo lavoro, sono di gran lunga più numerose rispetto agli ioni e agli elettroni: di fatto, la densità in numero di ioni ed elettroni è pari a solo $10^{-6} \div 10^{-7}$ volte quella delle molecole neutre.

In questo lavoro di tesi, ci si é occupati del comportamento dinamico di una singola *particella*, confrontando il moto di particelle Giano con quello di particelle omogenee di melamina (ossia di particelle analoghe senza calotta metallizzata). Negli esperimenti svolti, una singola particelle viene confinata in una regione spaziale limitata per mezzo di un anello di alluminio posto al centro dell'elettrodo inferiore della camera a plasma, che si carica negativamente nel plasma creando un'efficace buca di potenziale di confinamento. Per poter visualizzare il moto delle particelle all'interno della camera a plasma si è fatto uso di un microscopio non convenzionale (*long working distance microscope*) dotato di un'ottica a lunga distanza che permette di mettere a fuoco le particelle anche a distanze dell'ordine della decina di centimetri con una risoluzione dell'ordine del micron. Le immagine viene acquisita da una telecamera ad elevato frame rate, in modo da poter risolvere temporalmente la traiettoria.

Si sono analizzati i meccanismi che potrebbero generare la propulsione di particelle Giano nel plasma. È inoltre utile cercare di confrontare l'ordine di grandezza di questi meccanismi per riuscire a stimarne l'effetto relativo sulle particelle.

1. L'adsorbimento e diffusione degli ioni da parte della particella, che nel caso di particelle passive dá vita ad una forza agente lungo la verticale, potrebbero essere spazialmente non omogenei a causa di una non omogenea distribuzione di carica

sulla superficie della particella Giano. Questo fenomeno darebbe origine ad una forza agente sul piano orizzontale ($F_{\text{asym. ion drag}}$) ed in particolare essa sarebbe diretta dalla faccia carica piú negativamente, e quindi in grado di adsorbire e deviare piú efficacemente ioni, verso l'altra. Dalla letteratura si deduce che la faccia carica piú negativamente sia quella di materiale dielettrico. Una stima per eccesso di questa forza é stata fatta partendo dal presupposto che solo metà della particella collezioni ioni, considerando il contributo della diffusione degli ioni trascurabile. Il risultato di questa stima dà un limite superiore a quest'effetto pari a $F_{\text{asym. ion drag}} = 1{,}5 \times 10^{-19}\,\text{N}$.

2. Un'ulteriore forza agente come meccanismo direzionale di propulsione sulla particella é la forza dovuta alla pressione di radiazione alternata del laser (F_{laser}), che assume valori diversi se il laser colpisce la faccia di pura melamina o la parte ricoperta di platino. Considerando pari ad uno il coefficiente di riflettanza del platino e nullo quello della melamina, si é potuta fornire una stima per eccesso della differenza nel valore assoluto di questa forza in due casi limite. Nel caso di potenza del laser massima usata negli esperimenti di questo lavoro, vale a dire 99 mW, si ottiene $F_{\text{laser, MF}} = 1{,}2 \times 10^{-15}\,\text{N}$ e $F_{\text{laser, Pt}} = 2{,}6 \times 10^{-15}\,\text{N}$. La forza agente sul lato ricoperto di platino è dunque al massimo pari a più del doppio di quella agente sul lato di pura melamina. Poiché molto probabilmente la particella compie un moto di rotazione su se stessa nel plasma per effetto di gradienti di carica e/o di temperatura sulla sua superficie, la forza dovuta alla pressione di radiazione agirà su di essa con un modulo che varia nel tempo fra i due valori calcolati con la stessa frequenza di rotazione della particella.

3. In presenza della luce laser, si genera un gradiente di temperatura sulla superficie della particella Giano dovuto all'anisotropia di assorbimento ottico tra le due calotte emisferiche (metallizzata e non) della particella. Di conseguenza, durante gli urti delle molecole neutre del gas con la particella, queste trasferiranno alla particella una quantitá di moto che dipende dalla temperatura del punto della superficie urtato. Questo meccanismo dá origine ad una forza fotoforetica (spesso detta anche "fototermoforetica", o anche più semplicemente "termoforetica", per analogia alla forze che si originano su particelle disperse in un liquido o in un gas neutro per effetto della presenza di un gradiente di temperatura), che punta dalla faccia della particella a temperatura maggiore a quella a temperatura minore: $F_{\Delta T}$. Attraverso un bilancio di energia sulla particella si può stimare, considerando in prima approssimazione nulla la resistenza termica di contatto fra la melamina e il platino, una minima differenza di temperatura fra le due facce con un approccio a parametri semi-concentrati e con un metodo iterativo di risoluzione delle equazioni di bilancio. Con questo minimo ΔT si può fare una stima per difetto della forza fotoforetica agente sulla particella, ottenendo $F_{\Delta T} = 1{,}1 \times 10^{-18}\,\text{N}$.

4. Le due facce della particelle sono caratterizzate inotre da due diversi "coefficienti di accomodamento", che sono definiti come il rapporto fra il numero di molecole che vengono completamente termalizzate per effetto dell'interazione con la superficie della particella (ossia che assumono dopo l'urto una temperatura cinetica pari a quella della superficie e una corrispondente distribuzione termica dei momenti) rispetto al numero totale di molecole che impattano con la superficie stessa. Piú il coefficiente di accomodamento é alto, piú alta é la temperatura cinetica media delle molecole che lasciano la superficie ed é dunque piú alta la quantitá di moto trasferita alla particella durante l'urto. Questo meccanismo dá origine ad un'ulteriore forza ($F_{\Delta\alpha}$) che punta dalla faccia con coefficiente di accomodamento piú alto verso l'altra. A differenza che nel caso predente, tuttavia, questo ulteriore effetto è presente anche quando le perticelle non vengano illuminate dal laser: questa forza necessita infatti che la temperatura superficiale della particella sia maggiore della temperatura del fluido circostante, ma, se in acqua l'illuminazione laser é necessaria per generare questa differenza di temperatura fra la particella e il fluido, nel caso in cui il fluido sia un plasma la presenza stessa del plasma costituisce una fonte di calore in grado di scaldare la particella. Pertanto, si tratta a tutti gli effetti di un effetto puramente "termoforetico". Poiché il coefficiente di accomodamento melamina in argon non é noto in letteratura, una stima per eccesso di questa forza é stata fatta considerando la massima differenza possibile fra i due assumento un'espressione del tipo

$$\begin{aligned} F_{\text{neutrals}} &= \pi r_p^2 k_b n_0 \Big(\alpha_{\text{Pt}} T_{\text{Pt}} + (1-\alpha_{\text{Pt}}) T_0 - \alpha_{\text{MF}} T_{\text{MF}} - (1-\alpha_{\text{MF}}) T_0 \Big) \\ &= \pi r_p^2 k_b n_0 T_0 \Big(\alpha_{\text{Pt}} \left(\frac{T_{\text{Pt}}}{T_0} - 1 \right) - \alpha_{\text{MF}} \left(\frac{T_{\text{MF}}}{T_0} - 1 \right) \Big), \end{aligned}$$

dove n_0 è la densità in numero delle molecole neutrali del plasma, T_0 è la temperatura del gas, T_{Pt} è la temperatura della faccia ricoperta di platino e α_{Pt} il suo coefficiente di accomodamento, T_{MF} e α_{MF} sono la tempeartura e il coefficiente di accomodamento della faccia di pura melamina e r_p è il raggio della particella. Il risultato, nel caso di sola $F_{\Delta\alpha}$, che significa per $T_{\text{Pt}} = T_{\text{MF}}$, cioé in caso di laser spento, è $F_{\Delta\alpha} = 6{,}7 \times 10^{-13}\,\text{N}$ per pressione del gas pari a 1,33 Pa.

Nel caso in cui almeno uno di questi effetti non fosse trascurabile, la particella Giano sarebbe sottoposta ad un meccanismo di propulsione autonoma che la renderebbe attiva anche nel plasma. In letteratura si annoverano calcoli analitici e simulazioni numeriche del moto di singole particelle attive confinate in una buca di potenziale armonico in ambiente "smorzato" (*overdamped*), quale una soluzione acquosa. Questi risultati sono le previsioni teoriche esistenti piú vicine al caso sperimentale oggetto di questo lavoro e il fatto che i plasmi utilizzati negli esperimenti siano invece ambienti "non smorzati" (*undamped*) permette un paragone solo qualitativo fra la teoria e i risultati sperimentali. Le simulazioni prevedono che, se la forza agente come meccanismo di propulsione sulla particella attiva

non dipende dal tempo, quest'ultima percorra traiettorie circolari con la stessa frequenza con cui ruota su se stessa. Il raggio r_c previsto per queste traiettorie circolari è tale che $r_c \propto \frac{F}{\omega}$, dove F è il valore assoluto della forza agente sulla particella come meccanismo di propulsione e ω è la frequenza di rivoluzione della particella attorno al centro della buca di potenziale. É previsto inoltre che la frequenza di rivoluzione ω corrisponda alla frequenza di rotazione della particella su se stessa. Se il valore assoluto della forza è invece variabile nel tempo con una frequenza detta "di propulsione" ν, sono invece previste traiettorie chiuse a forma di coccarda in caso di rapporto ν/ω razionale e traiettorie che non si chiudono e riempiono l'area di un cerchio in caso di rapporto irrazionale. Se il rapporto ω/ν è intero positivo n, le traiettorie previste hanno una forma asimmetrica rispetto al centro della buca di potenziale e in particolare presentano $n-1$ petali interni alla traiettoria: per $n = 1$ la traiettoria prevista è una cardioide, per $n = 2$ un limaçon con un ricciolo interno, e così via. Anche nel caso di forza di propulsione dipendente dal tempo, vale l'approssimazione $r \propto \frac{F}{\omega}$.

I dati ottenuti sperimentalmente sono stati analizzati grazie all'utilizzo combinato dei due software `ImageJ` e `Python`. Con il primo si é trovata la posizione della particella frame per frame, con il secondo si sono scritti codici per calcolare le velocità, il raggio della traiettoria r_c, la frequenza di rivoluzione ω, la velocità lineare della particella $v = r\omega$ e la sua temperatura cinetica.

Il risultato principale degli esperimenti svolti su singole particelle Giano nel plasma sono le molteplici forme delle traiettorie osservate: alcune hanno forma circolare, altre di limaçon o di epicicloide bilobata, altre più genericamente di epitrocoide. Alcune particelle hanno poi mostrato traiettorie particolarmente complesse e non riconducibili anessun tipo di moto periodico: la loro forma é stata perció definita randomica. Un'epitrocoide é definita come una ruletta ottenibile come curva tracciata da un punto fissato ad un cerchio di raggio r, posto ad una distanza d dal centro, quando il cerchio rotola all'esterno di un altro cerchio di raggio R. Le particelle la cui traiettoria ha forma circolare o di epitrocoide con $R > r$ sono state denominate particelle Giano "circolanti", quelle la cui traiettoria ha forma di limaçon o di epicicloide bilobata sono state chiamate particelle Giano "a cuore", con riferimento alla letteratura, e le particelle la cui traiettorie avesse forma randomica sono state denominate particelle Giano "random". La denominazione fa ovviamente riferimento alla forma della traiettoria percorsa dalle particelle e non alla forma delle particelle in sè. Questo risultato costituisce un segno evidente della presenza di fenomeni di "moto attivo" di queste particelle nei plasmi e le forze ipotizzate in questo lavoro come meccanismi di propulsione in questo ambiente sono le quattro elencate sopra. Sono anche stati svolti esperimenti durante i quali l'anello di alluminio atto al confinamento delle singole particelle era stato traslato di circa 2 cm rispetto al centro dell'elettrodo inferiore della camera. Il fine di questa serie di esperimenti é la verifica che che il meccanismo di "moto attivo" delle particelle Giano sia effettivamente dovuto ad un meccanismo di propulsione autonoma della particella nel plasma e non ad effetti "collaterali". É possibile infatti che anche

particelle regolari ("passive") compiano un moto circolare nel caso in cui l'anello non sia posizionato esattamente al centro dell'elettrodo per via di uno dei seguenti meccanismi. Il primo meccanismo "collaterale" si verifica nel caso in cui la particella non sia confinata esattamente in corrispondenza del centro dell'elettrodo inferiore. Infatti, in tal caso essa sarebbe sottoposta ad una rottura della simmetria del sistema a causa della presenza di un flusso ambipolare di ioni ed elettroni che diffonde dal centro della camera verso i suoi bordi. Finché la particella si trova al centro della camera non risente di questo effetto, ma nel caso in cui l'anello atto al confinamento sia traslato rispetto al centro della camera, allora la superficie della particella é soggetta a un flusso di particelle cariche che turba il sistema, rompendone la simmetria. La traiettoria prevista per un simile caso di rottura di simmetria per particelle "passive" confinate in una buca di potenziale armonica é essa stessa circolare. Un secondo fenomeno "collaterale" che potrebbe indurre anche una particella non sottoposta ad alcun meccanismo di propulsione autonoma a moversi di moto circolare é la deformazione della buca di potenziale generata dalla presenza dell'anello a causa della focalizzazione del laser. La focalizzazione del laser in un punto non corrispondente al centro della buca di potenziale (cosa certa nel caso in cui l'anello venga spostato rispetto al centro dell'elettrodo) potrebbe infatti generare un secondo minimo di potenziale e la particella potrebbe percorrere una traiettoria circolare fra questi due minimi. Il terzo ed ultimo effetto "collaterale" ipotizzato é la presenza di una seconda buca di potenziale confinante dovuta alla distribuzione spaziale degli ioni nel plasma. Essa é piccata al centro della camera e quindi in corrispondenza del centro dell'elettrodo inferiore. Questo implica un confinamento, seppur piú debole di quello dovuto all'anello di alluminio, della particella al centro della camera. Nel momento in cui l'anello venga traslato le due buche di potenziale non genererebbero piú due minimi esattamente sovrapposti, ma separati da una distanza pari al decentramento dell'anello rispetto all'elettrodo inferiore della camera. Nel caso in cui il meccanismo che genera il moto circolare fosse uno di questi, gli effetti della traslazione dell'anello lo mostrerebbero con chiarezza. Il risultato di questi esperimenti ha confermato invece che questi effetti non sono la causa della forma circolare delle traiettorie.

Un altro risultato notevole degli esperimenti svolti é la presenza di forme non circolari nelle traiettorie delle particelle Giano. Se ne deduce che il valore assoluto della forza di propulsione agente sulle singole particelle vari nel tempo con una cossiddetta frequenza di propulsione ν. In particolare, sono state avanzate delle ipotesi in merito al motivo per cui il valore assoluto della forza di propulsione dovrebbe cambiare nel tempo. Come giá accennato, la particella Giano molto probabilmente ruota su se stessa e i meccanismi che dipendono dall'orientazione della particella sono stati analizzati:

- $F_{\text{asym. ion drag}}$ dipende dall'orientazione della particella Giano poiché il flusso di ioni è diretto dall'alto verso il basso. Se le due facce della particella sono rivolte l'una verso il basso e l'altra verso l'alto, allora non si genera asimmetria nell'adsorbimento

e diffusione degli ioni e $F_{\text{asym. ion drag}} \simeq 0$; in caso contrario questa forza é presente ed assume il suo valore massimo nel caso in cui il piano che separa le due facce si posizioni lungo la verticale. Nel caso dunque in cui la particella Giano ruotasse su se stessa, $F_{\text{asym. ion drag}}$ assumerebbe valori compresi fra zero ed il suo valore massimo con la stessa frequenza a cui la particella ruota su se stessa.

- F_{laser} dipende dall'orientazione della particella Giano perché il suo effetto sulla particella dipende dalla faccia che essa rivolge al laser. Come giá anticipato, dunque, questa forza assume valori compresi fra i due riportati sopra, anche in questo caso con la stessa frequenza con cui la particella ruota su se stessa.

- Come giá accennato, nel caso di sfere di pura melamina-formaldeide con deformazioni o difetti sulla loro superficie, una cosiddetta "macchia calda", dovuta alla rifrazione e riflessione della luce laser, si puó generare sulla superficie della faccia della particella non rivolta verso il laser. Essa darebbe vita ad un cosiddetto meccanismo di "fotoforesi negativa", che ha verso opposto rispetto alla direzione della luce incidente (il nome ha lo scopo di distinguerlo dal meccanismo di "fotoforesi positiva", che é la pressione di radiazione, e di fatto consiste in un semplice meccanismo di fotoforesi dovuto ad un gradiente di temperatura che peró causa un moto della particella in verso sempre opposto a quello della luce laser incidente). Combinando gli effetti della "macchia calda" presente sempre sulla faccia della particella non rivolta verso il laser e del gradiente di temperatura che si genera per via dei due diversi materiali componenti la superficie della sfera e che si riorienta continuamente quindi durante il moto di rotazione su se stessa della particella, ne risulta una variazione nel tempo del valore assoluto della fotoforesi dovuta al gradiente di temperatura *totale* sulla superficie della particella. La creazione di questa "macchia calda" nel caso delle particelle Giano non é mai stata provata ed é stata presa in considerazione in questo lavoro solo per completezza. Quest'ultimo meccanismo é dunque il meno plausibile dei tre.

La variazione temporale del valore assoluto di alcune delle forze agenti sulla particella Giano su cui ci si é focalizzati si basa sull'ipotesi che la particella routi attorno ad un asse diverso da quello congiungente i centri delle due facce. In tal caso, la frequenza di propulsione della forza e la frequenza di rotazione della particella su se stessa sarebbero uguali ($\nu = \omega$).

Questo risultato lascia tuttavia aperta una domanda fondamentale: come spiegare le traiettorie osservate caratterizzate da forma diversa da quella di cardiode? Le traiettorie circolari sono infatti previste nel caso di forza di propulsione non dipendente dal tempo, che peró nelle condizioni di questo lavoro vuol dire per asse di rotazione della particella corrispondente all'asse congiungente i centri delle due facce. In tal caso $F_{\text{asym. ion drag}} = 0$, F_{laser} assume un valore costante e quindi non costituisce piú un meccanismo di propulsione autonoma della particella e le due forze "fotoforetiche", $F_{\Delta\alpha}$ e $F_{\Delta T}$, agiscono in

direzione verticale, lungo la quale peró la particella é confinata. Di conseguenza, nessun meccanismo di propulsione autonoma della particella sarebbe presente per questo caso. La contraddizione in termini é che una particella non sottoposta a meccanismi di propulsione autonoma dovrebbe muoversi di moto Browniano semplice e non di moto circolare.
Le altre traiettorie osservate implicano invece un rapporto ν/ω diverso dall'unità, che va in aperta contraddizione con quanto appena discusso. L'unica traiettoria coerente con le considerazioni svolte é la cardioide, che é prevista numericamente per il caso di $\nu = \omega$. Questa domanda non trova una spiegazione soddisfacente in questo lavoro e resta una domanda aperta sull'argomento. Non bisogna ad ogni modo dimenticare che le traiettorie previste analiticamente e numericamente che si stanno usando come termine di paragone sono state previste per il caso di particelle attive in ambiente "smorzato", mentre il plasma in cui le particelle Giano sono state disperse nel presente lavoro é un ambiente "non smorzato", cosa che rende il paragone sensato fintanto che si rimanga su un livello qualitativo. É dunque ragionevole che non tutto ció che é stato osservato nell'arco di questo lavoro di tesi venga spiegato dai risultati previsti.

Una volta che il comportamento delle particelle Giano ha dunque confermato che la natura peculiare della loro superficie le rende attive anche nei plasmi, si é proceduto con esperimenti mirati a studiare le forze agenti sulle particelle. In particolare, si é sfruttato il fatto che variare alcuni parametri sperimentali implica automaticamente variare il valore assoluto delle forze agenti. Ci si è concentrati sui seguenti parametri:

- potenza del laser (valori utilizzati: 0 mW, 14 mW, 99 mW)
- potenza della radio-frequenza (valori utilizzati: 1 W, 5 W, 20 W)
- pressione dell'argon (valori utilizzati: 1,3 Pa, 4 Pa, 6,7 Pa, 10 Pa, 13,3 Pa).

Variando la potenza del laser, le conseguenze sono sulla forza dovuta alla pressione di radiazione e sulle due fotoforesi: $F_{\text{laser}} \propto$ potenza del laser, $F_{\Delta T} \propto$ potenza del laser, $F_{\Delta\alpha} \propto$ potenza del laser. Variando la potenza della radio-frequenza, le conseguenze sono sulla forza dovuta al trascinamento asimmetrico degli ioni: $F_{\text{asym. ion drag}}$ cresce al crescere della potenza della RF. Variando la pressione dell'argon, le conseguenze sono su tutte le forze eccetto quella associata alla pressione di radiazione: $F_{\Delta T} \propto p_{Ar}$, $F_{\Delta\alpha} \propto p_{Ar}$ e $F_{\text{asym. ion drag}}$ cresce al crescere della pressione.

Le evidenze sperimentali raccolte offrono diversi spunti di riflessione.

Un primo risultato di fondamentale importanza emerge dai risultati degli svolti variando la potenza dell radio-frequenza applicata. Essi hanno infatti evidenziato che la forza dovuta alla collezione asimmetrica degli ioni sulle due facce é sicuramente trascurabile rispetto alle altre. Sembra infatti che la forza netta agente sulla particella, valutata grazie al rapporto esistente fra F, ω ed r, dimunuisca invece che aumentare al crescere della potenza della radio-frequenza. É dunque evidente che altri fattori giochino un ruolo dominante sulla debole forze dovuta al flusso asimmetrico degli ioni. D'altronde, questo risultato era stato

teoricamente previsto dai conti svolti in questo lavoro che hanno condotto ad un valore di limite massimo di questa forza inferiore rispetto ai valori stimati per qualsiasi altra delle forza ipotizzate come meccanismi di propulsione sulle particelle Giano nel plasma. Va aggiunto inoltre che si tratta di un risultato previdibile considerando che la densitá di numero delle molecole neutrali é superiore di $6 \div 7$ ordini di grandezza rispetto a quella di ioni ed elettroni.

Un altro caso notevole é il diverso comportamento osservato nei tre tipi di particelle Giano identificati al variare della potenza del laser.

Per bassi valori di pressione del gas argon, ad esempio, le cosiddette particelle "a cerchio" mostrano traiettorie piú piccole all'aumentare della potenza del laser e il rapporto fra F, ω ed r suggerisce che la forza netta agente sulla particella sia a questa inversamente proporzionale, implicando che $F_{\Delta\alpha}$ debba agire in verso opposto rispetto a F_{laser} e $F_{\Delta T}$. Infatti, come spiegato in precedenza, $F_{\Delta\alpha}$ si manifesta anche in assenza del laser, contrariamente a $F_{\Delta T}$ e F_{laser}. Nel caso in cui il valore di F_{laser} fosse trascurabile rispetto a $F_{\Delta T}$, allora il comportamento osservato si spiegherebbe solo nel caso in cui le due forze "fotoforetiche" si contrastassero. I valori assoluti dei due meccanismi "fotoforetici" dovrebbero essere quindi necessariamente comparabili e la differenza calcolata in precedenza non puó che essere eccessiva. Poiché il valore di $\Delta\alpha$ usato nei calcoli é il massimo possibile, é evidente come $F_{\Delta\alpha}$ sia stata effettivamente sovrastimata, contrariamente a $F_{\Delta T}$, calcolato invece a partire dal minimo valore possibile di ΔT. In caso in cui invece l'effetto di F_{laser} dovesse essere dominante rispetto a quello di $F_{\Delta T}$ in tal caso, siccome F_{laser} assume un valore maggiore quando il laser colpisce la faccia ricoperta di platino della particella Giano, questo significherebbe che il verso di $F_{\Delta\alpha}$ suggerito in precedenza non sia corretto, anche se questa seconda ipotesi sembra essere meno attendibile. Nel caso in cui invece le tre forze abbiano valore fra loro comparabile, esse dunque interagirebbero fra loro in un modo difficile da prevedere.

Per alti valori della pressione dell'argon, il punto di minimo della forza agente sulla particella viene registrato in corrispondenza di valori intermedi della potenza del laser. Dato che F_{laser} non dipende dalla pressione del gas e che $F_{\Delta\alpha}$ e $F_{\Delta T}$ ne dipendono entrambe linearmente, é plausibile che una differenza nei coefficienti moltiplicativi della pressione per le due forze "fotoforetiche" renda $F_{\Delta T} \simeq F_{\Delta\alpha}$ per potenza del laser intermedia e $F_{\Delta T} > F_{\Delta\alpha}$ per potenza massima. Questo costituisce un'ulteriore riprova del fatto che i valori assoluti delle due forza "fotoforetiche" debbano essere comparabili.

Per quanto concerne invece le particelle Giano "a cuore", affinchè una simile traiettoria sia possibile, la forza di propulsione deve essere variabile nel tempo. Le forme di limaçon e di epicicloide bilobata sono piú marcate per alti valori della potenza del laser e assenti in caso di laser spento. Questo prova che delle sicuramente la variazione nel tempo della forza di trascinamento asimmetrica degli ioni non é quella dominante, ulteriore conferma della trascurabilitá di questa forza rispetto alle altre. Per queste particelle Giano il parametro che più conta è invece proprio la variazione della forza netta agente sulla particella nel

tempo.

Le particelle Giano "random" infine non mostrano nessuna dipendenza particolare dalla potenza del laser.

Gli esperimenti svolti variando la pressione dell'argon rivelano infine che, per pressioni crescenti e in assenza di laser, la forza agente sulle particelle aumenta. Poichè, come dedotto dai risultati dei precedenti esperimenti, la forza dovuta alla collezione asimmetrica degli ioni è trascurabile, $F_{\Delta\alpha}$ rappresenta in assenza di laser l'unica forza in gioco. Il risultato ottenuto prova dunque il fatto che all'aumentare della pressione del laser, e con essa della densità di molecole neutrali, $F_{\Delta\alpha}$ aumenti. Al contrario, a un aumento della potenza del laser corrisponde un valore della forza approssimativamente costante, indipendente dalle variazioni della pressione del gas. Un comportamento di questo tipo è in perfetto accordo con la teoria, dato che F_{laser} non dipende dalla pressione del gas e le due fotoforesi ne dipendono entrambe linearmente e tendono inoltre a compensarsi. Sebbene l'esiguo numero di elementi statistici a disposizione precluda la possibilità di trarre conclusioni attendibili, è indubbio che una trattazione più completa debba escludere la possibilità di considerare i due meccanismi di fotoforesi separatamente l'uno dall'altro. A corollario di quanto detto, si precisa che le attuali conoscenze teoriche sulla forza fotoforetica si applicano a fluidi neutrali e non ai plasmi, di conseguenza alcuni importanti fattori vengono inevitabilmente trascurati.

Dei diversi altri esperimenti compiuti, quelli riguardanti le particelle "passive", vale a dire pure sfere di melamina–formaldeide, hanno confermato quello che già la letteratura riporta relativamente al loro comportamento nei plasmi, mentre quelli incentrati sullo sviluppo temporale del comportamento delle particelle Giano non hanno fatto emergere nessuna dipendenza particolare dal fattore tempo.

I risultati qui proposti dimostrano che le particelle Giano si muovono di moto attivo nei plasmi e indagano brevemente le forze agenti su di esse in qualità di meccanismi di propulsione. É auspicabile che questo lavoro sia di impulso a nuove attività di ricerca ad esso correlate, come l'impostazione di un'impalcatura teorica del problema delle particelle natanti in ambienti non smorzati, lo sviluppo di una trattazione completa del caso di forze "fotoforetich" agenti nei plasmi, o l'approfondimento e la continuazione di questa stessa analisi con ulteriori osservazioni, ma soprattutto all'osservazione di altri tipi di particelle notoriamente attive in soluzione acquosa, così da evidenziare le differenze con le particelle giá osservate e consentire la scelta di quelle più consone ad essere sospese in gruppi nel plasma, aprendo la strada allo studio dei moti collettivi della materia attiva in ambiente non smorzato. Se gli esperimenti a terra si riveleranno sufficientemente interessanti, si potrebbe anche pensare di svolgerne in condizioni di microgravità, durante una campagna di volo parabolico o sulla Stazione Spaziale Internazionale.

Contents

List of Figures

List of Tables

Introduction

This thesis work has been performed together with the reaserch group on Complex Plasmas of the DLR (Deutsches Zentrum für Luft- und Raumfahrt – German Aerospace Centre), Institute of Materials Physics in Space, Wessling, Germany. The aim of my work has been to study the behaviour of micrometric particles with peculiar spatial anisotropy properties dispersed in a plasma, to highlight the presence of "active motion" phenomena of the particles themselves, to analyse their trajectories and to investigate the physical origin of these effects.

Dusty plasmas are low-temperature plasmas containing solid microparticles (dust) which are charged. The topic is very interesting because dusty plasmas play an important role in astrophysics applications, as they are present in planetary rings, comet tails, interplanetary and interstellar clouds, and in concern with space exploration, as they are also present in the vicinity of artificial satellites and space stations. Nowadays, an important application of complex plasmas is understanding better fusion plasmas. "Complex plasmas" is the name given to dusty plasmas created in laboratories for research purposes. The particles studied so far in complex plasmas are so-called "passive" particles and they perform a simple Brownian motion due to collisions with plasma ions, electrons and neutrals.

Recently, the attention of the research community studying particles dispersed in fluids has been drawn on so–called "active" particles, which show an "amplification" of Brownian motion due to the effects of autonomous self–propulsion (for example in the case of bacteria) or to the peculiar nature of their shape or surface, which makes them anisotropic in the presence of non-equilibrium situations, such as the presence of thermal or chemical gradients on the particle surface. The result is that a certain direction of motion is preferred. A very successful class of artificial swimmers are the so–called Janus particles: they are named after the two-faced Roman god Janus as they are dielectric colloids half–covered with thin layers of catalytic materials. These peculiar active particles ware chosen as the subject of the present work and the ones used are $9{,}27(10)\,\mu$m diameter melamine–formaldehyde spheres half–covered with $10{,}0(1)\,$nm of platinum. When suspended in water these particles perform an active motion because of the chemical reactions catalysed by the metal. However, the behaviour of these particles in

an ionized gas is so far a completely unexplored field, both theoretically and experimentally. Therefore, my experiments provide, therefore, the first experimentally collected data about active particles in a plasma environment.

Since both active matter and complex plasmas are topics of great interest, it is *a fortiori* even more interesting to study active particles in a complex plasma environment. As it often happens in science, it is still not clear what this research will bring to complex plasma and active matter research communities, but it is for sure something new. Something interesting and already clearly useful for complex plasma research community is that Janus particles are an extreme case of non-perfect regular particles. In fact, they are strongly asymmetric and it happens sometimes that regular particles become weakly asymmetric and give rise to behaviours similar to the ones of active particles, even if much weaker [1] [2]. Another field of possible useful application of studying active particles in complex plasma environment is the one of particles moving violently in fusion devices, like fast particles in tokamak plasmas. All these reasons together create a great interest nowadays in proceeding with these studies.

My experiments have been performed with single Janus particles in low–temperature weakly ionized plasmas. The reason is that the aim is to focus on the physics of one single Janus particle in this new environment without the influence of other particles, which would completely change the physics of the phenomenon.

As Janus particles are in my case immersed in a low-temperature plasma and not in an aqueous solution, the mechanisms that make them active in that environment are not present. In particular, the aim of my work is to understand if Janus particles are active in a complex plasma environment and in this case to analyse the self–propulsion mechanisms in plasmas. For this reason, I focused on the forces acting on single Janus particles that could work as propulsion mechanisms and I studied them experimentally. Mine is the first step of the research about active particles in a complex plasma environment and the next one will be studying groups of active particles in this environment. These groups of particles can be properly called *active matter* instead of active particles and the collective behaviour of active matter in complex plasma environment are likely to be studied in the future.

The work is therefore structured as follows:

1. In chapter 1, a brief introduction to what complex plasmas and active matter are will be presented, together with the reasons why they are interesting and useful fields of research.

2. In chapter 2, the experimental setup and the particular Janus particles that I have used will be presented.

3. In chapter 3, the forces most probably acting in my case, which means on the Janus particles used in complex plasma environment, will be hypothesized and treated in

depth. A rough estimation of their strength will also be made in order to understand which ones are stronger and which are weaker. In the end of this chapter, I will also discuss the existing theory about active particles in a harmonic potential well in an overdamped environment. As I have also confined the Janus particles in a potential well in my experiments, this theory is the closest to my case and in chapter 5 a qualitative comparison of my results with this theory will be performed.

4. In chapter 4, the experiments performed in order to understand if these forces actually make Janus particles active in plasma and to better understand how the forces act and if their theoretically predicted relative strength is correct will be presented.

5. In chapter 5, the results of the experiments will be reported and some conclusions based on the results will be drawn. The results numerically predicted for active particles in a harmonic potential well in an overdamped environment will be compared with my experimental results. Also the results that I obtain in chapter 3 about the forces that I have hypothesized to act on the single Janus particle in the experimental environment that I used will be compared to my experimental results.

6. In the conclusive part the conclusions about my work will be drawn and I will also go through the possible future developments of my work.

In the appendix, some of the codes that I have written in order to perform the analysis are reported.

Chapter 1

Complex plasmas and active particles

1.1 Introduction to complex plasmas

Complex or dusty plasmas are low-temperature plasmas containing solid particles, which get charged in the plasma [3]. Usually these particles have micrometric dimensions. The charges are usually negative, but in particular cases they can be positive. Dusty plasmas are quite natural in space: they are present in planetary rings, comet tails, interplanetary and interstellar clouds, in the vicinity of artificial satellites and space stations. Dusty plasmas are also investigated in laboratories and they are usually called complex plasmas to distinguish dusty plasmas specially designed for such investigations from natural dusty plasmas. The particles are large enough to be visualized individually and this is the reason why their motion can be easily tracked. This makes it possible to investigate phenomena at the most fundamental single particle kinetic level. The enormous increase of interest in complex plasmas was triggered in the mid 1990s by the laboratory discover of plasma crystals.

In general, complex plasmas can be generated either with radio-frequency discharges or direct current ones. The experiments performed with them can be ground-based or they can be in microgravity conditions. The complex plasmas used for this work have been generated with a radio-frequency discharge and the experiments performed are ground-based.

The particle charge is a very important parameter in complex plasma physics because it determines particle interactions with plasma electrons and ions, electromagnetic fields and particles themselves. In the absence of emission processes, the charge of particles immersed in a plasma of electrons and ions is negative because the electrons are much faster than the ions and, thus, their thermal flow is much higher. While becoming increasingly negatively

charged, the particle repulses the electrons more and more intensively: the absolute magnitude of the particle charge grows until the electron and ion fluxes on the surface are balanced. For this reason, the surface potential of the dust particle is determined by the electron temperature. Apart from collection of ions and electrons from the plasma, another important effect that could make the particles positively charged exists. It is the emission of electrons from the particle surface through thermoionic, photoelectric and secondary electron emission processes. They are important in rocket engines, upper atmosphere, space and some peculiar laboratory experiments, but not in the ones I performed.

In case of ground-based experiments, the particle levitates in a sheath region over the lower electrode of the chamber in which the plasma is. The sheath region grows from the negatively charged lower electrode to the quasi-neutral plasma bulk. The particle levitates in this region because the electric field present in it generates on the particle an electric force that balances the gravitational force acting on it. This sheath region is characterized by a high degree of plasma anisotropy.

1.1.1 Forces on particles

The forces acting on dust particles in plasmas in ground-based are briefly listed. In the vertical direction they are:

- gravitational force: $F_g = mg$, where m is the particle mass
- electric force: $F_e = ZeE$, where Ze is the particle charge and E is the electric field
- ion drag force: it is caused by the momentum transfer from the flowing ions to the charged particles. Ion flows are usually induced due to large-scale electric fields that always exist in plasmas. An ion flow directed downward is present in the plasma sheath because of the strong electric field present in it.

  The ion drag force consists of two parts often referred as collection and orbital forces. The collection force is associated with momentum transfer from the ions that are collected by the dust particle, while the orbital force is due to the momentum transfer from the ions that are scattered in the electric field of the grain, but that are not collected [4].

In the horizontal direction the usual acting forces are the neutral drag force and the radiation pressure force in case particles are observed with a strong light beam, like a laser. I will focus on the second one in chapter 3 because of reasons that will be clear later on. Neutral drag force is the main mechanism responsible for friction when a particle is moving through a stationary plasma, because ion and electron number densities are too low compared to the neutral one as the ionization fraction is in the order of $10^{-6} \div 10^{-7}$. When the Knudsen number is large and the relative velocity u_d between the particle and the gas is small compared to the thermal velocity of neutrals, which is most of the cases,

it comes up that $F_n \propto -u_d n_n v_n$, where n_n is the neutral numnber density and v_n is the neutral thermal velocity.

1.1.2 Applications

As already mentioned, complex plasmas can be studied experimentally at the kinetic individual particle level, which is something only possible for most of the systems when they are static or, at best, they exhibit secular variations. Moreover, the characteristic time and length scales of complex plasmas are "stretched" with respect to atomic or molecular systems by typically a factor of a million: atomic systems have scales $\sim 1\,\text{Å}$ and complex plasmas $\sim 100\,\mu\text{m}$. This allows studies at all the relevant physical parameters in "slow motion" and "high resolution". This peculiar characteristic of complex plasmas make them useful in order to study fundamental physics at the kinetic single particle level of a lot of phenomena, such as:

- Crystals: many aspects of crystal physics, e.g. waves, are well reproduced at the kinetic level. The interesting tasks for the future lie in the area of understanding the role of defects in thermodynamics, magnetized and anisotropic crystals. Crystalline structures such as bcc, fcc and hcp, as well as their coexistence, have been already found for certain plasma and particle parameters.

- Phase transitions: detailed kinetic studies of phenomena such as melting and crystallization with complex plasmas will complement the present understanding of the elementary processes considerably. This includes nucleation as well as the dynamics and structure of crystallization fronts.

- Fluids: in concern with cooperative phenomena in fluid flows and self-organization of fluid flows from laminar shears to turbulence investigations at the kinetic level promise a rich field of research for the years to come. In particular, some of the issues to investigate are Kelvin-Helmholtz and Rayleigh-Taylor instabilities, interpenetrating flows, nonequilibrium phase transitions, multi-fluid systems and their interfaces.

and so on. These examples are just to give an idea of the very interesting and important physics phenomena that can be deeply investigated at the kinetic individual particle level. Also liquid to gas transition and viceversa, surfaces, magnetization and exotic systems can be studied with complex plasmas.

Dusty plasmas have also been present in various industrial applications for many decades. Studying complex plasmas experimentally can help to overcome issues related to the presence of dust in industrial plasmas. For example, in the beginning of the 1990s it became clear that a large part of contamination found on the surface of silicon wafers after the manufacturing was was not because of insufficient cleaning, but in fact was an inevitable consequence of plasma etching and deposition technologies. Research

about complex plasmas can be useful to understand better another very interesting field: dust particles in magnetic confinement fusion devices. They mainly originate during the plasma-surface interaction and it has become obvious that dust represents a serious safety hazard in the development of ITER project. The main problem is the presence of tritium due to the parts of ITER made of graphite and carbon composites. Dust can also affect the plasma performance and stability as well as the fusion device operation. Thus, the problem of removing dust particles from thermonuclear devices represents one of the most important scientific and technological problems. Moreover, in concern with the forefront field of novel atomic batteries for electrical power supply of spacecrafts, automatic weather stations, antisubmarine buoys and so on, research on complex plasmas is very important.

1.2 Introduction to active particles

Differently from passive Brownian particles, active particles, also known as self-propelled Brownian particles or micro- and nanoswimmers, are capable of taking up energy from their environment and convert it into directed motion [5]. Thanks to this property, active matter systems feature a series of behaviours not attainable by matter at thermal equilibrium, including, for example, swarming and the emergence of collective properties. While the motion of passive Brownian particles is driven by equilibrium thermal fluctuations due to random collisions with the molecules of the surrounding fluid, the active particle behaviour shows an interplay between random fluctuations and active swimming which drives them far from equilibrium. They are, in fact, perfect ideal models systems for non-equilibrium physics.

Originally, self-propelled particles have been studied to model swarm behaviour of animals. The interesting thing is that some of these behaviours are turning out to be universal, as they are independent of the type of animals that constitute the swarm. For this reason it is now a challenge for theoretical physics to find minimal statical models that universally describe swarming.

Active particles can be either biological or manmade objects. For what concerns the first ones, self-propulsion is a common feature of microorganisms which allows them to explore the surrounding environment when looking for nutrients or when escaping toxic substances. Two paradigmatic examples are Escherichia coli and spermatozoa. For what concerns manmade active particles, they can be very different and they are driven by different types of self-propulsion mechanisms. Examples of both biological and manmade active particles are shown in figure 1.1.

From the point of view of application, active particles can be useful for a series of challenges that the society is facing thanks to their core functionalities: transport, sensing and manipulation. The challenges are personalized healthcare, environmental sustainability and security. Micro- and nanoswimmers can, in fact, be used as micro- and nanoscopic cargos in several applications, from the targeted delivery of drugs, biomarkers,

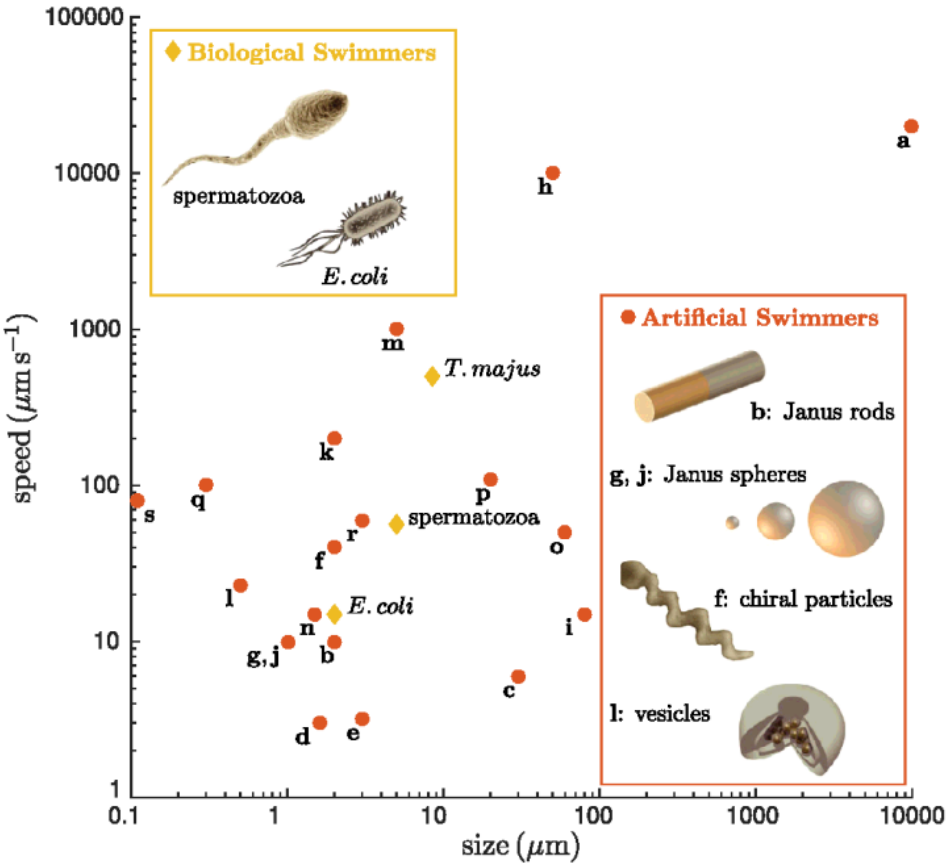

Figure 1.1: Biological and manmade active particles functions of their speed and size. The insets show some examples. The others letters correspond to: (a) PDMS platelets coated with Pt, (c) Linear chains of DNA-linked magnetic colloidal particles attached to red blood cells, (d) Janus spherical particles wih a catalytic Pt patch, (e) DNA-linked anisotropic doublets composed of paramagnetic colloidal particles, (h) Catalytic microjets, (i) Water droplets containing bromine, (k) Rod-shaped particles consisting of Au and Pt (or Au and Ru) segments, (m) Colloidal rollers made of PMMA beads, (n) Polymeric spheres encapsulating most of an antiferromagnetic hematite cube, (o) Water droplets, (p) Janus microspheres with Mg core, Au nanoparticles, and TiO_2 shell layer, (q) Hollow mesoporous silica Janus particles, (r) Janus particles half-coated with Cr, (s) Enzyme-loaded polymeric vesicles.

Table 1.1: Self-propulsion mechanisms of different kinds of Janus spheres

Microswimmer	Propulsion mechanism	Medium	Dim.	Max. Speed
Janus spherical particles with a catalytic Pt patch	Self-diffusiophoresis catalyzed by a chemical reaction on the Pt surface	H_2O_2 aqueous solution	1,6 μm	3 $\mu m\,s^{-1}$
Janus particles half-coated with Au	Self-thermophoresis due to local heating at the Au cap	Aqueous solution	1 μm	10 $\mu m\,s^{-1}$
Janus particles with light-absorbing patches	Local demixing of a critical mixture due to heating associated to localized absorption of light	Critical mixture	0,1 to 10 μm	10 $\mu m\,s^{-1}$
Janus microspheres with Mg core, Au nanoparticles and TiO_2 shell layer	Bubble thrust generated from the Mg-water reaction	Aqueous solution	20 μm	110 $\mu m\,s^{-1}$
Hollow mesoporous silica Janus particles	Catalysis powered by Pt or by three different enzymes (catalase, urease and glucose oxidase)	Aqueous solution	50 to 500 μm	100 $\mu m\,s^{-1}$
Janus particles half-covered with Cr	AC electric field	Aqueous solution	3 μm	60 $\mu m\,s^{-1}$

or contrast agants in healthcare applications to the autonomous depollution of water and soils contaminated because of bad waste management, climate changes, or chemical terrorist attacks in sustainability and security applications.

Since I will use a particular kind of active particles in my experiments, which are called Janus particles, I will spend now a few words about them. Janus particles are dielectric colloids partially coated with thin layers of catalytic materials like platinum or palladium. They are named after the two-faced Roman god Janus. For my experiments I used 9,27 μm diameter melamine-formaldehyde spheres half-covered with 10 nm of platinum. When these particles are immersed in an aqueous solution enriched with H_2O_2, they locally decompose it into H_2O and O_2. This reaction is catalyzed by the metal coating and a local concentration gradient is generated, which leads to self-diffusiophoresis. Also hematite has been used instead of platinum or palladium, as it acts as catalyst only when illuminated by blue light. This makes the particle motion easier to control. Also, when Janus particles are illuminated by strong laser light, a temperature gradient can generate on the particle and phoretic motion can take place. In this case, also optical forces can be present and they can be difficult to distinguish from the phoretic mechanism. Finally, self-propulsion can also be caused by a spontaneous symmetry breaking of the electric charge distribution around the particle if it is immersed in a conducting fluid and in presence of an electrical field. In table 1.1 the propulsion mechanisms of different Janus particles are listed.

Summary of chapter 1

Complex or dusty plasmas are low-temperature plasmas containing micrometric solid particles, which become negatively charged in the plasma. Dusty plasmas are quite natural in space; they are usually called “complex plasmas“ when investigated in laboratories. As the particles are large enough to be visualized individually, their motion can be easily tracked and this makes it possible to investigate phenomena at their most fundamental single particle kinetic level, which is a kind of investigation that can be carried out only on static systems or, at best, when they exhibit secular variations. Moreover, the characteristic time and length scales of complex plasmas are "stretched" with respect to atomic or molecular systems by a factor of typically a million: atomic systems have scales $\sim 1\,\text{Å}$ and complex plasmas $\sim 100\,\mu\text{m}$. The forces acting on regular particles in complex plasmas are: gravitational force in the case of ground-based experiments, electric force, ion and neutral drag forces. The fields of application of complex plasma physics go from crystals to fluids and phase transitions, and so on. In addition, research about complex plasmas can be useful to understand better another important field: dust particles in magnetic confinement fusion devices.

Active particles, also known as self-propelled Brownian particles or micro- and nanoswimmers, are defined as particles able to take up energy from their environment and convert it into direct motion. The direct consequence of this is that active particles are able to drive themselves far from equilibrium. Examples of active particles are natural and artificial objects capable of self-propulsion. Among biological swimmers it is worth to mention *spermatozoa* and *Escherichia coli*, while a very successful class of artificial swimmers are Janus particles: they are named after the two-faced Roman god Janus as they are dielectric colloids half covered with thin layers of catalytic materials. The different mechanisms making them active in aqueous solutions are listed in table 1.1.

Chapter 2

Experimental setup

In this chapter I will briefly describe the experimental setup that I used to perform my experiments with Janus and pure MF particles as well as the Janus particles I used. I performed my experiments in the Research Group on Complex Plasmas of the DLR (Deutsches Zentrum für Luft- und Raumfahrt, that is the German Space Agency) in Oberpfaffenhofen, Germany.

2.1 GEC chamber and vacuum system

The GEC (Gaseous Electronics Conference RF Reference Cell) chamber is where the experiments have been performed. This kind of chamber was initiated in 1988 in Minneapolis in order to give specifications of discharge geometry, setup and minimum diagnostic tool set for better data comparison under similar conditions about applications in low-temperature plasma physics. In fact, before that moment, in laboratories of different institutions where they used to work with low-temperature plasmas, they had different chambers and data from different groups were very difficult to compare.

Every GEC is made of stainless steel, it has a 25,1 cm inner diameter and eight flanges on its sides in order to provide simple access to whatever it's needed: pumps, gas inlets, plasma diagnostic probes and various devices. The main vacuum chamber of a GEC is shown in figure 2.1.

In figure 2.2 it is possible to see what the GEC of the group looks like; all the main components are pointed out. Numbers and letters refer to figure 2.6 and to the following parts of the description.

In particular, the GEC chamber that I used is modified. The modifications performed with respect to the usual chamber are:

- A stainless steal cap with a 20 cm diameter hole is attached to the big flange on top of the chamber instead of a closed cap. This choice has been made in order to

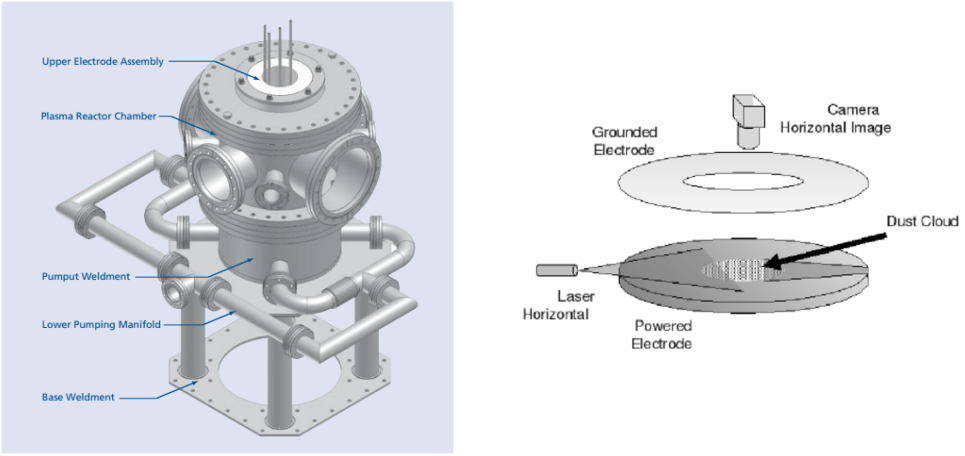

(a) *What a standard GEC RF Reference Cell looks outside*

(b) *What the used GEC RF Reference Cell looks inside*

Figure 2.1: Gaseous Electronics Conference RF Reference Cell

have the possibility of seeing what is inside the chamber every time, also during experiments. In usual GECs a closed cap is used. A 22 cm diameter glass plate is located on this top steel cap and it is not permanently attached to it, but it just lies over it: the big Δp between the inside and the outside of the chamber keeps it blocked.

- The lower electrode is larger than usual in order to obtain larger plasma crystals. In fact, even if I have not used the GEC to observe crystals but single particles, experiments with crystals are the routine ones performed with it.

In figure 2.3 it is possible to see the GEC used from different perspectives and in case of both plasma off and on.

The gas used to create plasma is argon and the colour of ionized argon is the one you can see in detail in figure 2.4. Argon is provided from a regular gas bottle connected to the chamber through a flow controller (see figure 2.6).

In particular, when plasma is off argon is already inside the chamber, but the RF power is off, so the gas is not ionized and it is just transparent. On the other side, when plasma is on the RF power has been turned on. Ionization is created with a RF and not with a DC (direct current) discharge in order to obtain several operational advantages. In particular, knowing that the typical value for ion plasma frequency is $\omega_{p,i} = 2\,\text{MHz}$ in case of argon and that the one for electron plasma frequency is $\omega_{p,e} = 0{,}5\,\text{GHz}$, for an AC (alternative current) discharge three frequency regimes can be defined:

- low frequency discharge: $\omega < \omega_{p,i}$: ions and electrons respond to the oscillating electric field

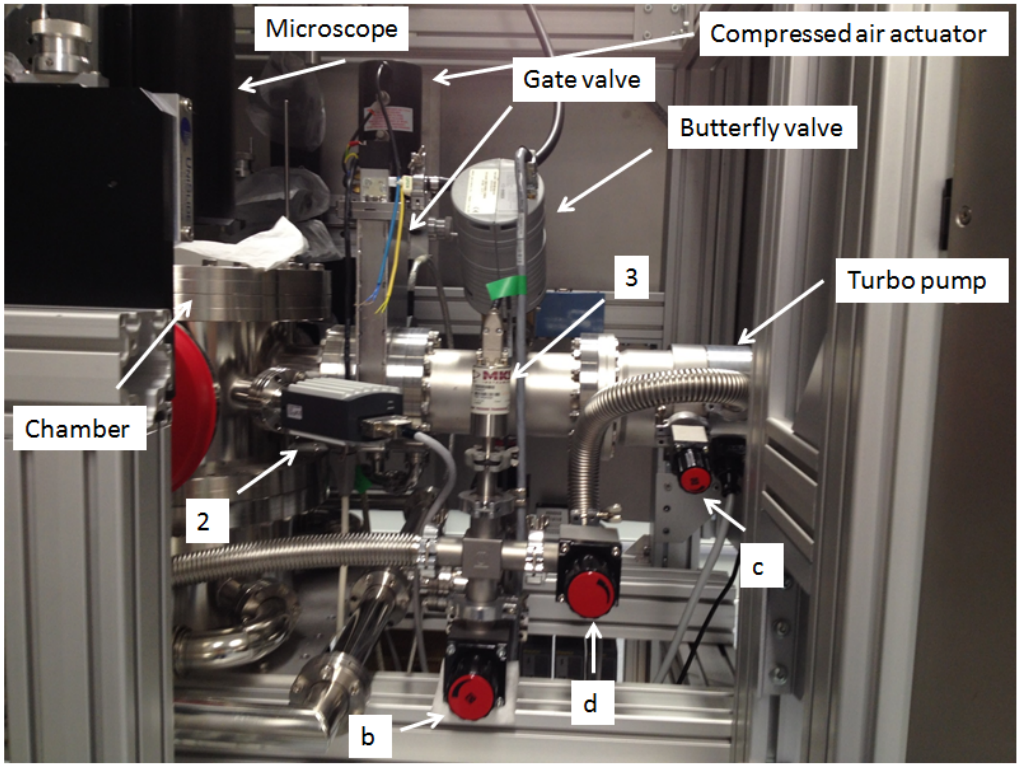

(a) *GEC seen from its left side*

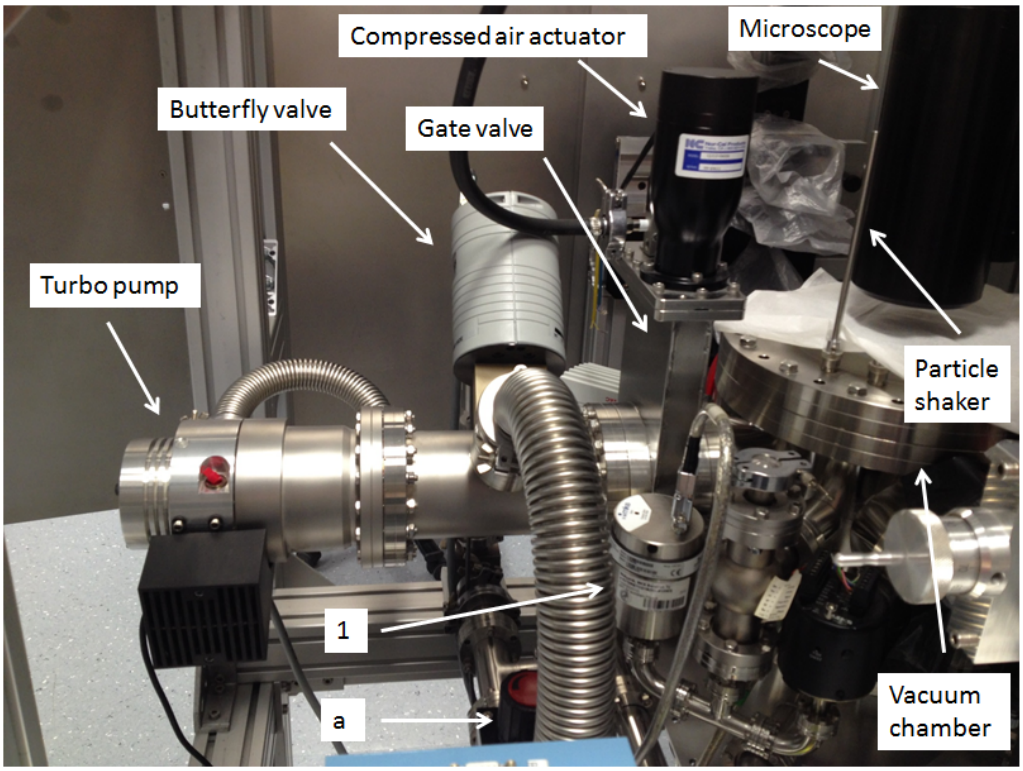

(b) *GEC seen from its right side*

Figure 2.2: Main components of the GEC used

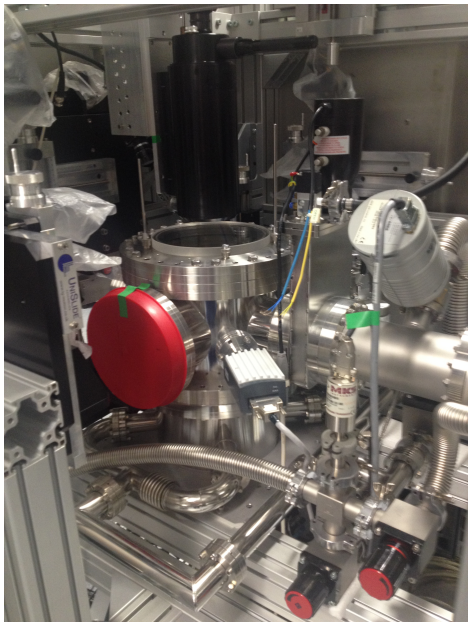

(a) *GEC seen from its left side before switching the RF power on: plasma off*

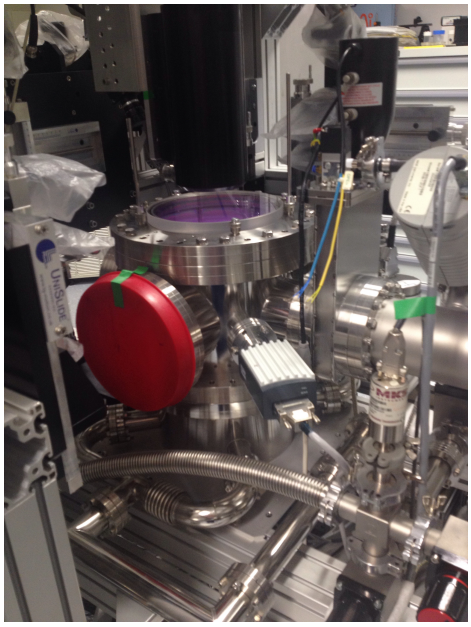

(b) *GEC seen from its left side after switching the RF power on: plasma on*

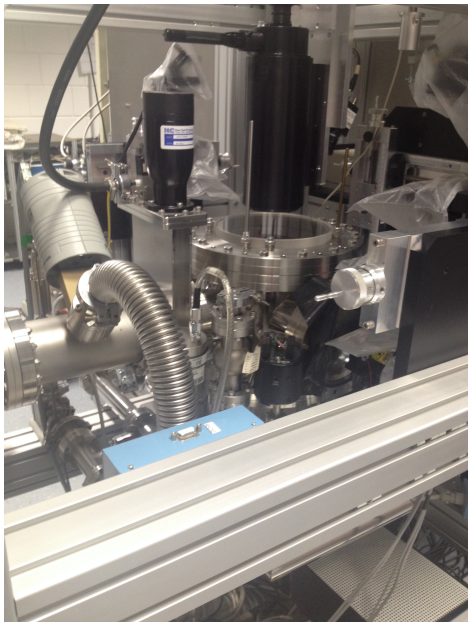

(c) *GEC seen from its right side before switching the RF power on: plasma off*

(d) *GEC seen from its right side after switching the RF power on: plasma on*

Figure 2.3: Perspectives and plasma of the GEC chamber used

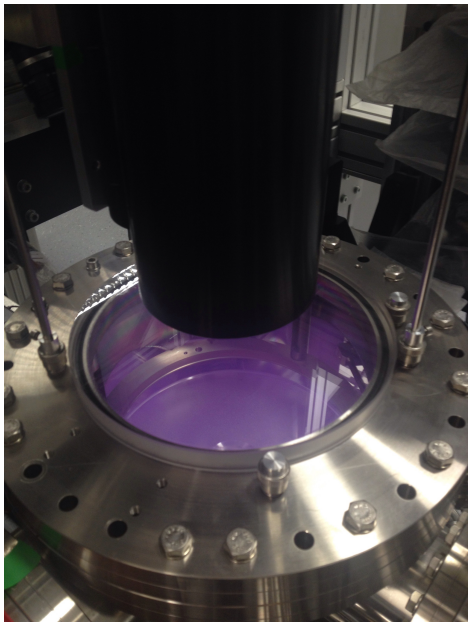

Figure 2.4: Argon plasma

- RF discharge: $\omega_{p,i} < \omega_{RF} < \omega_{p,e}$: only electrons respond to the oscillating electric field, while ions respond to its time-average
- hyper-frequency discharge: $\omega > \omega_{p,e}$: neither ions nor electrons respond to the oscillating electric field

In particular, in case of RF discharge the typical value for the frequency is 13,56 MHz not for a physical reason, but because the ISM (Industrial, Scientific and Medical) agreed on this value for power applications. Higher frequencies (VHF) would work better for several physical reasons, but from a technological point of view they are more expensive and need Faraday screening.

Notice that the lower electrode is a plate, while the upper one has a ring shape.

The lower electrode is connected to the RF (radio frequency) generator shown in figure 2.5 which provides an electric field at the standard frequency of 13,56 MHz up to 300 W. It is a commercial *Dressler Cesar* RF generator. In this picture the RF power - left value - was set to 5 W, the most used value for the present work, and the reflected power - right value - is 0 W. It is important that the reflected power is always null, otherwise it can damage the device. This RF generator has some problems in finding automatically - "AUTO" in figure 2.5 - a *matching condition* which makes the reflected power null, so it must always be set manually. The *matching condition* is in fact the condition in which C_T and C_L, the two capacitances inside the device, are coupled in such a way that makes the reflected power null. The manually set values are respectively 118 and 814, as it can be seen under the value of the reflected power in figure 2.5. After pushing the button "MAN"

Figure 2.5: The RF generator

on the right, the lower buttons, "$C_T <$", "$C_T >$" and "$C_L <$", "$C_L >$", are used in order to regulate the capacitance values.

The lower electrode is also connected to a water cooling device. The reference temperature used during all my experiments is 22,9 °C.

The GEC is connected to a vacuum system because experiments with complex plasmas require high vacuum and a precise dosage of gas, argon in this case. A flow diagram of the vacuum system is shown in figure 2.6. Numbers refer to various pressure measurement devices which are explained in the following papers and letters refer to valves; both pressure measurement devices and valves are addressed with the same nomenclature of figure 2.2.

Pressure can go down until 10^{-7} mbar and two pumps are used in order to reach such low pressures. The first one is a Scrollvac SC 5D roughing pump which creates pre-vacuum and the second one is a Leibold TURBOVAC 151 turbo pump (see figure 2.2). The pressure in the for-vacuum line is measured with a baratron (number 3 in figures 2.6 and 2.2) and its output is the value "PR1" in mbar on the MKS PR 4000 controller that can be seen in the first picture of figure 2.7.

When running plasma exact pressure control is demanded the gate valve to the turbo pump is closed and the turbo pump is connected to the chamber through a butterfly valve (see figures 2.6 and 2.2). This last one controls the gas outflow of the chamber with a rotating disk and it keeps the pressure at the desired value. In fact, the gas pressure is maintained constant during the operations and it is set with the *set point a* of the pressure controller in Torr (see "SP A" in the lower device of figure 2.7). When the pressure

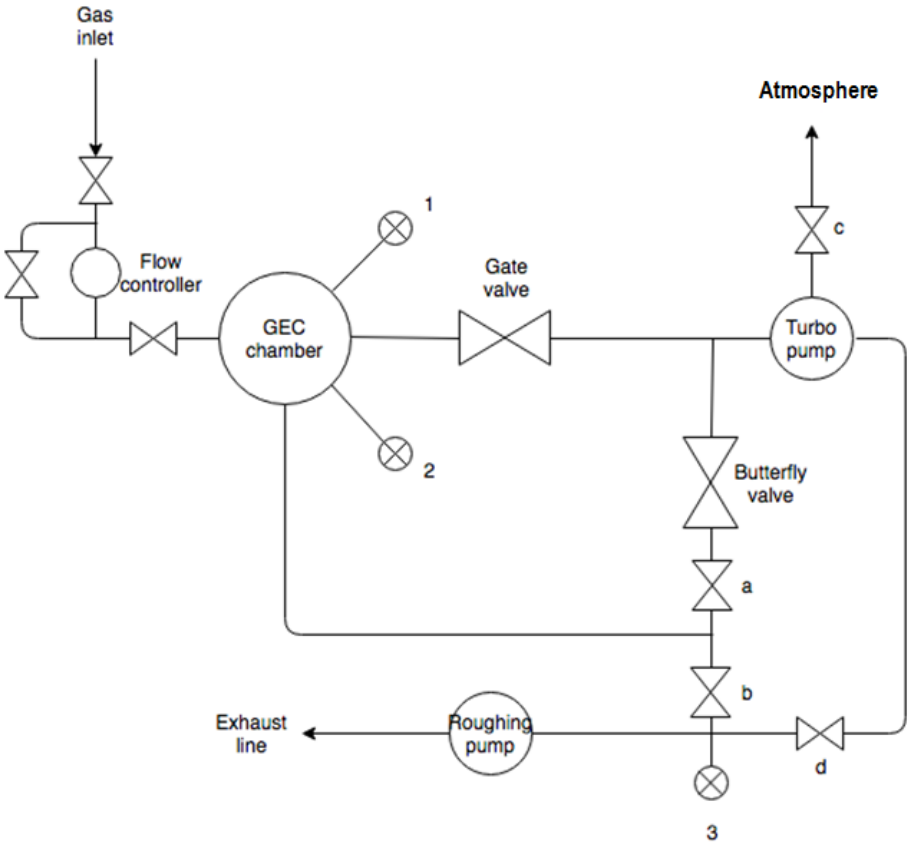

Figure 2.6: The flow diagram of the vacuum system which includes the numbers for the pressure measurement devices and the letters for the valves which refer to figure 2.2 and to the text

measured in the chamber is < *set point a*, then the rotating disk closes a little bit in order to let less gas molecules move to the turbo pump; when on the other hand it is > *set point a*, then the disk opens more in order to let more gas flow to the turbo pump. The gas inflow from the argon bottle is regulated through the flow controller shown in figure 2.6 and its value is shown in sccm as "FL2" on the MKS PR 4000 controller in the first image of figure 2.7. In fact, this device is connected both to the baratron number 3 and to the flow controller.

Apart from the baratron connected to the for-vacuum line (number 3), there are two other devices measuring the pressure and they measure it directly in the chamber. The first one is number 1 of figures 2.6 and 2.2. It is a baratron whose mechanism is based on a flexible capacitor and its range is 0,25 Torr: it is small and this lets the device be very precise in this range. The output of this baratron number 1 can be read in Torr on the MKS 600 Series pressure controller shown in the second picture of figure 2.7. In particular, the upper value on the pressure controller in the picture is the *set point a*, which we talked about referring to the butterfly valve's role, and the lower one is the pressure measured in the chamber. In the picture they are the same as it usually happens. It is important to be aware that the pressure read on this controller is 25 % lower than the true one.

The third device measuring the pressure is a combination of a ionization manometer and a Pirani gauge. It measures the pressure directly in the chamber, it appears with the number 2 in figures 2.6 and 2.2 and its output is shown in Torr by the read-out in figure 2.8. This system can work in a wide range of pressures because the manometer works in the low-pressure regime, while the Pirani gauge works in the high-pressure regime. This device is then more precise than the baratron number 1 in the low-pressure regime, but the baratron is more precise in its range.

The presence of two different devices measuring the pressure in the chamber is due to the fact that plasma pressure is a very important parameter to keep under control and for this reason some redundancy is a good idea. Furthermore, the output pressure of the combination ionization manometer and Pirani gauge depends on the type of gas, while the one of the baratron number 1 does not. During the experiments, the observed value is the output of the baratron number 1 on MKS 600 Series pressure controller (second picture of figure 2.7).

Now that the vacuum system has been explained in detail, how to perform experiments with single particles will be investigated. In order to inject particles in the plasma, a particle dispenser is used. I injected the single particles simply shaking gently the shaker connected to the dispenser on top of the chamber. The particle dispenser can be seen in figure 2.9 and the shaker in figure 2.2. Every time I injected more than one particle I switched off the RF power and I started the plasma again. In fact, when the RF is off also the electric field that compensates gravity is off and the particles fall on the lower electrode and they lie there.

In order to record the motion of the single particle with the microscope small field of

(a) *MKS PR 4000 controller showing the pressure measured by the baratron connected to the for-vacuum line (number 3) and the gas inflow measured by the flow controller*

(b) *MKS 600 Series pressure controller showing the fixed set point a and the pressure value measured in the chamber by baratron number 1*

Figure 2.7: MKS controllers

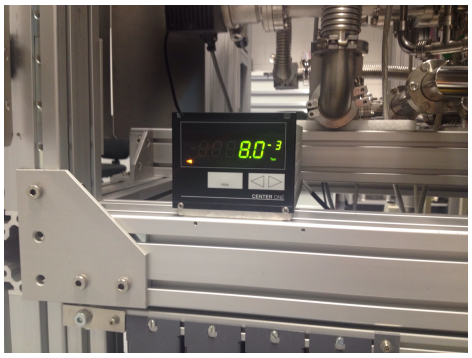

Figure 2.8: Read-out of the pressure measured by the combination of ionization manometer and Pirani gauge

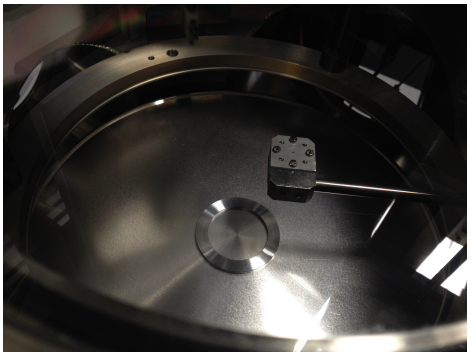

Figure 2.9: Janus particle dispenser

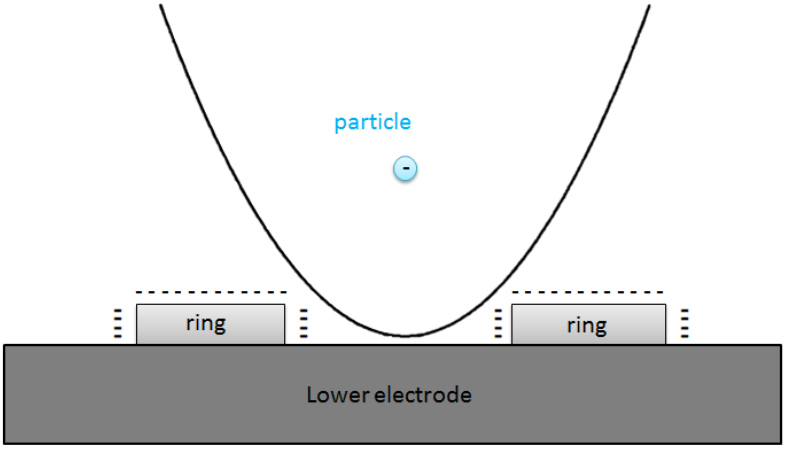

Figure 2.10: Potential well generated by the ring

view, an aluminium ring is put in the middle of the lower electrode. It can be clearly seen in figure 2.9. This is because also the ring, like the particles and like every object inserted in the plasma, charges negatively and its presence creates a potential well which confines the particle motion. See figure 2.10.

2.2 Detection setup

In order to see the suspended single particles it is necessary to illuminate them with a laser beam. For the present experiments a horizontal and a vertical laser sheets are used. The horizontal is much more powerful that the vertical: for this reason in the following chapter just its power will be taken into account. The horizontal laser wavelength is 660 nm and the vertical one is 635 nm. Both are in the visible range and in particular they are red. The vertical one is just necessary if a plasma crystal must be seen from the side,

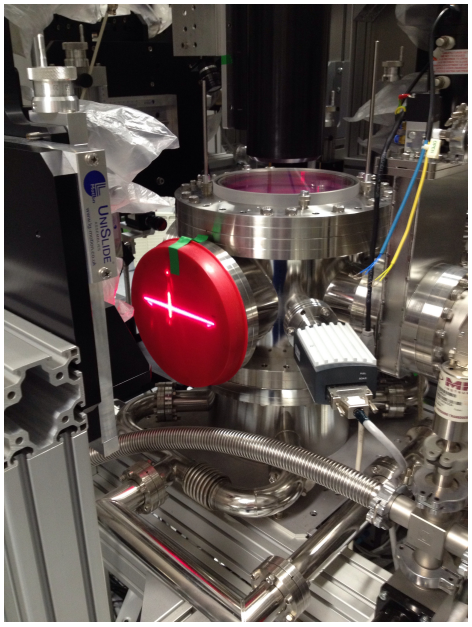

Figure 2.11: Horizontal and vertical lasers on

for example to verify that the plasma crystal is two-dimensional. In my single-particle experiments it is therefore unnecessary. See the lasers in figure 2.11.

A 4 Mega-Pixel CMOS camera and a long distance microscope constitute the imaging system used: see figure 2.12.

The FASTCAM Mini WX100 is a high-speed camera which delivers exceptional high resolution imaging performance by providing 2048x2048 pixel resolution at 1080 fps, 1920x1080 pixel full HD resolution at 2000 fps and frame rates up to 80 000 fps at reduced image resolution. Standard operational features of the FASTCAM Mini WX include a mechanical shutter to allow remote system calibration, Gigabit Ethernet Interface for a reliable system control with high-speed data transfer to PC, and the ability to switch off cooling fans to eliminate vibration when recording at high magnifications (see last picture of figure **??**). In figure 2.13 it is shown what the camera looks like without the microscope and some more performance specifications are reported.

The software used to control the camera is called PFV (Photron FASTCAM Viewer): its layout is shown in figure 2.14.

Every time I performed a recording, the PFV software generated a text file (`.cih` extension) with all the details about the recording. All information is divided into five groups named:

- `Camera Information Header`, with date and time of recording, information about the camera, recording rate in fps, shutter speed in s, trigger mode, number of frames, image width and height in pixels, number of colour bits and so on: an extract of

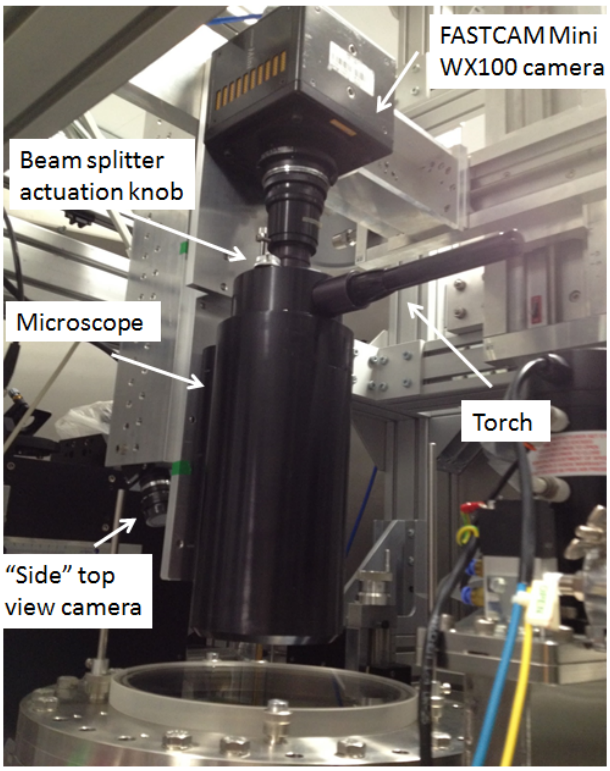

Figure 2.12: Imaging system: camera and microscope

(a) *FASTCAM Mini WX100 camera*

Model	Mini WX50	Mini WX100
Full Frame Performance	750fps 2048 x 2048 pixels	1,080fps 2048 x 2048 pixels
Maximum Frame Rate	Type 67.5K: 67,500fps (256 x 32 pixels)	Type 80K: 80,000fps (256 x 32 pixels)
Minimum Exposure	Global electronic shutter minimum exposure time independent of frame rate 2.7µs	
Inter-Frame Time (for PIV)	2.6µs	
Ruggedized Mechanical Calibration Shutter	Standard feature	
Dynamic Range (ADC)	12-bit monochrome 36-bit color	
Memory Capacity Options	8GB: 1,361 frames at full resolution 16GB: 2,726 frames at full resolution 32GB: 5,457 frames at full resolution	
Memory Partitions	Up to 64 memory segments	
Region of Interest	Selectable in steps of 256 pixels (horizontal) x 32 pixels (vertical)	
Trigger Inputs	Selectable +/- TTL and switch closure FET input 0V +/-12V (H level +2.5V to +12V)	
Trigger Delay	Programmable on selected input / output triggers: 100ns resolution	
Input / Output	Input: Trigger (TTL/Switch), sync, ready, event, IRIG Output: trigger, sync, ready, rec, exposure	
Trigger Modes	Start, end, center, manual, random, random reset, image trigger, time lapse	
Time Code Input	IRIG-B	
External Sync	+/- TTL Variable frequency sync FET input 0V +/-12V (H level +2.5V to +12V)	
Camera Control Interface	High-speed Gigabit Ethernet	
Image Data Display	Memory status, Frame rate, shutter speed, trigger mode, date/time, status, real time / IRIG time, frame count, resolution, LUT and comment	
Saved Image Formats	BMP, TIFF, JPEG, PNG, RAW, RAWW, MRAW, AVI, WMV, FTIF, MOV - Images can be saved with or without image data and in 8-bit, 16-bit or 36 bit depth of sensor where supported	
Supported OS	Microsoft Windows operating system including: XP, Vista, 7, 8, 8.1, 10 (32/64-bit)	

(b) *Camera performance specifications*

Figure 2.13: Camera and performance specifications

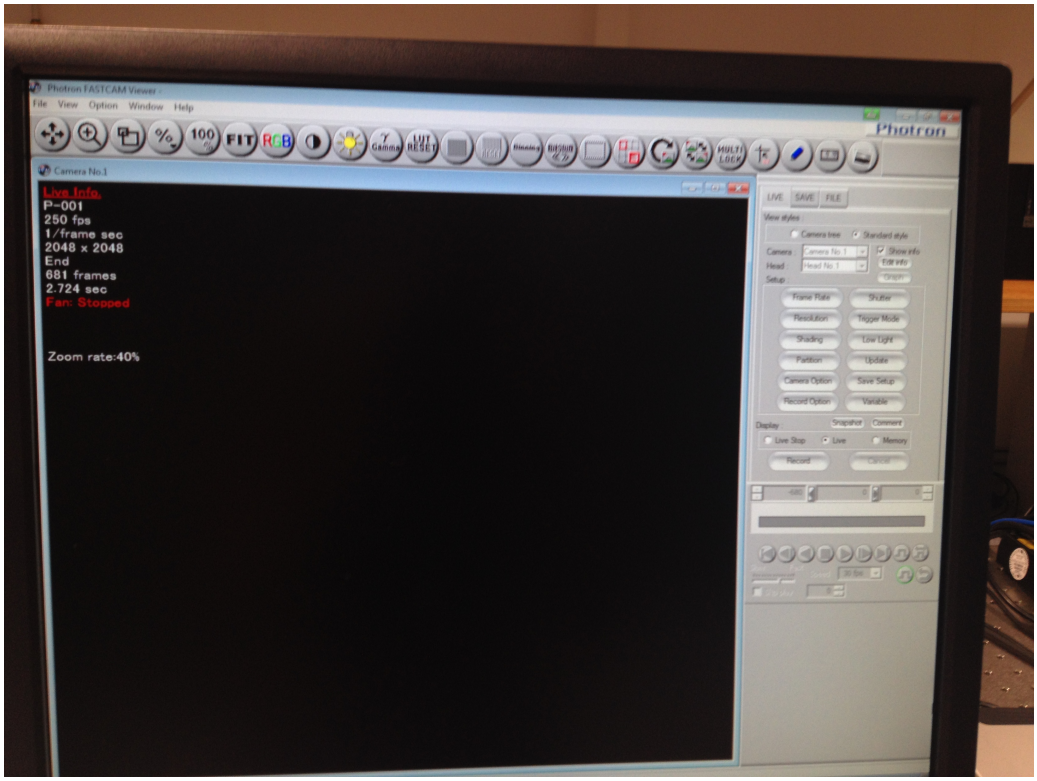

Figure 2.14: Layout of the software PFV

```
#Camera Information Header
Date : 2018/5/9
Time : 15:33
Camera Type : FASTCAM Mini WX100 type 80KM - 16GB
Head Type : Unknown Child Device
Camera ID : 10
Camera Number : 0
Head Number : 1
Max Head Number : 1
Scene Name :
User Defined Camera Name : Camera No.1
Session Number :
Date Record : Unknown
Time Record : Unknown
Trigger Time : 0
Record Rate(fps) : 50
Shutter Speed(s) : 1/50
Trigger Mode : Start
Original Total Frame : 2726
Total Frame : 2726
Start Frame : 0
Correct Trigger Frame : 0
Save Step : 1
Image Width : 2048
Image Height : 2048
Color Type : Mono
Color Bit : 8
File Format : Png
EffectiveBit Depth : 12
EffectiveBit Side : Lower
Partition Number: 1
```

Figure 2.15: Extract of the `.cih` file generated by the PFV software during a recording

this part is shown in figure 2.15

- `Photron Fastcam Viewer Version Information`
- `System Information`, that is:
  - `OS : Windows 7 Enterprise (x64) Service Pack 1 (version 6.1 Build 7601)`
  - `Memory :  16326MB RAM`
  - `Processor :  Intel(R) Core(TM) i7-4790 CPU @ 3.60GHz`
  - `DirectX : DirectX 11`
- `Device Information`, that is just the number of devices, in my case always only 1
- `Device 1 (Current)`.

Apart from the camera, a microscope is needed for single particle analysis. The long distance microscope used is a Questar QM 100 whose working range is 15 cm to 35 cm and whose resolution is 1,1 μm at 15 cm. A torch can be connected to it, see figure 2.12, in case one wants to record a particle motion without switching the lasers on. When the torch is used, since a light beam must go down to the chamber and another one must go back to the microscope and they are not supposed to overlap, the beam splitter actuation knob of figure 2.12 must be switched. It is interesting to note that with the normal light coming out of the torch it was not possible to observe the particles because it was too bright. For this reason a resistor of 3,3 Ω was inserted in the torch in order to lower its brightness and to see the particle's shadow well. I am talking about its shadow because when the particle is observed with the laser light, then the particle is white on a black background because the light seen by the camera is the one scattered by the particle. The

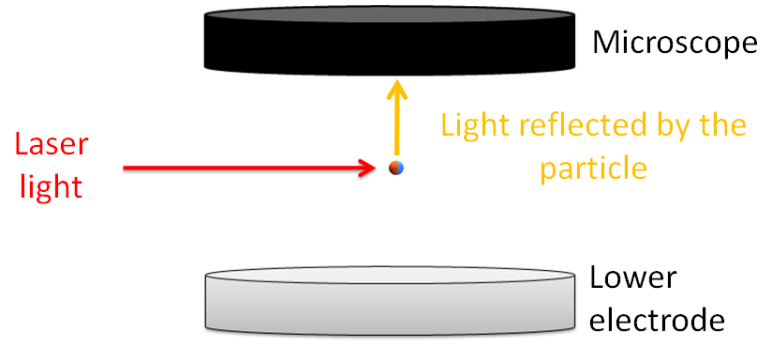

(a) *Optical model in case of laser light*

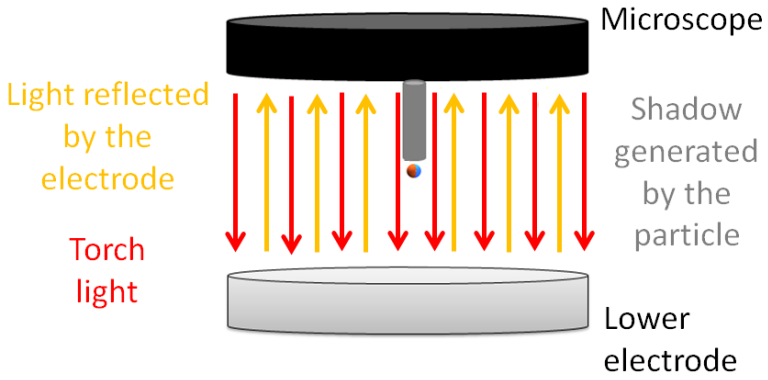

(b) *Optical model in case of torch light*

Figure 2.16: Difference in the recorded images when the laser and when the torch are used

electrode is in fact not hit by the laser (see figure 2.1). On the other hand, when the particle is observed with the torch light, then the particle is black on a white background because the light hits the electrode and it reflects it back. Since the particle shields light coming to the long distance microscope and to the camera from the electrode, it gives rise to a shadow. See figure 2.16 for a simplified illustration of the optical model and figure 2.17 for two recorded images in the two cases of lasers and torch on. This simple model can explain why, in case of illumination coming from the torch, particle tracking gives the problem called "pixel locking" I describe in section 4.1.1.

Apart from the FASTCAM Mini WX100 camera software, the single particles moving in the plasma can also be seen from a monitor connected to the "side" top view camera in figures 2.12 and 2.18.

The single particle confined in the potential well generated by the ring recorded by the "side" top view camera is shown in figure 2.19. The impression is that the particle does not seem located in the centre of the electrode, but this is just because of the angular view

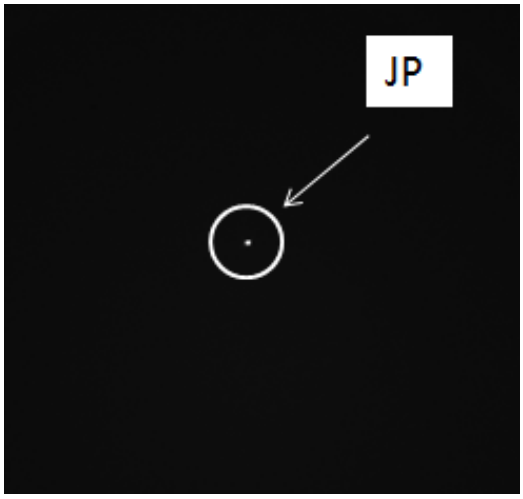

(a) *Janus particle observed with laser light*

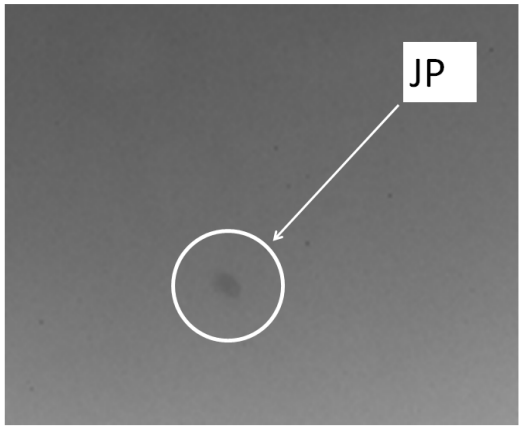

(b) *Janus particle observed with torch light*

Figure 2.17: Simple optical model. The red arrows are the input light, in one case from the laser and in the other from the torch, and the yellow ones are the reflected light. The parts hit by the reflected light are the white ones in the recorded frames.

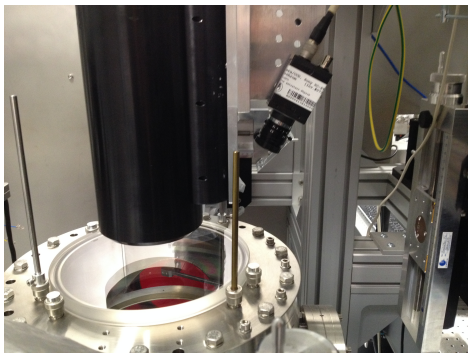

Figure 2.18: "Side" top view camera

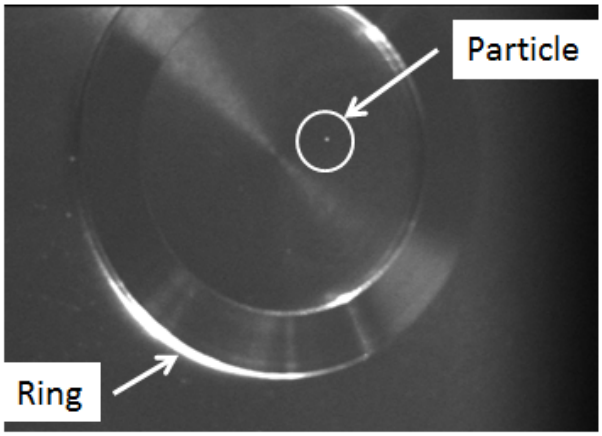

Figure 2.19: Suspended particle trapped in the potential well generated by the aluminium ring. Image from the "side" top view camera.

of this camera.

2.3 The Janus particles used

All Janus particles that I used in my experiments have been produced in the same way. The starting point is pure melamine formaldehyde (MF) particles that the group buy from a German company called *Microparticles GmbH*, whose headquarter is in Berlin. Melamine formaldehyde, which can also be called melamine resin or simply melamine, is a hard thermosetting plastic material made from melamine and formaldehyde by polymerization. The idealized subunit of a MF resin and the pure MF particle property table provided by *Microparticles GmbH* can be seen in figure 2.20.

In particular, the MF particles used have a diameter of 9,27(10) μm. These pure MF particles are then exactly half-covered with 10 nm of platinum by Ali Kaouk in DLR, Institute of Materials Physics, Cologne. The following steps constitute the MF particle covering procedure:

1. MF particles are dispersed in isopropanol (99.99%, *Sigma Aldrich*) at 0,5 mg/10 ml
2. the solution is mixed in a vortexer
3. silicon wafer pieces are cleaned in an ultrasonic bath with:
   - water + soap
   - water
   - ethanol

   consecutively

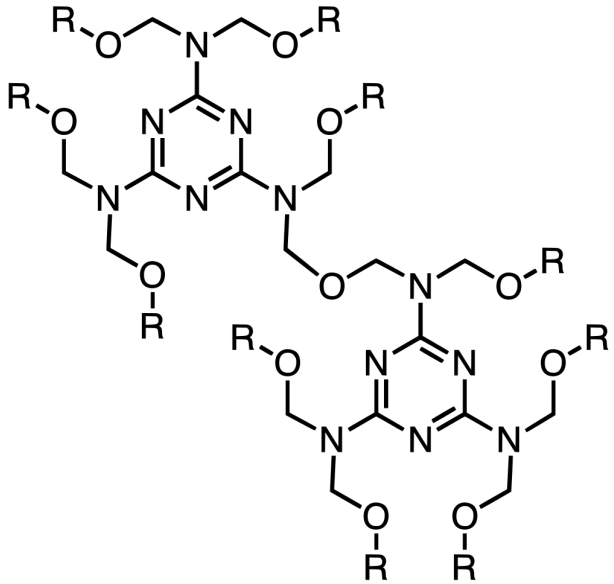

(a) *Idealized subunit of a MF resin*

Properties	MF-Particles
Density	1,51 g/cm³
Refractive index	1,68
Particle diameter	300 nm -12 µm
Monodispersity	CV < 5%
Particle shape	spherical
Surface charge	> pH5 anionic
Functional groups	methylol, imino
Hydrophilicity/Hydrophobicity	hydrophilic
Crosslinking	crosslinked
Porosity	non-porous
Temperature stability	to 250 °C
Mechanical strength	robust
Solubility in acids and bases	insoluble
Stability in solvents without swelling	water, alcohols, all solvents and oils
Biocompatibility	biocompatible

(b) *MF particle properties table provided by Microparticles GmbH*

Figure 2.20: Melamine formaldehyde particles

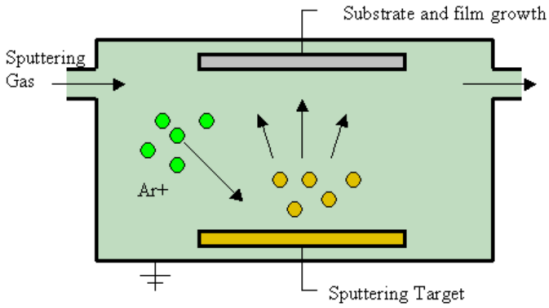

Figure 2.21: Sputter deposition

4. a silicon wafer is covered with drops of this solution when inclined at an angle of 10°
5. the solution dries over the silicon wafer while it is still inclined
6. the particles are half covered with a 10,0(1) nm platinum sputter in a PVD (physical vapour deposition) setup
7. Janus particles are scraped off with a sharp scalpel from the wafers into a vial and sealed under nitrogen to stop them from getting humid.

The physical vapour deposition of step 6 is also known as magnetron sputtering and it is a procedure in which the material, platinum in the present case, goes from a condensed phase to a vapour phase and then back to a thin film condensed phase. A RF plasma is used to remove platinum atoms from a solid metal target and make them condense onto the silicon wafer covered with MF particles.

The used sputtering parameters are:

- 120 s duration
- 10^{-4} mbar pressure
- 60 mA current.

Plasma is a normal magnetron plasma. See figure 2.21 to have an idea of how the sputter deposition procedure works and see figure 2.22 for what the particle should look like at the end. The red side represents the half-covered with platinum, while the blue one is the pure MF. All Janus particles are exactly half covered with platinum.

I observed both pure MF and Janus particles under the optical microscope and I compared the way they look like. The problem is that the platinum layer is too thin (10 nm) to be observed with the optical microscope of the research group because its resolution is not high enough: it works with white light and not with laser light. Figures 2.23 and 2.24 show what I observed: MF and Janus particles look identically under the optical microscope I have used.

Figure 2.22: Simplified illustration of a Janus particle

The only different feature of Janus particles is that some of them look darker than others. This effect is possibly due to the platinum layer facing upwards, that is facing the microscope. In fact, these Janus particles have not been observed directly from the same silicon wafer used to cover half of their surface with platinum in the PVD setup, but they were moved to another wafer. When they fall, their angular orientation is random and this is why the platinum layer can face upwards, downwards or any other direction. The brightness of two Janus particles has been studied and it has turned out to be actually slightly different: see figure 2.25.

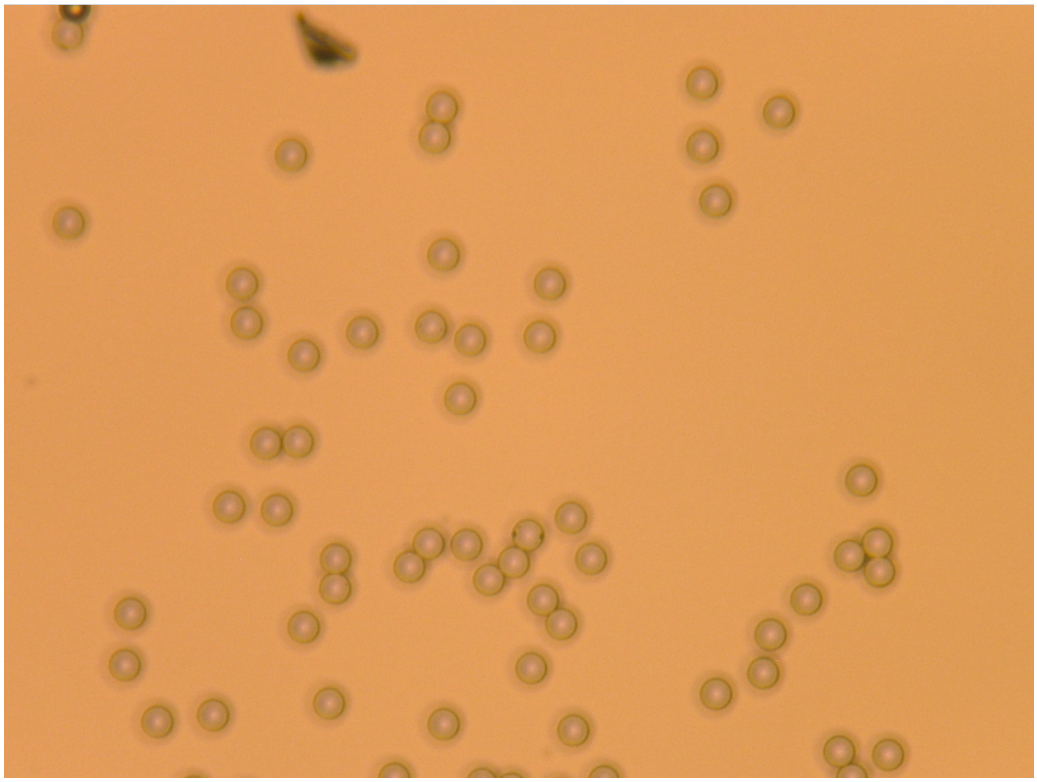

(a) 9,27 μm *diameter pure MF particles under the optical microscope*

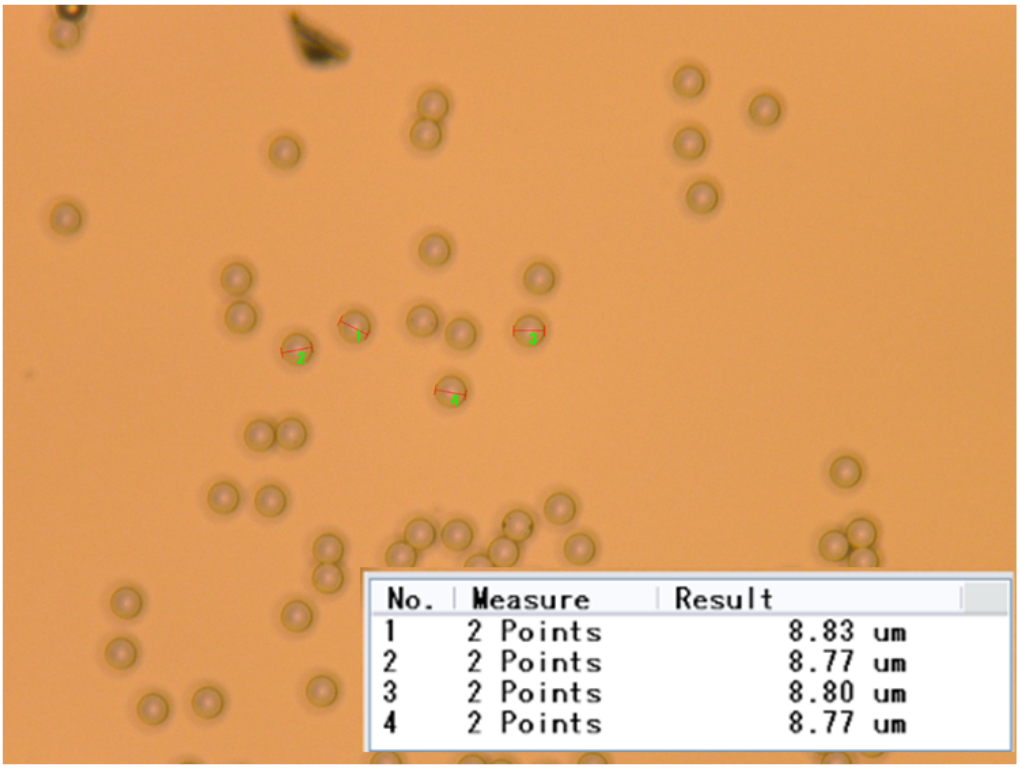

(b) *MF particle measured diameters*

Figure 2.23: MF particles under the optical microscope

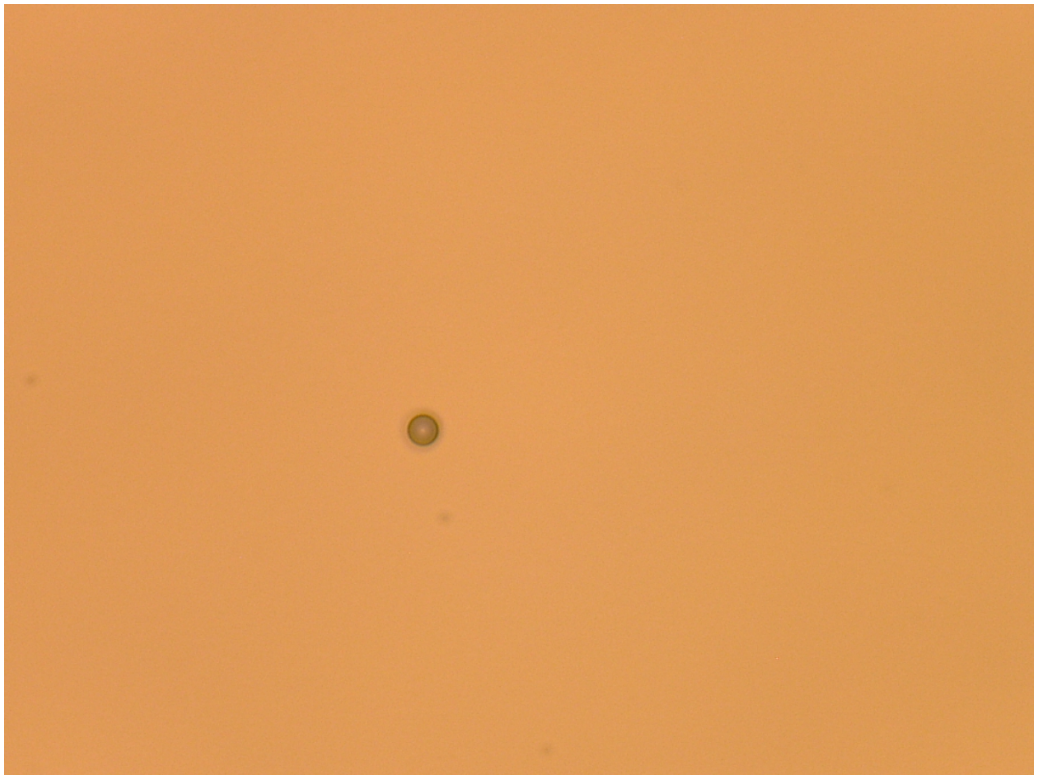

(a) 9,27 μm *diameter Janus particles under the optical microscope*

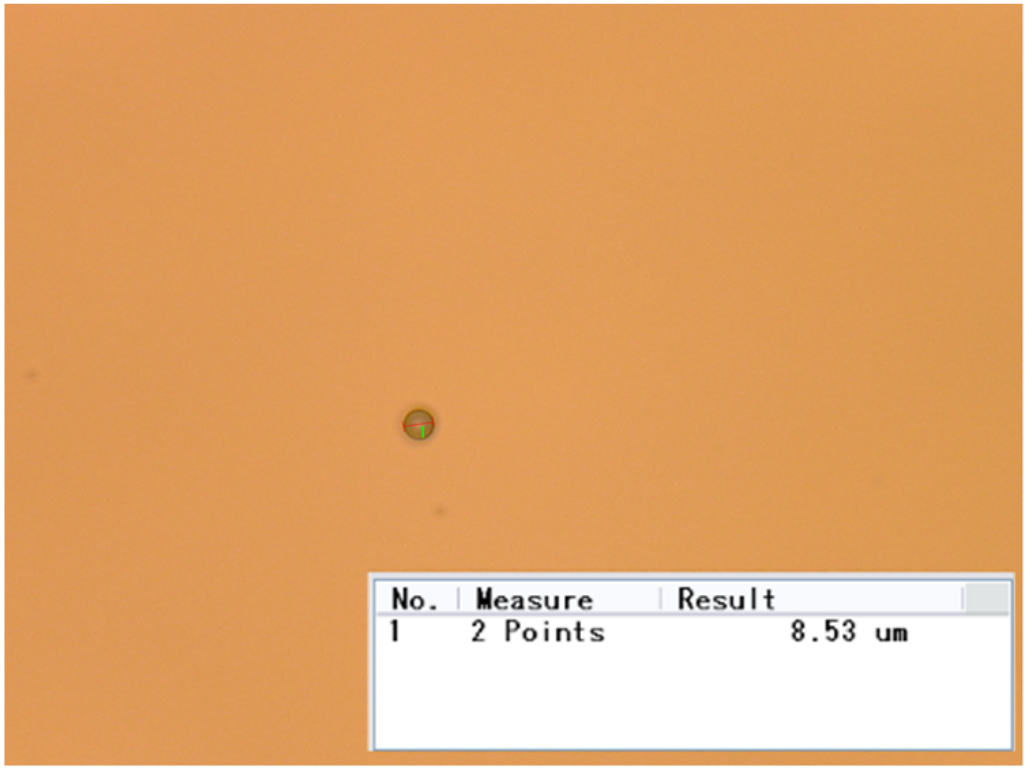

(b) *Janus particle measured diameter*

Figure 2.24: Janus particles under the optical microscope

(a) *Couple of Janus particles under the optical microscope*

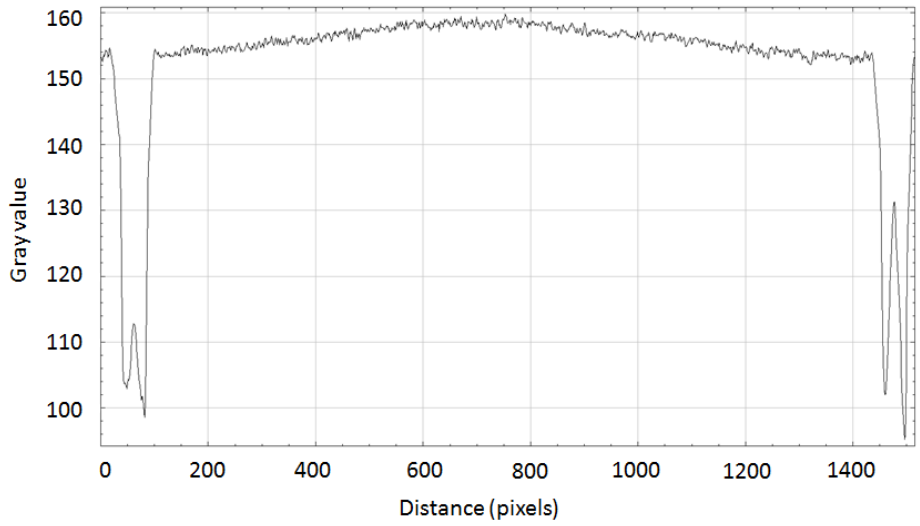

(b) *Couple of Janus particle brightness: the right one is brighter than the left one*

Figure 2.25: Couple of Janus particles and their brightness under the optical microscope

Summary of chapter 2

A GEC (*Gaseous Electronics Conference RF Reference Cell*) chamber was used to perform the experiments. The gas used is argon, ionized with a 13,6 MHz radio-frequency. As the upper electrode of the chamber is shaped as a ring and as the GEC chamber I used had been modified substituting the usual closed top cap with one having a 20 cm diameter hole, the single Janus particles suspended in the plasma sheath were observed and recorded with a top camera and a long working distance microscope connected to it. Two different experimental setups were used. When the particle was illuminated on its side with a laser light, it was possible to see the light reflected upward with the camera. Differently, when the white light of a torch coming from upwards was used to illuminate the particles, the particle shadow could be seen with the camera, as the metallic lower electrode reflects much more light than the particle (see figure 2.16). The Janus particles used are 9,27(10) μm diameter melamine-formaldehyde spheres produced by *Microparticles GmbH*, half covered with 10,0(1) nm of platinum with a PVD setup by Ali Kaouk in DLR, Cologne.

Chapter 3

Theoretical background

In this chapter I will describe the mechanisms of the various forces acting on the Janus particles I studied in the plasma environment. I will focus only on the forces than can cause Janus particles to be active, that means forces that can be considered as a "small engine" driving the particle out of equilibrium. During my analysis, I will also give an order of magnitude of their strength in order to have an idea of their relative importance. Demonstrating that a net resulting force is acting on Janus particles due to their peculiar structural asymmetry leads to the conclusion that, differently from pure MF particles, these ones are active particles because they are able to drive themselves far from equilibrium. Then I will particularly focus on the existing theory for active particle behaviour in overdamped environments in order to lay the foundations for a qualitative comparison between the outcome of my experiments and what is numerically predicted. Obviously, this comparison, which will be performed in section 5.1, can be just qualitative and not quantitative because the highly rarefied plasma used in my experiments provides the particles with an undamped environment.

3.1 Forces acting on the Janus Particles in Plasmas

The forces described in this section only act on Janus particles and not on pure MF particles, because of the asymmetric nature of Janus particles. These forces are hypotheses about what could make Janus particles active in the plasma environment I used during my experiments. In fact, the propulsion mechanisms that make them active in aqueous solutions are not present in the experimental environment used: chemical reactions, catalysis, and so on. However, it will be observed that local heating of particles and the effect of AC electric field of table 1.1 are propulsion mechanisms also hypothesized for my case.

The forces described in chapter 1 do not act as propulsion mechanisms, but they are just due to external fields. They are gravity and electrostatic force, whose effect is the

vertical confinement of the particle, and Epstein drag force which acts in the horizontal direction, that means in the xy plane.

In particular, the following forces can act on the Janus particle as "small engines" that would lead it out of equilibrium. These forces are:

1. Asymmetric ion drag force
2. Radiation pressure force
3. Photophoresis due to a temperature gradient on the particle surface, that is an asymmetric neutral drag force caused by a temperature difference
4. "Photophoresis" due to different accommodation coefficients, that is a neutral drag force caused by different accommodation coefficients of MF and platinum.

Is it very important to make a comment about the names of the forces that I use in the present work. In principle, apart from asymmetric ion drag, they are all "sides of the same coin": they are all kinds of photophoresis. One problem about nomenclature is that different authors use different names for the same thing. In principle, "photophoresis" is a force related to light, which is mainly laser light in my case as white light from the torch is not strong enough to be compared with it. Some authors distinguish between "direct photophoresis" and "inverse photophoresis". By the first one they mean the one that I call radiation pressure force and that can also be found in literature as "positive photophoresis". By the second one they mean the force resulting from a gradT established on the particle surface as a result of the action of a light beam and the subsequent asymmetric drag of the surrounding molecules that drives the particle in a specific direction. Sometimes and mainly in Russian scientific tradition it can also be found under the term "photothermophoresis" that is as much a self-explaining name as seldom used: for this reason I will not use this term in my work, but I will call it "photophoresis due to a gradT". It is important to note that even the term "thermophoresis" would not be adequate to describe the phenomenon because it usually refers to a temperature difference in the gas molecules themselves and not on the particle surface. This term is anyway used sometimes in literature (see Ref. [3]). It can also happen for particles with a homogeneous surface that the side of the particle which does not face the light source becomes hotter than the one facing it for reasons due to refraction and reflection and the particle moves towards the light source. This is again a kind of photophoresis due to a gradT and this can happen to pure MF particles, but it is called "negative photophoresis" by the same authors who refer to radiation pressure as "positive photophoresis". For the sake of clarity, I will use the term "negative photophoresis" for this case in the present work. One last consideration about it: "negative photophoresis" is a particular case of "indirect photophoresis", which I call "photophoresis due to a gradT" and which can cause a motion in every direction, depending on the gradT on the particle surface. "Negative photophoresis", on the other side, causes

a motion in the opposite direction with respect to the light beam hitting the particle. As it will be explained soon, for Janus particles the platinum covering plays an important role and this originates a generic "inverse photophoresis" due to a gradT. It must be kept in mind that in a plasma environment a gradT can also be present in the absence of laser irradiation because of the heating up of the particle due to the presence of the plasma itself and due to different emittance coefficients of the two materials. "Photophoresis due to a difference in accommodation coefficients" is also present in the absence of laser irradiation in plasma environment. In order for it to be present, in fact, the particle must be hotter than the surrounding environment, but the plasma is a heat source itself. This means that "photophoresis" due to a difference in accommodation coefficients acts both in the cases of laser light on and off. It becomes stronger as the difference between the plasma temperature and the particle temperature becomes larger. Photophoresis due to a gradT will depend even more strongly on the laser power because laser light is a strong heat source for the particle. I will use quotation marks to refer to "photophoresis" due to a difference in accommodation coefficients because in the plasma environment the presence of the light beam is not necessary in order to generate this force. I will go on using the term "photophoresis" for the sake of coherence with the referenced papers.

The forces acting on active particles cause the propulsion mechanisms that characterize them [5]. In particular, two kinds of propulsion can be distinguished:

- Propulsion mechanism powered by local energy conversion
- Propulsion mechanism due to external fields.

A classical example of the first one is phoretic transport due to some gradient on the particle surface, i.e. chemical, electrostatic or thermal gradient. If a particle generates its own local gradient, a self-phoretic motion can take place. This propulsion mechanism requires some type of asymmetry in the particle properties. Self-propulsion can otherwise emerge in the case of spontaneous symmetry breaking without the particle being asymmetric itself.

Propulsion due to external fields is based on a swimming motion achieved by the periodic non-reciprocal geometrical deformation or reorientation of the particle body in the external field. Also application of alternating electric fields on asymmetric particles has been predicted to lead to propulsion.

In some cases, a combination of both these propulsion mechanisms is possible.

3.1.1 Asymmetric ion drag force

By this name I mean the net force acting on the Janus particle in the xy plane due to an asymmetry of the ion flow on the particle caused by the different materials composing its surface. The most negatively charged surface attracts more ions and this means that more momentum is transferred to it. This mechanism transforms a vertical flow of ions into a

force acting on the horizontal plane and it results in phoretic transport. Asymmetric ion drag is a propulsion mechanism due to local energy conversion.

The plasma I worked with is collisionless because:

$$\begin{cases} \frac{r_p}{l} << 1 \qquad \text{for both } l_e \text{ and } l_i \\ \\ \frac{r_p}{\lambda_{d,e}} << 1 \end{cases} \tag{3.1}$$

where l_e and l_i are the electron and ion mean free paths M.F.P. in the plasma and $\lambda_{d,e}$ is the electron Debye length:

$$\lambda_{d,e} = \sqrt{\frac{\varepsilon_0 k_b T_e}{n_e e^2}} \tag{3.2}$$

and with ε_0 the vacuum permittivity, $n_e \simeq 2 \times 10^9\,\mathrm{cm}^{-3} = 2 \times 10^{15}\,\mathrm{m}^{-3}$ and $K_b T_e \simeq 2{,}5\,\mathrm{eV} = 4 \times 10^{-19}\,\mathrm{J}$:

$$\lambda_{d,e} \simeq 2{,}6 \times 10^{-4}\,\mathrm{m} = 260\,\mu\mathrm{m}. \tag{3.3}$$

This means that the first condition of equation 3.1 is verified.

The minimum of l_e and l_i is the last one because the cross section for the ions is much larger than the one for electrons and a good estimation for it is the M.F.P. λ computed in section 3.1.4 as $\lambda \simeq 0{,}1\,\mathrm{cm} = 1\,\mathrm{mm}$. Even the second condition of equation 3.1 is verified.

The Janus particle cannot be thought as an electric dipole because the problem of the charge distribution on dust particles is not trivial at all. Ref. [7] furnishes an example on how much the charge distribution on a dust particle in a plasma can be complicated. The electric charge on the dielectric side of the Janus particle will be strongly anisotropic and it will show peaks. The charge corresponding to these peaks can be even much higher than the particle charge on the metallic side [8].

A rough estimation of the strenght of this force can be done. First, as it has been explained in chapter 1, there are two main contributions to this force: collection of ions on the particle surface and deflection of them due to **E** generated by the charge distribution on the particle. I am supposing in the following that just the first contribution, which is the strongest, is not negligible because the non-homogeneity of the particle charge is no longer important when far enough from the particle. An upper estimate of this force could be done considering just the first contribution and under the hypothesis that half of the JP collects ions and half does not:

$$F_{\text{asymm. ion drag}} \sim qJ \tag{3.4}$$

where q is the momentum of ions, that is:

$$q = m_i v_{th,ion}$$

where m_i is the ion mass and $v_{th,ion}$ is the thermal velocity of ions, and J is the flow of ions, that is:

$$J \sim \pi a^2 n_i u (1 + \frac{e\varphi_s}{m_i u^2})$$

where a is the particle radius, n_i the ion density, u the ion velocity, e the elementary charge and φ_s the surface potential.

But:

$$J \sim \pi a^2 n_i u$$

Because:

$$\frac{e\varphi_s}{mu^2} \sim 1$$

Setting:

- $m_i = m_{Ar} = 39{,}95\,\mathrm{u} = 6{,}6 \times 10^{-26}\,\mathrm{kg}$
- $v_{th,ion} = \sqrt{\frac{k_b T}{m_i}}$, with $T = T_i \sim T_n = 296\,\mathrm{K}$
- $a = 4{,}635\,\mu\mathrm{m}$
- $n_i \sim 5 \times 10^8\,\mathrm{cm}^{-3}$ *internal reference*
- $u \sim \sqrt{\frac{k_b T_e}{m_i}}$, with $k_b T_e \sim 3\,\mathrm{eV}$ *internal reference*

then:

$$q = 1{,}7 \times 10^{-23}\,\mathrm{kg\,m\,s^{-1}}$$

$$J \simeq 9 \times 10^3\,\mathrm{s}^{-1}$$

so:

$$F_{\text{asymm. ion drag}} \simeq 1{,}5 \times 10^{-19}\,\mathrm{N} \tag{3.5}$$

This situation never occurs, so this result is just an upper estimate. In particular, the situations closer to this description, even if still not corresponding to it, are (a) and (b) of figure 3.10.

Note that this result is an upper estimate for the net force acting on the particle due to asymmetric ion drag, while the result for the photophoresis due a temperature gradient is a lower estimate of that force: we considered in fact null thermal contact resistance between platinum and MF. It is then evident that the contribution of photophoresis due to a ΔT is much more important than the one due to asymmetric ion drag.

3.1.2 Radiation pressure force

The radiation pressure force is exerted on a particle if it is exposed to a beam of light. Radiation pressure is the momentum per unit area per unit time transferred from photons to a surface. Radiation pressure force is then radiation pressure multiplied by the surface

the force is acting on. If a beam of photons strikes the particle, some photons will be reflected and others will be transmitted or absorbed. All these three processes contribute to the radiation pressure force. An example of radiation pressure force acting are the tails of comets: they always point away from the Sun because of the radiation pressure exerted by sinlight. In laboratory experiments, this force is significant only for very light particles and intense light [9].

This force is a propulsion mechanism of the Janus particle not powered by local energy conversion, but it is the only mechanism based on external field action. In fact, as it will be treated in detail, the Janus particle is most probably spinning and the radiation pressure force acts in different ways on the particle depending on which face turns to the laser beam. This means reorientation of the particle body and actually alternating force due to the laser light.

Let us try to estimate the different values of this force depending on which side faces the laser. If we suppose for a moment that the Pt-layer has a reflectance $\varrho = 1$ and that the MF side has a reflectance $\varrho = 0$, then this force can be double when the Pt-layer is facing the laser. In particular, the value of this force changes with the same frequency as the particle rotates at.

Now let us obtain a rough estimation of the order of magnitude of this force:

$$F_{\text{laser}} = q\frac{n_1 \pi r_p^2 q_s{}''}{c} \tag{3.6}$$

with:

$$q_s{}'' = \frac{P}{Lw} \tag{3.7}$$

where:

- q is a dimensionless coefficient that is determined by the reflection, transmission and absorption of photons by the particle. It was measured for MF particles and the value of $q = 0.94 \pm 0.11$ is reported in Ref. [9]. Let us assume that for platinum $q \sim 2$ in the hypothesis that all photons are reflected and in the approximation that the platinum layer is a flat disk at normal incidence [9].
- n_1 is the refractive index of the medium around the particle, that is ~ 1
- r_p is the particle radius
- c is the speed of light
- P is the laser power
- L is the length of the laser plane at the particle position. In particular, I measured $l = 22{,}5\,\text{cm}$ for the distance between the laser source and the centre of the chamber, where the particle is. The angular size of the laser sheet is $\vartheta = 25°$, that means (see figure 3.1) $L = 10\,\text{cm}$

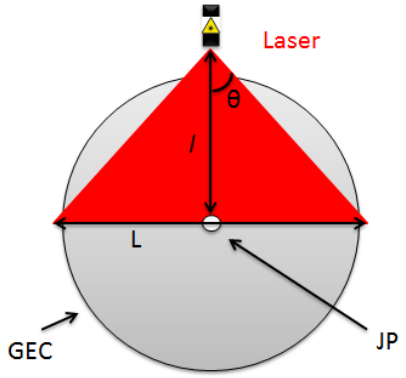

Figure 3.1: Geometry related to the laser beam

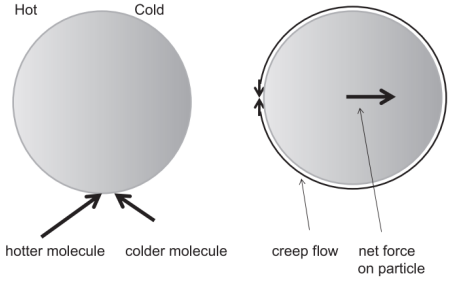

Figure 3.2: Photophoresis due to a temperature gradient on the particle [6]

- w is its width, that is the FWHM of the laser sheet $\sim 170\,\mu$m

$$\text{For} P = 14\,\text{mW}: \begin{cases} F_{\text{laser, MF}} = 1{,}7 \times 10^{-16}\,\text{N} \\ F_{\text{laser, Pt}} = 3{,}8 \times 10^{-16}\,\text{N} \end{cases} \tag{3.8}$$

$$\text{For} P = 99\,\text{mW}: \begin{cases} F_{\text{laser, MF}} = 1{,}2 \times 10^{-15}\,\text{N} \\ F_{\text{laser, Pt}} = 2{,}6 \times 10^{-15}\,\text{N} \end{cases} \tag{3.9}$$

In conclusion, the result is that for the fixed laser power radiation pressure force in the case of platinum facing the laser beam is approximately twice as large as in the case of MF facing the light.

3.1.3 Photophoresis due to a temperature gradient

First, it must be specified that the surface temperature of the particle, which has nothing to do with its kinetic temperature, has been demonstrated to be higher than the surrounding gas temperature (see Ref. [10], [11], [12], [13]). For this reason, it is clear that the neutral

flow cannot cool the particle down to the gas temperature, that is room temperature in my case. In particular, the gas pressure in my experiments is even lower than the minimum one set in these references and, since when decreasing the pressure the particle temperature increases compared to the one of the neutrals, it is even more likely that my particles are not in thermal equilibrium with the neutrals. This ΔT between the particle and its surroundings is probably due to low pressure and to the inefficient energy exchange during the collisions of the neutrals with the particle surface. This also means that when a non-zero gradT is present on the particle, then it mostly will not be modified by collisions with the plasma atoms.

The mechanism which causes this force is the following. Due to accommodation, the gas molecules colliding on the warmer side of the particle leave the surface faster, resulting in a force which is directed from the warmer to colder side of the particle. If the direction of "positive" and "negative photophoreses" just depend on the direction of the laser beam and not on the particle orientation, the direction of photophoresis due to gradT acting on the Janus particles that I used depends just on the particle orientation. For this reason, differently from "positive" and "negative photophoreses", it cannot be called a "space-fixed" force [6].

In the present case of weakly-ionized plasma environment the molecules causing the force are the plasma neutrals, as the ionization fraction is quite low, around $10^{-6} \div 10^{-7}$.

It is very important to keep in mind that this force cannot be completely separated from the "photophoresis" due to the difference in the accommodation coefficients because the temperature gradient is in this case mainly due to the different materials which obviously have different accommodation coefficients. This is the reason why these two mechanisms always act together. For sake of simplicity they will be considered separately, despite they act together. It is hard to predict how these forces will work separately, but it is even harder when they combine. In section 3.1.5 this problem will be approached, but for now the forces will be considered separately.

This force is caused by a thermal gradient on the particle and results in phoretic transport. Photophoresis due a gradT is, moreover, a propulsion mechanism due to local energy conversion.

This photophoresis is seldom acting on pure MF particles, just when they are deformed: see Ref. [1].

This force should become stronger as the laser power increases, because it is the main heat source. I think that it is directed from MF to platinum, because MF should heat up more when the 660 nm laser is on because of its higher absorption coefficient at this wavelength. In figure 3.3, platinum and MF absorption spectra in the visible range are shown. See also Ref. [35] and Ref. [36] for what concerns platinum nanoparticle absorption spectrum. But this is just an educated guess of my own, because it cuold be that the platinum deposited on my MF particles has a particularly low absorption as it seems quite opaque; but the absorption cannot be measured and for this reason I will use in the

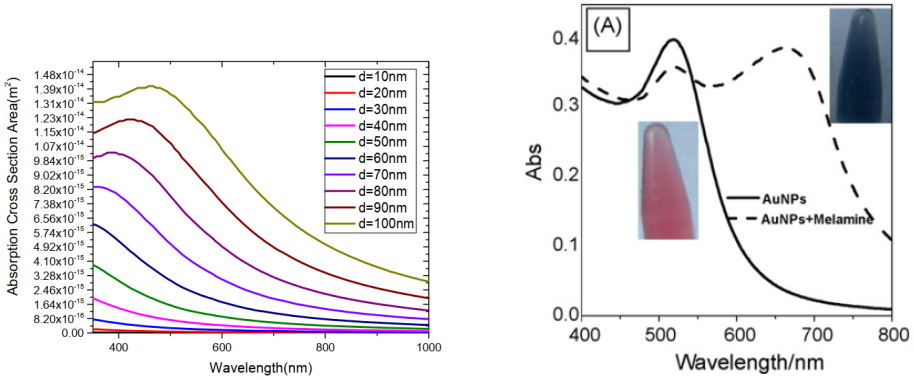

(a) *Absorption cross section area for 10 sizes of platinum nanospheres of varying diameter. In my case, platinum layer width is* 10 nm *and the black line corresponding to* 10 nm *diameter particles is the lowest and it is really negligible. Ref:The Simulation of the Optical Characteristics of Platinum and Platinum/Silica Nanoparticles*

(b) *Absorption spectra of Au nanoparticles in the absence (solid line) and in presence of melamine (dashed line): MF adds a peak between about* 600 *and* 700 nm. *Reference: Visual detection of Melamine in milk products by label-free gold nanoparticles*

Figure 3.3: Platinum nanoparticles and MF absorption spectra

present work the values present in literature. In this case, photophoresis would go from platinum to MF. The main point is that a temperature difference establishes on the Janus particle surface.

Nevertheless, actually there will also be a temperature difference when the laser is off because the idea of having the same temperature all over the surface of a particle is not realistic even when the surface is made of one single material, then in case of Janus particle it will be even less likely to happen. This means that "photophoresis" due to $\Delta\alpha$ and photophoresis due to gradT are always acting and they are always acting together.

Let us proceed with an estimation of the order of magnitude of this third force. In a free molecular regime, in a gas (not ionized) and in the case of a surface with homogeneous accommodation coefficient but a temperature gradient on it:

$$F_{\Delta T} = \frac{\pi}{24}\alpha d^2 p \frac{\Delta T}{T} \tag{3.10}$$

where α is the accommodation coefficient, d is the particle diameter, p is the gas pressure, T is the average particle temperature, ΔT is the temperature difference between the particle two faces and gradT is the temperature gradient on the particle surface.

The values of the parameters in the formula are the following:

- $\alpha = 0.55$ is the accommodation coefficient in argon in low pressure range (0 to 100 mTorr), measured for a Pt surface taking all possible precautions to ensure clean surfaces [14]. This is the only value that I have, because I do not have a value for α

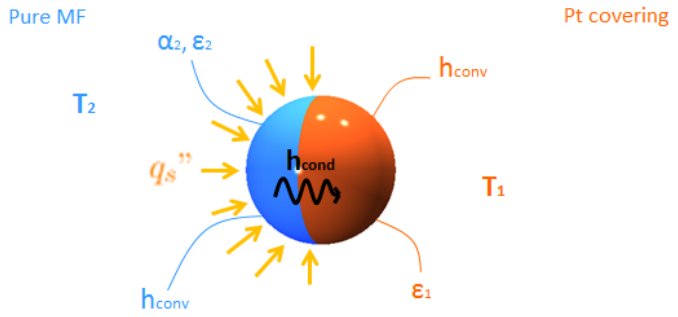

Figure 3.4: Sketch of the energy balance equation for the two sides of the Janus particle in case of semi-lumped parameters approach

for MF and I do not have any dependence on the surface temperature.

- $d = 9{,}27\,\mu$m.
- $p = 1{,}33\,$Pa as it is the mainly used plasma pressure.
- ΔT has been calculated as follows: considering that talking about convection in a classical way is not a precise approach because argon is ionized - in fact it is a plasma and not just a gas - and it is so rarefied, adding that the particle spin is unknown and would influence the heat equation in time and space, then trying to estimate a gradT in a sophisticated way having a not negligible uncertainty on all parameters is completely pointless. For this reason, I used a semi-lumped parameter model instead of a distributed parameters one, as a more precise one would make little sense for such a small particle. I also considered the system in steady state. Calling T_1 and T_2 the particle platinum-covered half and the non covered one temperatures, in the hypothesis that one value of temperature for each half gives a sufficiently precise description of the physical situation, a rough estimation of ΔT, that is $T_2 - T_1$ can be done using an iterative procedure in order to find T_1 and T_2 from the energy balance on the two particle sides.

  The energy balance for the non-covered pure MF side is:

$$\alpha_2 \overline{q_s"} - h_{\text{conv}}(T_2 - T_{\text{Ar}}) - \varepsilon_2 \sigma (T_2^4 - T_{\text{wall}}^4) - h_{\text{cond}}(T_2 - T_1) = 0 \tag{3.11}$$

  The one for the platinum-covered one is:

$$h_{\text{cond}}(T_2 - T_1) - h_{\text{conv}}(T_1 - T_{\text{Ar}}) - \varepsilon_1 \sigma (T_1^4 - T_{\text{wall}}^4) = 0 \tag{3.12}$$

  See figure 3.4 for equation parameters.

  In particular:

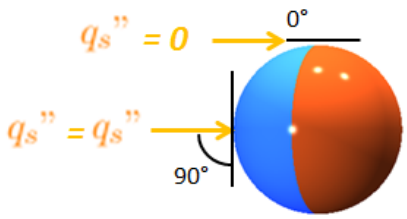

Figure 3.5: Incident laser power as function of the incidence angle

- T_1 and T_2 are the unknown variables
- $T_{\mathrm{Ar}} = T_{\mathrm{wall}} = T_{\mathrm{amb}} = 22{,}9\,^{\circ}\mathrm{C} \simeq 296\,\mathrm{K}$ are the gas and the wall temperatures
- α_1 and α_2 are the values of the absorption for the two surfaces
- $\overline{q_s"}$ is the average laser power per unit surface. In particular, this is because when the laser impacts on the particle's surface with an incidence angle of 90° the incident laser power is simply q_s", but when the angle is 0°, then the incident power is null: see figure 3.5. $\overline{q_s"}$ was calculated as:

$$\overline{q_s"} = \frac{q_s"}{4\pi} \int_{-\pi/2}^{\pi/2} \cos\vartheta \, d\vartheta \tag{3.13}$$

that gives:

$$\overline{q_s"} = \frac{q_s"}{2\pi} \tag{3.14}$$

with $q_s" = 1{,}98 \times 10^3\,\mathrm{W\,m^{-2}}$, so: $\overline{q_s"} = 3{,}2 \times 10^2\,\mathrm{W\,m^{-2}}$.

- $\alpha_2 = 0.4$ is MF absorbance at 660 nm, which is the illumination laser wavelength, while $\alpha_1 = 0$ is the estimated value for platinum.
- ε_1 and ε_2 are platinum and MF emissivities, whose values are respectively $\varepsilon_1 = 0.075$ [15] and $\varepsilon_2 = 0.95$ [16]
- σ is the Stephan-Boltzmann constant $5{,}670\,373 \times 10^{-8}\,\mathrm{W\,m^{-2}\,K^{-4}}$
- h_{cond} is the conductive coefficient and is given by:

$$h_{\mathrm{cond}} = \frac{k_{\mathrm{MF}}}{L_c} \tag{3.15}$$

where k_{MF} is the MF heat conductivity $0{,}5\,\mathrm{W\,m^{-1}\,K^{-1}}$ and L_c is the characteristic length of the system:

$$L_c = \frac{V}{A} = \frac{d}{6}, \tag{3.16}$$

where V is the particle volume, A its total surface and d its diameter. Performing

the calculations, I found:

$$L_c = 1{,}5 \times 10^{-6}\,\mathrm{m} \tag{3.17}$$

and so:

$$h_{\mathrm{cond}} = 3{,}3 \times 10^{5}\,\mathrm{W\,m^{-2}\,K^{-1}} \tag{3.18}$$

– h_{conv} can be estimated by solving the following system of equations:

$$\begin{cases} Nu = 2 \qquad for \qquad v_f \to 0 \\ \\ Nu = \frac{h_{\mathrm{conv}} d}{k_{\mathrm{plasma}}} \end{cases} \tag{3.19}$$

with Nu the Nusselt number, k_{plasma} the plasma heat conductivity and v_f the fluid velocity. $v_f \to 0$ because the particle is rotating very slowly (see below) and because the plasma is very rarefied. Considering that the plasma is a weakly ionized gas, k_{plasma} is calculated treating the plasma as a gas using the theory of thermal conductivity for monoatomic gases [17] as:

$$k_{\mathrm{plasma}} = k_{\mathrm{Ar}} = 2{,}63 \times 10^{-23} \frac{\sqrt{T_{\mathrm{Ar}}/M'}}{\sigma^2 \Omega_v} \tag{3.20}$$

with T_{Ar} in K, M', which is the molecular weight, in $\mathrm{kg\,mol^{-1}}$ and σ, which is the molecule characteristic dimension d, in m. Ω_v is the dimensionless collision integral:

$$\Omega_v = A(T^*)^{-B} + Ce^{-DT^*} + Ee^{-FT^*}. \tag{3.21}$$

In particular, $A = 1.16145$, $B = 0.14874$, $C = 0.52487$, $D = 0.77320$, $E = 2.16178$, $F = 2.43787$ and $T^* = \frac{K_b T}{\varepsilon}$. ε is the minimum of the pair potential energy and for Argon $\varepsilon/K_b = 142{,}1\,\mathrm{K}$ from Ref. [18]. In particular, equation 3.21 is valid only if $0.3 \leq T^* \leq 100$ and in my case $T^* = 2.1$.

Making the calculations:

$$\Omega_v = 1.16 \tag{3.22}$$

and, with $T_{\mathrm{Ar}} = 296\,\mathrm{K}$, $\sigma = d = 9{,}27\,\mu\mathrm{m}$ and $M' = 3{,}99 \times 10^{-2}\,\mathrm{kg\,mol^{-1}}$, then:

$$k_{\mathrm{plasma}} = k_{\mathrm{Ar}} = 2{,}3 \times 10^{-11}\,\mathrm{W\,m^{-1}\,K^{-1}}. \tag{3.23}$$

Using equation 3.19, it turns out that

$$h_{\mathrm{conv}} = \frac{2k_{\mathrm{plasma}}}{d} \tag{3.24}$$

and the result is:

$$h_{\text{conv}} = 0{,}5\,\text{W}\,\text{m}^{-2}\,\text{K}^{-1} \tag{3.25}$$

The result for T_1 and T_2 calculated with this semi-lumped parameter approach is:

$$T_1 = 308{,}783\,78\,\text{K} \tag{3.26}$$

and

$$T_2 = 308{,}783\,82\,\text{K}. \tag{3.27}$$

ΔT is then about $4 \times 10^{-5}\,\text{K}$.

The platinum coating in this procedure was considered just in concern with its emittance and its absorption which was approximated as null. It could be actually that platinum, which does not absorb the laser light, is colder than MF, more than estimated by the computed difference. It just depends on thermal resistivity of the contact between the two materials, that is impossible to estimate. If platinum absorption was higher than what estimated, then the temperature difference would be reversed and it would depend again on the unknown thermal contact between platinum and MF.

Another way of estimating gradT was developed by Rubinowitz (1920):

$$\text{gradT} = \frac{\overline{\text{q}_\text{s}"}}{2(\text{k}_\text{MF} + \text{k}_\text{plasma})} \tag{3.28}$$

that gives $\Delta T = d\,\text{gradT} = 3 \times 10^{-3}\,\text{K}$.

If the method that I used does not take into consideration the thermal resistance of the contact between platinum and MF, this method does not even consider the presence of a second material on the particle surface. For this reason in the following I will use my result and not this oversimplified one.

- $T = 308{,}7838\,\text{K}$, calculated as the average value between my values T_1 and T_2.

The result for the absolute value of the force using the parameters explained and computed above is:

$$F_{\Delta T,\text{max}} \simeq 1{,}1 \times 10^{-18}\,\text{N}. \tag{3.29}$$

This result is a lower estimation of the force because I considered null thermal resistance of the contact between MF and platinum. The actual ΔT is for sure higher that the one estimated. In particular, considering all the uncertainties about the various parameters, it is also possible that platinum becomes hotter than MF, it depends on the absorption coefficients.

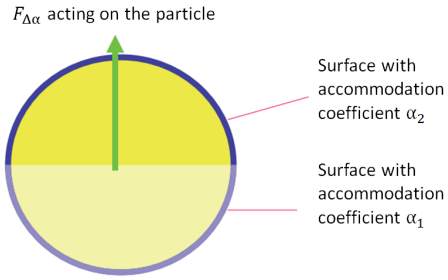

Figure 3.6: "Photophoresis" due to different accommodation coefficients on the particle

3.1.4 "Photophoresis" due to different accommodation coefficients

Let us consider a particle in a gas, whose surface temperature is T_s higher than the temperature T_0 of the surrounding gas. A gas molecule hitting the particle surface can acquire some of the thermal energy of the hot particle and be reflected with a velocity corresponding to a temperature T, which is obviously higher than T_0. Tha accommodation coefficient is defined as:

$$\alpha = \frac{T - T_0}{T_s - T_0}. \tag{3.30}$$

$\alpha = 0$ is case of no accommodation: $T = T_0$ and $\alpha = 1$ in case of full accommodation: $T = T_s$. The value of α depends on both the material forming the particles as well as its surface structure and the gas.

At the locations of higher accommodation coefficient, the molecules are reflected with a higher average velocity, resulting in a thrust on the particle from the location of higher to the ones or lower accommodation coefficient [6]. This force actually requests a heat source in order to be present and the plasma itself, even when laser is off, provides heat [10].

This force is caused by a gradient of physical properties of the particle on its surface and results in phoretic transport. "Photophoresis" due a $\Delta\alpha$ is, moreover, a propulsion mechanism due to local energy conversion.

This force is always present and is slightly depend on the laser power: it becomes larger as the difference between T_s and T_0 grows. Anyway, photophoresis due a temperature gradient should depend more strongly on the laser power. I have no idea about the direction of it because I don't have reliable data regarding accommodation coefficients. I just have data on α in argon in low pressure region (0 to 100 mTorr), measured for a Pt surface taking all possible precautions to ensure clean surfaces [14], which is $\alpha = 0.55$. In order to perform a rough estimation of the force, MF accommodation coefficient will be set to be null. In general accommodation coefficients of metals are higher than accommodation coefficients of non metals, so this should not be a too wrong guess about the coefficients. Of course, the resulting force estimated with these values is a higher estimate of the force as this $\Delta\alpha$ is the maximum possible.

In order to have an idea of this mechanism strength, a rough estimation can be done. In a gas, for a surface characterized by homogeneous temperature but two different accommodation coefficients:

$$F_{\Delta\alpha} = \frac{1}{2\bar{c}} \frac{\gamma - 1}{\gamma + 1} \frac{1}{1 + (p/p^*)^2} \frac{\Delta\alpha}{\bar{\alpha}} H \tag{3.31}$$

with $\bar{c}$ = mean molecular velocity, $\gamma = c_p \ / \ c_v$, p = gas pressure, p^* is a reference pressure, $\Delta\ \alpha = \alpha_2 - \alpha_1$, $\bar{\alpha} = \frac{1}{2}\ (\alpha_1 + \alpha_2)$, with α_1 and α_2 = accommodation coefficients of the two surfaces, and H = net energy flux transferred by the gas molecules.

However, this formula hides all the difficulty of the problem in that H factor. In fact, it can be found with an energy balance on the collision mechanism of neutrals with the particle surface. The problem is that this mechanism is not known and it makes the formula impossible to use.

For this reason, the method presented in next section has been used.

3.1.5 Photophoretic mechanisms acting together

Let us start considering the very general case of figure 3.4. The net force acting on the Janus particle of the figure is due to the different pressures exerted on it by the gas molecules. When they arrive on the surface they have approximately the same temperature as the surrounding gas and for this reason the pressure exerted by the incoming molecules on the particle surfaces is the same. The difference is due to the energy of the neutrals leaving the surface, that can be caused either by a temperature difference between the surfaces or by a difference in their accommodation coefficients. Let us start from the general case in which both the surfaces have different temperatures as well as different accommodation coefficients.

Calling:

- n_0 the gas neutral number density
- T_0 the gas temperature
- T_1 the platinum-covered side temperature
- α_1 the platinum accommodation coefficient
- T_2 the pure MF side temperature
- α_2 the MF accommodation coefficient
- r_p the particle radius,

then each force can be computed as the gas pressure multiplied by the area of the particle and then the two forces can be subtracted in order the find the net one. The

particle section πr_p^2 has been used as area, as the only interesting component of the force is the one on the xy plane. One of the interpretations of the accommodation coefficient is:

$$\alpha = \frac{\text{number of molecules completely accommodated}}{\text{total number of molecules leaving the surface}}.$$

Let us assume that all the neutrals hitting the surface leave it, that the temperature of a completely accommodated molecule is the same temperature as the particle surface (T_1 or T_2) and that the temperature of a non-accommodated one is the same as the gas (T_0). The completely accommodated molecules number density is αn_0 and the one of non-accommodated molecules is $(1-\alpha)n_0$. Then:

$$\begin{aligned} F_{\text{neutrals}} &= \pi r_p^2 k_b n_0 \Big(\alpha_1 T_1 + (1-\alpha_1)T_0 - \alpha_2 T_2 - (1-\alpha_2)T_0\Big) \\ &= \pi r_p^2 k_b n_0 T_0 \Big(\alpha_1\left(\frac{T_1}{T_0} - 1\right) - \alpha_2\left(\frac{T_2}{T_0} - 1\right)\Big) \end{aligned} \tag{3.32}$$

I called the net force *neutrals* because it is the total force due to the neutrals, while asymmetric ion drag is obviously caused by ions and radiation pressure is due to the laser.

Now, let us consider the three different cases:

1. $T_1 = T_2 = T$. This leads to:

$$F_{\text{neutrals}} = F_{\Delta\alpha} = |\pi r_p^2 k_b n_0 T_0 \left(\frac{T}{T_0} - 1\right)\Big(\alpha_1 - \alpha_2\Big)|, \tag{3.33}$$

   which actually means that:

$$F_{\Delta\alpha} \neq 0 \iff T \neq T_0,$$

   which is theoretically predicted for "photophoresis" due to $\Delta\alpha$: it can exist only in the presence of a source of heat.

   This is only the absolute value of the force because its direction goes from the locations of higher to lower accommodation. Anyway, without the module the obtained force goes from 1 to 2 if positive and viceversa if negative.

   $T_1 = T_2 = T$ when the laser power is off. The code I already used to compute iteratively T_1 and T_2 in section 3.1.3 obviously gives $T_1 = T_2 = T_0$ for q_s" $= 0$. However in literature it is known that plasma itself constitutes a source of heat for the particle, even though the reasons for this are not clear yet. Therefore, let us consider $T = 300\,\text{K}$, which is really just a few degrees over $T_0 = 296\,\text{K}$. This is a really rough estimation, as in this case T should be higher since T_1 and T_2 should have been higher in section 3.1.3. However, the heating mechanisms caused by plasma are not known yet and so I chose the value $T = 300\,\text{K}$ as it is higher than

T_0, but smaller than T_1 and T_2 when laser is on.

The parameters are:

- $T = 300\,\mathrm{K}$
- $r_p = 4{,}635\,\mu\mathrm{m}$
- $n_0 = \frac{p}{k_b T_0}$
- $T_0 = 296\,\mathrm{K}$
- $\alpha_1 = 0.55$ as explained in section 3.1.4
- $\alpha_2 = 0$: this is because the accommodation coefficient for MF in argon is unknown. Moreover, non metals usually have an accommodation coefficient lower than metals. The result will be an overestimation of the force because $\alpha_2 = 0$ gives the maximum possible $\Delta\alpha$. As the actual value of α_2 cannot be too different from this one, the estimation will anyway result close to the actual value of the absolute value of the force.

The result is:

- $F_{\Delta\alpha} = 6{,}7 \times 10^{-13}\,\mathrm{N}$ for $p = 1{,}3\,\mathrm{Pa}$
- $F_{\Delta\alpha} = 2{,}0 \times 10^{-12}\,\mathrm{N}$ for $p = 4\,\mathrm{Pa}$
- $F_{\Delta\alpha} = 5{,}0 \times 10^{-12}\,\mathrm{N}$ for $p = 10\,\mathrm{Pa}$
- $F_{\Delta\alpha} = 6{,}7 \times 10^{-12}\,\mathrm{N}$ for $p = 13{,}3\,\mathrm{Pa}$

The fact that the result is positive means that the force goes from 1 to 2, that is from the platinum-covered side to the pure MF side, that is from locations of higher to lower accommodation, as theoretically predicted.

Laser irradiation will make this force even stronger because it heats particle up and $F_{\mathrm{neutrals}} \propto T$. The precise calculation of the combined effect of the two will be performed in the following.

This result shows that this force is the strongest one: in fact, even if this result is an upper estimation, it is orders of magnitude higher than the results for all the other forces.

2. $\alpha_1 = \alpha_2 = \alpha$. This is the case when $F_{\Delta\alpha} = 0$ and only $F_{\Delta T}$ is present. The equation becomes:

$$F_{\mathrm{neutrals}} = F_{\Delta T} = |\pi r_p^2 k_b n_0 T_0 \alpha \left(\frac{T_1 - T_2}{T_0} \right)|. \tag{3.34}$$

If $T_1 = T_2 = T$, then $F_{\Delta T} = 0$, as it should be.

Performing the calculations using:

- $T_1 = 308{,}783\,78\,\mathrm{K}$ and $T_2 = 308{,}783\,82\,\mathrm{K}$, which are the temperatures out of my code found in section 3.1.3 and which lead to $\Delta T = 4 \times 10^{-5}\,\mathrm{K}$

- $\alpha = 0.55$
- $r_p = 4{,}635\,\mu\text{m}$
- $n_0 = \frac{p}{k_b T_0}$
- $T_0 = 296\,\text{K}$
- $p = 1{,}33\,\text{Pa}$,

the result is:

$$F_{\Delta T} = 6{,}7 \times 10^{-18}\,\text{N}. \tag{3.35}$$

The direction of this force goes from the location of higher to lower temperature. This is the reason why the fact that the outcome of equation 3.34 is negative constitutes another validation of the correctness of the proposed formula 3.32: the negative result means in fact that the force goes from 2 to 1. The value obtained with equation 3.34 is only the absolute value of the force.

This calculations have given a second estimate of photophoresis due the temperature gradient of the particle, which has actually always been treated as a ΔT because of the semi-lumped parameter approach. The obtained value are actually similar, mutually compatible.

With T_1 and T_2 used, $F_{\Delta T} << F_{\Delta \alpha}$. If this was true, the main contribution to the overall photophoretic mechanism would be the one of $F_{\Delta \alpha}$.

3. General case in which both $F_{\Delta \alpha}$ and $F_{\Delta T}$ are acting together. The main contribution will probably be due to $F_{\Delta \alpha}$ both in terms of module and the force direction. Anyway, considering the complete model and performing the calculations leads to a more complete description and understanding of the problem.

   Using in equation 3.32 the following values:

   - $T_1 = 308{,}783\,78\,\text{K}$
   - $T_2 = 308{,}783\,82\,\text{K}$
   - $\alpha_1 = 0.55$
   - $\alpha_2 = 0$
   - $r_p = 4{,}635\,\mu\text{m}$
   - $n_0 = \frac{p}{k_b T_0}$
   - $T_0 = 296\,\text{K}$
   - $p = 1{,}33\,\text{Pa}$,

the result is:

$$F_{\text{neutrals}} = 2{,}1 \times 10^{-12}\,\text{N} \tag{3.36}$$

As the result is positive, it means that this force goes from 1 to 2, that is from the platinum-covered side to the pure MF one. This is the same direction of pure $F_{\Delta\alpha}$. The absolute of the force is also close to the one of $F_{\Delta\alpha}$ for the same value of the gas pressure.

The result of the direction of the forces is that they are opposite: $F_{\Delta T}$ points from pure MF side to the platinum-covered one as the MF temperature is higher and $F_{\Delta\alpha}$ points from the platinum-covered side to the pure MF one as the platinum accommodation coefficient is higher. If I am wrong about both this conclusions, then the two forces have anyway opposite direction, but if I am wrong about just one, then they have the same direction. This is actually not so important as the dominant one is $F_{\Delta\alpha}$ because its value is orders of magnitude higher than the one of $F_{\Delta T}$.

In conclusion, $F_{\Delta\alpha}$ is the only force, together with asymmetric ion drag, acting when laser power is off; F_{neutrals}, which is comprehensive of both photophoretic mechanisms, acts together with the radiation pressure and the asymmetric ion drag forces when laser power is on. As the ion drag force is much weaker than the others, when the laser power is off the total acting force is $\simeq F_{\Delta\alpha}$ and when the laser power is on the only two acting forces are the radiation pressure force and F_{neutrals}. Obviously, also gravitational and electric forces are always present, but I just focused on the forces acting as "small engines" capable of making Janus particles active.

It must be specified that most probabily the difference between the temperatures of the two sides of the Janus particle will be bigger than what comes out of my calculation. In fact, as I have no way to estimate the thermal contact resistance between the MF and the platinum, I considered it null. This means that the force due to ΔT will be bigger than what estimated in both the present section and section 3.1.3. The uncertainty is then not only on the direction of the force for the reasons already explained, but also on its module.

3.2 Janus particle spin

As explained in section 3.1.1, the charge distribution on the particle surface is not trivial at all and for this reason the particle is not likely to be a dipole oriented in the electric field of the plasma sheath. It is highly probable that Janus particles rotate because of their not perfectly spherical shape [6] and especially because of the symmetry breaking due to the two different materials of the particle surface. This symmetry breaking concerns gravity because of the platinum weight and it concerns charge and temperature because

or their non-homogeneous distributions. In general, even for MF particles there can be a symmetry breaking due to non-uniform temperature of their surface or non-uniform ion drag acting on them. For the case of Janus particles, this contribution is for sure much stronger because of their own asymmetric nature. The dominant contribution of the particle orientation is probably due to gravity because the Pt covered side is heavier. As it will be shown in section 4.1.1, the platinum mass is $m_{Pt} = 2{,}7 \times 10^{-14}\,\mathrm{kg}$ with an associated gravitational force:

$$F = mg = 2{,}6 \times 10^{-13}\,\mathrm{N} \tag{3.37}$$

that causes a torque equal to:

$$M = Fr_p = 1{,}2 \times 10^{-20}\,\mathrm{N\,m}. \tag{3.38}$$

I tried to study experimentally Janus particle spin through the resonances in the power spectrum of the particle image brightness because the idea is that the platinum-covered side is brighter than the other because platinum reflects the laser light more than MF. It is also possible that the platinum layer is darker because of light absorption actually, but anyway the idea is to try to catch an oscillation in the brightness profile in time through a peak in the frequency. The results of this analysis will be discussed in section **??**.

If a particle is spinning, considering that in a collisionless plasma like the one I used the spinning motion is dominant with respect to the Brownian rotational diffusion, then it is possible to give a rough estimation of what the spinning frequency would be. In my case, the rotational frequency ω of the particle can be roughly estimated as follows:

$$Hp: \begin{cases} Equilibrium\,situation \\ Molecular\,regime \end{cases}$$

$$\frac{1}{2}k_bT = \frac{1}{2}I\omega^2$$

with:

$$I = \frac{2mr^2}{5}$$

Even if we are in the molecular regime, the equilibrium hypothesis is not valid if Janus particles are active particles. As already said, the main aim of my work is actually to give an answer to the question about Janus particle activity in plasmas and the conclusions will be discussed in detail in chapter 5: in particular, it will be clear that they are actually active. Nevertheless, this result is just to give a rough idea about particle spinning frequency and this is the best I can do.

The calculation gives:

$$\omega = 27{,}0\,\mathrm{s}^{-1} = 4{,}3\,\mathrm{Hz} \qquad \text{for} \quad T_{\text{kin, min}} \sim 300K \tag{3.39}$$

and

$$\omega = 139{,}5\,\mathrm{s}^{-1} = 22{,}2\,\mathrm{Hz} \qquad \text{for} \quad T_{\text{kin, max}} \sim 8000K \tag{3.40}$$

This range of values will be the one studied more carefully in the particle image brightness fast Fourier transform analysis.

3.3 Theory about active particles in overdamped environments

If the forces described in section 3.1 are really acting on the particle, we should observe something similar to the theoretical predictions in Ref. [19]. The comparison can only be qualitative because the plasma at the low densities I worked with is an undamped environment.

Let us make a brief parenthesis before describing the theoretical model. In general, damping is an important factor in an oscillatory system that has the effect of reducing, restricting or preventing its oscillations; damping is produced by processes that dissipate the energy stored in the oscillation. An environment can be defined as:

- overdamped: the system returns (exponentially decays) to equilibrium without oscillating
- critically damped: the system returns to equilibrium as quickly as possible without oscillating
- underdamped: the system oscillates (at reduced frequency compared to the undamped case) with the amplitude gradually decreasing to zero
- undamped: the system oscillates at its natural resonant frequency without experiencing significant decay of its amplitude.

In particular:

$$\text{Undamped environment} \iff \nu_E << \nu_{\text{Einstein}}$$

where ν_E is the Epstein drag rate and ν_{Einstein} is the Einstein frequency, that is the oscillation frequency of one particle when its nearest neighbours, which are six in the case of two-dimensional crystals, are fixed. In particular, in the conditions used $\nu_{\text{Einstein}} = 30 \div 50\,\mathrm{s}^{-1}$ [20]. For what concerns the Epstein drag rate ν_E, a simple formula in which

you use certain kinds of units of measurement and you get s^{-1} as a result, is [21]:

$$\nu_E = K_\gamma \frac{p_g}{\varrho r_p} \tag{3.41}$$

where p_g is the argon pressure, which is $1{,}33\,\mathrm{Pa} = 9{,}98\,\mathrm{mTorr}$, ϱ is MF density $1{,}51\,\mathrm{g\,cm^{-3}}$, r_p is the particle radius $4{,}635\,\mu\mathrm{m}$ and K_γ is a factor that for argon is:

$$K_\gamma = 1{,}18\,\mu\mathrm{m\,g\,mTorr^{-1}\,cm^{-3}} \tag{3.42}$$

However, this value of K_γ is affected by the Epstein gas drag force coefficient δ that Epstein estimated to be $\delta_E = 1{,}39$, but that for my experimental conditions has been measured to be $\delta_{\mathrm{group}} = 1{,}26$ [9]. Considering this correction, a better value for K_γ will be called K_Γ in order to distinguish the two of them:

$$K_\Gamma = K_\gamma \frac{\delta_{\mathrm{group}}}{\delta_E} \tag{3.43}$$

that leads to $K_\Gamma = 1{,}07\,\mu\mathrm{m\,g\,mTorr^{-1}\,cm^{-3}}$.

With this value of K_Γ the resulting Epstein drag rate is:

$$\nu_E = 1{,}53\,\mathrm{s^{-1}} \tag{3.44}$$

As $1{,}53\,\mathrm{s^{-1}} << 30 \div 50\,\mathrm{s^{-1}}$, the condition of undamped environment is true.

Coming back to the theoretical model, it describes a single swimmer dynamics confined in a harmonic trap in two spatial dimensions. The external potential, which is assumed to be symmetric and centred in the origin, is given by:

$$U(x, y) = \frac{\lambda_0}{2}(x^2 + y^2), \tag{3.45}$$

where λ_0 is the potential strenght. The self-propulsion is modeled by an effective force:

1. $$\mathbf{F} = F_0\mathbf{u} \tag{3.46}$$

   in case of time-independent self-propulsion

2. $$\mathbf{F}(t) = F_0[1 + \cos(\nu t + \vartheta)]\mathbf{u} \tag{3.47}$$

   in case of time-dependent self-propulsion.

$\mathbf{u}$ is the Janus particle orientation:

$$\mathbf{u} = (\cos\varphi, \sin\varphi). \tag{3.48}$$

The rotational motion of a particle in an overdamped environment is governed by a single Langevin equation for the orientation angle φ:

$$\frac{d}{dt}\varphi(t) = \omega \tag{3.49}$$

in case of vanishing brownian noise (see following). ω is the spinning frequency of the particle I talked about in the previous section. ν in the equation of time-dependent self-propulsion is the so-called propulsion frequency and ϑ is the initial phase.

Two cases need to be distinguished in order to go on with this theoretical description:

1. Time-independent self-propulsion.

   The Langevin equations describing the two-dimensional motion can be solved analytically and the result is that, after an initial regime, the microswimmer approaches a circular swimming path which is independent on the initial conditions. The limit cycle is described by the following equations:

   $$\frac{1}{r_p}x(t) = \frac{F_0}{\lambda_0^2+\omega^2}[\lambda_0\cos(\omega D_r t+\varphi_0)+\omega\sin(\omega D_r t+\varphi_0)] \tag{3.50}$$

   $$\frac{1}{r_p}y(t) = \frac{F_0}{\lambda_0^2+\omega^2}[\lambda_0\sin(\omega D_r t+\varphi_0)-\omega\cos(\omega D_r t+\varphi_0)] \tag{3.51}$$

   where r_p is the particle radius and D_r is the rotational short-time diffusion constant. The radius r_c of this limit cycle is

   $$\frac{r_c}{r_p} = \frac{F_0}{\sqrt{\lambda_0^2+\omega^2}} \tag{3.52}$$

   and the particle moves along it with a frequency ω, which is equal to the spinning frequency of equation 3.49. The cycle is shown in figure 3.7.

2. Time-dependent self-propulsion.

   A simplified expression for the trajectories in this case is:

   $$\begin{aligned}\frac{1}{r_p}x(t) = \frac{F_0}{\lambda_0^2+\omega^2}[&\lambda_0\cos(\omega D_r t+\varphi_0)+\omega\sin(\omega D_r t+\varphi_0)+\\ \frac{\lambda_0}{2}\cos((\omega+\nu)D_r t+\varphi_0+\vartheta)&+\frac{\omega+\nu}{2}\sin((\omega+\nu)D_r t+\varphi_0+\vartheta)\\ +\frac{\lambda_0}{2}\cos((\omega+\nu)D_r t+\varphi_0-\vartheta)&+\frac{\omega+\nu}{2}\sin((\omega+\nu)D_r t+\varphi_0-\vartheta)]\end{aligned} \tag{3.53}$$

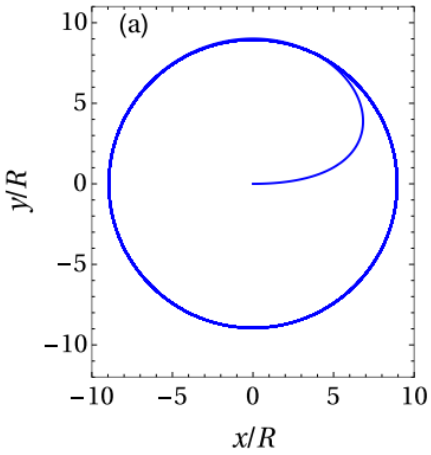

Figure 3.7: Noise-free trajectory predicted for active particle confined in a harmonic trap in an overdamped environment in case of time-independent self-propulsion force. The initial position of the active particle is supposed to be in the centre of the trap. The parameters are: $F_0 = 100$, $phi_0 = 0$, $\lambda_0 = 10$ and $\omega = 5$ [19].

$$\begin{aligned}\frac{1}{r_p}y(t) = \frac{F_0}{\lambda_0^2+\omega^2}[\lambda_0\sin(\omega D_r t+\varphi_0) - \omega\cos(\omega D_r t+\varphi_0)+\\ \frac{\lambda_0}{2}\sin((\omega+\nu)D_r t+\varphi_0+\vartheta) - \frac{\omega+\nu}{2}\cos((\omega+\nu)D_r t+\varphi_0+\vartheta)\\ +\frac{\lambda_0}{2}\sin((\omega+\nu)D_r t+\varphi_0-\vartheta) - \frac{\omega+\nu}{2}\cos((\omega+\nu)D_r t+\varphi_0-\vartheta)].\end{aligned} \tag{3.54}$$

In particular, some cases need to be distinguished:

- if the ratio ν/ω is irrational, the trajectory will never close and eventually fill a circular area around the trap centre
- if the ratio ν/ω is rational, the swimming paths, according to equations 3.53 and 3.54, are the closed rosette-like curves shown in figure 3.8. Most of the occurring trajectories have a rotational symmetry around the trap centre, but if $\omega = n\nu$ with n=1,2,3... the trajectories are asymmetric. The reason is the synchronous oscillation of the self-propulsion force and the particle orientation, which leads to the formation of the second "petal" exactly on top of the first one. This trajectories are in fact called "single-petal" trajectories with $n-1$ inner ones. The *cardioid* generated in the case $\omega = \nu$ is also called "heart-like" trajectory. The maximum distance from the trap centre depends on ω, ν and even on λ_0. This dependence is shown in figure 3.9.

It has to be specified that mine is vanishing Brownian noise case. Brownian noise is caused by gas atoms colliding with the particle and, if present, it causes rotational diffusion of the particle; rotational diffusion would prevent spinning to happen with a constant frequency. The reason why Brownian noise can be considered negligible is dominant

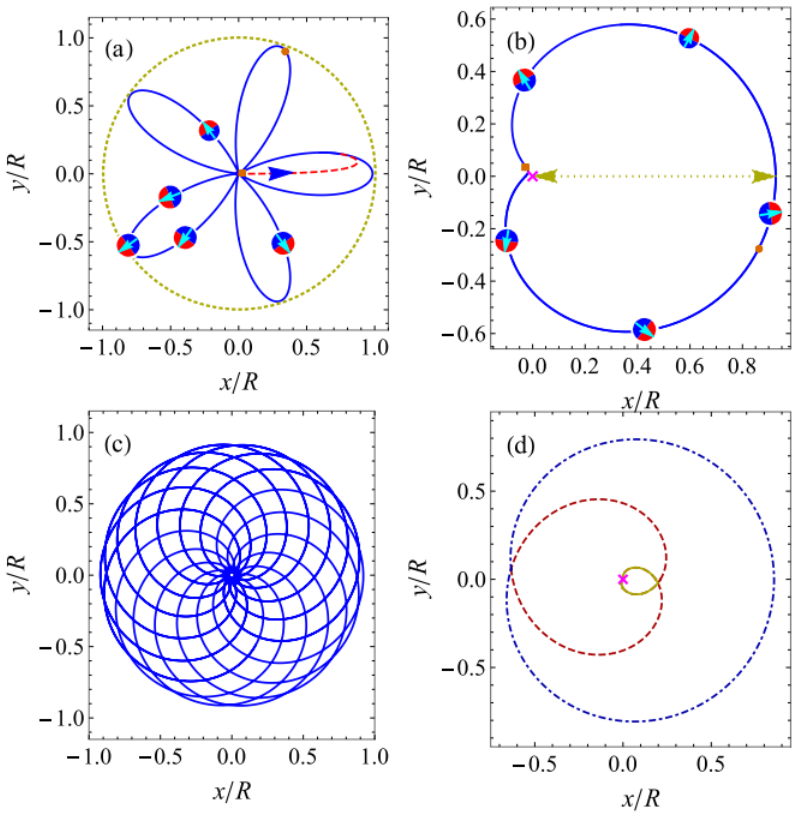

Figure 3.8: Noise-free trajectories predicted for active particle confined in a harmonic trap in an overdamped environment in case of time-dependent self-propulsion force. For all the plots $F_0 = 1$, $\varphi_0 = \vartheta = 0$, $\lambda_0 = 2$ and $\omega = 5$. In figure (a) the initial position of the active particle is supposed to be in the centre of the trap and the red dashed line represents the initial regime. The parameters for the various plots are: (a) $\omega = 0.1$ and $\nu = 0.5$, (b) $\omega = \nu = 0.7$, (c) $\omega = 0.75$ and $\nu = 0.7$, (d) $\omega = 1.2$ and $\nu = 0.4$. In cases (a) and (c) the ration between the frequencies is constant and they are closed rosette-like curves, in case (b) $\omega = \nu$ and for this reason the trajectory is a *cardioid*, in case (d) $\omega = 3\nu$ and for this reason the trajectory is asymmetric with respect to the centre of the trap and there are two inner petals in the *cardioid* [19].

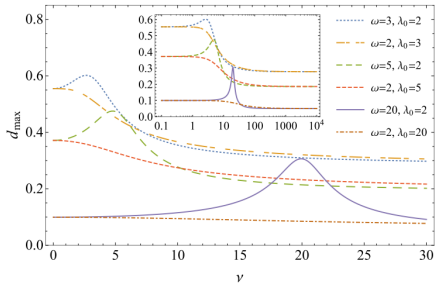

Figure 3.9: Maximum distance from the trap centre of a noise-free circle swimmer with temporally varying self-propulsion in a constant harmonic trap as a function of ν for $F_0 = 1$ and $\vartheta = 0$ [19].

particle-to-gas motion with non-zero velocity, which is valid in the molecular regime. It was demonstrated that the present regime is the molecular one in section 3.1.1.

Also the dynamics of a circle swimmer with time-dependent self-propulsion can be interesting in my case. In the theoretical model of the paper [19] the self-propulsion force absolute value is modelled by:

$$\mid F \mid = F_0[1 + \cos(\nu t + \vartheta)]$$

where ν is the so-called *propulsion frequency* and ϑ is the initial phase. Now the point is why in my case should F change in time with a fixed frequency ν. In principle, ν has nothing to do with the particle spinning frequency ω because the spinning motion should be just related to changes in the direction of the force acting on the particle. Nevertheless, I have a couple of hypotheses about why the *modulus* of the net force could change due to the particle spin. If these hypotheses are true, then $\nu = \omega$.

My hypotheses are:

1. Dependence of the asymmetry of ion drag force on the particle orientation.

   It is important to notice that this contribution will not be the dominant one for sure since the force due to asymmetric ion drag comes out to be the weakest force from my calculations in the previous sections. But it is still interesting to consider this hypothesis.

   Considering that the ion flow is always directed downward the plasma sheath, when the platinum-covered side is facing upwards, then the ion drag force has no reason to be asymmetric because of the homogeneous charge distribution on this side. On the contrary, if the particle is oriented any other way, the ions could be deviated differently by the parts of the surface with a different charge. In particular, if the non-covered side is facing upward, the asymmetry of the charge is due to the insulating nature of the MF, as explained before; otherwise, the different charge on the two sides plays the role of deviating the ions differently. These different situations could lead to a different net force acting on the particle due to the ions. In particular, if the rotational frequency of the particle was higher than the ion plasma frequency, then the net force due to ions would result in a time average over the different values assumed by it. The values calculated in section 3.2 are both much lower than the ion plasma frequency ω_{pi}, which is about 2 MHz obtained with the following calculation:

   $$\omega_{pi} = \sqrt{\frac{n_i z^2 e^2}{\varepsilon_0 m_i}}$$

   This means that the ions have enough time to "recognize" that the situation is changing and they can adapt to the new one. This means that the effect of the asymmetric drag force acting on the particle is changing in time and with the same

frequency as the spinning frequency of the particle. See figure 3.10

2. Coupling between gradT of the particle surface due to the two different materials and negative photophoresis.

   I have not considered so far that the particle could also heat up more on the side not facing the laser. This can happen for pure MF particles and this mechanism can be called negative photophoresis. In fact, the MF particle surface heats up more on the side not directly facing the laser for reasons related to refraction and reflection [22]: because of their transparency a "hot ring" forms on this side at an angle between 30° and 60° from the laser plane: see figure 3.11. This have been experimentally proved by the group in Ref. [1].

   Since my Janus particles are pure MF spheres half covered with 10 nm of platinum, this mechanism could also take place in my case, even if the presence of the platinum makes it difficult to predict if it is actually happening or not.

   As photophoresis due to gradT is not among the strongest forces and as negative photophoresis is again a weak contribution and it is not even sure if is present, this contribution to the time-dependence is not only just a hypothesis of mine, but, if present, it is very weak, probably comparable with the first contribution.

   The direction of this negative photophoresis never changes because it just depends on the laser direction and not on the particle orientation, while the direction of the photophoresis due to the gradT due to the different materials is just related to the particle and so it changes with particle orientation. In particular, in the three following situations the *modulus* of the total force changes this way: platinum-covered side facing towards the laser, non-covered side facing towards the laser, platinum-covered side facing upwards or downwards. See figure 3.12.

   The hot spot due to reflective nature of MF is always on the side which does not face the laser because the spinning frequency of the particle is much smaller than the inverse of the characteristic time of conductive thermal equilibration. On the other side, gradT rotates together with the particle because convection due to plasma neutrals is not fast enough to cool down the pure MF side while it is not facing the laser beam. In fact, if all my assumptions are correct, the pure MF side is heated up by the laser more than the platinum-covered one thanks to its large absorption coefficient at the laser beam wavelength when heated directly by it. The proof of the low efficiency of the convection process is the fact that the temperature of the particle surface is always higher than the one of the surrounding in these conditions, as mentioned before.

   In particular, the spinning frequency of the particle has been estimated to be between 4,3 Hz and 22,2 Hz and the time required for thermal equilibration can be roughly

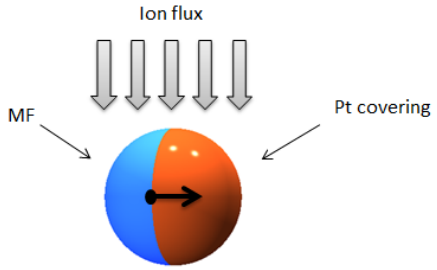

(a) *Pt on the right hand side: the black arrow is the force resulting from asymmetric ion drag, which should be stronger on the surface collecting more ions, which is the MF because it is a dielectric material and for this reason more negatively charged*

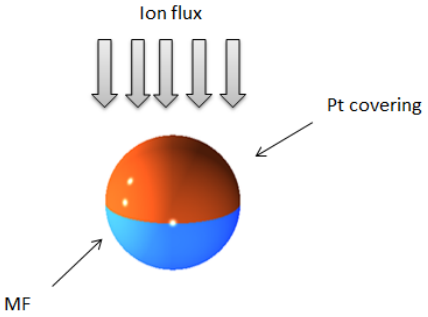

(b) *Pt facing the ion flux: in principle there should be no net force resulting from asymmetric ion drag, because in this case it is symmetric. This comes from the fact that the charge on a conductive surface like Pt is homogeneous, which means that ions are collected in the same way by the two sides of the particles*

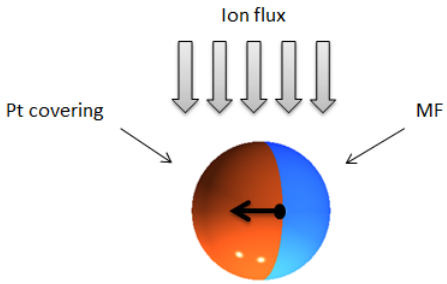

(c) *Pt on the left hand side: the black arrow is the force resulting from asymmetric ion drag, which should be stronger on the surface collecting more ions, that is the MF because it is a dielectric material and for this reason more negatively charged*

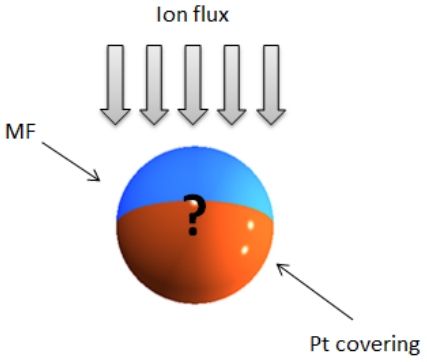

(d) *MF facing the ion flow: the charge distribution on a dielectric material just like MF is not homogeneous and it is unknown. For this reason there can be a net force resulting from asymmetric ion drag, but it is not possible to determine the direction of the net force because the charge distribution of MF is unknown. Anyway, probably in this case the resulting force is close to zero.*

Figure 3.10: Dependence of asymmetric ion drag force on Janus particle orientation

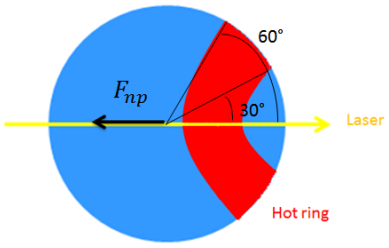

Figure 3.11: Hot ring on a pure MF particle in the negative photophoresis scenario: F_{np} is the negative photophoretic force

estimated as:

$$\tau = \frac{{r_p}^2}{\alpha}$$

with:

$$\alpha = \frac{k}{\varrho c_p}$$

Setting:

- $r_p = 4{,}635\,\mu\text{m}$
- $k = 0{,}5\,\text{W m}^{-1}\,\text{K}^{-1}$ from Ref. [23]
- $\varrho = 1{,}51\,\text{g cm}^{-3}$
- $c_p = 1200\,\text{J kg}^{-1}\,\text{K}^{-1}$ from [24].

The result is:

$$\tau = 7{,}7 \times 10^{-5}\,\text{s}$$

In particular, the inverse of the spinning frequency, which is the time required for a complete round, is between $4{,}5 \times 10^{-2}\,\text{s}$ and $0{,}2\,\text{s}$: this time is much longer than the one required to reach thermal equilibrium.

3. Dependence of radiation pressure force on particle orientation.

   This contribution will be the strongest for what concerns time dependence, as radiation pressure force is $3 \div 4$ orders of magnitude stronger than both force due to asymmetric ion drag and photophoresis due gradT.

   In this case, no comparison between characteristic times is required because the effect of the laser is immediate. As shown above, the force acting when the platinum-layer is facing the laser can be twice as big as the one acting when the pure MF is facing it. This means that the absolute value of this force depends on time with the same frequency as the particle is spinning at. See figure 3.13.

These three are therefore my hypotheses about why the *absolute value* of the net force acting on the particle should change in time with a certain frequency ν. In particular, this

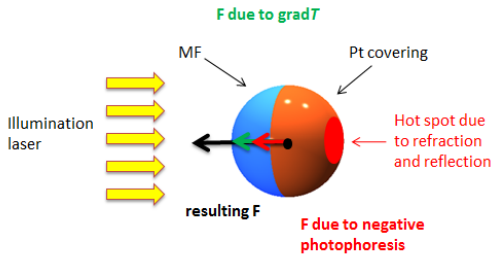

(a) *MF facing the laser*

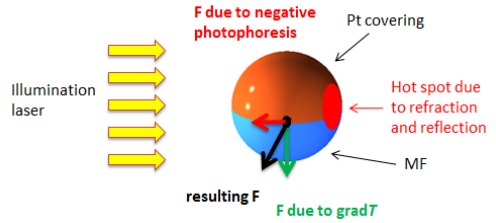

(b) *Pt facing upward*

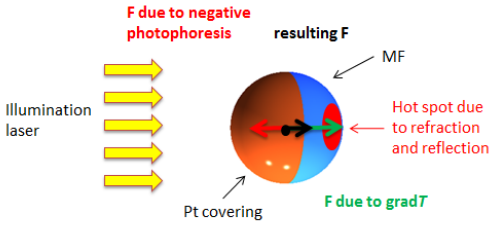

(c) *Pt facing the laser*

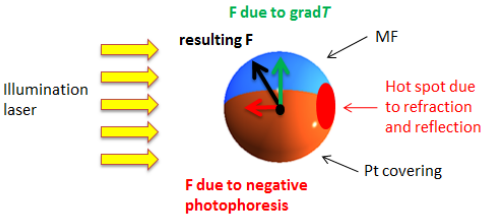

(d) *MF facing upward*

Figure 3.12: Dependence of the net force resulting from photophoresis due to a temperature gradient and negative photophoresis on different Janus particle orientations: the green arrows are the force due to the temperature gradient on the JP, the red arrows are the one due to the addition of the possible hot spot generated by refraction in MF of the laser light - it is always on the side not facing the laser - and the black arrows are the net force resulting from their combination

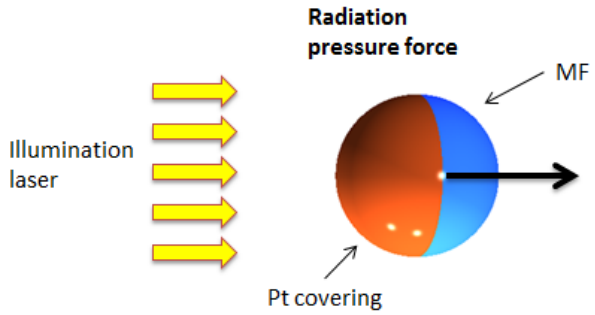

(a) *Platinum facing the laser: the force due to radiation pressure is represented by the black arrow and it obviously has the same direction as the laser*

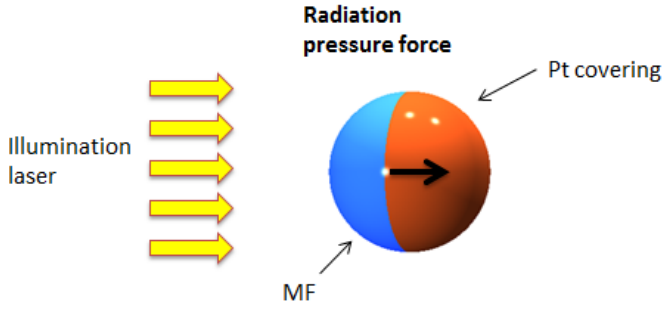

(b) *MF facing the laser: the force due to radiation pressure is about half of the one in the previous case.*

Figure 3.13: Dependence of the radiation pressure force on different Janus particle orientations

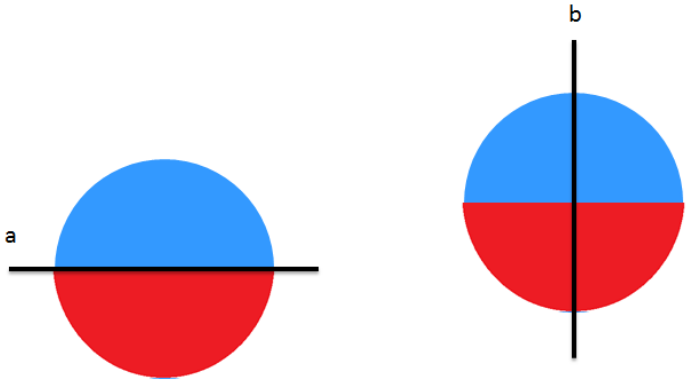

(a) *Rotational axis a* **(b)** *Rotational axis b*

Figure 3.14: Possible rotational axes

frequency ν should be equal to the particle spinning frequency ω if this conjectures are correct.

Moreover, it is important to note that these time dependent mechanisms act only if the particle is spinning around the rotational axis "a" of figure 3.14 and not if the rotational axis is "b". This is because, if the rotational axis is "b", then the platinum layer always faces downward and neither the net force due to asymmetric ion drag nor radiation pressure force nor the combination of negative photophoresis and photophoresis due to gradT change in time.

Summary of chapter 3

The forces hypothesised acting as propulsion mechanisms on the Janus particles dispersed in the plasma are the following.

1. Asymmetric ion drag force ($F_{\text{asym. ion drag}}$): the ion drag force acting along the vertical direction is caused by the adsorption and diffusion of ions, which flow from the top down. As the particle has an inhomogeneous charge distribution on its surface due to the different materials composing the two faces, the interaction with ions will be asymmetric. As the most negatively charged face collects and diffuses ions more effectively, more momentum will be transferred to this half of the particle than to the other one and this will generate a force pointing from this face to the other one.

2. Alternating radiation pressure force (F_{laser}): this force depends on the optical properties of the material hit by the light and actually MF and platinum have different optical absorption properties. This means that, if the particle spins around the rotational axis "a" of figure 3.14, this force will assume values that oscillate between the two values assumed on the two different faces, with the same frequency as the Janus particle is spinning at.

3. Photophoresis due to a temperature gradient on the particle surface ($F_{\Delta T}$): a temperature gradient generates on the particle surface when the laser is on because of the different thermal and optical properties of the materials composing the particle surface. When a gas neutral molecule collides with the particle surface, it leaves the surface with an energy that depends on the surface temperature. The higher the surface temperature, the higher the momentum transferred from the neutrals to the particle is. Therefore, a net force which points from the face at higher to the one at lower temperature generates. This mechanism will be even more complicated in a plasma, but a complete treatment of photophoresis in a plasma environment does not exist so far. Moreover, the temperature gradient could exist on the particle even in the absence of laser power because the plasma itself is a source of heat. However, even if this was true, for sure the temperature difference between the two faces will be larger the higher the laser power is.

4. "Photophoresis" due to different accommodation coefficients ($F_{\Delta\alpha}$): an accommodation coefficient is defined as the ratio between the number of "completely accommodated" molecules leaving the surface and the total number of molecules colliding with it. The "completely accommodated" molecules are the ones that leave the particle surface with a kinetic temperature that is equal to the surface temperature. The other molecules leave it with a temperature that is in between their initial one, which is equal to the gas temperature, and the surface temperature. The higher the accommodation coefficient, the larger the momentum transferred by the neutrals to the particle is: this generates a net force on the particle pointing from the surface of higher to the surface of lower accommodation coefficient. So far, also in this case the contribution of plasma ions and electrons has not been studied in detail in literature. This force requires the particle temperature to be higher than the surrounding fluid one. I call the force "photophoresis" (in quotes) because this is the name given to this force in literature, as usually a light source is required to make the particle hotter than its surrounding, but in this case the plasma is a sufficient source of heat.

The last two forces should always be considered together as the momentum transferred by the neutrals to the particle depends both on its temperature and on its accommodation coefficient.

With the aim of comparing at least thei orders of magnitude of the forces, I tried to evaluate the absolute value and the direction of each force as follows.

1. Considering negligible the contribution of ion diffusion, an upper estimate of $F_{\text{asym. ion drag}}$ can be done hypothesising that half of the particle collects ions and half does not. The result is $F_{\text{asym. ion drag}} \simeq 1{,}5 \times 10^{-19}\,\text{N}$. The direction of the force is from the most negatively charged face to the other, that is from the pure MF side to the platinum–coved one, as it is well known in literature that the dielectric particles in plasmas get more negatively charged than the metallic ones.

2. For laser power equal to 14 mW:

$$\begin{cases} F_{\text{laser, MF}} = 1{,}7 \times 10^{-16}\,\text{N} \\ F_{\text{laser, Pt}} = 3{,}8 \times 10^{-16}\,\text{N} \end{cases}$$

   For laser power equal to 99 mW:

$$\begin{cases} F_{\text{laser, MF}} = 1{,}2 \times 10^{-15}\,\text{N} \\ F_{\text{laser, Pt}} = 2{,}6 \times 10^{-15}\,\text{N} \end{cases}$$

   This force always has the same direction as the laser and it pushes the platinum side stronger than the MF one.

3. Using a semi–lumped parameter approach and considering the thermal contact between platinum and MF negligible, a lower estimate of the ΔT which generates on the particle surface was done: $\Delta T \simeq 4 \times 10^{-5}\,\mathrm{K}$, which leads to: $F_{\Delta T} \simeq 1{,}1 \times 10^{-18}\,\mathrm{N}$. As the platinum is more reflective than MF, the hottest face was estimated to be MF: this force was therefore estimated to point from the MF to the platinum–coved side.

4. Using the accommodation coefficient that can be found in literature for platinum in gas argon and considering the maximum possible $\Delta\alpha$ between the two faces, an upper estimate was done: $F_{\Delta\alpha} \simeq 6{,}7 \times 10^{-13}\,\mathrm{N}$. If MF accommodation coefficient is guessed to be lower than the platinum one, then the force should point from the platinum–coved side to the other.

If at least some of these forces are not negligible, then the single Janus particles should be active in plasmas. Some simulations exist in literature for the trajectories of circle swimmers in a harmonic potential well in case of "overdamped" environments. In this case, if the propulsion force acting on the particle is time-independent, then the particle trajectory has been computed to be circular. The radius of the circle is proportional to the ratio between the absolute value of the force and the rotational frequency ($r \propto F/\omega$) and the rotation frequency is equal to the particle spinning frequency. If the force acting on the particle is time-dependent, then the trajectories can assume different shapes as a function of the ratio between the rotational (spinning) frequency ω and the propulsion frequency ν, which is defined as the frequency at which the propulsion force changes over time. Three mechanisms have been hypothesised to depend on the Janus particle orientation. This would imply that the propulsion force depends on time with the same frequency as the particle is spinning at ($\nu = \omega$). The mechanisms are $F_{\text{asym. ion drag}}$, F_{laser} and $F_{\Delta T}$ in case of coupling of the described ΔT with a "hot spot" which generates from reflection and refraction on the side of the particle not facing the laser. These forces actually depend on time just if the particle spins around axis "a" of figure 3.14. Moreover, it is important to keep in mind that the comparison between this theoretical result obtained for an "overdamped" environment and the experimental results I obtained in an "undamped" environment can be just qualitative.

Chapter 4

Analysis and Experiments

In this chapter I will present the methods that I used in order to analyse particle behaviour in plasma and I will present the experiments that I performed in order to try to understand it better, especially changing various experimental parameters. The aim of my experimental work is, in fact, to understand as well as possible the acting forces discussed in chapter 3 from an experimental point of view.

For every series of the experiments performed, I analysed more than one particle in order to obtain some statistics about the results. Moreover for each particle I performed more than one recording because I needed one every time I changed one parameter in order to get a response about what happened to the particle after changing something. In particular, every recording consists of 2726 frames recorded at a speed of 50 frames per second (fps).

4.1 Analysis

I would like to clarify how particle mass was calculated, as it is an important parameter used in all the following analysis:

$$m_{\mathrm{MF}} = \varrho_{\mathrm{MF}} V_{\mathrm{MF}} \tag{4.1}$$

where V_{MF} is the particle volume and ϱ_{MF} is the melamine-formaldehyde density:

$$\varrho_{\mathrm{MF}} = 1{,}51 \, \frac{\mathrm{g}}{\mathrm{cm}^3} \tag{4.2}$$

from [25] and:

$$V_{\mathrm{MF}} = \frac{4}{3} \pi r_p^3 \tag{4.3}$$

with r_p particle radius:

$$r_p = 4{,}635 \, \mu\mathrm{m}. \tag{4.4}$$

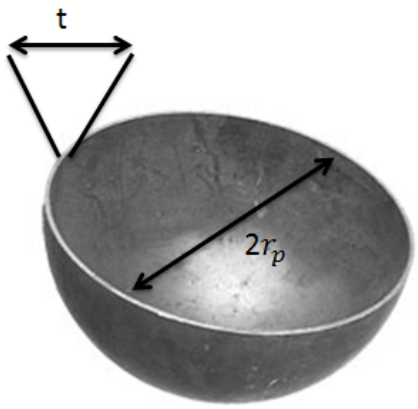

Figure 4.1: Simple representation of platinum coating

The result is:

$$V_{\mathrm{MF}} = 4{,}2 \times 10^{-16}\,\mathrm{m}^{-3} \tag{4.5}$$

and:

$$m_{\mathrm{MF}} = 6{,}3 \times 10^{-13}\,\mathrm{kg}. \tag{4.6}$$

The additional contribution to the mass due to the 10 nm of platinum covering half of the particle can be calculated as follows. As the volume V_{Pt} of the platinum layer is:

$$V_{\mathrm{Pt}} = 2\pi r_p^2 t \tag{4.7}$$

with t the platinum layer thickness, the result is:

$$V_{\mathrm{Pt}} = 1{,}3 \times 10^{-18}\,\mathrm{m}^3. \tag{4.8}$$

Platinum covering mass can be found multiplying this value for the platinum density. Actually, every PVD machine is different and the resulting sputtered platinum density has never been measured. The actual sputtered platinum density is approximately 98% of its bulk density of $21{,}45\,\mathrm{g\,cm}^{-3}$, which is given in Ref. [26] for a setup and a sputter source similar to the one used by Ali Kaouk in Cologne. The result of platinum contribution to Janus particle mass is:

$$m_{\mathrm{Pt}} = 2{,}7 \times 10^{-14}\,\mathrm{kg}. \tag{4.9}$$

The total mass of the particle is the sum of m_{MF} and m_{Pt}:

$$m = 6{,}6 \times 10^{-13}\,\mathrm{kg}. \tag{4.10}$$

In particular, an error can be associated with the particle mass as the uncertainty on

the particle radius given by *Micropartcles GmbH*, the company producing the pure MF particles, is:

$$\Delta r_p = 0{,}05\,\mu\text{m} \tag{4.11}$$

and:

$$\frac{\Delta V_{\text{MF}}}{V_{\text{MF}}} = 3\frac{\Delta r_p}{r_p} \tag{4.12}$$

from which $\Delta V_{\text{MF}} = 1{,}35 \times 10^{-17}\,\text{m}^3$. Considering ϱ_{MF} as a constant as the company does not give an error on it, then:

$$\Delta m_{\text{MF}} = \varrho_{\text{MF}} \Delta V_{\text{MF}} = 2{,}05 \times 10^{-14}\,\text{kg}. \tag{4.13}$$

An error relative to m_{Pt}, that is related to the error affecting the platinum layer's width, must be added. Considering that $\Delta t = 0{,}1\,\text{nm}$, then:

$$\frac{\Delta V_{\text{Pt}}}{V_{\text{Pt}}} = \sqrt{\left(2\frac{\Delta r_p}{r_p}\right)^2 + \left(\frac{\Delta t}{t}\right)^2}, \tag{4.14}$$

that leads to $\Delta V_{\text{Pt}} = 3{,}1 \times 10^{-20}\,\text{m}^3$, and

$$\Delta m_{\text{Pt}} = \varrho_{\text{Pt}} \Delta V_{\text{Pt}} = 6{,}7 \times 10^{-16}\,\text{kg} \tag{4.15}$$

In conclusion:

$$\Delta m = \sqrt{(\Delta m_{\text{MF}})^2 + (\Delta m_{\text{Pt}})^2} = 2{,}05 \times 10^{-14}\,\text{kg}. \tag{4.16}$$

4.1.1 Analysis with `ImageJ` and `Python`

I used `ImageJ` to find the particle *centre of brightness* position frame by frame, which is returned by `ImageJ` with 5 decimal places. I also asked `ImageJ` to return the particle area and mean brightness frame by frame.

In particular, the output positions from `ImageJ` have been compared to another code often used by the group in order to check their precision. The result is that they are fully compatible.

Then I used `ImageJ` output as an input to my `Python` codes. The data that I calculated with Python in order to characterize and study Janus particle behaviour in plasmas are:

- Trajectory (see appendix A for the code). Figure 4.2 shows an example of a Janus particle trajectory over 2726 frames. All the figures of the present and following sections are from the same recording.

- Radius of the particle trajectory. It has been computed as the mean of the distances

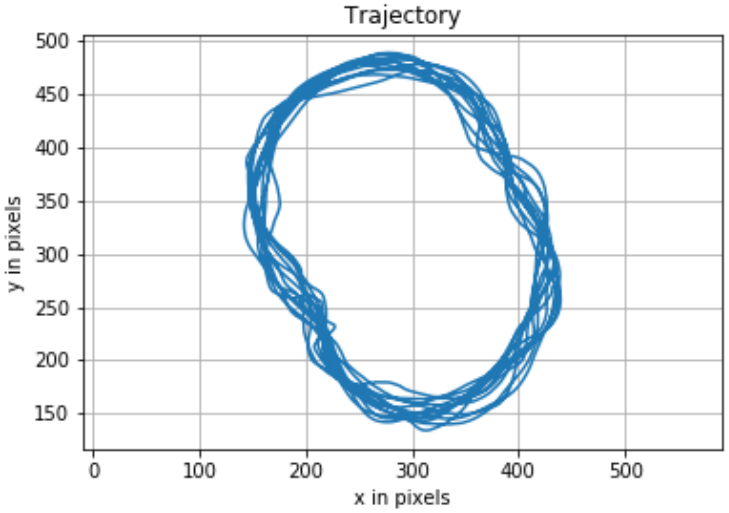

Figure 4.2: Example of a Janus particle trajectory over 2726 frames

$x_{\max} - x_{\min}$ and $y_{\max} - y_{\min}$, divided by two, which means:

$$r = \frac{1}{2}\frac{(x_{\max} - x_{\min}) + (y_{\max} - y_{\min})}{2}. \tag{4.17}$$

Its standard deviation has been computed as:

$$\Delta r = \frac{1}{4}\sqrt{(\Delta^2_{\text{diff, x}} + \Delta^2_{\text{diff, y}})}. \tag{4.18}$$

where $\Delta_{\text{diff, x}}$ and $\Delta_{\text{diff, y}}$ has been computed as:

$$\Delta_{\text{diff, x}} = \sqrt{2}\Delta x \tag{4.19}$$

and

$$\Delta_{\text{diff, y}} = \sqrt{2}\Delta y. \tag{4.20}$$

Δx and Δy are the uncertainties related to the particle x and y positions and they are 0.02 pixels, which means:

$$\Delta x = \Delta y = 0{,}04 \times 10^{-8}\,\text{m} \tag{4.21}$$

because 1 pix = 1,881 μm. The results is:

$$\Delta r = 2{,}0 \times 10^{-10}. \tag{4.22}$$

- Fast Fourier transform of the positions (see appendix B for the code). The interest

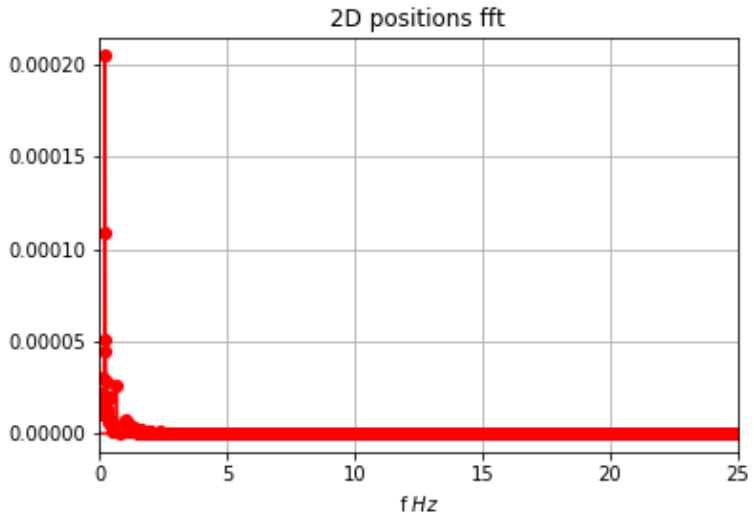

Figure 4.3: Example of the fast Fourier transform of a Janus particle two-dimensional positions over 2726 frames

in this result comes from the fact that this graph resonances are related to the characteristic frequencies of the system. Figure 4.3 shows an example of it.

- Fast Fourier transform of the particle mean and total brightness (see appendix C for the code), in order to check if the resonance frequencies match the possible spinning frequency calculated in section 3.2. Figure 4.4 shows an example of the fast Fourier transforms of mean and total particle brightnesses.

- One-dimensional and two-dimensional velocity frame by frame.

  The two-dimensional velocity has been calculated as follows:

  ```
  v_2D[i] = ( np.sqrt ( ((x_m[i+1]-x_m[i])**2)
  + ((y_m[i+1]-y_m[i])**2)) ) * fps,
  ```

  where `i` stays for the i-th frame, as v_{2D} is calculated frame by frame, `x_m[i+1]` is the subsequent frame particle x in meters, `x_m[i]` is the i-th frame x in meters, `y_m[i+1]` and `y_m[i]` is the same for particle y, `fps` is the camera speed in frames per second and `**2` means elevated to the power of 2.

  A similar calculation was performed for one-dimensional velocities:

  ```
  v_x[i] = (x_m[i+1] - x_m[i]) * fps
  ```
  (4.23)

  ```
  v_y[i] = (y_m[i+1] - y_m[i]) * fps
  ```
  (4.24)

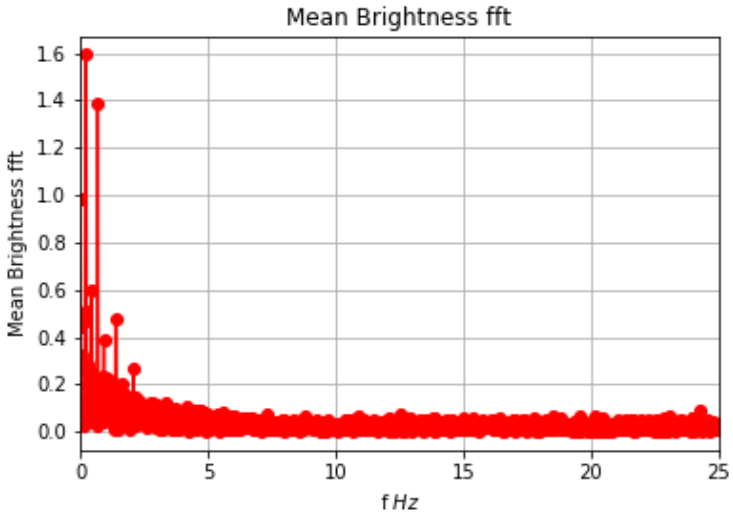

(a) *Fast Fourier transform of mean particle brightness*

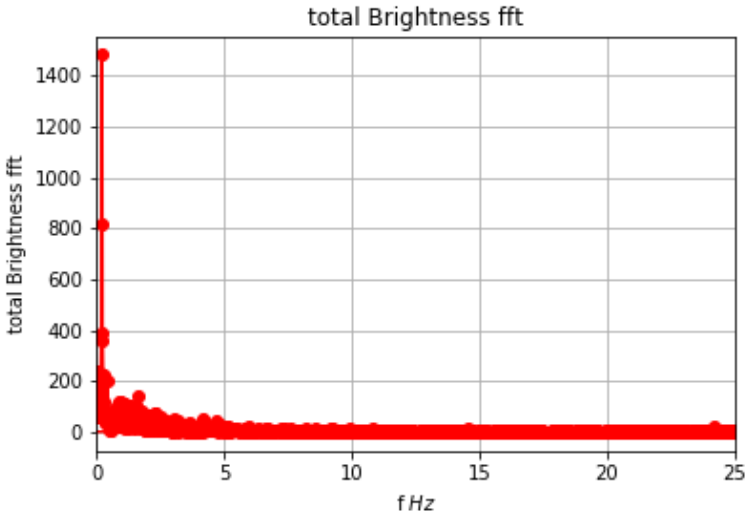

(b) *Fast Fourier transform of total particle brightness*

Figure 4.4: Fast Fourier transform of particle brightness

- Kinetic temperatures from velocities: T_{2D}, T_x, T_y.

  They are a first estimation for the particle temperature, which has nothing to do with the particle surface temperature, and they are also a good estimation in the case of random trajectories. They were calculated as follows:

  ```
  T_x=mass*meanvx2/Kb
  T_y=mass*meanvy2/Kb
  ```

  where `mass` is the particle mass, `Kb` is the Boltzmann constant and `meanvx2` and `meanvy2` are the mean squared one-dimensional velocity over all the frames calculated as follows:

  ```
  meanvx2 = np.mean(v_x2[:])
  meanvy2 = np.mean(v_y2[:])
  ```

  with:

  ```
  v_x2 = v_x**2
  v_y2 = v_y**2.
  ```

  v_x and v_y are two Python *lists* calculated as explained in equations 4.23 and 4.24. `np.mean` is a Python function from *numpy* package, imported as *np*, which calculates the mean of a list and `"[:]"` means *over all the elements of the list.*

  The errors associated with `T_x` and `T_y` could be calculated from:

  $$\frac{\Delta T_x}{T_x} = \sqrt{\left(\frac{\Delta m}{m}\right)^2 + \left(\frac{\texttt{errvx2}}{\texttt{meanvx2}}\right)^2} \tag{4.25}$$

  and

  $$\frac{\Delta T_y}{T_y} = \sqrt{\left(\frac{\Delta m}{m}\right)^2 + \left(\frac{\texttt{errvy2}}{\texttt{meanvy2}}\right)^2} \tag{4.26}$$

  where `errvx2` and `errvy2` are the errors associated with `meanvx2` and `meanvy2`. In particular:

  ```
  errvx2 = np.std(v_x2[:])
  errvy2 = np.std(v_y2[:])
  ```

  where `np.std` is another Python function from `numpy` package which calculates the standard deviation of a list.

  This method of estimating the temperature standard deviation gives however too high values. This is because the particle velocity can really vary a lot during the motion. So, I really think that a better way to estimate the uncertainty relatively to the kinetic temperature is the following. As $\Delta x = \Delta y = 0{,}04 \times 10^{-8}\,\mathrm{m}$, computing v_x as in equation 4.23, then:

  $$\Delta v_x = 2\Delta x \cdot fps = 0{,}002\,\mathrm{m\,s^{-1}}. \tag{4.27}$$

This value is maybe a little bit overestimated but, as two consecutive positions are not considered completely uncorrelated, their uncertainties are summed up in a non geometrical way. Therefore these are the steps I followed:

$$\frac{\Delta v_x^2}{v_x^2} = 2\frac{\Delta v_x}{v_x} \tag{4.28}$$

and

$$\Delta\texttt{meanvx2} = \frac{\sqrt{\sum_{i=1}^{2725}(\Delta v_x^2)^2}}{2725}, \tag{4.29}$$

as 2726 is the standard number of frames, and

$$\frac{\Delta T_x}{T_x} = \sqrt{\left(\frac{\Delta\texttt{meanvx2}}{\texttt{meanvx2}}\right)^2 + \left(\frac{\Delta m}{m}\right)^2}, \tag{4.30}$$

where Δm and m have been computed as in equation 4.16 and 4.10. This way the errors of the resulting temperatures of chapter 5 were computed. The same is valid for y.

The calculations above for the one-dimensional kinetic temperature are the result of energy equipartition theorem:

$$\frac{1}{2}k_b T_x = \frac{1}{2}m < v_x^2 >, \tag{4.31}$$

where $< \cdots >$ stands for the mean value of the argument. The same equation obviously holds also for T_y.

When T_x and T_y are similar, T_{2D} can be estimated as their mean value:

```
T[0] = (T_x + T_y)/2
```

with an associated error:

```
T[1] = np.sqrt((T_xsigma)**2 + (T_ysigma)**2)/2
```

from error propagation theory.

- One-dimensional and two-dimensional velocity distribution functions. See figure 4.5 for examples.

- Velocity distribution function fits with Maxwellian distribution for two-dimensional velocity and with Gaussian distribution for one-dimensional velocity.

  See 4.6 for examples. Notice that in the figure the blue curves are Gaussian and Maxwellian distribution functions computed from mean velocities and kinetic temperature, respectively. Here the importance of the blue curve is not relevant, but when the velocity histograms computed after subtracting the circular motion will be fitted it will matter much more (see figure 4.12).

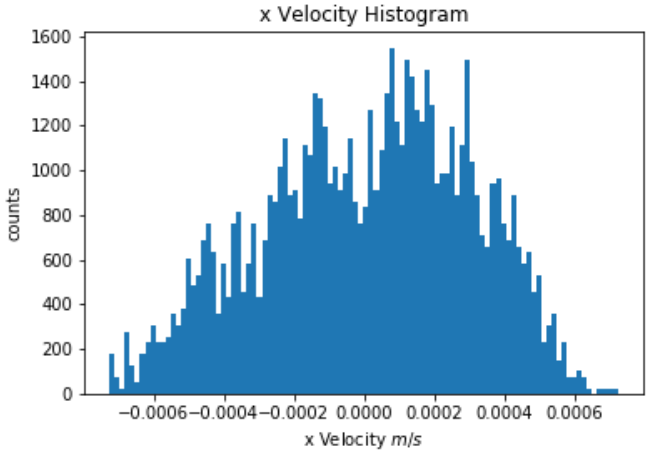

(a) *x one-dimensional velocity distribution function*

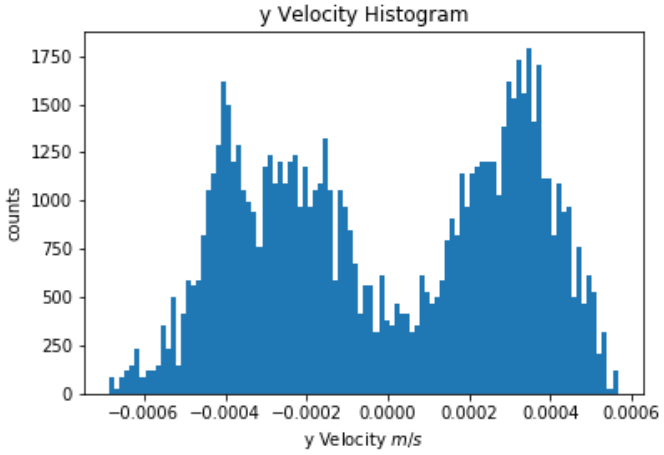

(b) *y one-dimensional velocity distribution function*

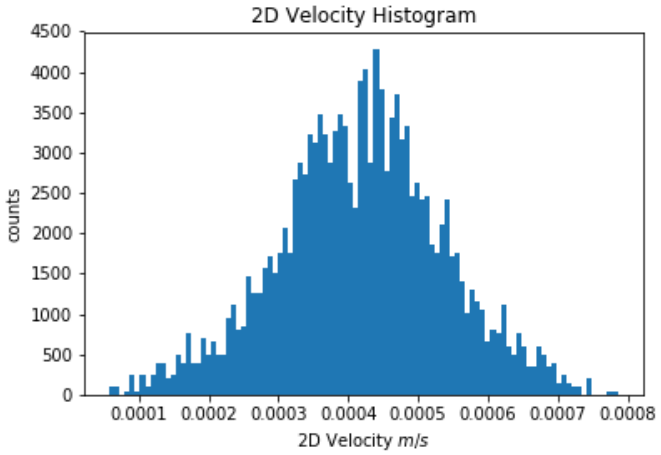

(c) *Two-dimensional velocity distribution function*

Figure 4.5: One- and two-dimensional velocity distribution functions

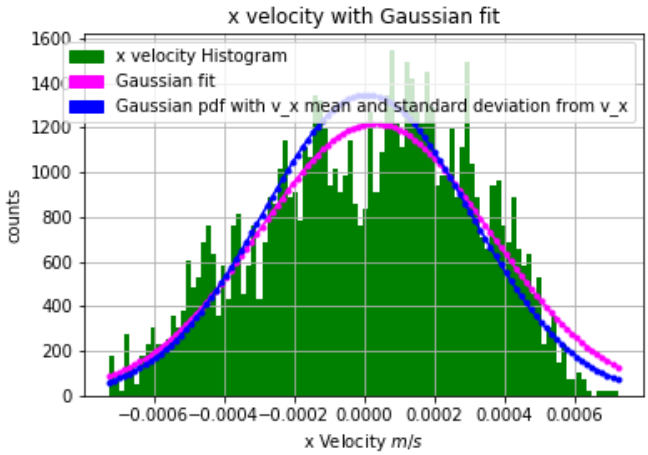

(a) *x one-dimensional velocity distribution function fitted with a Gaussian distribution function*

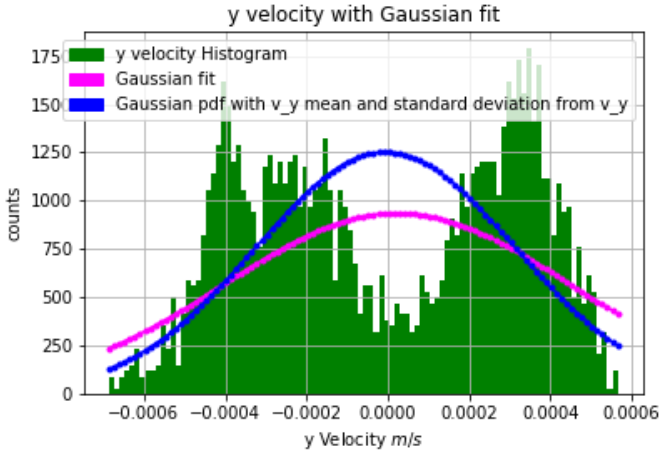

(b) *y one-dimensional velocity distribution function fitted with a Gaussian distribution function*

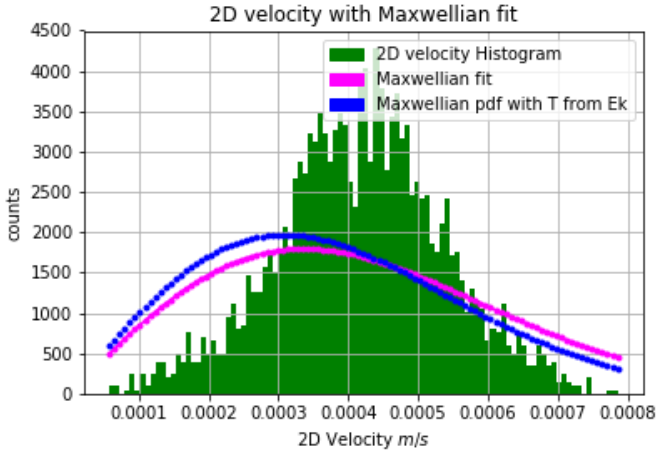

(c) *Two-dimensional velocity distribution function fitted with a Maxwellian distribution function*

Figure 4.6: One- and two-dimensional velocity distribution functions fitted with the proper distribution function

- Two-dimensional kinetic temperature from Maxwellian fit.

  Maxwellian distribution form is:

  $$f(v) = \frac{mv}{k_b T} e^{-\frac{mv^2}{2K_b T}} \tag{4.32}$$

  where m is the particle mass, v the two-dimensional velocity, K_b the Boltzmann constant and T the particle two-dimensional kinetic temperature.

  Using Python function `curve_fit` imported from `scipy.optimize` package the two-dimensional velocity histogram can be fitted obtaining T as output. In particular, `curve_fit` receives as input *f, xdata, ydata* and other not required parameters, for example an initial guess value of the parameters to fit in order to produce a faster and better output. Assuming that `ydata = f(xdata, *params) + eps`, where `f` means *function of* and `eps` means *an arbitrary small value*, the function outputs are:

  - `popt`, which is an array of optimal values for the parameters to fit so that the sum of the squared residuals of `f(xdata, *popt) - ydata` is minimized
  - `pcov`, which is a 2d array of the estimated covariance of `popt`.

  The diagonals provide the variance of the estimated parameter, so, in order to compute one standard deviation error on the parameters, I used `perr = np.sqrt(np.diag(pcov))`, where `np.sqrt` simply computes the square root of its argument.

  Considering that in my case `f` is Maxwellian distribution form, `xdata` are the `v_2D` values used as bins in abscissa for the two-dimensional velocity histogram and `ydata` are the values in ordinate of it, `popt` is in my case the fit value for T_{2D} and `perr` is its standard deviation. I gave as additional input `T[0]` as initial guess value of T_{2D}.

- One-dimensional kinetic temperatures from Gaussian fit.

  Gaussian distribution form is:

  $$f(v) = \frac{1}{\sqrt{2\pi\sigma^2}} e^{-\frac{(v-\mu)^2}{2\sigma^2}} \tag{4.33}$$

  where v is v_x or v_y, σ the standard deviation of v and μ the mean of v.

  I used again `curve_fit` to fit μ and σ and to compute their standard deviations.

  From:

  $$\sigma = \sqrt{\frac{k_b T}{m}} \tag{4.34}$$

  I calculated T_x and T_y. Calling $\Delta\sigma$ the standard deviation of σ, I computed the

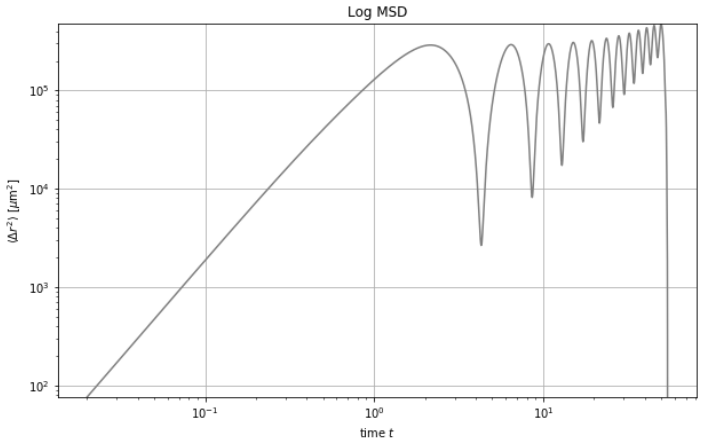

Figure 4.7: Example of MSD in logarithmic scale computed over 2726 frames

standard deviation of the temperature as:

$$\frac{\Delta T_x}{T_x} = \sqrt{\left(2\frac{\Delta\sigma}{\sigma}\right)^2 + \left(\frac{\Delta m}{m}\right)^2}. \tag{4.35}$$

The same for T_y.

- Mean squared displacement MSD (see appendix **??** on page ?? for the code). See figure 4.7 for an example.

- Temperature from MSD [27].

  It has been known since 1905 thanks to Einstein [28] that the MSD of a Brownian particle over a time t can be related to the properties of its environment or to its own properties:

  $$< x^2 >= 2Dt \qquad \text{for} \quad t >> \tau_p \tag{4.36}$$

  $$< x^2 >= \frac{k_b T}{m} t^2 \qquad \text{for} \quad t << \tau_p \tag{4.37}$$

  wihere $D = \mu K_b T$ is the diffusion constant and τ_p the momentum relaxation time, because at $t << \tau_p$ the motion is ballistic.

  Moreover, equations 4.36 and 4.37 are valid in the case of a free Brownian particle, while for a particle confined in a harmonic potential well in presence of friction the equation of motion is:

  $$m\ddot{x} = -m\gamma\dot{x} + R(t) - m\omega_0^2 x \tag{4.38}$$

  where $\gamma = \frac{1}{\tau_p}$ is the damping coefficient, $R(t)$ the fluctuating force due to collisions and ω_0 the particle resonance frequency. My aluminium ring creates a confining

potential well which can be well approximated with a harmonic well in its centre, where the particle motion takes place. MSD solution of 4.38 is [29] [30]:

$$< x^2 >= \frac{2k_bT}{m\omega_0^2}[1 - e^{\frac{\gamma t}{2}}\{\cos(\hat{\omega}t) - \frac{\gamma}{2\hat{\omega}}\sin(\hat{\omega}t)\}] \tag{4.39}$$

with $\hat{\omega} = \sqrt{\omega_0^2 - \frac{\gamma}{2}^2}$.

In the case of a dusty plasma, unwanted mechanical or electronic oscillations require equation 4.38 to be modified as follows [27]:

$$m\ddot{x} + m\gamma\dot{x} + m\omega_0^2 x = R(t) + \sum_{oscill} a_i \cos(\omega_i t), \tag{4.40}$$

where a_i and ω_i are the amplitude and the frequency of individual oscillations within the system. The solution is:

$$< x^2 >= \frac{2k_bT}{m\omega_0^2}[1 - e^{\frac{\gamma t}{2}}\{\cos(\hat{\omega}t) - \frac{\gamma}{2\hat{\omega}}\sin(\hat{\omega}t)\}] + \sum_{oscill} C_i \cos(\omega_i t + \varphi_i). \tag{4.41}$$

When $t << \tau_p$, the particle moves ballistically and equation 4.41 reduces in two dimensional case to:

$$< r^2 >= \frac{2k_bT}{m}t^2 \tag{4.42}$$

τ_p is the momentum relaxation time, that is basically the average time in which the particle loses a big part of its original momentum due to scattering events. In particular, it can be computed as the inverse of the Epstein drag rate. As the Epstein drag rate ν_E has been computed in equation 3.44 to be $\nu_E = 1{,}53\,\mathrm{s}^{-1}$, its inverse is:

$$\tau_p = \frac{1}{\nu_E} = 0{,}66\,\mathrm{s}. \tag{4.43}$$

I made a parabolic fit of the first four MSD points, that means over $t = 0{,}08\,\mathrm{s}$, which is much smaller than τ_p, and I found a fitting parameter A of $< r^2 >= At^2$ I calculated T_{2D} from:

`T=popt[0]*mass/Kb/2.`

Here `popt[0]` is the A parameter fitted by `curve_fit`. The initial guess value of A that I gave to the function was calculated as follows:

`AfromT=(2*Kb*T[0]/mass).`

In concern with the error associated with T_{2D} calculated from MSD fit, it has been computed from

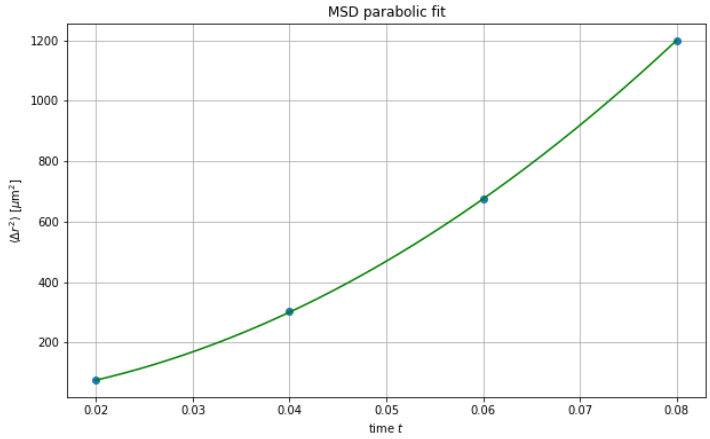

Figure 4.8: Example of MSD initial part parabolic fit

$$\frac{\Delta T}{T} = \sqrt{\left(\frac{\texttt{perr[0]}}{\texttt{popt[0]}}\right)^2 + \left(\frac{\Delta m}{m}\right)^2} \tag{4.44}$$

with:

`perr = np.sqrt(np.diag(pcov))`,

as usual, and `Dmass` $= \Delta m$ and `m` $= m$ from equations 4.16 and 4.10.

See figure 4.8 for an example of the parabolic fit of the MSD first four points.

- Subtraction of the circular motion and rotation frequency from sinusoidal fitting.

  This step of the analysis was performed just for those trajectories whose shape resembles a circle of something similar. In particular, I computed the mean values of x and y over all the frames and I plotted the difference between x or y and their mean value in time, that are the Python lists `random_x` and `random_y` calculated frame by frame as follows:

  `random_x[i]=x[i]-mean_x`
  `random_y[i]=y[i]-mean_y`.

  See figure 4.9 for an example of the plot of `random_x[i]` and `random_y[i]`.

  Then, again using `curve_fit`, I fitted their evolution in time with a generic sinusoidal function:

  $$y = A\sin(\omega t + \varphi) + c, \tag{4.45}$$

  where the free parameter A is the amplitude of the sine, ω is the rotational frequency of the particle periodic motion in $\mathrm{rad\,s^{-1}}$ and φ and c are other fitted parameters.

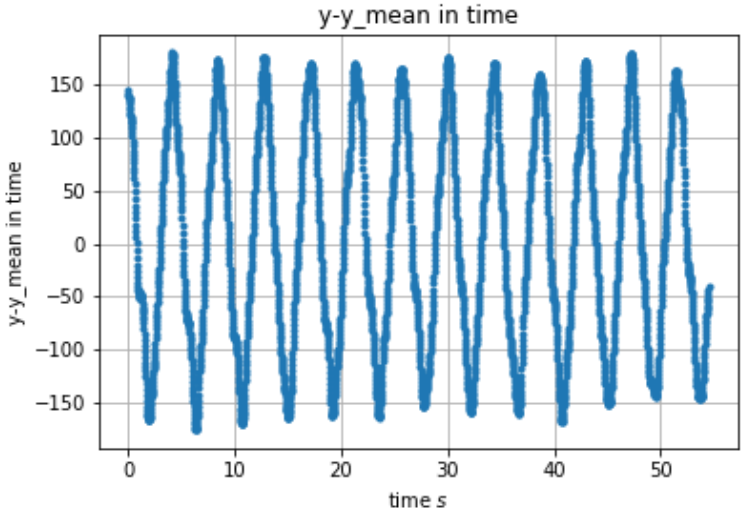

(a) *Difference between x and its mean value in time*

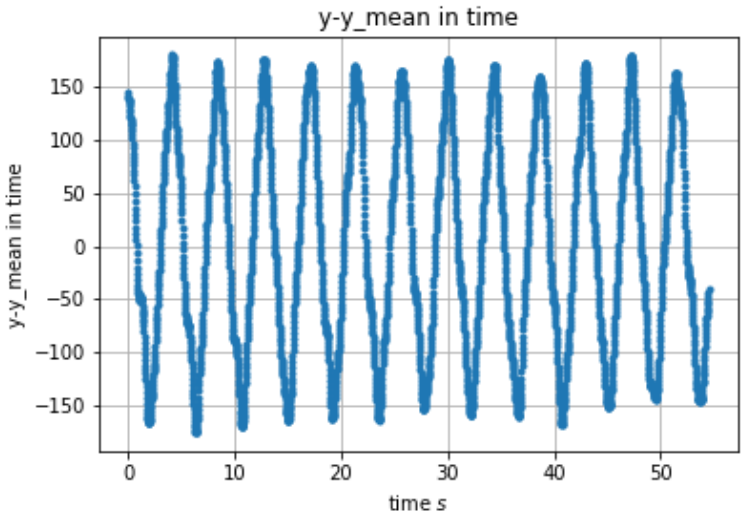

(b) *Difference between y and its mean value in time*

Figure 4.9: Trend of the difference between positions are their mean values in time

In particular, I computed the rotational frequencies that will be reported in chapter **??** as follows:

$$f_{\mathrm{rot}} = \frac{\Omega}{2\pi} \tag{4.46}$$

in Hz, both for x and y coordinates. The standard deviation of ω can be extracted from the results of the `curve_fit` function as explained before. From $\Delta\omega$ the standard deviation related to f_{rot} can be computed as:

$$\Delta f_{\mathrm{rot}} = \frac{\Delta\omega}{2\pi}. \tag{4.47}$$

The linear velocity v associated to the circular motion has been computed as:

$$v = f_{\mathrm{rot}} r, \tag{4.48}$$

both for x and y coordinates, where r is the trajectory radius calculated as in equation 4.17. In consequence:

$$\Delta v = v\sqrt{\left(\frac{\Delta f_{\mathrm{rot}}}{f_{\mathrm{rot}}}\right)^2 + \left(\frac{\Delta r}{r}\right)^2}, \tag{4.49}$$

where the radius standard deviation has been computed as in equation 4.22.

After subtracting this sinusoidal function from the x and y coordinates frame by frame, I obtained the particle motion random component, which is the only one contributing to the particle kinetic temperature and from which I computed it for the particles doing this kind of periodic motion superimposed to the random one. I called these x and y just related to the particle random motion `Dx` and `Dy`, which I computed frame by frame as follows:

```
Dx[i]=random_x[i]-sinx[i]
Dy[i]=random_y[i]-siny[i]
```

See figure 4.10 for `random_x` and `random_y` sinusoidal fit.

- Rotational angle as a function of time.

  The distance of the particle from the centre of the trajectory, which is `(mean_x,mean_y)`, belongs to a half-line that forms an angle with the half-line starting form `(mean_x,mean_y)` and going horizontally towards right. The angle is considered positive when starting form the horizontal half-line and reaching anti-clockwise the half-line the distance of the particle position from `(mean_x,mean_y)` belongs to. I will call this angle as rotational angle. I calculated it as a function of time the following way (@ corresponds to a tabulator space):

  ```
  alpha=np.ones(len(x))
  for i in range(len(x)):
  ```

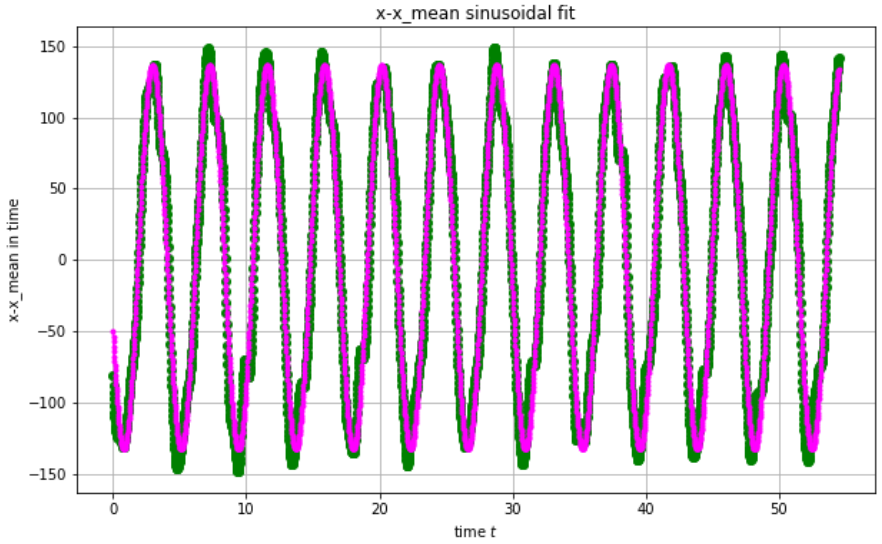

(a) *Sinusoidal fitting of the difference between x and its mean value in time*

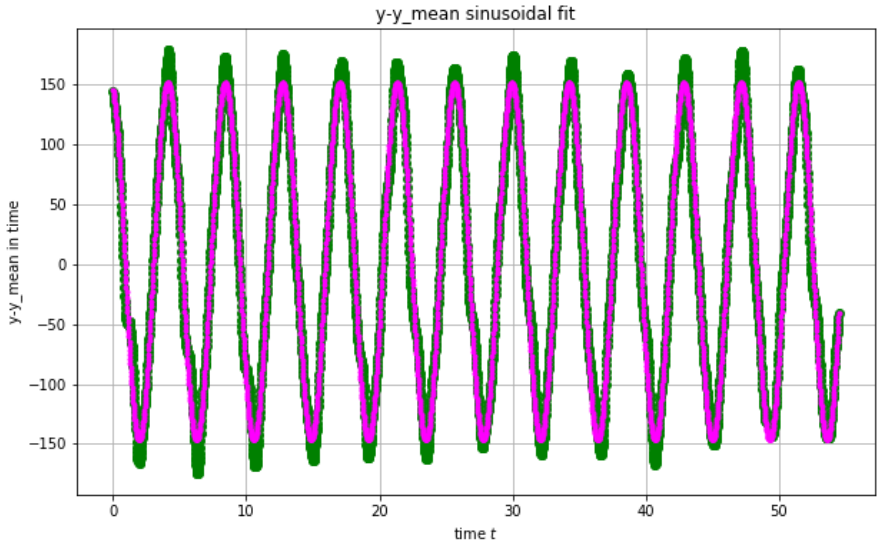

(b) *Sinusoidal fitting of the difference between y and its mean value in time*

Figure 4.10: Sinusoidal fitting of the difference between the positions and their mean value in time

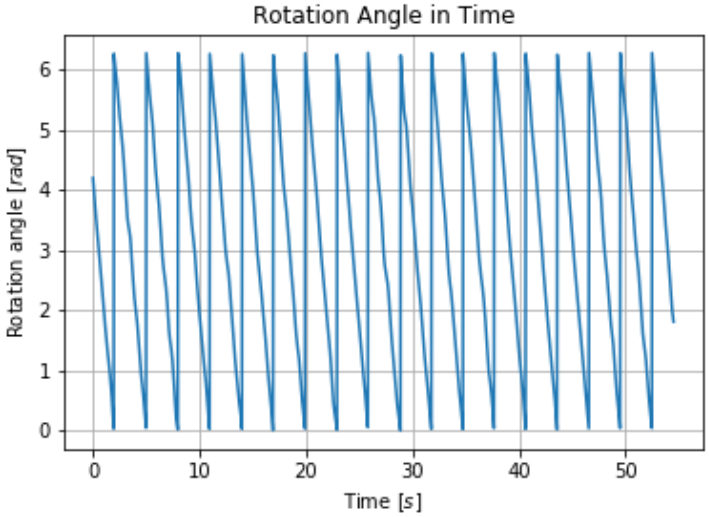

Figure 4.11: Example of rotational angle in time for a circular trajectory

```
@ if ((y_m[i]-mean_y)>0) and ((x_m[i]-mean_x)>0):
@@ alpha[i]=np.arctan((y_m[i]-mean_y)/(x_m[i]-mean_x))
@ if ((y_m[i]-mean_y)>0) and ((x_m[i]-mean_x)<0):
@@ alpha[i]=(np.pi/2)+((np.pi/2)+np.arctan((y_m[i]-mean_y)/(x_m[i]-mean_x)))
@ if ((y_m[i]-mean_y)<0) and ((x_m[i]-mean_x)<0):
@@ alpha[i]=(np.pi)+np.arctan((y_m[i]-mean_y)/(x_m[i]-mean_x))
@ if ((y_m[i]-mean_y)<0) and ((x_m[i]-mean_x)>0):
@ alpha[i]=(np.pi*3/2)+((np.pi/2)+np.arctan((y_m[i]-mean_y)/(x_m[i]-mean_x))).
```

Then I plotted it and an example of it in case of a circular trajectory is shown in figure 4.11. If the angle is growing in time, then the particle is moving anti-clockwise, otherwise clockwise. The jump from 2π to 0 or viceversa is caused by passing through the horizontal half-line.

- The temperature just due to the random component of the particle motion.

  I calculated it with the three previously explained procedures starting from `Dx` and `Dy`:

  1. kinetic temperatures: T_x, T_y and T_{2D}
  2. two-dimensional temperature from Maxwellian fit
  3. one-dimensional temperatures from Gaussian fit
  4. two-dimensional temperature from MSD initial part parabolic fit

  For the last three ones see figure 4.12. Notice once more that all the figures shown in the present and the next section are the the result of the analysis of the same

recording. It is really different what is shown in figure 4.6 and 4.12: the only thing that changes is that the histogram is created with "complete" velocities in case of figure 4.6 and with velocities computed from positions after subtracting the circular motion in figure 4.12.

- New velocity distribution functions and new temperature from Maxwellian fitting
- Comparison of Gaussian and Maxwellian functions resulting from fitting with the ones calculated with `v_x`, `v_y` and the kinetic temperature, respectively. The "comparison" Maxwellian curve was calculated as follows:

  ```
  maxwellian =(mass/Kb/T[0])*bins_v2D*
  np.exp(-(mass*(bins_v2D**2)/2/Kb/T[0]))
  ```

  where `mass` is particle mass, `Kb` the Boltzmann constant and `T[0]` the two-dimensional kinetic temperature. The "comparison" Gaussian curve as:

  ```
  gaussian_vx = (1/np.sqrt(2*np.pi*(v_x_sigma**2)))*
  np.exp(-(bins_vx-v_x_mean)**2/2/(v_x_sigma**2))
  ```

  where `np.pi` is π, `v_x` the single frame one-dimensional x velocity, `v_x_mean` the mean value of v_x python list and `v_x_sigma` its standard deviation.

  This comparison is made to distinguish between the velocity two components better. The first one is related to self-propelling, due to which the particle moves with constant angular velocity, along the geometrical shape of the trajectory, in the parabolic potential well. The second one is related to thermal agitation. Statistical mechanics postulates that the velocity distribution in this case is the Maxwellian distribution shifted in velocity space according to the hydrodynamics velocity.

- New MSD and new temperature obtained from the fit of the initial part of MSD curve. See figure 4.13 for the example associated with the analysis I am showing. Even if the difference between figures 4.8 and 4.13 is not easy to notice, the two fits return two different values for A and consequently two different temperatures.
- Pixel locking.

  In principle, the particcle positions given by `ImageJ` should have the fractional part homogeneously distributed over all the possible values it can assume because there is no reason why the fractional part should always be the same or it should never assume certain values. Moreover, for some reasons not fully understood, sometimes it happens that just some values are assumed by the fractional part of the positions or that some values are particularly frequent with respect to others instead of appearing all with the same frequency. This phenomenon is called pixel locking and when it is present the positions found by the program are no longer reliable. See figure 4.14 in order to have a look at what fractional parts of x and y look like without pixel

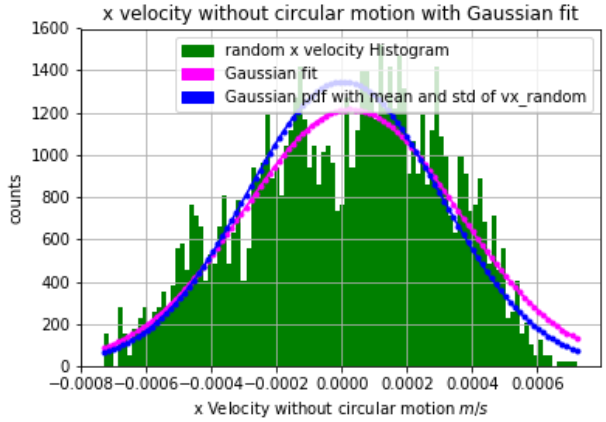

(a) *x one-dimensional velocity distribution function, computed after subtracting the circular motion, fitted with a Gaussian distribution function*

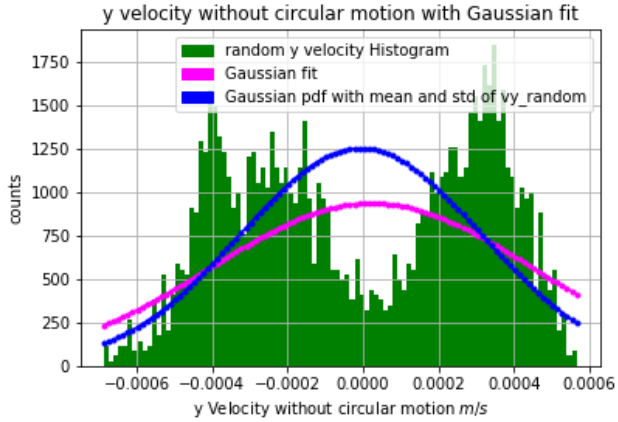

(b) *y one-dimensional velocity distribution function, computed after subtracting the circular motion, fitted with a Gaussian distribution function*

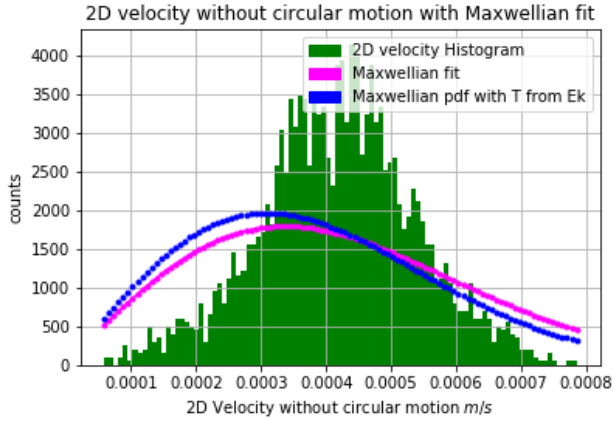

(c) *Two-dimensional velocity distribution function, computed after subtracting the circular motion, fitted with a Maxwellian distribution function*

Figure 4.12: One- and two-dimensional velocity distribution functions, computed after subtracting the circular motion, fitted with the proper distribution functions

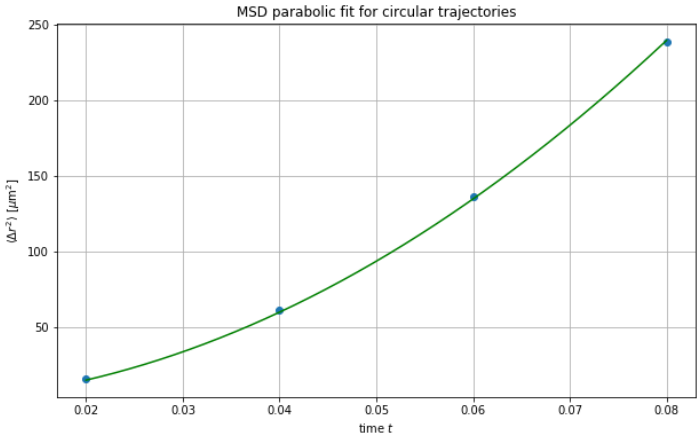

Figure 4.13: Example of MSD initial part parabolic fit where MSD is computed with the positions obtained after subtracting the circular motion

locking. The first two images show examples of fractional part of x and y versus the frame number in case of no pixel locking and the third one comes from graphing the fractional part of y and x one versus the other again in the case of no pixel locking.

Figure 4.15 on the other hand gives an example of fractional parts of x and y when some pixel locking is present. In particular in its last image it is possible to see some spots were the fractional parts tend to concentrate.

The graphs of the figure were created just considering the fractional part of the positions:

```
fractional_x=np.ones(frames)
fractional_y=np.ones(frames)
for j in range(frames):
      fractional_x[j]=round(math.modf(data2[j][3])[0],3)
      fractional_y[j]=round(math.modf(data2[j][4])[0],3)
```

where the function `math.modf(number)` from the `math` package returns a two-dimensional array whose first value is the result of subtracting to `number` its integer part and the second value is just `number` integer part. The built-in function `round(number,ndigits)` returns the value `number` rounded to `ndigits` after the decimal point. Then the fractional parts `fractional_x` and `fractional_y` are plotted versus the frame number as per the first and last two graphs of figure 4.15 and then one versus the other.

The positions found with `ImageJ` seldom have the problem of pixel locking and

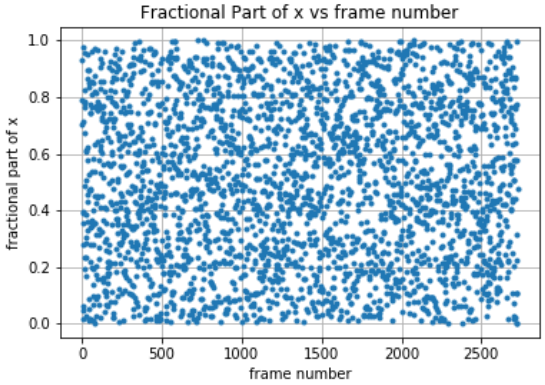

(a) *Fractional part of x vs frame number*

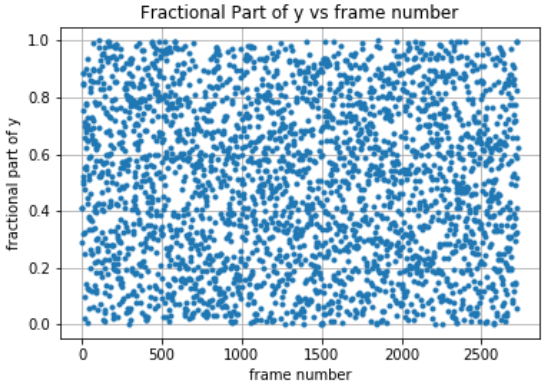

(b) *Fractional part of y vs frame number*

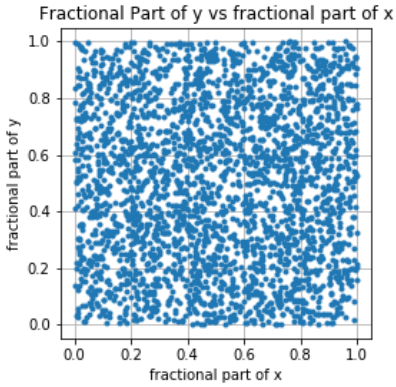

(c) *Fractional part of y vs fractional part of x*

Figure 4.14: Pixel locking absent

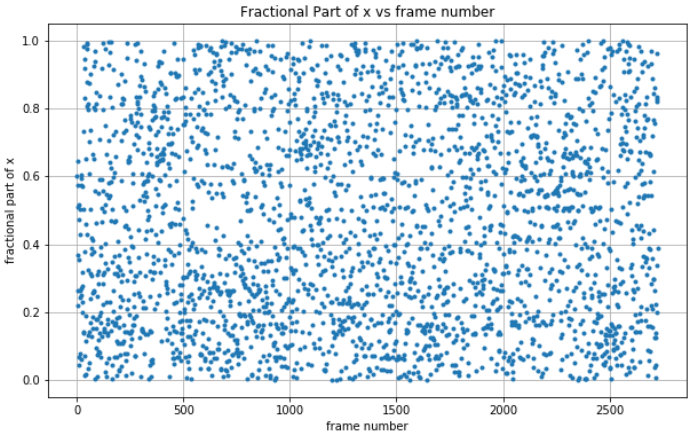

(a) *Fractional part of x vs frame number*

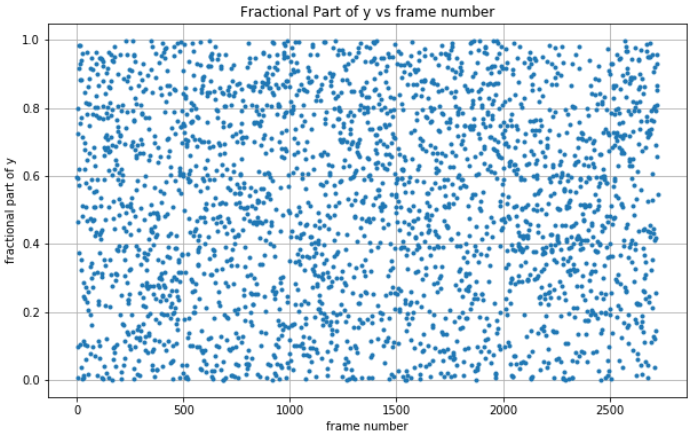

(b) *Fractional part of y vs frame numberg*

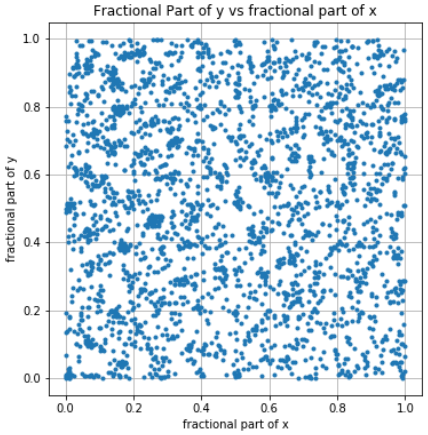

(c) *Fractional part of y vs fractional part of x*

Figure 4.15: Pixel locking weakly present

mainly just for the frame sequences recorded with the laser off and the torch on.

4.1.2 Analysis with `Trackpy`

I also used a Python package for particle tracking whose name is `Trackpy` [31]. I used it just in order to check the results of the analysis performed starting with `ImageJ` and in cases with `ImageJ` it has been impossible for me to track the particle position in time. This is because the program gives a lot of pixel locking in my case. The reason could be that imaging with the microscope does not return a Gaussian shape of the particle, while `trackpy.batch`, the `Trackpy` function locating the particle, actually locates properly just Gaussian-like blobs. Figure 4.16 shows an example of fractional parts of x and y positions returned by `Trackpy`. They have been actually obtained for a different recording with respect to all the other figures showing parts of the analysis. In particular, the analysis previously shown in the section is one of the few cases for which `Trackpy` does not return pixel locking.

Some of the shown results for the case of laser off have been obtained with `Trackpy`, but the velocity distribution functions computed with `Trackpy` are never shown because they are not reliable because of pixel locking.

It is interesting to underline that pixel locking does not give any problems for some parts of the analysis such as tracking the trajectory or computing the kinetic temperature or the temperature out of MSD initial part parabolic fit, but, for example, it causes big problems with the velocity distribution functions.

In figure 4.17, a frame is shown with a Janus particle in which the particle has been found and circled by `Trackpy`.

4.2 Experiments

In this section, I provide a list of the experiments performed and for each of them an explanation of the reason why they have been performed and a brief description of how they were performed. The experimental setup used is the one described in chapter 2.

It needs to be specified that all the experiments have been performed in undisturbed conditions because in every case just before recording:

- the fan of the turbo pump has been switched off
- the gas flow in the vacuum chamber has been switched off
- the light in the laboratory has been switched off
- the camera cooling fan has been switched off: see figure 4.18.

As already explained in the introduction the aim of the present work is to verify if Janus particles are active also in complex plasma environment. In particular, it is important

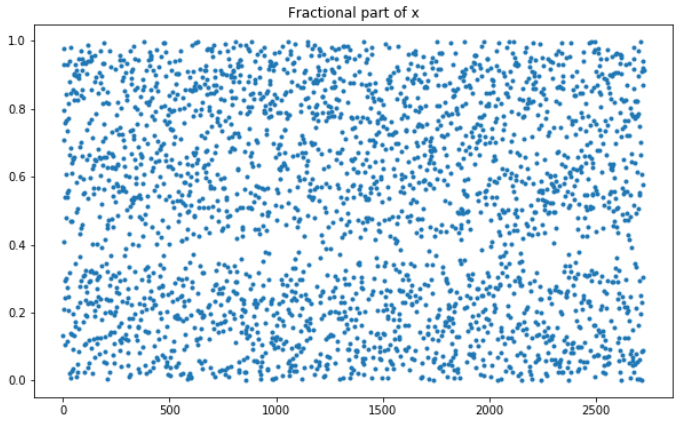

(a) *Fractional part of x vs frame number when pixel locking is present*

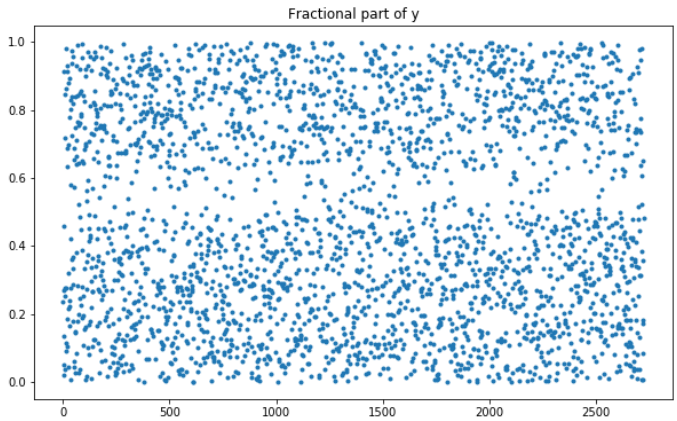

(b) *Fractional part of y vs frame number when pixel locking is present*

Figure 4.16: Fractional parts of x and y returned by `Trackpy` in case of pixel locking present

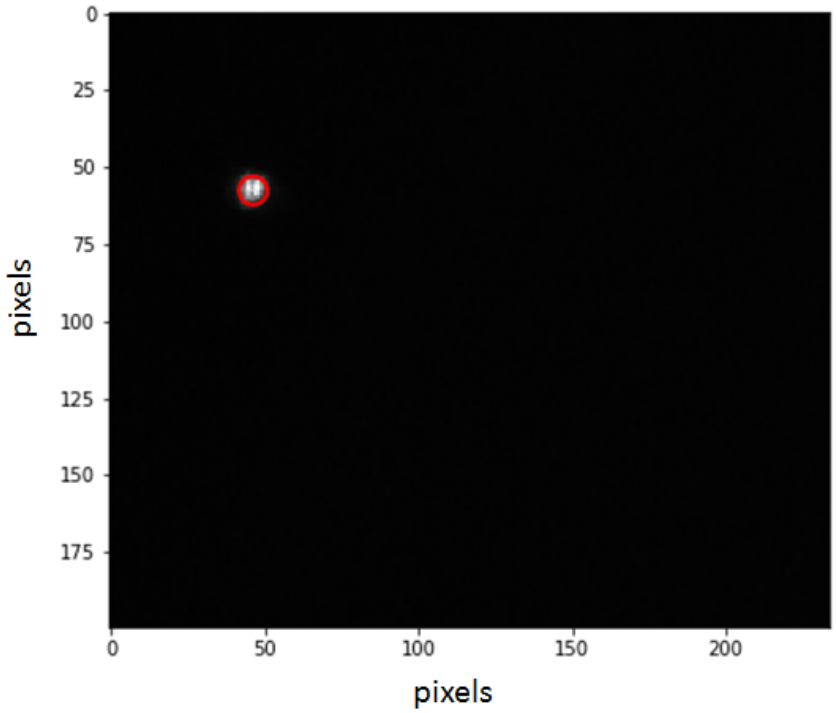

Figure 4.17: A Janus particle in the first frame of one experiment found by `Trackpy`

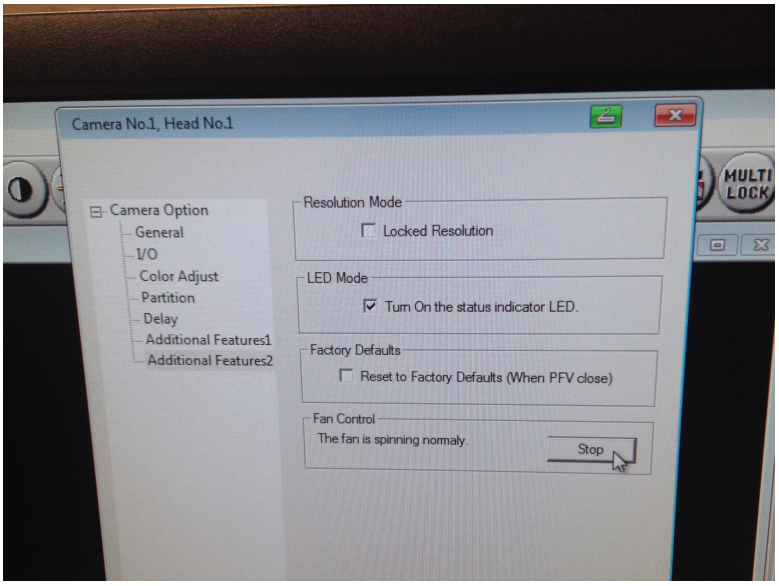

Figure 4.18: "Camera option" of PFV software: fan control

to understand which forces among the ones discussed in chapter 3 are acting or at least which ones are more important. Just to recall them, the forces acting on a Janus particle as self-propulsion mechanisms in plasma are:

1. Radiation pressure force
2. "Photophoresis" due to different accommodation coefficients
3. Photophoresis due to a temperature gradient on the particle surface
4. Asymmetric ion drag force

The calculations in chapter 3 leading to an estimation of these forces can in principle be verified experimentally. The expectation is that, if Janus particles are active in plasmas thanks to the action of these forces, then the observed trajectories should resemble the ones discussed in section 3.3. While observing single Janus particle trajectories, I used to change some parameters in order to understand something about the acting forces. Then I also performed experiments with pure MF particles having the same dimensions of the Janus particles used, which were actually produced starting from them. These experiments were done in the same conditions as the ones with Janus particles, in order to have the possibility of making a direct comparison between the two types of particles. As already mentioned, in the past some experiments with single MF particles were performed in the group.

4.2.1 Experiments where the laser power was varied

The horizontal laser powers used for these experiments are:

1. 0 mW
2. 14 mW
3. 99 mW.

The pictures of the setup with different horizontal laser powers applied are shown in figure 4.19. During these experiments RF power was kept at 5 mW and plasma pressure at 1,33 Pa.

The two self-propelling mechanisms depending on the laser power are radiation pressure and photophoresis due to the temperature gradient grad$T$ on the particle surface:

$$\text{Radiation pressure} \propto \text{laser power}$$

$$\text{grad}T \text{ induced photophoresis} \propto \text{laser power}$$

$$\Delta\alpha \text{ induced "photophoresis"} \propto \text{laser power}$$

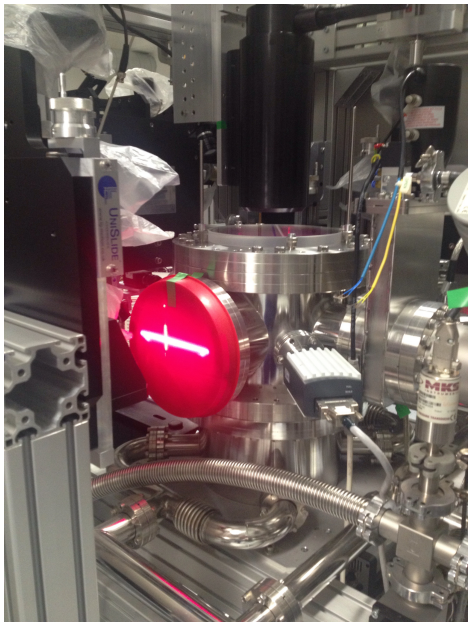

(a) 99 mW *horizontal laser power*

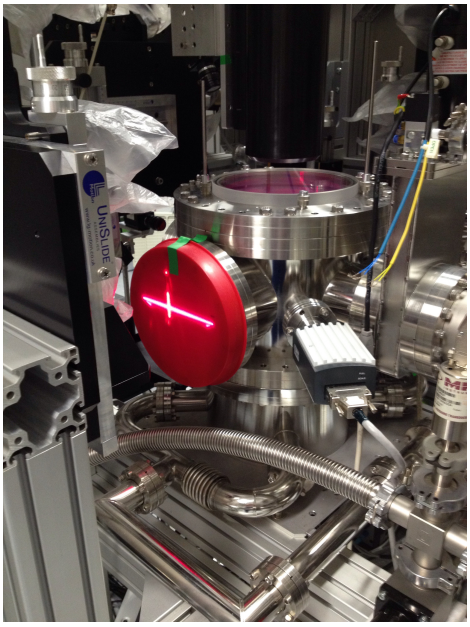

(b) 14 mW *horizontal laser power*

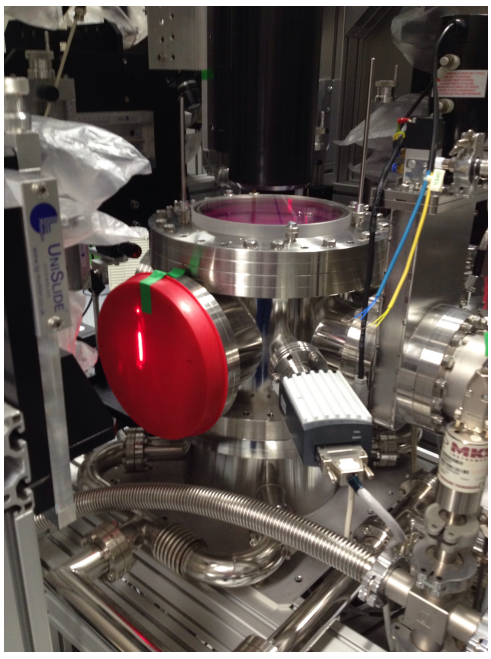

(c) 0 mW *horizontal laser power*

Figure 4.19: Different horizontal laser powers used

For this reason, the aim of this series of experiments is to understand if these forces are present and how Janus particle behaviour depends on them. In particular, if these forces are actually acting on the Janus particles, then their effect should be stronger the stronger the laser power is. Of course, these conclusions are not firm and everything needs to be considered with caution. In fact:

- the theory of photophoresis is not easily applicable to particles in plasmas because of the presence of charged particles
- the two photophoretic mechanisms act together
- the thermal insulating nature of the MF makes the temperature distribution on its surface not as trivial as I assumed in my calculations of section 3.1.3
- the particle is most probably spinning.

Unfortunately, these forces act together and just changing the laser power there is no clue of shifting their contributions. The only way of separating them is changing the gas pressure at high laser power because the radiation pressure force is fixed with the laser power, while photophoreses become larger with gas pressure, see section 4.2.3.

Anyway, both the combined effect of photophoreses and radiation pressure are not weak forces as far as predicted by my calculations of chapter 3, so the expected effect of a change in the laser power is strong.

The whole analysis described in section 4.1.1 was performed on all the single Janus particle motions recorded changing the laser power; the changes in the trajectory shape, kinetic temperature and all other data extracted from the analysis have been analysed.

4.2.2 Experiments where the RF power was varied

The different RF powers used for this series of experiments are:

1. 1 W
2. 5 W
3. 20 W.

During these experiments plasma pressure was kept at 1,33 Pa.

Two important plasma parameters change with RF power: the ion density and the electron temperature:

$$n_i \quad \text{increases with} \quad \text{RF power}$$

$$T_e \quad \text{increases with} \quad \text{RF power}$$

The aim of these experiments is to understand what is the relative importance of the ion drag force and if this result matches the theoretical predictions in section 3.1.1. The bigger n_i and T_e are, the stronger the ion drag force should be:

$$\text{Asymmetric ion drag} \propto n_i$$

$$\text{Asymmetric ion drag} \propto T_e$$

My calculations have shown that the net force due to the asymmetric ion drag is really small compared to the other ones acting and if this theoretical prediction was true, then it would mean that changing the ion drag force should not change things much.

Also the laser power was changed during these experiments in order to consider even the dependence of the changes with RF power on the laser power. For example, if photophoresis due to the grad$T$ on the particle surface is absent in case of zero laser power, then maybe it is possible to observe something more related to asymmetric ion drag effects with the laser power off.

4.2.3 Experiments where the gas pressure was varied

The different gas pressures used are:

1. 1,3 Pa
2. 4,0 Pa
3. 6,7 Pa
4. 10,0 Pa
5. 13,3 Pa.

During these experiments RF power was kept at 5 mW.

Two important parameters change with the gas pressure: neutral density and electron temperature:

$$n_n \propto p$$

$$T_e \quad \text{increases with} \quad \frac{1}{p}$$

where p is the gas pressure.

Also the ion density changes with neutral density, because, if the RF power is fixed, the ion over neutral number ratio is fixed and the relative importance of the two forces does not change:

$$n_i \propto n_n$$

This series of experiments is aimed to study what happens when the number of gas molecules is increased. In particular, the monitored forces are supposed to be the photophoresis due to grad$T$ and the one due to different accommodation coefficients. In fact, as already explained, they are actually mechanisms driven by the collisions of neutrals

with the particle. The larger the number of neutrals, the larger both these forces should be. Moreover, when neutral density is increased, the ion density increases too and for this reason also asymmetric ion drag should increase.

$$\text{grad}T \text{ induced photophoresis} \propto n_n$$

$$\Delta\alpha \text{ induced "photophoresis"} \propto n_n$$

$$\text{Asymmetric ion drag} \propto n_i$$

When so many parameters change, then it is not trivial at all to understand what happens to Janus particles during these experiments. The shape of the trajectory performed and the particle temperature are observed while the gas pressure is changing.

As before, also the laser power was changed in this series of experiments. This is because photophoresis due to grad$T$ strongly depends on it, while "photophoresis" due to $\Delta\alpha$ does not. For this reason, using the laser power in the experiments makes it possible to observe how the first mechanism works and in particular, as already mentioned, to distinguish between its contribution and the one of radiation pressure, while in the 0 mW laser power experiments of this series it is possible to observe how the second mechanism works. It is important to always keep in mind that the action of the two photophoretic mechanisms can never be separated completely because of their intrinsic nature. In addition, always keep in mind that "photophoresis" due to $\Delta\alpha$ can act alone or almost alone as the temperature gradient with the laser off is even smaller than when it is on, while the mechanisms of radiation pressure and photophoresis due to the temperature gradient not only are always acting together, but they also always act in the presence of the "photophoresis" due to $\Delta\alpha$, which is always there.

4.2.4 Temporal-development experiments

These experiments are aimed to take into account a possible sputtering of the platinum layer due to the plasma action. In particular, if this sputtering process really happens, then a transition from Janus particle to pure MF particle behaviour should take place with time. It is also interesting to see if there is anything that influences the particle behaviour and if this factor changes alone. For example, one parameter that could autonomously change in time is Janus particle spinning and in particular the rotational axis of the particle and the spinning frequency. The spinning mechanism is in fact not fully understood, but just hypothesized with reasonable motivations.

4.2.5 Experiments with the confining ring shifted

As it will be shown in chapter 5, it is very common to observe circular trajectories for Janus particles, like the one shown in figure 4.2. This series of experiments has the important

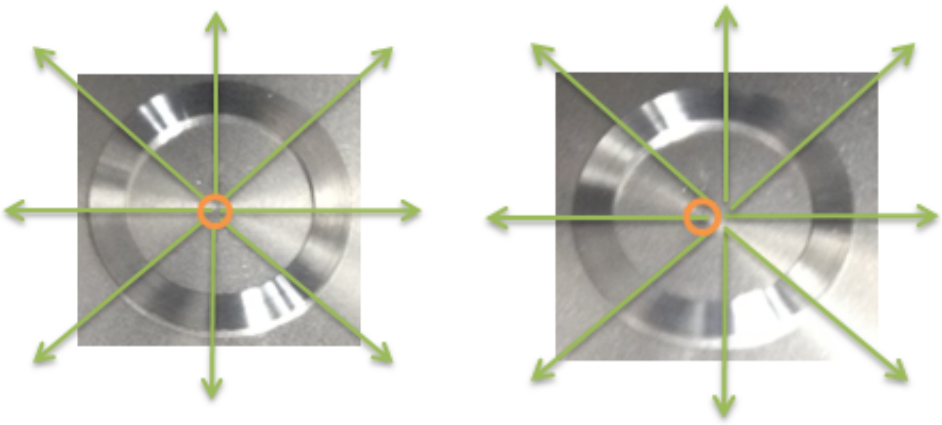

(a) *Schematic representation of the interaction of the ion flow with the particle when the ring is centred on the lower electrode*

(b) *Schematic representation of the interaction of the ion flow with the particle when the ring is not centred on the lower electrode*

Figure 4.20: Interaction of the ion flow with the particle. The particle position is represented by the orange circle and the ion flow by green arrows.

aim to check if the circular motion of Janus particles is caused by factors other than the four forces taken into account so far. If this was true, it would mean that the circular motion shown by the particles is not a proof of their active nature.

In particular, the factors that could cause a circular motion by themselves, without having anything to do with a self-propulsion mechanism, are:

- Ion flow going from the centre of the lower electrode to the edges due to ambipolar diffusion: see figure 4.20.

  If the confining ring was not perfectly centred on the lower electrode, then the Janus particle would be in an environment characterized by a broken symmetry due the ion flow and this asymmetry might make its trajectory circular [32]. For this reason, after shifting the ring I expect to see a much bigger effect that would lead to a much stronger circular motion. This would prove that the circular behaviour is due to the fact that the ring is not perfectly centred on the lower electrode and that it has nothing to do with the Janus particle activity in plasmas. On the other hand, if the effect of symmetry breaking due to ion flow was weak, then no significant changes should be observed if the ring is shifted. Actually this symmetry breaking due to ion flow is not very likely to be the cause of the circular motion because the direction of the particle circular motion is not always the same, not even for one particle it is the same, while the ion flow always goes in the same direction with respect to the ring.

- Distortion of the shape of the potential well due to the focus of the laser: an additional potential well may appear next to the main one and this may cause the co-presence of two potential minima. See figure 4.21 for a schematic representation.

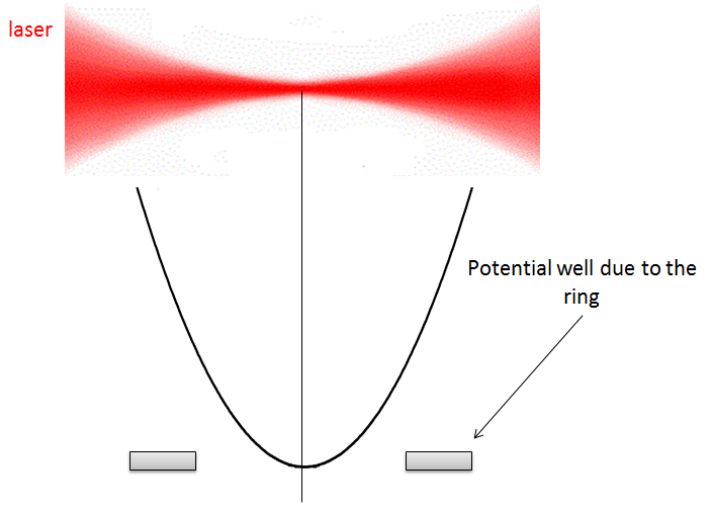

(a) *Shape of the resulting potential well in the case the minimum of the potential well due to the presence of the ring and the beam waist are aligned*

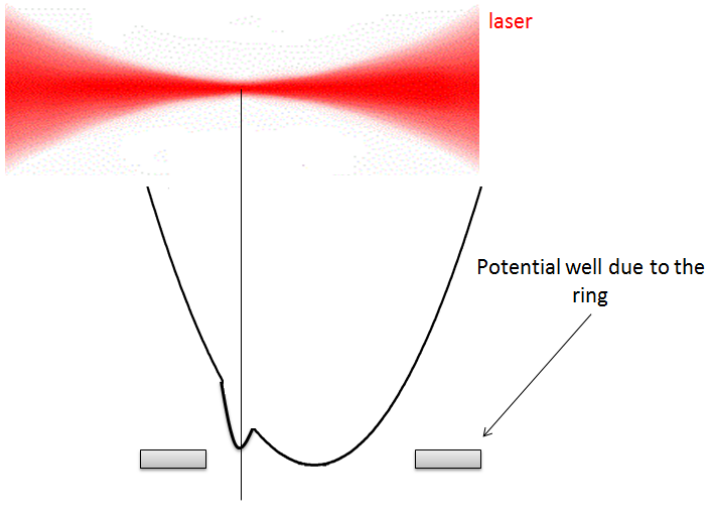

(b) *Shape of the resulting potential well in the case the beam waist is shifted with respect to the minimum of the potential well due to the presence of the ring*

Figure 4.21: Shape of the potential well according to the confining ring position

In particular, if the beam waist was small enough, then the relative minimum would be important enough to have an effect on the particle trajectory. This is anyway not likely to be my case, because the laser beam was defocused a little bit specifically to avoid this kind of consequences. But, if this was the cause of the circular motion of the particles, then when the ring is shifted in this series of experiments the circularity of the motion would become stronger and clearer, with a larger radius and a less smeared circumference. Otherwise, if this effect is too weak to cause a circular motion, than the result would be the same as usual. In particular, considering that the particle would move in a three-dimensional "doughnut" generated by the two minima, then the diameter of the circular motion would be as large as the ring shift. Of course, also this second effect can be the cause of a rotation just if in the other experiments the ring was not perfectly centred on the lower electrode.

- Co-presence of two different confining potential wells.

  One is due to the ring and the other to the ion density distribution in the plasma. The two central parts of the wells could produce two close minima in the overall confining potential well which would induce a circular motion. The mechanism is basically the same as before, but the second minimum would be caused by something different. See figure 4.22 for a simple representation of the situation.

  The discussion about what the results can tell us is the same as in the previous case.

In order to perform these experiments, the ring was shifted by 2 mm with respect to the centre of the lower electrode: see figure 4.23 for the setup used in these experiments. Note that the ring shift was estimated by measuring the distance of the camera from its usual position. Actually, I moved the camera in order to have the particles in the centre of the microscope field of view once again.

4.2.6 Experiments with pure MF particles

A very important step of this work is the comparison between pure MF and Janus particles in plasmas. In fact, the mechanisms that lead Janus particles to self-propulsion do not act on pure MF particles. They are described in detail in section 3.1. Below, a short list of the reasons why these mechanisms do not act on MF particles is included:

1. The ion drag force is symmetric on a pure MF particle and so there does not exist a net force acting on the particle due to its asymmetry.

2. Radiation pressure acts just as an external force: there is no conversion of this force into self propulsion because of the homogeneity of pure MF particle surface.

3. The grad$T$ on pure MF particle surface is null because there are no different materials with different optical or thermal properties on it. Even negative photophoresis is not

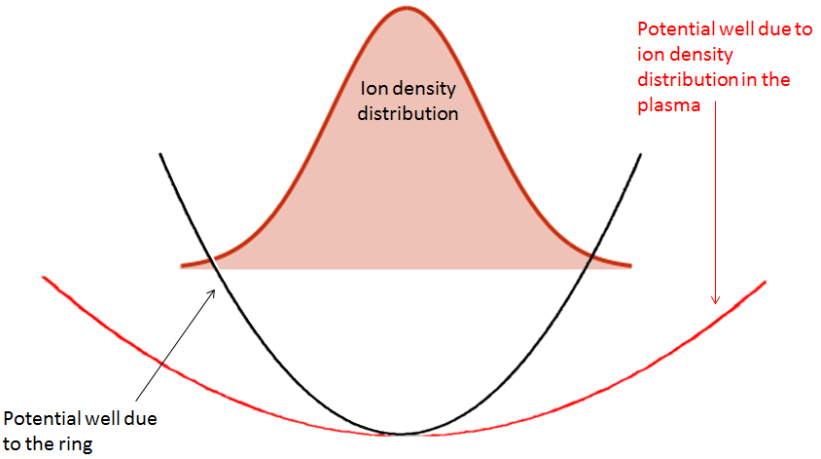

(a) *Case in which the potential well due to the ring and the one due to ion density distribution in plasma are perfectly aligned: the ring is perfectly centred on the lower electrode*

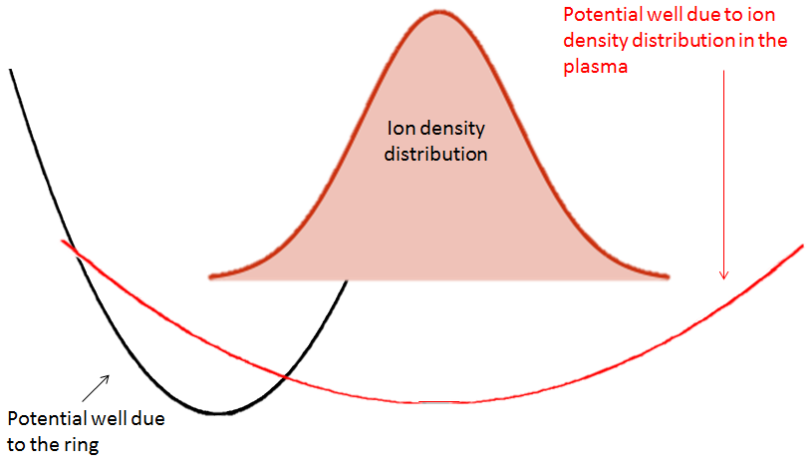

(b) *Case in which the potential well due to the ring and the one due to ion density distribution in plasma are not aligned: the ring is shifted with respect to the centre of the lower electrode*

Figure 4.22: Relative position of the potential well due to the confining ring and the one due to the ion density distribution in plasma according to the ring position

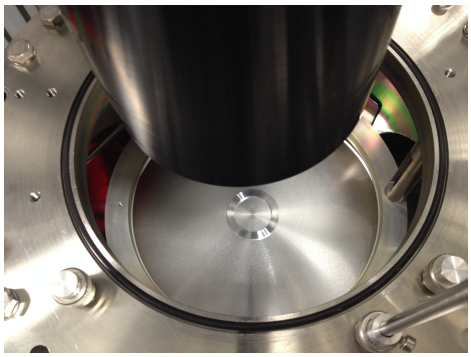

(a) *Picture of the ring centred on the lower electrode*

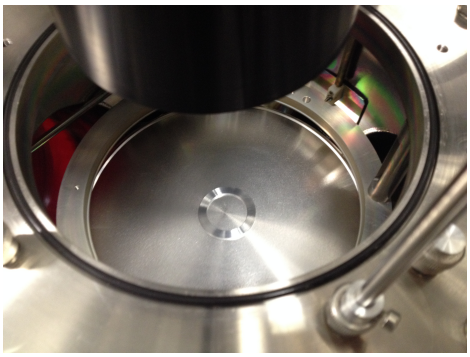

(b) *Picture of the ring shifted* 2 mm *with respect to the centre of the lower electrode*

(c) *Picture of the camera after moving it. The black line was traced with a pen before moving the camera.*

(d) *Zoom-in of the previous picture*

Figure 4.23: Setup for experiments with the confining ring shifted by 2 mm

present in general, but just in very specific cases: in fact, it has been observed in the past that negative photophoresis produces a measurable effect on MF particles just if they are damaged with deformations or defects [1] and this is true just for a very small percentage of them.

4. The accommodation coefficient is always the same on the MF particle surface because of its homogeneity.

For this reason, pure MF particles are "passive" and Jaunus particles should be active. In the past in the group tens of MF particles have been observed [33]: they have always moved with a passive Brownian motion and almost never showed the peculiar trajectories discussed in section 3.3. For the three cases in which they showed a circular behaviour, an educated guess is that those particles had some rare damage on their surfaces. The trajectories of all other pure MF particles were random.

I added to all those observations some more. In particular, I observed pure MF particles with exactly the same diameter as my Janus particles, which means that the only difference between the two is the thin platinum layer.

For all the experiments performed with single MF particles, the same aluminium ring generating the confining potential well that has been used for single Janus particle experiments has been positioned in the centre of the lower electrode.

Summary of chapter 4

The experiments were performed with single Janus particles suspended in the plasma generated with a 13,6 MHz RF frequency from argon gas in a GEC (*Gaseous Electronics RF Reference Cell*) chamber. Their aim was to highlight the presence of "active motion" of the Janus particles in the plasma and to analyse the four forces acting on the Janus particles as propulsion mechanisms from an experimental point of view. The series of experiments performed are:

- experiments where the laser power was varied (used values: 0 mW, 14 mW, 99 mW): F_{laser}, $F_{\Delta T}$, $F_{\Delta\alpha} \propto$ laser power
- experiments where the RF power was varied (used values: 1 W, 5 W, 20 W): $F_{\text{asym. ion drag}}$ increases with RF power
- experiments where the gas pressure was varied (used values: 1,3 Pa, 4,0 Pa, 6,7 Pa, 10,0 Pa, 13,3 Pa): $F_{\Delta T}$, $F_{\Delta\alpha} \propto$ laser power and $F_{\text{asym. ion drag}}$ increases with RF power
- temporal-development experiments
- experiments with the confining ring 2 mm shifted with respect to the centre of the lower electrode: the aim of this series of experiments is to verify that the "active" behaviour of Janus particle is actually due to a self-propulsion mechanism and not to:
  - symmetry breaking caused by the ion flow going from the centre of the chamber to its edges due to ambipolar diffusion
  - distortion of the shape of the potential well due to the focus of the laser (an additional potential minimum may appear next to the main one and this may cause the co-presence of two potential minima)
  - co-presence of the confining potential well due to the presence of the ring and the potential well due to the ion density distribution in plasma (the two central parts of the wells could produce two close minima in the overall confining potential well which would induce a circular motion)

- experiments with regular MF particles.

For every series of the experiments performed, I analysed more than one particle in order to obtain some statistics about the results. Moreover, for each particle I performed more than one recording because one was needed every time I changed one parameter in order to get a response to what happened to the particle after changing something. In particular, every recording consists of 2726 frames recorded at a speed of 50 frames per second. I used the software `ImageJ` in order to trace the particle position in time and, starting from the particle positions, I wrote some codes on `Python` in order to:

- trace the particle trajectory
- compute its dimensions ("radius")
- produce the power spectrum of the particle position and brightness
- compute the one- and two- dimensional velocities frame by frame
- compute directly from velocities one- and two-dimensional kinetic temperatures
- plot one- and two-dimensional velocity distribution functions
- compute one- and two-dimensional kinetic temperatures with Gaussian and Maxwellian fit of the velocity distribution functions
- plot the Mean Squared Displacement (MSD)
- compute the temperature from the parabolic fit of the initial part of the MSD
- subtract the non-random component of the motion with a sinusoidal fit (in the case this was possible, then also the following steps were followed)
- plot the rotational angle in time
- compute the kinetic temperature from the isolated random component of the particle motion
- check if "pixel locking" was present.

Chapter 5

Results and discussion

In this chapter, I will report the results obtained performing the experiments described in the previous chapter. In particular, before going through the detailed results of all the experiments described, I will present the general result obtained with Janus particles and compare it with the general result obtained for MF particles. This comparison, together with the qualitative comparison between experimental trajectories of Janus particles and those numerically predicted in Ref. [19] and presented in section 3.3, will prove that Janus particles are active in complex plasma environment. This is beacuse the trajectories obtained can just be explained when a net propulsion force is acting on the particle. This means that the forces described in chapter 3 are actually acting on the Janus particles observed. In particular, some of the resulting trajectories can just be explained if the propulsion force is varying in time with a constant frequency and this will prove the validity of the theoretical discussion at the end of chapter 3.

After proving that Janus particles are active in plasmas in section 5.1, I will discuss the results of the more detailed experiments explained in chapter 4. These will lead to some conclusions about the acting forces and, in particular, the theoretical predictions about the relative strength of the forces in chapter 3 will be compared with the experimental results.

5.1 Janus particle activity in complex plasma environment

I observed different kinds of trajectories performed by Janus particles in the complex plasma environment used in my experiments. They are:

- circles
- *epitrochoids*

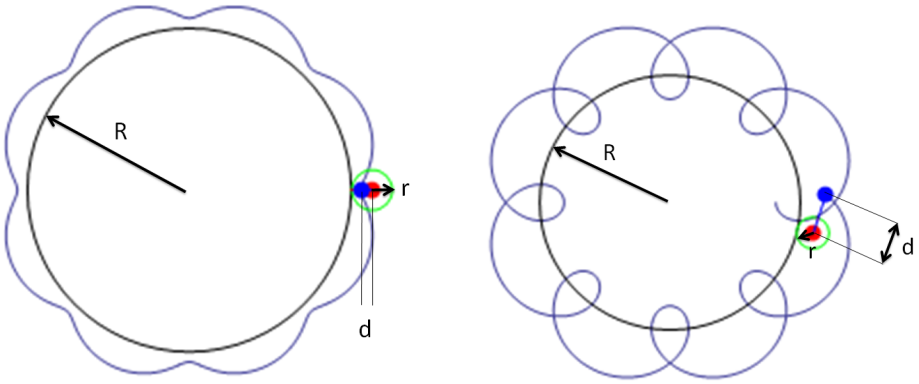

(a) *Epitrochoid with $R > r$ and $d < r$* **(b)** *Epitrochoid with $R > r$ and $d > r$*

Figure 5.1: Some of the observed trajectory shapes

- apparently random trajectories.

An *epitrochoid* is defined as a roulette traced by a point attached at a distance d from the centre of a circle of radius r rolling around the outside of a fixed circle of radius R. The observed *epitrochoids* are:

- *Epitrochoids* with $R > r$ and $d < r$ (see figure 5.1).
- *Epitrochoids* with $R > r$ and $d > r$ (see figure 5.1).
- *Epitrochoids* with $R = r$, which are called *limaçons*, with:
  - $d < r$: *dimpled limaçon*
  - $d = r$: *cardioid* or *epicycloid with* $k = 1$ or *limaçon with cusp*
  - $d > r$: *looped limaçon.*

  Note that *epicycloids* are particular kinds of roulettes produced by tracing the path of a chosen point on the circumference of a circle of radius r which rolls without slipping around a fixed circle of radius R. For *epicycloids* $k = R/r$. See figure 5.2 for these three geometrical figures in the same order.
- *Epitrochoids* with $R = 2r$, which are called *epicycloids with* $k = 2$ or *bilobed epicycloids*, with:
  - $d < r$: *dimpled*
  - $d = r$: *with cusps* or *nephroid*(see figure 5.3)
  - $d > r$: *looped*

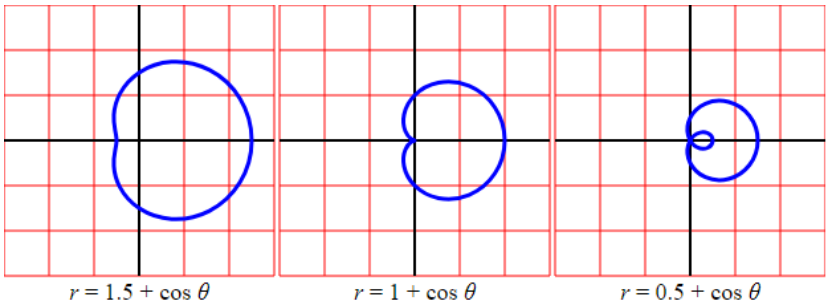

Figure 5.2: Limaçons: dimpled limaçon, cardioid (epicycloid with $k = 1$) and looped limaçon

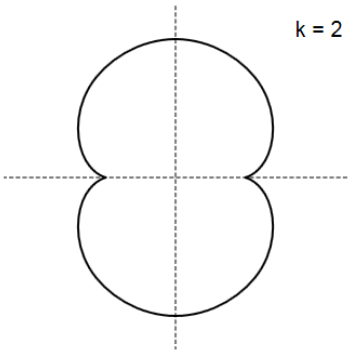

Figure 5.3: Nephroid

Circles and *epitrochoids*, in particular *cardioids* and *looped limaçons*, are numerically predicted for swimmers, which means active particles, in a harmonic trap. The self-propulsion mechanism of Janus particles in complex plasma environments is the result of the forces discussed in chapter 3, which are:

1. asymmetric ion drag force
2. radiation pressure force
3. photophoresis due to a temperature gradient on the particle surface, that is an asymmetric neutral drag force due to a temperature difference
4. "photophoresis" due to different accommodation coefficients, that is a neutral drag force due to different accommodation coefficients of MF and platinum.

Here, the results obtained in chapter 3 for the absolute values of the forces are reported. For laser light off:

- $F_{\text{ion drag}} \simeq 1{,}5 \times 10^{-19}\,\text{N}$
- $F_{\Delta\alpha} = 6{,}7 \times 10^{-13}\,\text{N}$ for $p = 1{,}3\,\text{Pa}$.

For laser light on:

- $F_{\text{ion drag}} \simeq 1{,}5 \times 10^{-19}\,\text{N}$
- $F_{\text{radiation pressure,MF}} = 1{,}2 \times 10^{-15}\,\text{N}$ and $F_{\text{laser,Pt}} = 2{,}6 \times 10^{-15}\,\text{N}$ for $P_{\text{laser}} = 99\,\text{mW}$
- $F_{\text{neutrals}} = 2{,}1 \times 10^{-12}\,\text{N}$ due to both photophoretic mechanisms.

For what concerns trajectories explainable with time-independent self-propulsion, the net force acting on a Janus particle could actually change its direction, for example because the particle spins, but not in absolute value. On the other hand, talking about time-dependent self-propulsion means that the absolute value of the propulsion force is changing in time with a certain propulsion frequency ν, according to the approach of Ref. [19]. In particular, the time dependence of the *absolute value* of the propulsion force can change for the reasons explained in section 3.3.

Now the focus must be placed on the reason why I observe both trajectories explainable with a time-independent absolute value of the propulsion force and trajectories explainable with a time-dependent one. The time-dependent mechanisms discussed in section 3.3 are recalled here:

- dependence of the asymmetry of ion drag force on the particle orientation
- coupling between grad T on the particle surface due to the two different materials and negative photophoresis

- dependence of radiation pressure force on particle orientation.

The first two forces are predicted to be much smaller than the third one and the second one is just a guess: it is not sure that a "hot spot" generates on the side not facing the laser on Janus particles. It must be observed that in absence of laser power there is no time-dependence of the propulsion forces. For this reason, the trajectories predicted for time-dependent absolute value of the propulsion force can be observed only in presence of laser illumination. In addition, considering that the forces listed above are time-dependent just if the particle is spinning around its axis "a" and not axis "b" in figure 3.14, my educated guess is that when regular circles are drawn by the particle moving in presence of laser lighting, then the torque due to gravitational force is predominant with respect to the particle rotation and for this reason the platinum-covered half of the particles always faces downward. This means that, if the Janus particle is spinning, it simply does it around axis "b". On the other hand, when the observed trajectories are *epitrochoids*, the particle is spinning around the axis "a".

All the trajectories drawn by the particles resemble one of the geometrical figures described in this section and for this reason all the trajectories shown in this chapter can be described by one of them. The trajectory shown in figure 4.2 for example is a *dimpled bilobed epicycloid*.

5.2 Comparison with MF particles

For what concerns MF particles, they had almost never showed either circular or *epitrochoidal* trajectories when previously observed as single particles in the experiments performed by the group. In my case, they very often showed circular trajectories or *epitrochoids* with $R > r$ and $d < r$. By very often, I mean that I observed seven circular trajectories in the nineteen recordings performed with six different pure MF particles. This result is not easy to explain because they are passive particles and none of the forces listed in chapter 3 acting on Janus particles act also on pure MF particles, as explained in section 4.2.6. In addition, they were observed very rarely in the past and those few cases can be probably explained as MF particles with a non-perfectly spherical shape. Forces like photophoresis or asymmetric ion drag could have acted on such particles making them active because of their particular shape. Unfortunately, they were not observed under the optical microscope because this is not an easy nor a usual procedure and for this reason mine is just a hypothesis.

However, as already mentioned, some experiments with both Janus and pure MF particles were performed with the confining ring shifted by 2 mm with respect to the centre of the lower electrode. For what concerns pure MF particles, I observed one of them in these experimental conditions and it showed a circular trajectory three times out of three and it never happened before that a pure MF showed a circular trajectory

100% of the times. In particular, after moving the ring back to the centre of the lower electrode, they never showed those kinds of trajectories any more, but just random ones. The random trajectories are the result which is easy to explain because they match the expected behaviour of passive particles and because they have always been observed in the past. Combining the facts that:

- before moving the ring, a lot of trajectories were not random
- while the ring was shifted by 2 mm, all the trajectories were not random
- after moving the ring back to the centre of the lower electrode, all the trajectories were random,

a possible explanation is that the ring was in the beginning not perfectly in the centre and for this reason the asymmetry of the ion flow on the particle may have caused the circular shape of the trajectories, as explained in Ref. [19]. This explanation of what made pure MF particles behave like active is anyway not valid for Janus particles, because they showed circular and *epitrochoidal* behaviour with the same occurrence before, during and after moving the ring: the effect of the asymmetric ion flow acting on MF particle must be just a small perturbation for Janus particles compared to all the other forces acting on them.

In figure 5.4, the trajectories of one of the observed pure MF particles before moving the confining ring are shown. Some results of the analysis of this particle motion are provided in Tables 5.1 and 5.2. The standard deviation of the trajectory radius is always the Δr of equation 4.22. In all the tables showing temperature results presented after 5.2, only two-dimensional temperatures are shown. In Table 5.2, also T_x and T_y are shown in order to give the reader an idea about their difference. In all the tables only the kinetic temperature is present because it constitutes a good estimator of the particle temperature. In section 5.4, also the particle temperature computed with the methods described in section 4.1.1 will be presented for one meaningful case, in order to demonstrate that the kinetic temperature is a good estimator of the particle temperature. Let me just recall that the particle temperature I talk about in the present chapter and I show in the results has nothing to do with the particle surface temperature, but it is related to the particle speed.

In figure 5.5, the trajectories of the pure MF particle observed while the confining ring was 2 mm shifted with respect to the centre of the lower electrode are shown: they are all circular. The main results of the analysis of this particle motion are provided in Tables 5.3 and 5.4.

In figure 5.6, a trajectory of a pure MF particle observed after shifting the confining ring back to the centre of the electrode is shown. The main results of the analysis of this particle motion are provided in Table 5.5.

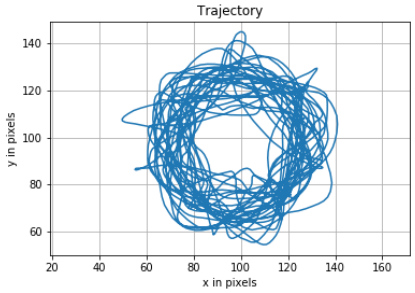

(a) *First observed trajectory with* 99 mW *of laser power: it can be described as a circle or as an epitrochoid with* $R > r$ *and* $d < r$

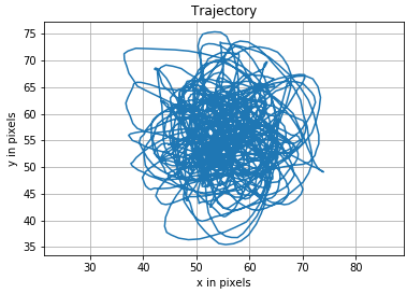

(b) *Second observed trajectory with* 14 mW *of laser power: random*

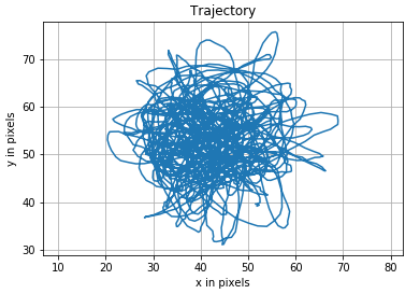

(c) *Third observed trajectory with* 0 mW *of laser power: random*

Figure 5.4: Observed trajectories for a pure MF particle before shifting the confining ring at different laser powers. They are shown in the same chronological order as they have been recorded during the experiment.

Table 5.1: Data about one of the observed pure MF particle before shifting the confining ring, at different laser powers. Gas pressure was 1,33 Pa and RF power 5 W. r is the approximate trajectory radius or, in case of random trajectories, the radius of the area covered by the trajectory in meters. f_{rot} is the rotational frequency in circles per second, which means Hz. f_{rot} is defined only for non-random trajectories. v is the linear velocity and it has been calculated as $v = r f_{\text{rot}}$. Obviously, v is defined only for non-random trajectories. The results are shown in chronological order.

Laser power	r	f_{rot}		v	
		x	y	x	y
(mW)	(m)	(Hz)	(Hz)	(m s^{-1})	(m s^{-1})
99	$1{,}3 \times 10^{-4}$	$0.54 \pm 7{,}4 \times 10^{-5}$	$0.54 \pm 7{,}1 \times 10^{-5}$	$4{,}7 \times 10^{-5} \pm 3{,}2 \times 10^{-9}$	$4{,}6 \times 10^{-5} \pm 3{,}0 \times 10^{-9}$
14	$5{,}4 \times 10^{-5}$	-	-	-	-
0	$6{,}7 \times 10^{-5}$	-	-	-	-

Table 5.2: Kinetic temperature T_k and kinetic temperature after subtracting the circular motion $T_{\text{k,without circular motion}}$ of one of the observed pure MF particles before shifting the confining ring, at different laser powers. Gas pressure was 1,33 Pa and RF power 5 W. $T_{\text{k,without circular motion}}$ is obviously defined only for non-random trajectories. The results are shown in chronological order.

Laser power	T_k			$T_{\text{k,without circular motion}}$		
(mW)	T_x (K)	T_y (K)	T_{2D} (K)	T_x (K)	T_y (K)	T_{2D} (K)
99	1289.9 ± 603.4	1267.7 ± 598.2	1278.8 ± 424.8	1231.2 ± 576.0	1210.2 ± 571.0	1220.7 ± 405.5
14	485.3 ± 369.6	499.9 ± 375.1	492.6 ± 263.3	-	-	-
0	579.1 ± 403.8	476.6 ± 366.3	527.8 ± 272.6	-	-	-

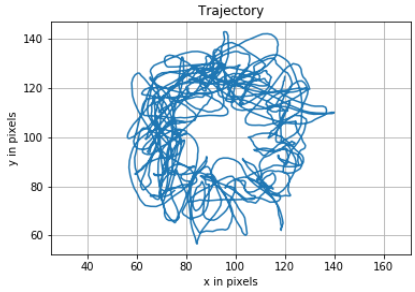

(a) *First observed trajectory with* 99 mW *of laser power: it can be described as a circle or as an epitrochoid with* $R > r$

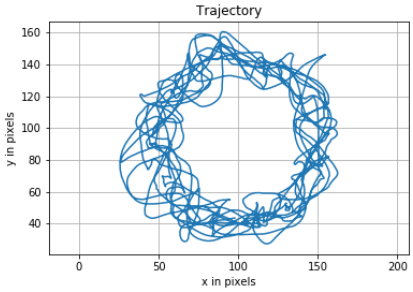

(b) *Second observed trajectory with* 99 mW *of laser power: it can be described as a circle or as an epitrochoid with* $R > r$

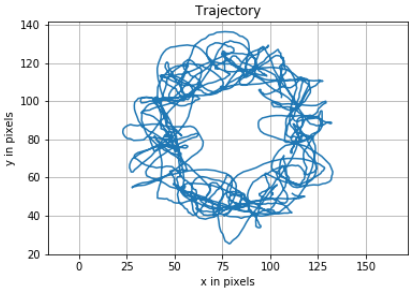

(c) *Third observed trajectory with* 0 mW *of laser power: it can be described as a circle or as an epitrochoid with* $R > r$

Figure 5.5: Observed trajectories for a pure MF particle when the confining ring was 2 mm shifted at different laser powers. They are shown in the same chronological order as they have been recorded during the experiment.

Table 5.3: Data about the observed pure MF particle while the confining ring was 2 mm shifted with respect to the centre of the lower electrode, at different laser powers. Gas pressure was 1,33 Pa and RF power 5 W. r is the approximate trajectory radius in meters; f_{rot} is the rotational frequency in circles per second, which means Hz. v is the linear velocity and it has been calculated as $v = rf_{\mathrm{rot}}$. The results are shown in chronological order.

Laser power	r	f_{rot}		v	
		x	y	x	y
(mW)	(m)	(Hz)	(Hz)	($\mathrm{m\,s^{-1}}$)	($\mathrm{m\,s^{-1}}$)
99	$1{,}2 \times 10^{-4}$	$0.07 \pm 7{,}9 \times 10^{-5}$	$0.07 \pm 8{,}0 \times 10^{-5}$	$5{,}1 \times 10^{-6} \pm 3{,}1 \times 10^{-9}$	$5{,}3 \times 10^{-6} \pm 3{,}2 \times 10^{-9}$
99	$1{,}9 \times 10^{-4}$	$0.2 \pm 4{,}1 \times 10^{-5}$	$0.2 \pm 4{,}0 \times 10^{-5}$	$8{,}2 \times 10^{-6} \pm 1{,}9 \times 10^{-7}$	$1{,}1 \times 10^{-5} \pm 2{,}9 \times 10^{-7}$
0	$1{,}6 \times 10^{-4}$	$0.14 \pm 6{,}3 \times 10^{-5}$	$0.14 \pm 5{,}6 \times 10^{-5}$	$7{,}8 \times 10^{-6} \pm 1{,}1 \times 10^{-7}$	$8{,}3 \times 10^{-6} \pm 9{,}8 \times 10^{-8}$

Table 5.4: Kinetic temperature of the observed pure MF particle while the confining ring was 2 mm shifted with respect to the centre of the lower electrode, at different laser powers. Gas pressure was 1,33 Pa and RF power 5 W. $T_{\mathrm{k,\ 2D}}$ is the two-dimensional kinetic temperature in K; $T_{\mathrm{k,\ 2D,\ nc}}$ is the two-dimensional kinetic temperature after subtracting the circular motion in K.

Laser power	$T_{\mathrm{k,\ 2D}}$	$T_{\mathrm{k,\ 2D,\ nc}}$
(mW)	(K)	(K)
99	537.8 ± 275.2	504.5 ± 260.4
99	833.7 ± 342.7	503.1 ± 260.0
0	670.4 ± 307.3	549.8 ± 271.9

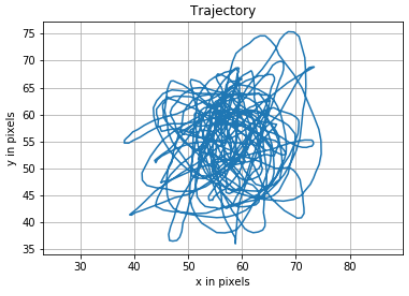

Figure 5.6: Observed trajectory for a pure MF particle after the confining ring has been shifted back to the centre of the lower electrode at 99 mW of laser power. It is a random trajectory.

Table 5.5: Kinetic temperature of one of the observed pure MF particle after moving the confining ring back in the centre of the lower electrode. Laser power was 99 mW, gas pressure was 1,33 Pa and RF power 5 W. r is the radius of the area covered by the trajectory in meters; $T_{\mathrm{k,\ 2D}}$ is the two-dimensional kinetic temperature in K; $T_{\mathrm{k,\ 2D,\ nc}}$ is the two-dimensional kinetic temperature after subtracting the circular motion in K.

Laser power	r	$T_{\mathrm{k,\ 2D}}$
(mW)	(m)	(K)
99	$5{,}3 \times 10^{-5}$	479.4 ± 367.4

5.3 Results of the experiments with Janus particles with the ring shifted with respect to the centre of the lower electrode

Recalling it from section 4.2.5, the three factors that could make Janus particles move along the observed trajectories and make them seem active, even if they were not, are:

- ion flow going from the centre of the lower electrode to the edges due to ambipolar diffusion, which causes symmetry breaking
- distortion of the shape of the potential well due to the focus of the laser: the absolute potential minimum could be accompained by a secondary one
- co-existence of two different confining potential wells.

The results of these experiments show an outcome that is about the same as the usual one for Janus particles. I observed in fact both circular trajectories and random ones and I also recorded one *nephroidal* trajectory. If the symmetry breaking caused by ion flow going from the centre of the lower electrode to the edges due to ambipolar diffusion was the reason of the non-random shape of the Janus particle trajectories, then under these experimental conditions Janus particles should not move along random trajectories. For this reason, my educated guess is that the contribution of ion flow due to ambipolar diffusion is much smaller than the forces acting on Janus particles as propulsion mechanisms. In addition, the dimensions of the trajectories remained almost the same as usual and they have never even got close to 2 mm. This is a clear indication that also the other two hypothesised causes of the circular motion of Janus particles are not the right explanation. It must be that the focus of the laser is not strong enough to distort the shape of the confining potential well due to the ring and that the potential well due to the ion density distribution is not important at all with respect to the confining one due to the ring. This leads to the conclusion that Janus particles are really active in plasmas because of the forces acting on them as propulsion mechanisms described in chapter 3.

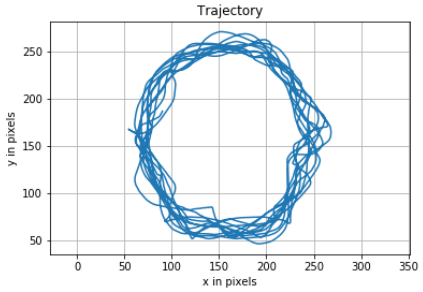

(a) *First observed trajectory with* 99 mW *of laser power: it can be described as a circle or as an epitrochoid with* $R > r$*. It could even remind of a dimpled epicycloid with* $k = 2$

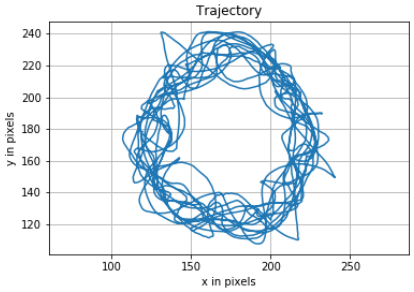

(b) *Second observed trajectory with* 14 mW *of laser power: it can be described as a circle or as an epitrochoid with* $R > r$

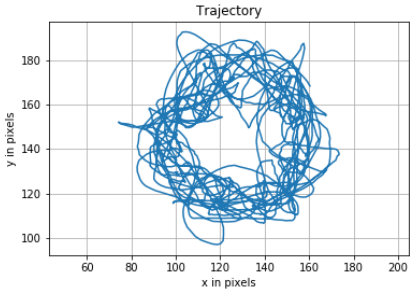

(c) *Third observed trajectory with* 0 mW *of laser power: it can be described as a circle or as an epitrochoid with* $R > r$

Figure 5.7: Trajectories of one of the observed Janus particles when the confining ring was 2 mm shifted at different laser powers. They are shown in the same chronological order as they have been recorded during the experiment.

The pure MF particle trajectories recorded in these experimental conditions are shown in figure 5.5. Some trajectories of one observed Janus particle are shown in figure 5.7 and they must be compared to the trajectories of figures 5.26. Some of the results of the analysis are reported in Tables 5.6 and 5.7.

5.4 Results of the experiments where the laser power was varied

A lot of Janus particles have been observed at the three different illumination laser powers listed in the previous chapter: 0 mW, 14 mW, 99 mW. The other experimental parameters used have been 5 W of RF power and 1,3 Pa of gas pressure.

Different Janus particles observed showed different behaviours and, for this reason,

Table 5.6: Data about the observed Janus particle of figure 5.7. The confining ring was 2 mm shifted with respect to the centre of the lower electrode, at different laser powers. Gas pressure was 1,33 Pa and RF power 5 W. r is the approximate trajectory radius in meters; f_{rot} is the rotational frequency in circles per second, which means Hz. v is the linear velocity and it has been calculated as $v = r f_{\mathrm{rot}}$. The results are shown in chronological order.

Laser power	r	f_{rot}		v	
		x	y	x	y
(mW)	(m)	(Hz)	(Hz)	($\mathrm{m\,s^{-1}}$)	($\mathrm{m\,s^{-1}}$)
99	$3{,}1 \times 10^{-4}$	$0.2 \pm 4{,}0 \times 10^{-5}$	$0.2 \pm 4{,}3 \times 10^{-5}$	$3{,}0 \times 10^{-5} \pm 2{,}5 \times 10^{-9}$	$3{,}0 \times 10^{-5} \pm 2{,}7 \times 10^{-9}$
14	$1{,}9 \times 10^{-4}$	$0.2 \pm 4{,}1 \times 10^{-5}$	$0.2 \pm 4{,}0 \times 10^{-5}$	$8{,}2 \times 10^{-6} \pm 1{,}9 \times 10^{-7}$	$1{,}1 \times 10^{-5} \pm 2{,}9 \times 10^{-7}$
0	$1{,}4 \times 10^{-4}$	$0.3 \pm 6{,}5 \times 10^{-5}$	$0.3 \pm 6{,}9 \times 10^{-5}$	$2{,}6 \times 10^{-5} \pm 3{,}0 \times 10^{-9}$	$2{,}5 \times 10^{-5} \pm 3{,}1 \times 10^{-9}$

Table 5.7: Kinetic temperature of the observed pure MF particle while the confining ring was 2 mm shifted with respect to the centre of the lower electrode, at different laser powers. Gas pressure was 1,33 Pa and RF power 5 W. $T_{\mathrm{k,\ 2D}}$ is the two-dimensional kinetic temperature in K; $T_{\mathrm{k,\ 2D,\ nc}}$ is the two-dimensional kinetic temperature after subtracting the circular motion in K.

Laser power	$T_{\mathrm{k,\ 2D}}$	$T_{\mathrm{k,\ 2D,\ nc}}$
(mW)	(K)	(K)
99	1729.9 ± 494.5	434.1 ± 241.5
14	1038.1 ± 382.6	536.0 ± 268.4
0	790.1 ± 333.6	536.6 ± 268.5

some categories of Janus particles were identified based on how the particle behaves:

- first kind of Janus particles: Janus particles with “heart-like“ trajectories. They are the particles drawing *limaçons* and *epicycloids with* $k = 2$ with their motion. "Heart-like" is actually the name given to *cardiods* in Ref. [19]. They are six out of the fourteen observed in total.
- Second kind of Janus particles: “circling“ Janus particles. They are the particles drawing pure circles or *epitrochoids* with $R > r$ with their motion. They are also six out of the fourteen observed in total.
- Third kind of Janus particles: “randomly moving“ Janus particles. They are particles whose motion is apparently random. They are two out of the fourteen observed in total.

It is important to note that the statistics on these particles is just related to the ones observed during these experiments. In fact, the statistics over all the particles observed during the experiments performed for the whole work shows that the "circling" Janus particles are more common than the Janus particles with “heart-like“ trajectories.

Each group of particles follows a rule of behaviour depending on the laser power:

- “heart-like“ Janus particles rule: the higher the laser power is, the bigger, cleaner and more *limaçon*-like or *epicycloidal with* $k = 2$ the trajectory is
- “circling“ Janus particles rule: the lower the laser power is, the bigger and cleaner the circular trajectory is
- “randomly moving“ Janus particles rule: there is not a clear dependence of the shape of the trajectory on the laser power.

What makes the trajectories “dirty“, which means more similar to *epitrochoids* with $R > r$ than to pure circles or pure *limaçons* and *epicycloids with* $k = 2$, could be the random motion that becomes stronger related to a higher kinetic temperature of the particle.

Moreover, the important parameter in order to have an idea about the force on the particle is not the trajectory radius, but it is the product between the radius and the rotational frequency. In fact, relating r_c, ω and F_0 as in equation 3.52:

$$\frac{r_c}{r_p} = \frac{F_0}{\sqrt{\lambda_0^2 + \omega^2}}, \tag{5.1}$$

which is valid in case of circular trajectories, it follows that roughly:

$$F_0 \propto r_c \omega. \tag{5.2}$$

Some examples of trajectories of “heart-like“ moving Janus particles are shown in figures 5.8, 5.9 and 5.10; in Tables from 5.8 to 5.13 some of the results of their analysis

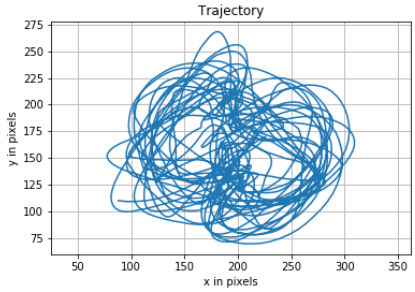

(a) *Observed trajectory for* **14 mW** *of laser power: it can be described as an epicycloid with* $k = 2$.

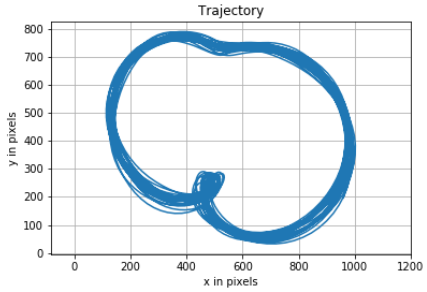

(b) *Observed trajectory for* **99 mW** *of RF power: it can be described as something in between a dimpled limaçon and an epicycloid with* $k = 2$.

Figure 5.8: Trajectories of one of the observed Janus particles at 5 W of RF power and 1,3 Pa of gas pressure, changing the laser power. They are shown in the same chronological order as they have been recorded during the experiment.

Table 5.8: Data about the observed Janus particle of figure 5.8. The RF power was 5 W and the gas pressure 1,3 Pa. r is the approximate trajectory radius in m; f_{rot} is the rotational frequency in circles per second, which means Hz; v is the linear velocity and it has been calculated as $v = r f_{\text{rot}}$. The results are shown in chronological order.

Laser power	r	f_{rot}		v	
		x	y	x	y
(mW)	(m)	(Hz)	(Hz)	(m s^{-1})	(m s^{-1})
14	$3{,}1 \times 10^{-4}$	$0.4 \pm 1{,}1 \times 10^{-4}$	$0.4 \pm 1{,}4 \times 10^{-4}$	$8{,}6 \times 10^{-5} \pm 1{,}2 \times 10^{-8}$	$7{,}3 \times 10^{-5} \pm 1{,}3 \times 10^{-8}$
99	$1{,}2 \times 10^{-3}$	$0.4 \pm 7{,}7 \times 10^{-5}$	$0.4 \pm 7{,}1 \times 10^{-5}$	$3{,}6 \times 10^{-4} \pm 3{,}2 \times 10^{-8}$	$3{,}0 \times 10^{-4} \pm 2{,}5 \times 10^{-8}$

are reported. In figure 5.11 radius, rotational frequency and an estimation of the force as $F = r f_{\text{rot}}$ in arbitrary units are plotted as a function of the laser power for the "heart-like" trajectories of figures 5.8, 5.9 and 5.10. No clear conclusions can be deduced for what concerns the force.

The theoretical predictions of Ref. [19] imply that the active particles performing "heart-like" trajectories are the ones driven by a time-dependent propulsion force, that means in my case the ones spinning around an axis such that the mechanisms making the net force time-dependent are active (axis a of figure 3.14). The fact that with the laser power off the trajectories are simply circles, as it would be for the case of time-independent propulsion force, is a clear sign that the laser power plays a major role among my hypotheses of section 3.3. In particular, the important contributions to the time-dependence of the force should be the so called "dependence of radiation pressure force on particle orientation" and, if actually present, "coupling between gradT of the particle surface due to the two different materials and negative photophoresis".

Table 5.9: Kinetic temperature of the observed Janus particle of figure 5.8. The RF power was 99 mW and the gas pressure 1,3 Pa. $T_{k,\,2D}$ is the two-dimensional kinetic temperature in K; $T_{k,\,2D,\,nc}$ is the two-dimensional kinetic temperature after subtracting the "circular" motion in K. Note that the more the trajectories depart from circular shape, the less $T_{k,\,2D,\,nc}$ is a good estimator of the kinetic temperature. The results are shown in chronological order.

Laser power (mW)	$T_{k,\,2D}$ (K)	$T_{k,\,2D,\,nc}$ (K)
14	5947.0 ± 923.5	4295.0 ± 764.9
99	132996.0 ± 5217.9	63692.9 ± 3240.3

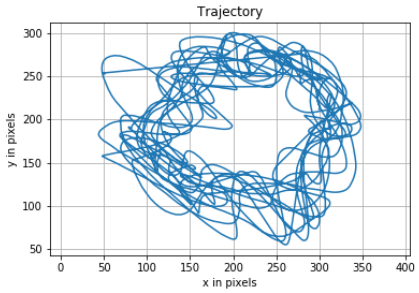

(a) *Observed trajectory for* **0 mW** *of laser power: it can be described as a dirty circle or an epitrochoid with R>r.*

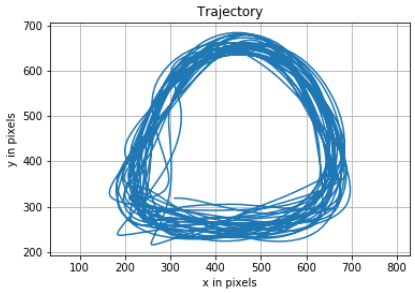

(b) *Observed trajectory for* **14 mW** *of RF power: it can be described as something similar to a circle.*

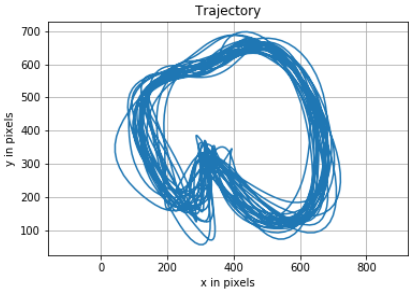

(c) *Observed trajectory for* **99 mW** *of laser power: it can be described as something between a cardioid and a dimpled bilobed epicycloid.*

Figure 5.9: Trajectories of one of the observed Janus particles at 5 W of RF power and 1,3 Pa of gas pressure, changing the laser power. They are not shown in the same chronological order as they have been recorded during the experiment.

Table 5.10: Data about the observed Janus particle of figure 5.9. The RF power was 5 W and the gas pressure 1,3 Pa. r is the approximate trajectory radius in meters; f_{rot} is the rotational frequency in circles per second, which means Hz; v is the linear velocity and it has been calculated as $v = r f_{\mathrm{rot}}$. The results are not shown in chronological order.

Laser power	r	f_{rot}		v	
		x	y	x	y
(mW)	(m)	(Hz)	(Hz)	($\mathrm{m\,s^{-1}}$)	($\mathrm{m\,s^{-1}}$)
0	$4{,}0 \times 10^{-4}$	$0.2 \pm 8{,}8 \times 10^{-5}$	$0.2 \pm 8{,}9 \times 10^{-5}$	$6{,}9 \times 10^{-5} \pm 1{,}3 \times 10^{-8}$	$5{,}6 \times 10^{-5} \pm 1{,}0 \times 10^{-8}$
14	$7{,}2 \times 10^{-4}$	$0.5 \pm 3{,}6 \times 10^{-5}$	$0.5 \pm 5{,}3 \times 10^{-5}$	$2{,}6 \times 10^{-4} \pm 9{,}0 \times 10^{-9}$	$2{,}3 \times 10^{-4} \pm 1{,}2 \times 10^{-8}$
99	$9{,}4 \times 10^{-4}$	$0.5 \pm 6{,}9 \times 10^{-5}$	$0.5 \pm 1{,}1 \times 10^{-4}$	$2{,}9 \times 10^{-4} \pm 2{,}2 \times 10^{-8}$	$2{,}8 \times 10^{-4} \pm 3{,}4 \times 10^{-8}$

Table 5.11: Kinetic temperature of the observed Janus particle of figure 5.9. The RF power was 5 W and the gas pressure 1,3 Pa. $T_{\mathrm{k,\ 2D}}$ is the two-dimensional kinetic temperature in K; $T_{\mathrm{k,\ 2D,\ nc}}$ is the two-dimensional kinetic temperature after subtracting the "circular" motion in K. Note that the more the trajectories depart from circular shape, the less $T_{\mathrm{k,\ 2D,\ nc}}$ is a good estimator of the kinetic temperature. The results are not shown in chronological order.

Laser power	$T_{\mathrm{k,\ 2D}}$	$T_{\mathrm{k,\ 2D,\ nc}}$
(mW)	(K)	(K)
0	9231.1 ± 1135.5	7715.9 ± 1035.5
14	49715.5 ± 2861.2	7795.0 ± 1037.3
99	84413.1 ± 3947.6	47306.5 ± 2771.9

Table 5.12: Data about the observed Janus particle of figure 5.10. The RF power was 5 W and the gas pressure 1,3 Pa. r is the approximate trajectory radius in meters; f_{rot} is the rotational frequency in circles per second, which means Hz; v is the linear velocity and it has been calculated as $v = r f_{\mathrm{rot}}$. The results are not shown in chronological order.

Laser power	r	f_{rot}		v	
		x	y	x	y
(mW)	(m)	(Hz)	(Hz)	($\mathrm{m\,s^{-1}}$)	($\mathrm{m\,s^{-1}}$)
0	$4{,}6 \times 10^{-4}$	$0.3 \pm 2{,}0 \times 10^{-5}$	$0.3 \pm 2{,}1 \times 10^{-5}$	$1{,}1 \times 10^{-4} \pm 3{,}1 \times 10^{-9}$	$1{,}0 \times 10^{-4} \pm 3{,}1 \times 10^{-9}$
14	$2{,}6 \times 10^{-4}$	$0.3 \pm 3{,}7 \times 10^{-5}$	$0.3 \pm 3{,}9 \times 10^{-5}$	$4{,}6 \times 10^{-5} \pm 3{,}4 \times 10^{-9}$	$3{,}8 \times 10^{-5} \pm 2{,}9 \times 10^{-9}$
99	$3{,}1 \times 10^{-4}$	$0.3 \pm 1{,}5 \times 10^{-4}$	$0.3 \pm 1{,}0 \times 10^{-4}$	$5{,}4 \times 10^{-5} \pm 1{,}4 \times 10^{-8}$	$6{,}9 \times 10^{-5} \pm 1{,}2 \times 10^{-8}$
99	$3{,}7 \times 10^{-4}$	$0.4 \pm 3{,}6 \times 10^{-4}$	$0.4 \pm 2{,}2 \times 10^{-4}$	$9{,}2 \times 10^{-5} \pm 4{,}2 \times 10^{-8}$	$1{,}0 \times 10^{-4} \pm 3{,}0 \times 10^{-8}$

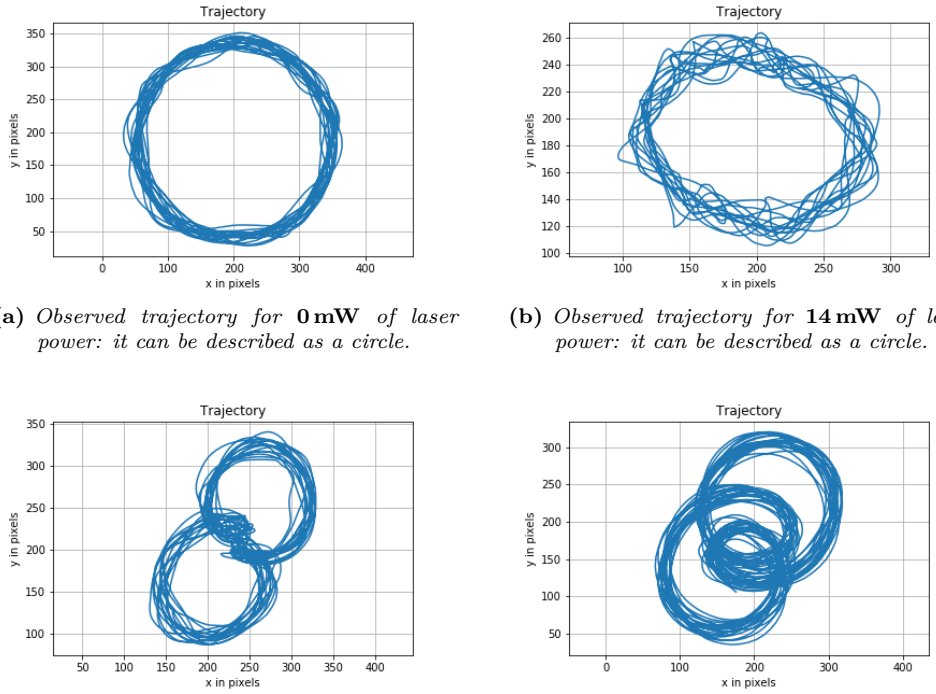

(a) *Observed trajectory for* **0 mW** *of laser power: it can be described as a circle.*

(b) *Observed trajectory for* **14 mW** *of laser power: it can be described as a circle.*

(c) *Observed trajectory for* **99 mW** *of laser power: it can be described as a looped epicycloid with* $k = 2$.

(d) *Observed trajectory for* **99 mW** *of laser power: it can be described as a looped epicycloid with* $k = 2$.

Figure 5.10: Trajectories of one of the observed Janus particles at 5 W of RF power and 1,3 Pa of gas pressure, changing the laser power. They are not shown in the same chronological order as they have been recorded during the experiment.

Table 5.13: Kinetic temperature of the observed Janus particle of figure 5.10. The RF power was 5 W and the gas pressure 1,3 Pa. $T_{\mathrm{k,\ 2D}}$ is the two-dimensional kinetic temperature in K; $T_{\mathrm{k,\ 2D,\ nc}}$ is the two-dimensional kinetic temperature after subtracting the "circular" motion in K. Note that the more the trajectories depart from circular shape, the less $T_{\mathrm{k,\ 2D,\ nc}}$ is a good estimator of the kinetic temperature. The results are not shown in chronological order.

Laser power (mW)	$T_{\mathrm{k,\ 2D}}$ (K)	$T_{\mathrm{k,\ 2D,\ nc}}$ (K)
0	8595.4 ± 1090.2	665.0 ± 299.0
14	1710.4 ± 491.7	638.7 ± 293.0
99	5678.0 ± 901.9	4254.4 ± 761.2
99	24745.0 ± 1942.3	22375.8 ± 1800.9

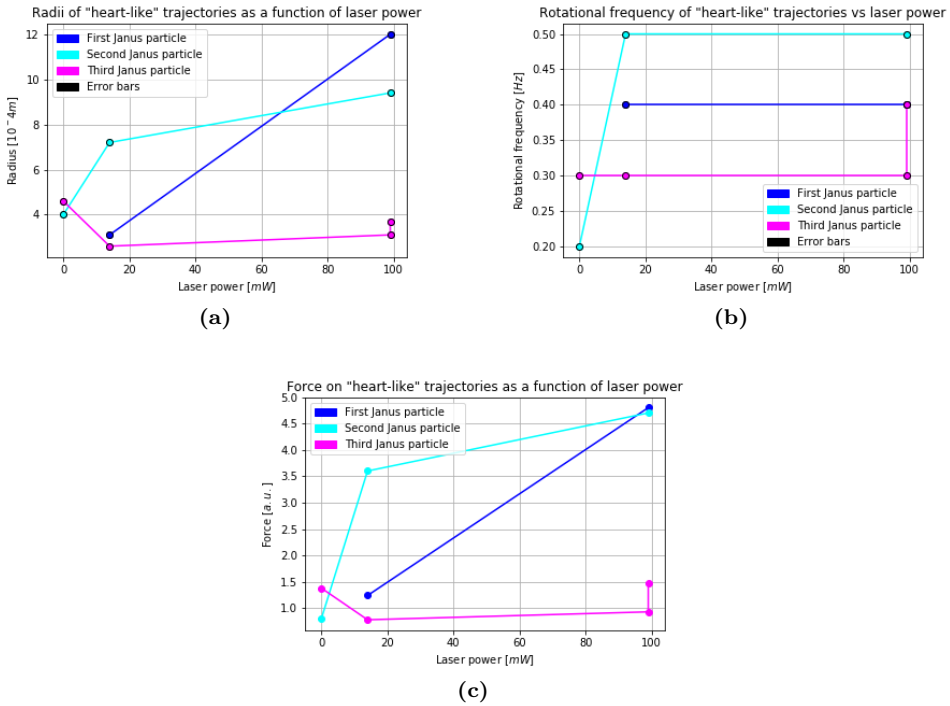

Figure 5.11: Radius of the trajectories, rotational frequency and force acting on the Janus particles shown in figures from 5.8 to 5.10 are plotted as functions of the laser power. The error bars cannot be seen as the errors are too small: they are orders of magnitude smaller than the values.

What I would say in conclusion for this first category of Janus particles is that the major role for the "heart-like" trajectories is played by the time-dependence of the net force acting on the Janus particles.

A couple of more details about the analysis are discussed in the following. Focusing on the Janus particle whose trajectories are shown in figure 5.10 and whose results are shown in Tables 5.12 and 5.13, the less the trajectory is circular, the larger $T_{k,\,2D,\,nc}$ is, as the sinusoidal fit is not good. For this reason, if for all non-random trajectories $T_{k,\,2D}$ is not any more a good estimator of the particle kinetic temperature, for non-circular trajectories even $T_{k,\,2D,\,nc}$ is not. See, as an example of the x and y positions after subtracting their mean as a function of time, figure 5.12 for trajectory (a) of figure 5.10 and figure 5.13 for trajectory (d) of figure 5.10.

The observed shapes of the trajectories are due to Janus particle activity in the plasma environment. As explained in chapter 1, active particles are able to drive themselves far from equilibrium and this makes the Gaussian and Maxwellian fits questionable. Moreover, if the procedure of subtracting the periodic regular motion of the particle is effective, like in case of trajectory (b) of figure 5.10, then just the random component of the motion is left and the Gaussian and Maxwellian fits of the velocity random component distribution function should be good, but if the procedure is not effective, like in case of trajectory (d) of figure 5.10, then the fits are anyway bad. See figures 5.14 and 5.15.

On the other side, for what concerns the second kind of JP, these "circling" ones, it seems that they are not subject to a time-dependent self-propulsion mechanism, which means that they spin around the axis b of figure 3.14, if they spin. As in general this "circling" Janus particles are the most common, this is a sign that gravitational force probably plays a major role in Janus particle orientation. What can be deduced from the results of these experiments is the following. The asymmetric ion drag force does not depend on laser power. If the particle was rotating around axis b of figure 3.14, then the two photophoretic mechanisms would act in principle, from the point of view of the simple semi-lumped parameters approach adopted in chapter 3, act in the vertical direction and the radiation pressure would not depend on time. The "circling" motion it self is, by the way, the proof that the single Janus particles are active. For this reason, it could be reasonable to think that the semi-lumped parameter approach is not enough in order to understand the particle behaviour. Or maybe simply the theoretical model of Ref. [19] is not precise enough for the case of an undamped environment and should be for this reason modified to adapt it to the environment of my experiments.

In figures 5.16 and 5.17, the trajectories of two "circling" Janus particles are shown. The results of 5.17 have been obtained for pressures higher than 1,3 Pa, in particular for 6,7 Pa and 13,3 Pa. In Tables from 5.14 to 5.17 some of the results of their analysis are reported.

In figure 5.18, the trajectory radius, rotational frequency and force acting in the cases of the "circular" trajectories shown in figures 5.16 and 5.17 are shown as functions of

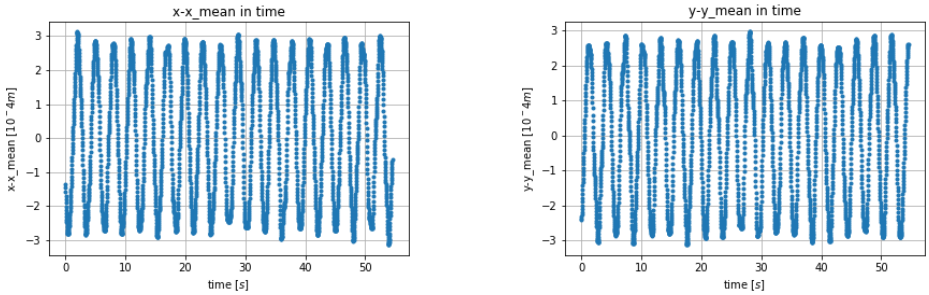

(a)

(b)

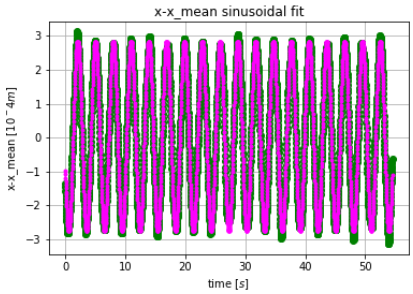

(c)

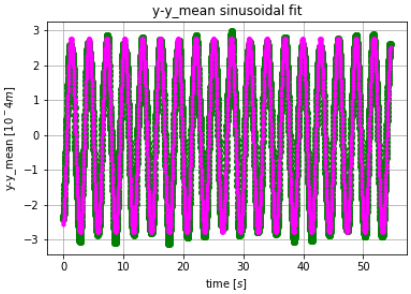

(d)

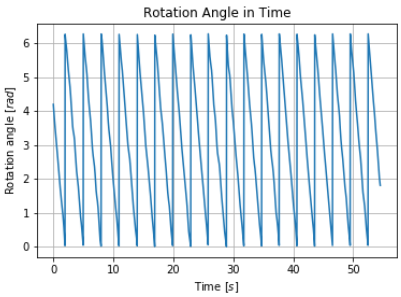

(e)

Figure 5.12: Good sinusoidal fit of the circular trajectory (a) of figure 5.10. The rotational angle as a function of time is also shown and it clearly proves that the trajectory is circular.

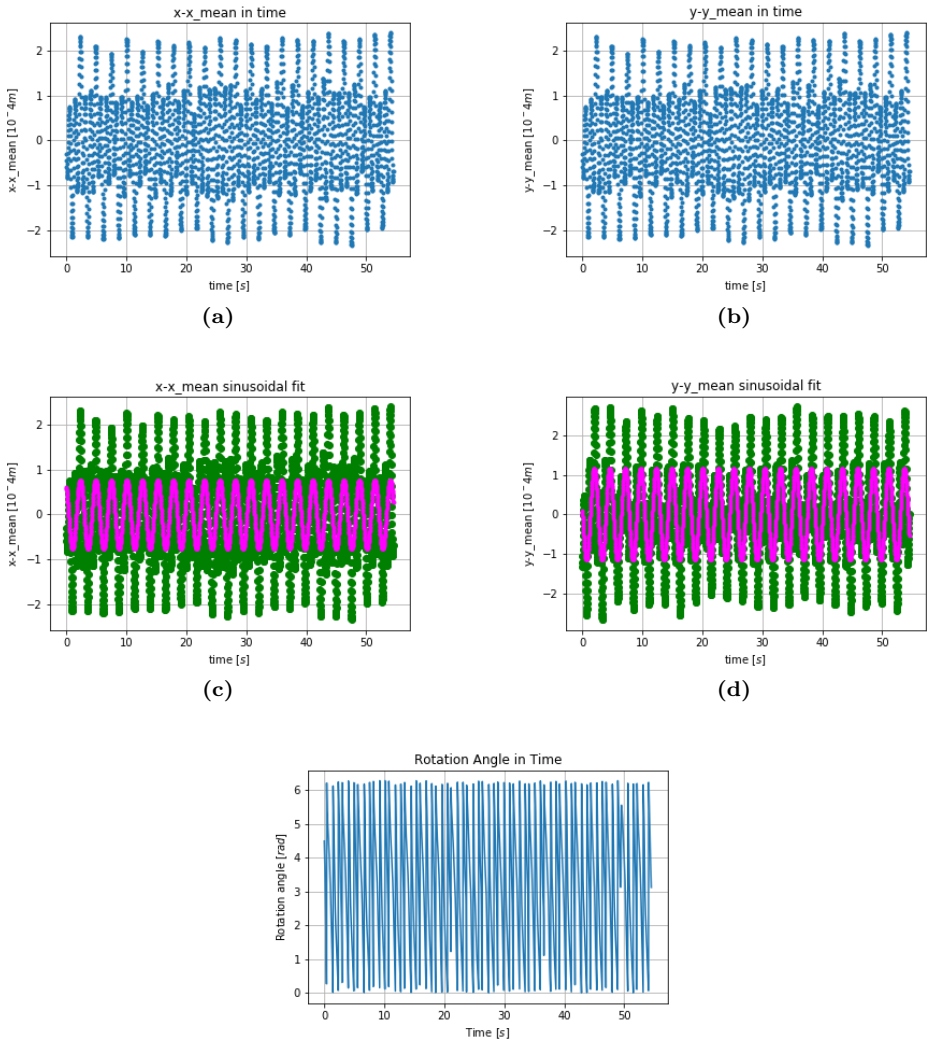

Figure 5.13: Bad sinusoidal fit of the *looped bilobed epicycloidal* trajectory (d) of figure 5.10. The fit should be done with the correct shape of the trajectory in order to compute a reliable result for the kinetic temperature. The rotational angle as a function of time is also shown.

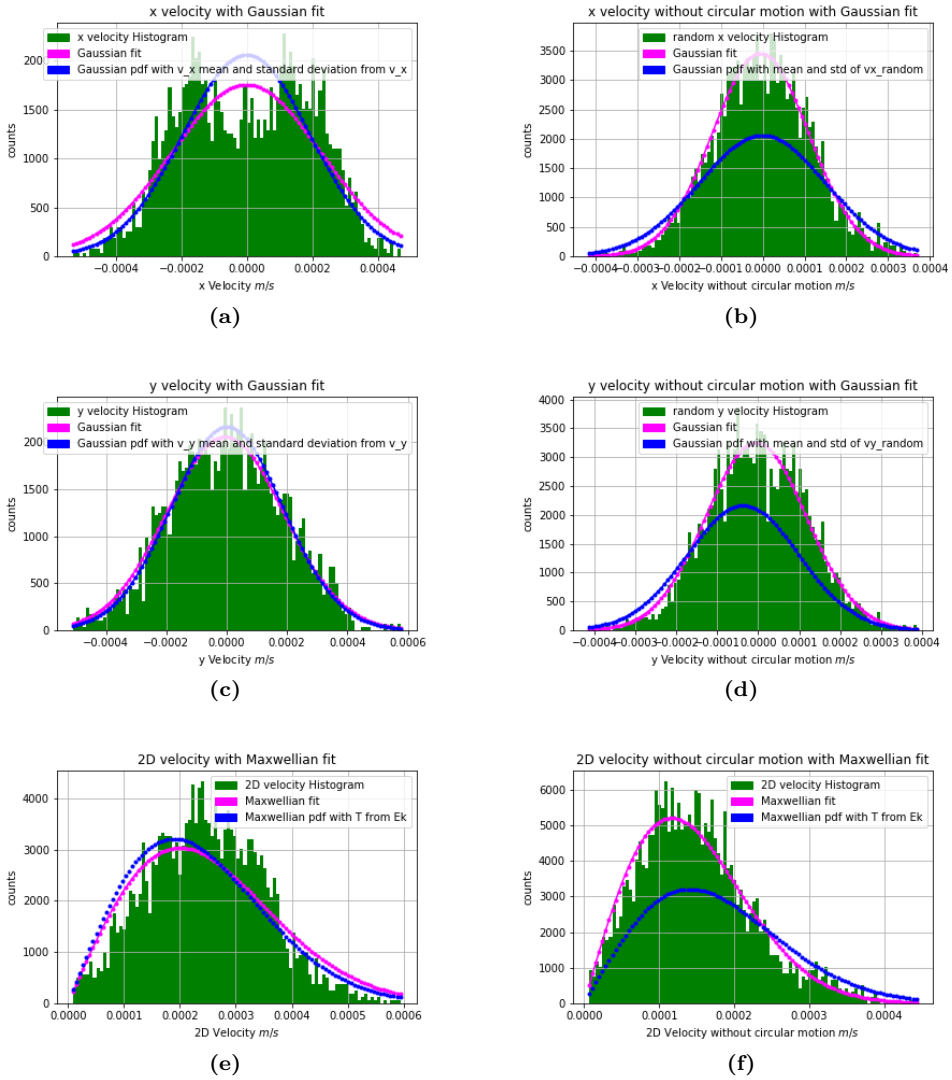

Figure 5.14: Gaussian and Maxwellian fits of velocity distribution functions before and after subtracting the circular motion for the case of trajectory (b) of figure 5.10. The results after the subtraction are very good as it is an effective process (see figure 5.12): the trajectory actually has a circular shape.

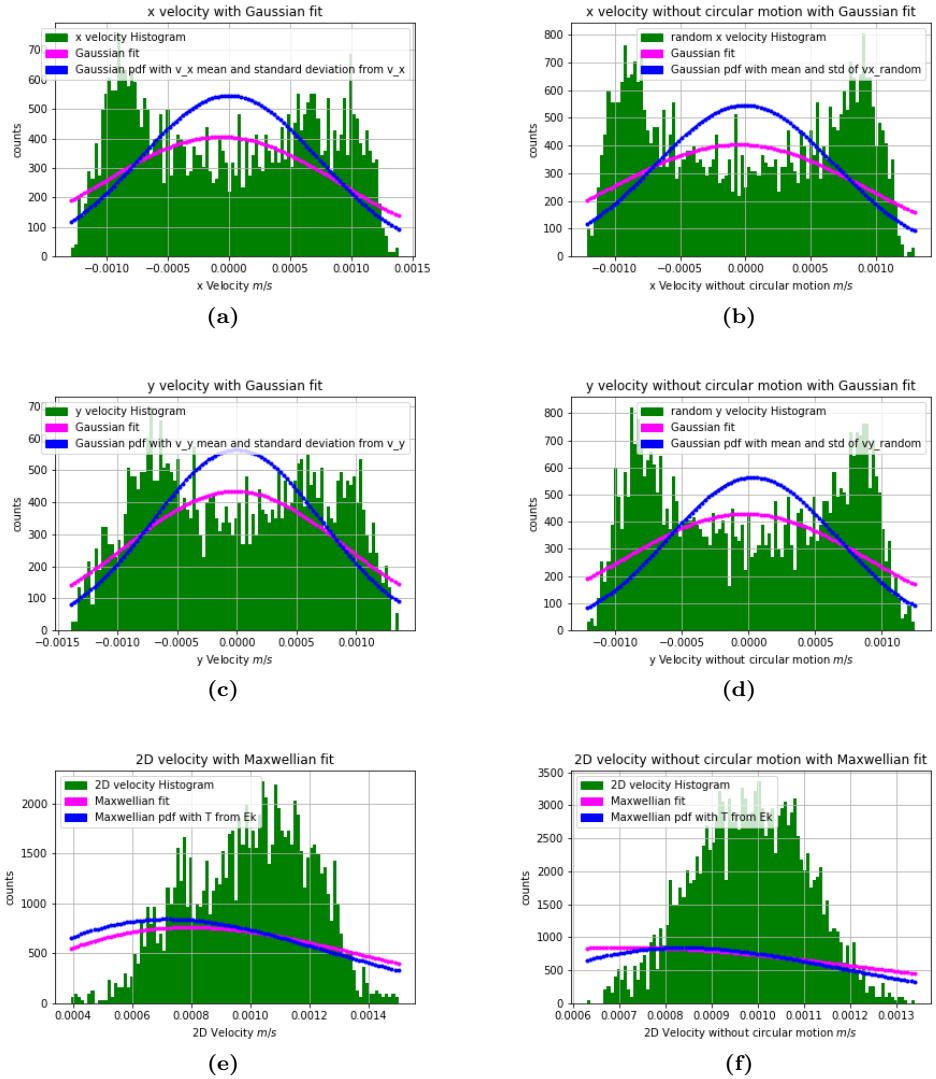

Figure 5.15: Gaussian and Maxwellian fits of velocity distribution functions before and after subtracting the circular motion for the case of trajectory (d) of figure 5.10. The results after the subtraction are not better as it is not an effective process (see figure 5.13): the trajectory does not have a circular shape.

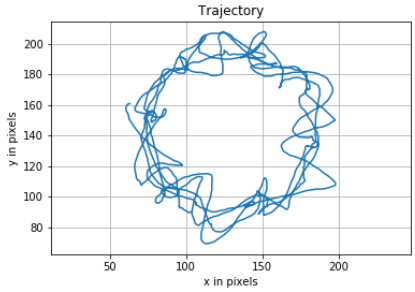

(a) *Observed trajectory for* **0 mW** *of laser power: it can be described as a circle.*

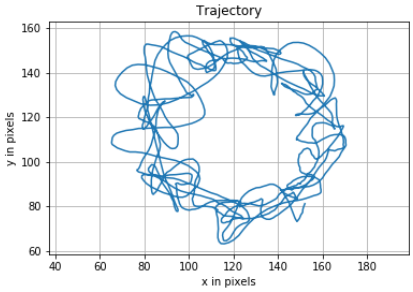

(b) *Observed trajectory for* **14 mW** *of laser power: it can be described as a circle.*

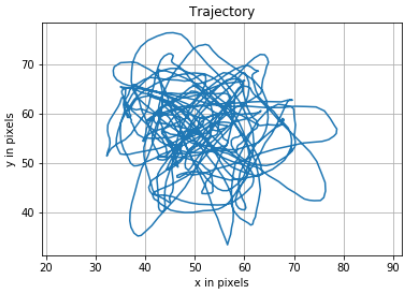

(c) *Observed trajectory for* **99 mW** *of laser power: it is random.*

Figure 5.16: Trajectories of one of the observed Janus particles at 5 W of RF power and 1,3 Pa of gas pressure, changing the laser power. They are not shown in the same chronological order as they have been recorded during the experiment.

Table 5.14: Data about the observed Janus particle of figure 5.16. The RF power was 5 W and the gas pressure 1,3 Pa. r is the approximate trajectory radius in meters; f_{rot} is the rotational frequency in circles per second, which means Hz; v is the linear velocity and it has been calculated as $v = r f_{\text{rot}}$. The results are not shown in chronological order.

Laser power	r	f_{rot}		v	
		x	y	x	y
(mW)	(m)	(Hz)	(Hz)	($\text{m}\,\text{s}^{-1}$)	($\text{m}\,\text{s}^{-1}$)
0	$2{,}0 \times 10^{-4}$	$0.2 \pm 3{,}7 \times 10^{-5}$	$0.2 \pm 3{,}2 \times 10^{-5}$	$2{,}0 \times 10^{-5} \pm 2{,}4 \times 10^{-9}$	$2{,}0 \times 10^{-5} \pm 2{,}1 \times 10^{-9}$
14	$1{,}5 \times 10^{-4}$	$0.2 \pm 4{,}8 \times 10^{-5}$	$0.2 \pm 5{,}3 \times 10^{-5}$	$1{,}6 \times 10^{-5} \pm 2{,}5 \times 10^{-9}$	$1{,}5 \times 10^{-5} \pm 2{,}6 \times 10^{-9}$
99	$8{,}3 \times 10^{-5}$	–	–	–	–

Table 5.15: Kinetic temperature of the observed Janus particle of figure 5.16. The RF power was 5 W and the gas pressure 1,3 Pa. $T_{k,\,2D}$ is the two-dimensional kinetic temperature in K; $T_{k,\,2D,\,nc}$ is the two-dimensional kinetic temperature after subtracting the "circular" motion in K. Note that the more the trajectories deviate from circular shape, the less $T_{k,\,2D,\,nc}$ is a good estimator of the kinetic temperature. The results are not shown in chronological order.

Laser power (mW)	$T_{k,\,2D}$ (K)	$T_{k,\,2D,\,nc}$ (K)
0	712.0 ± 316.7	463.9 ± 249.7
14	587.2 ± 287.5	458.0 ± 248.0
99	538.3 ± 275.3	-

Table 5.16: Data about the observed Janus particle of figure 5.17. The RF power was 5 W. r is the approximate trajectory radius in meters; f_{rot} is the rotational frequency in circles per second, which means Hz; v is the linear velocity and it has been calculated as $v = r f_{rot}$. The results are not shown in chronological order.

Pressure (Pa)	Laser (mW)	r (m)	f_{rot} x (Hz)	f_{rot} y (Hz)	v x ($m\,s^{-1}$)	v y ($m\,s^{-1}$)
6.7	0	$1{,}3 \times 10^{-4}$	$0.3 \pm 9{,}1 \times 10^{-4}$	$0.3 \pm 5{,}3 \times 10^{-5}$	$2{,}6 \times 10^{-5} \pm 4{,}2 \times 10^{-8}$	$2{,}1 \times 10^{-5} \pm 2{,}2 \times 10^{-9}$
6.7	14	$1{,}6 \times 10^{-4}$	$0.04 \pm 3{,}8 \times 10^{-4}$	$0.04 \pm 1{,}3 \times 10^{-4}$	$3{,}8 \times 10^{-6} \pm 1{,}9 \times 10^{-8}$	$3{,}9 \times 10^{-6} \pm 7{,}2 \times 10^{-9}$
6.7	99	$3{,}7 \times 10^{-4}$	$0.05 \pm 9{,}9 \times 10^{-5}$	$0.04 \pm 8{,}8 \times 10^{-5}$	$1{,}9 \times 10^{-5} \pm 1{,}0 \times 10^{-8}$	$1{,}3 \times 10^{-5} \pm 1{,}3 \times 10^{-8}$
13.3	0	$7{,}0 \times 10^{-4}$	$0.2 \pm 1{,}1 \times 10^{-4}$	$0.2 \pm 8{,}8 \times 10^{-5}$	$7{,}5 \times 10^{-5} \pm 2{,}7 \times 10^{-8}$	$7{,}8 \times 10^{-5} \pm 2{,}1 \times 10^{-8}$
13.3	14	$9{,}0 \times 10^{-4}$	$0.1 \pm 4{,}6 \times 10^{-5}$	$0.1 \pm 3{,}9 \times 10^{-5}$	$6{,}6 \times 10^{-5} \pm 1{,}3 \times 10^{-8}$	$7{,}4 \times 10^{-5} \pm 1{,}3 \times 10^{-8}$
13.3	99	$1{,}7 \times 10^{-3}$	$0.1 \pm 4{,}4 \times 10^{-5}$	$0.1 \pm 4{,}1 \times 10^{-5}$	$1{,}1 \times 10^{-4} \pm 2{,}3 \times 10^{-8}$	$1{,}4 \times 10^{-4} \pm 2{,}6 \times 10^{-8}$

Table 5.17: Kinetic temperature of the observed Janus particle of figure 5.17. The RF power was 5 W. $T_{k,\,2D}$ is the two-dimensional kinetic temperature in K; $T_{k,\,2D,\,nc}$ is the two-dimensional kinetic temperature after subtracting the "circular" motion in K. Note that the more the trajectories deviate from circular shape, the less $T_{k,\,2D,\,nc}$ is a good estimator of the kinetic temperature. "n.r." stays for "non-reliable", in case of problems analysing the trajectory, usually with `Trackpy`. The results are not shown in chronological order.

Gas pressure (Pa)	Laser power (mW)	$T_{k,\,2D}$ (K)	$T_{k,\,2D,\,nc}$ (K)
6.7	0	963.3 ± 361.4	848.7 ± 339.2
6.7	14	550.3 ± 393.7	519.6 ± 373.7
6.7	99	696.2 ± 442.8	568.8 ± 391.0
13.3	0	n.r.	n.r.
13.3	14	4877.4 ± 1176.3	520.2 ± 373.9
13.3	99	15483.3 ± 2114.9	922.7 ± 498.2

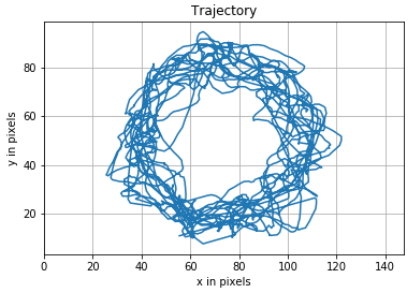

(a) *Observed trajectory for* **0 mW** *of laser power and* **6,7 Pa** *of gas pressure: it can be described as a circle.*

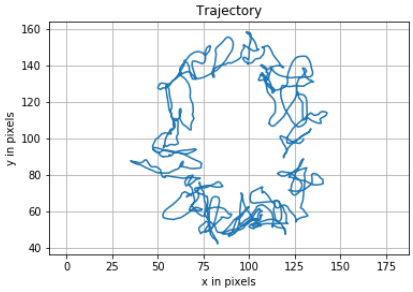

(b) *Observed trajectory for* **14 mW** *of laser power and* **6,7 Pa** *of gas pressure: it can be described as a circle.*

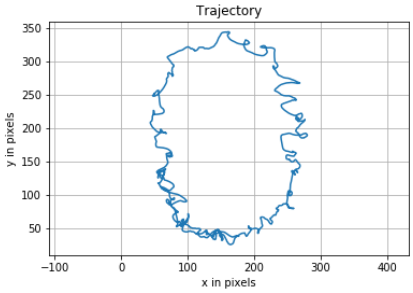

(c) *Observed trajectory for* **99 mW** *of laser power and* **6,7 Pa** *of gas pressure: it can be described as a circle.*

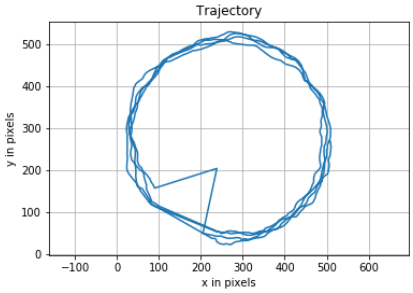

(d) *Observed trajectory for* **0 mW** *of laser power and* **13,3 Pa** *of gas pressure: it can be described as a circle. The triangle does not make any sense: it is due to* `Trackpy` *problems in tracking the particles that I used for the reasons explained in section 4.1.2.*

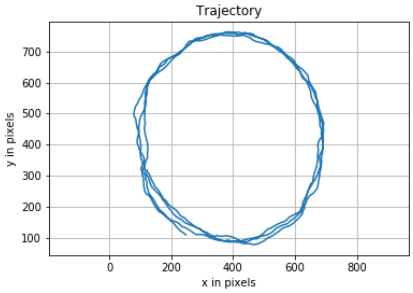

(e) *Observed trajectory for* **14 mW** *of laser power and* **13,3 Pa** *of gas pressure: it can be described as a circle.*

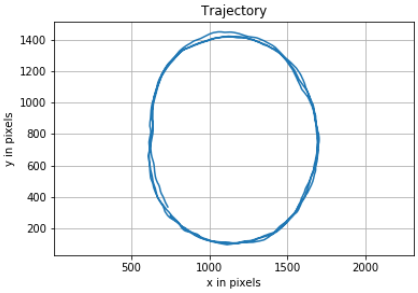

(f) *Observed trajectory for* **99 mW** *of laser power and* **13,3 Pa** *of gas pressure: it can be described as a circle.*

Figure 5.17: Trajectories of one of the observed Janus particles at 5 W of RF power and 1,3 Pa of gas pressure, changing the laser power. They are not shown in the same chronological order as they have been recorded during the experiment.

pressure and laser power. In figure 5.19, the behaviour of the force acting on the particle is shown as a function of laser power in case of gas pressure value of 1,3 Pa. The general trend of the force in case of 1,3 Pa of gas pressure is that is becomes smaller when increasing laser power: see particles "first" and "second" of figure 5.19 and see trend between 14 and 99 mW of laser power of the "fourth" particle. In conclusion, the only true exception is the "third" particle of figure 5.19 and actually in that case the force is just slightly larger for stronger laser power. As the "fotoforetic" force due to the difference in the accommodation coefficients of MF and platinum $F_{\Delta\alpha}$ has turned out to be the only force acting in case of laser off, the action of the other two forces has the effect of making the net force acting on the particle weaker. I deduced it because:

- for intermediate laser power (14 mW), when F_{laser} and photophoresis due to a gradT are present but not at their maximum, the net force is smaller than for the case of laser off
- for strong laser power (99 mW), when F_{laser} and photophoresis due to a gradT are at their maximum, the net force becomes even smaller.

This means that alternating radiation pressure force F_{laser} and photophoresis due to temperature gradient which generates on the particle $F_{\Delta T}$, or at least one of the two, must have absolute values comparable to the one of $F_{\Delta\alpha}$ and opposite directions with respect to it. The first consequence is that, as the estimation for the absolute value of F_{laser} cannot be too wrong, I must have actually underestimated the value of $F_{\Delta T}$ considering the minimum possible ΔT that could generate on the particle surface and overestimated $F_{\Delta\alpha}$ considering the maximum possible $\Delta\alpha$. If the value of F_{laser} was close to the value of $F_{\Delta\alpha}$ and the value of $F_{\Delta T}$ was much smaller than the two of them, as predicted in chapter 3, as F_{laser} pushes surely the platinum–cover face stronger, then the predicted direction of $F_{\Delta\alpha}$, which is from the platinum–cover face to the pure MF, would be wrong and it must be supposed that the MF accommodation coefficient is larger than the platinum one. On the other hand, if the values of $F_{\Delta\alpha}$ and $F_{\Delta T}$ were comparable and the value of F_{laser} weaker, then this would imply that the direction of the two forces is opposite, so they could be either the way predicted in chapter 3 or the other way around. Otherwise it is also possible that both F_{laser} and $F_{\Delta T}$ have values comparable to $F_{\Delta\alpha}$ and in this case they three would exhibit an interplay difficult to predict. It should always be remembered that a better way to evaluating the action of the "photophoretic" mechanisms would be, when having reliable values for the temperatures of the two surfaces, to consider them together. For this reason, the picture could be not as simple as I am describing it. Note that also $F_{\Delta\alpha}$ could become a little bit larger with laser power, but I think that this dependence on laser power will be weaker than the one of $F_{\Delta T}$.

For what concerns the results for higher pressures, that is 6,7 Pa and 13,3 Pa, the net force shows a minimum for 14 mW of laser power instead of 99 mW. The reason why the behaviour is not exactly the same as at lower pressure is not still clear, as nothing should

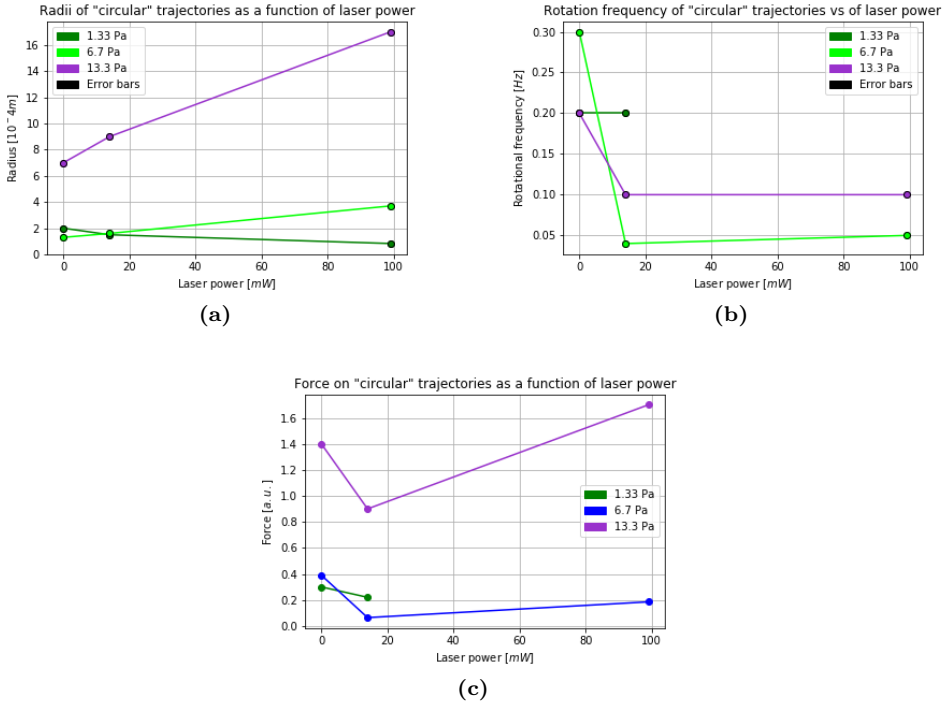

Figure 5.18: Radius of the trajectories, rotational frequency and force acting on the Janus particles shown in figures 5.16 and 5.17 are plotted as functions of the laser power.

change because radiation pressure force does not depend on gas pressure and as the two photophoretic mechanisms should both depend on pressure linearly (see equations 3.33 and 3.10). A possible educated guess of mine is that the coefficients play a role and $F_{\Delta T}$ becomes bigger than $F_{\Delta\alpha}$ at the same laser power for higher pressure. For this reason, if at 1,3 Pa $F_{\Delta T}$ should become comparable to $F_{\Delta\alpha}$ when it is at its maximum, that is for 99 mW of laser power, at higher pressures they seem to be comparable at 14 mW of laser power, while at 99 mW $F_{\Delta T}$ could become even stronger than $F_{\Delta\alpha}$ and play a major role. The consequence of this is that the most likely conclusion of the ones listed above is that $F_{\Delta\alpha}$ and $F_{\Delta T}$ have comparable absolute values and opposite directions.

In order to be sure that the explanation of the different behaviour of “heart-like“ and “circling“ Janus particles has nothing to do with the fact that the first ones are agglomerates of particles, I observed the interference figures of some of the Janus particles with “heart-like“ trajectories defocusing the lens of the side camera. I compared the motion of the observed strips, which were moving downwards and not rotating in the xy plane, with the results of Ref. [34]. The outcome of my analysis is that none of the observed particles are agglomerates, but they are all single particles. For this reason, my educated guess about the axis they are spinning around seems to me to be the most logical one, even if the situation is still not clear.

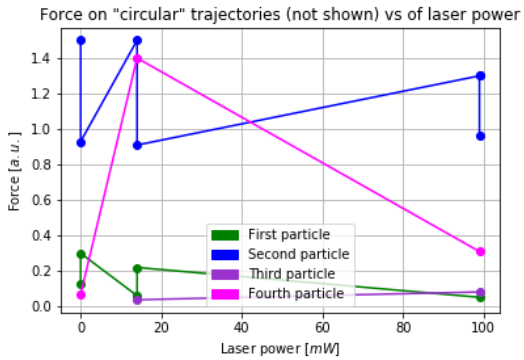

Figure 5.19: Force in arbitrary units acting on some of the "circling" Janus particles observed at 1,3 Pa as a function of the laser power. The trajectories are not shown in the present work, but the last three ones of the "first" Janus particle in figure 5.16.

5.5 Results of the experiments where the RF power was varied

The different RF powers used for this series of experiments are: 1 W, 5 W and 20 W. The gas pressure used is 1,3 Pa.

In light of the results of the experiments performed changing the RF power, I identified different rules of behaviour for the different categories of Janus particles observed:

- "Heart-like" and "circling" Janus particles: the trajectory dimension and the rotational frequency become slightly smaller as RF power is increased in the cases of both 99 and 0 mW of laser power.

  In particular, for two out of the three observed Janus particles, which were both "heart-like", the rule is followed perfectly: this kind of Janus particles seem to follow it better. For the other one, the rule is followed only after some time. In addition, it has to be considered that for one of the two "heart-like" Janus particles the experiment was done only after some time. Therefore, the general idea is that the rule is better followed as time goes on.

- "Randomly moving" Janus particles:

  – for 99 mW of laser power: the area covered by the trajectory and the thermal agitation become slightly larger as RF power is increased

  – for 0 mW of laser power: the area covered by the trajectory and the thermal agitation become slightly smaller as RF power is increased.

  This rules are valid for 100% of the particles observed, which means for two out of two.

Table 5.18: Data about the observed Janus particle of figure 5.20. Laser power was 99 mW and and gas pressure 1,3 Pa. r is the approximate trajectory radius in meters; f_{rot} is the rotational frequency in circles per second, which means Hz; v is the linear velocity and it has been calculated as $v = rf_{\text{rot}}$. The results are not shown in chronological order, but for increasing RF power values.

RF power	r	f_{rot}		v	
		x	y	x	y
(W)	(m)	(Hz)	(Hz)	(m s^{-1})	(m s^{-1})
1	$5{,}1 \times 10^{-4}$	$0.4 \pm 5{,}3 \times 10^{-5}$	$0.4 \pm 4{,}5 \times 10^{-5}$	$1{,}3 \times 10^{-4} \pm 9{,}0 \times 10^{-9}$	$1{,}2 \times 10^{-4} \pm 7{,}5 \times 10^{-9}$
5	$4{,}5 \times 10^{-4}$	$0.2 \pm 3{,}1 \times 10^{-5}$	$0.2 \pm 2{,}4 \times 10^{-5}$	$6{,}5 \times 10^{-5} \pm 4{,}3 \times 10^{-9}$	$7{,}7 \times 10^{-5} \pm 4{,}0 \times 10^{-9}$
20	$3{,}1 \times 10^{-4}$	$0.2 \pm 4{,}0 \times 10^{-5}$	$0.2 \pm 3{,}1 \times 10^{-5}$	$3{,}8 \times 10^{-5} \pm 3{,}8 \times 10^{-9}$	$4{,}9 \times 10^{-5} \pm 3{,}7 \times 10^{-9}$

In figure 5.20, the trajectories of a "heart-like" moving Janus particle are shown. The laser power is 99 mW and the gas pressure is 1,3 Pa. The shape of the trajectory, which can be described as a *dimpled epicycloid with* $k = 2$ is clearer for small RF power. In figure 5.21 the trend of the trajectory radius, rotation frequency, linear velocity and force acting on the particles (this last one in arbitrary units) versus RF power are shown. Let me recall from section 4.1.1 that the radius, that is no more a proper term for non-circular trajectories is just aimed to be a measure of the dimensions of the trajectory. It has been computed as:

$$r = \frac{1}{2}\frac{(x_{\max} - x_{\min}) + (y_{\max} - y_{\min})}{2}. \tag{5.3}$$

The radius clearly becomes smaller increasing the RF power and f_{rot} is basically staying constant. So, even if equation 3.52 relating r_c, ω and F_0 is not exact for non-circular trajectories, something similar is valid for trajectories in case of time-dependent propulsion force (see Ref. [19]), and for this reason it is anyway valid that $F_0 \propto \omega r_c$. If f_{rot}, which is ω is constant and r_c is decreasing, this also means that F_0 is decreasing, as shown in figure 5.21. This is actually in contradiction with what should happen for increasing RF power to asymmetric ion drag force. It can be deduced then, there are other effects stronger than asymmetric ion drag force that play a major role when RF power is changed. This could mean that the force resulting from the asymmetric ion drag is weaker than the photophoretic mechanisms and oscillating radiation pressure. This experimental evidence is strongly supported by the consideration that ion density is much lower than neutral density in the weakly ionized plasma that I used for my experiments:

$$n_i \sim 10^{-6 \div -7} n_n,$$

that could mean that the forces due to neutrals, which are the photophoretic mechanisms, are stronger than the one due to ions.

In figure 5.22, the trajectories of an observed “randomly“ moving Janus particles are

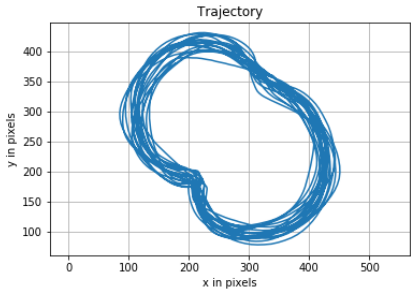

(a) *Observed trajectory for* **1 W** *of RF power: it can be described as a dimpled epicycloid with* $k = 2$.

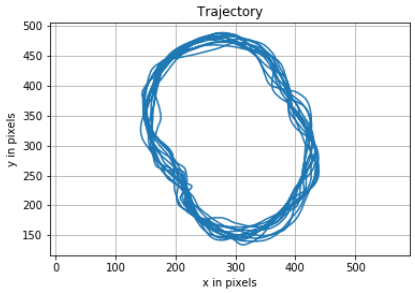

(b) *Observed trajectory for* **5 W** *of RF power: it can be described as a dimpled epicycloid with* $k = 2$.

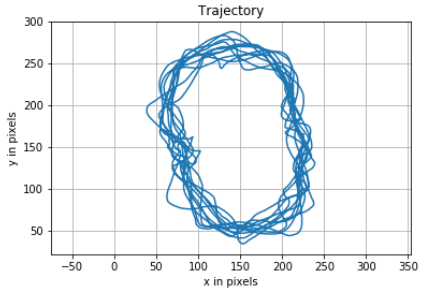

(c) *Observed trajectory for* **20 W** *of RF power: it can be described as a dimpled epicycloid with* $k = 2$.

Figure 5.20: Trajectories of one of the observed Janus particles at 99 mW of laser power and 1,3 Pa of gas pressure, changing the RF power. They are not shown in the same chronological order as they have been recorded during the experiment, but they are shown from the lower to the higher RF power value.

Table 5.19: Kinetic temperature of the observed Janus particle of figure 5.20. Laser power was 99 mW and gas pressure 1,3 Pa. $T_{\mathrm{k,\ 2D}}$ is the two-dimensional kinetic temperature in K; $T_{\mathrm{k,\ 2D,\ nc}}$ is the two-dimensional kinetic temperature after subtracting the circular motion in K. Note that the more the circle is precise the lower is $T_{\mathrm{k,\ 2D,\ nc}}$ as the procedure of subtracting the circular motion is more effective obviously. The results are not shown in chronological order, but for increasing RF power values.

RF power (W)	$T_{\mathrm{k,\ 2D}}$ (K)	$T_{\mathrm{k,\ 2D,\ nc}}$ (K)
1	12806.1 ± 1370.6	4120.4 ± 748.9
5	4525.1 ± 803.6	887.6 ± 345.6
20	1884.6 ± 516.3	688.4 ± 304.2

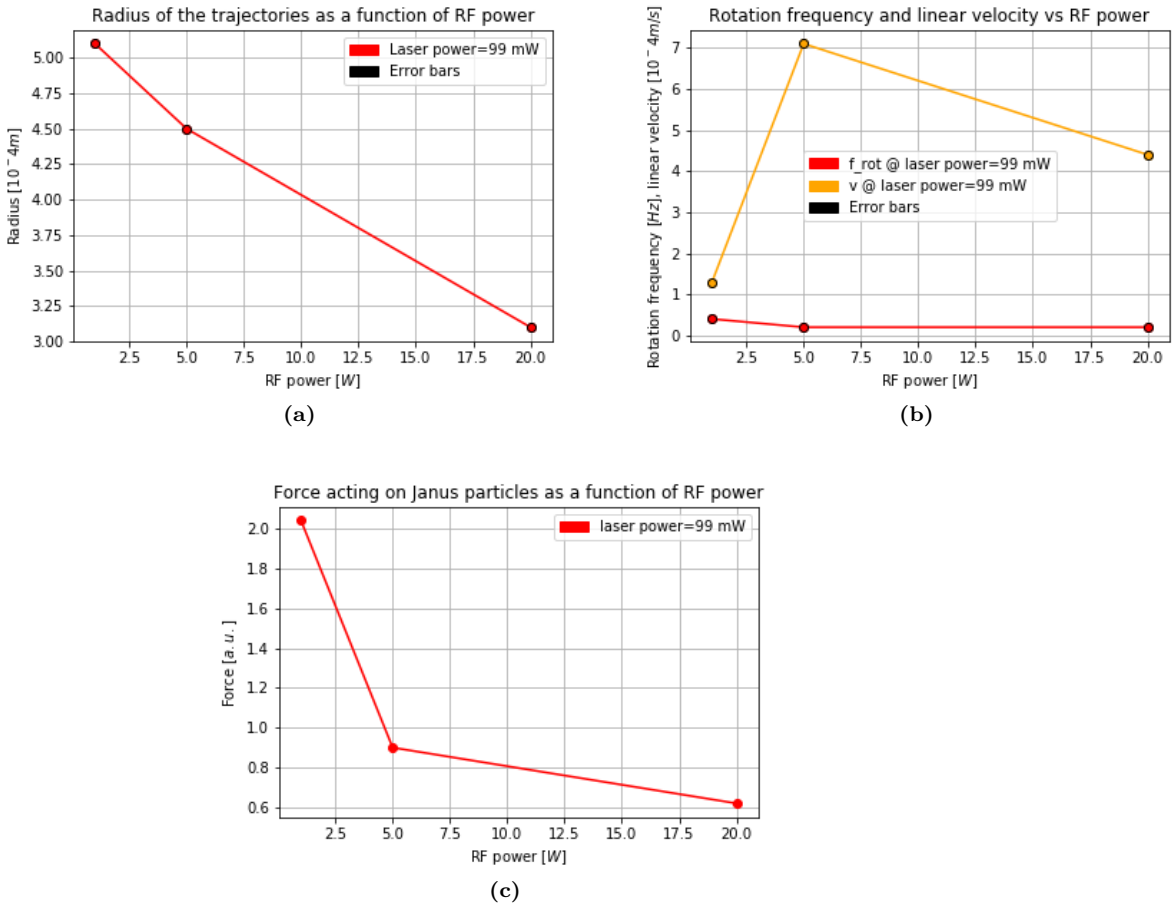

Figure 5.21: Parameters of the trajectories and force as functions of the RF power for the trajectories shown in figure 5.20. The plotted values for f_{rot} and v are obtained as a mean between the values for x and y. The error bars cannot be seen, even if they are plotted, because they are orders of magnitude smaller than the plotted values.

Table 5.20: Kinetic temperature of the observed Janus particle of figure 5.22. Laser power was 99 mW and gas pressure 1,3 Pa. $T_{k,\,2D}$ is the two-dimensional kinetic temperature in K. The results are not shown in chronological order, but for increasing RF power values. The results with laser off are reported before the ones obtained with laser on.

RF power (W)	laser power (mW)	r (m)	$T_{k,\,2D}$ (K)
1	0	$3{,}7 \times 10^{-4}$	9850.6 ± 1569.7
5	0	$1{,}4 \times 10^{-4}$	2408.8 ± 570.9
20	0	$1{,}1 \times 10^{-4}$	1070.4 ± 388.5
1	99	$7{,}3 \times 10^{-5}$	760.8 ± 327.4
5	99	$1{,}4 \times 10^{-4}$	2072.3 ± 541.7
20	99	$4{,}6 \times 10^{-4}$	22135.1 ± 1829.4

shown. In Table 5.20, some meaningful data are reported and their trend with RF power is shown in figure 5.23. The error bars are not visible because they are too small. It is possible to see that, as the "rules" of behaviour already reported, the "radius", that means the dimensions, of the trajectory becomes smaller with RF power in case of no laser power and larger in case of strong laser power. A plot of the kinetic temperature as a function of time is also reported for this case, as this value assumes an important meaning in case of random trajectories, while for non-random trajectories it is less easy to associate a physical meaning to the kinetic temperature. The kinetic temperature behaves exactly as the radius. There is no clear rule in this case in order to connect directly F_0 and r_c as the trajectory is not circular and for this reason no guesses can be made about the absolute value of the force based on the area covered by the particle during its motion. If the random trajectories were actually very complicated rosette-like closed curves (see image (c) of figure 3.8), then, since $F_0 \propto r_c\omega$ for them, the fact that the radius becomes larger or smaller with RF power, considering ω constant as I have no way of estimating it, would mean that also the force acting on the particle becomes larger or smaller with RF power. But no reliable suppositions can be done about it.

For the last trajectory of figure 5.22, the results for the particle two-dimensional temperature calculated in all the ways shown in section 4.1.1 are reported in Table 5.21 and figure 5.24. The conclusion is that the kinetic temperature is a good estimate of the particle temperature and this is the reason why I reported only it in this chapter. I do this comparison now because random trajectories are particularly suitable for talking about kinetic temperature. The Maxwellian fit of the two-dimensional velocity distribution function and the parabolic fit of the initial part of the MSD are shown in figure 5.25.

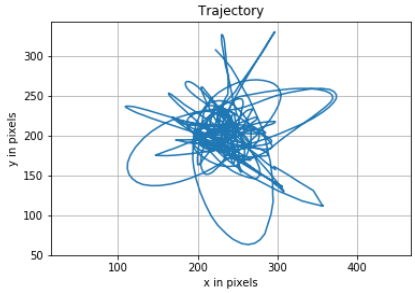

(a) *Observed random trajectory for* **1 W** *of RF power and* **0 mW** *of laser power.*

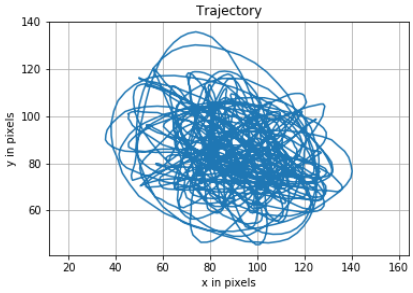

(b) *Observed random trajectory for* **5 W** *of RF power and* **0 mW** *of laser power.*

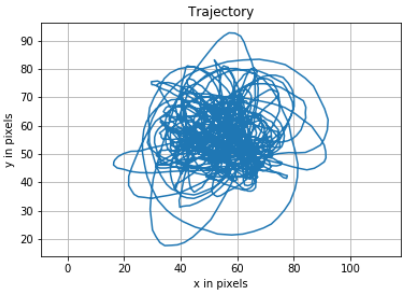

(c) *Observed random trajectory for* **20 W** *of RF power and* **0 mW** *of laser power.*

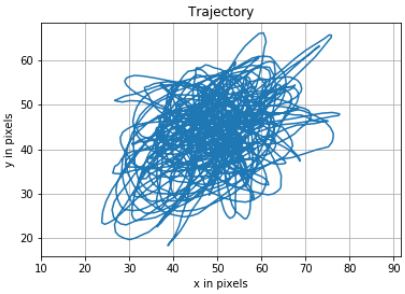

(d) *Observed random trajectory for* **1 W** *of RF power and* **99 mW** *of laser power.*

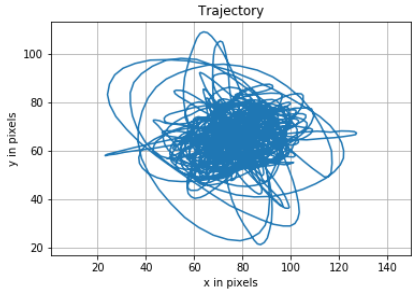

(e) *Observed random trajectory for* **5 W** *of RF power and* **99 mW** *of laser power.*

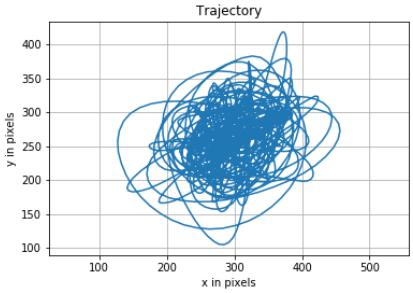

(f) *Observed random trajectory for* **20 W** *of RF power and* **99 mW** *of laser power.*

Figure 5.22: Trajectories of one of the observed Janus particles at 1,3 Pa of gas pressure, changing the RF power. The other experimental parameters are reported under each image. They are not shown in the same chronological order as they have been recorded during the experiment, but they are shown from the lower to the higher RF power value. The results with laser off are reported before the ones obtained with laser on.

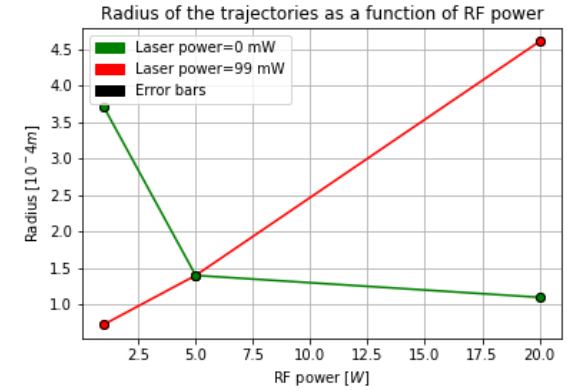

(a)

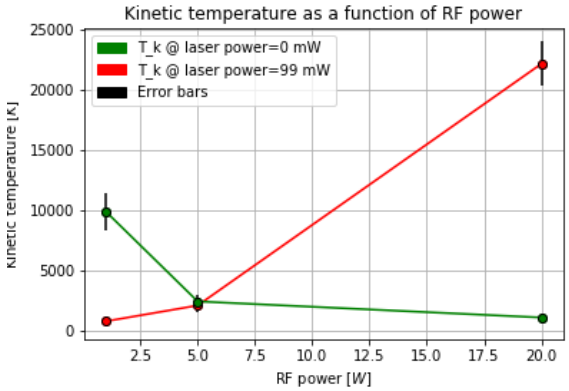

(b)

Figure 5.23: Parameters of the trajectories as functions of the RF power for the trajectories shown in figure 5.22. The plotted values for f_{rot} and v are obtained as a mean between the values for x and y.

Table 5.21: Two-dimensional temperature for the case of the last trajectory in figure 5.22 described in section 4.1.1.

$T_{k,2D}$ (K)	22135.1 ± 1829.4
$T_{\mathrm{Maxw,2D}}$ (K)	21608.6 ± 593.9
T_{MSD} (K)	21445.2 ± 0.03

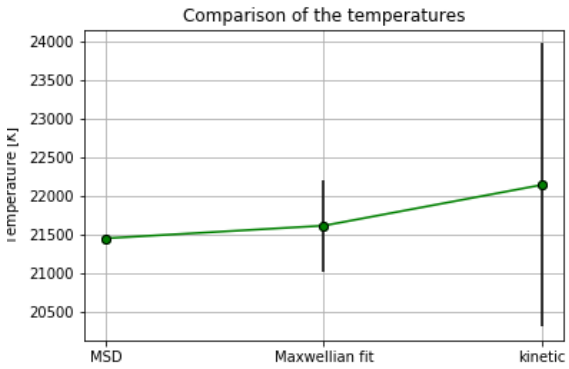

Figure 5.24: Comparison of the two-dimensional temperature values obtained with the different methods described in section 4.1.1 for the last trajectory shown in figure 5.22. The conclusion is that the kinetic temperature is a good estimator of the particle temperature, apart from being also the most direct one.

5.6 Results of the experiments where the gas pressure was varied

The gas pressures used for this series of experiments are 1,3 Pa, 4,0 Pa, 6,7 Pa, 10,0 Pa and 13,3 Pa. The RF power has always been set equal to 5 W.

All the Janus particles observed during this sequence of experiments are "circling" Janus particles and I have been able to identify some rules of behaviour also in this case. As anticipated in section 4.2.3 of chapter 4, the behaviour is actually different for different laser powers. In fact, I identified two different rules of behaviour for different laser powers used:

- 0 mW of laser power (1 particle observed): the trajectory becomes larger as the pressure is increased. The rule is better followed as time goes on.
- 99 mW of laser power (2 particles observed): the trajectory becomes smaller as the pressure is increased. The rule is better followed as time goes on.

The observed trajectories of the particle illuminated with 99 mW laser power are shown in figure 5.26 and some results are reported in Tables 5.22 and 5.23.

In figure 5.27, more details about the first trajectory in figure 5.26 are shown because it is not a clear circle. The pressure in this case is 1,3 Pa. The difference between the x position and its mean, which is supposed to be the centre of the circle, and the same for y are shown. The sinusoidal fits of these curves are also shown. The explanation for this behaviour could be the following. I was going decreasing the gas pressure and this measurement has been done just after the one at 4 Pa. Maybe the particle was still adapting its motion to the new pressure. On the other hand, just to give an example of

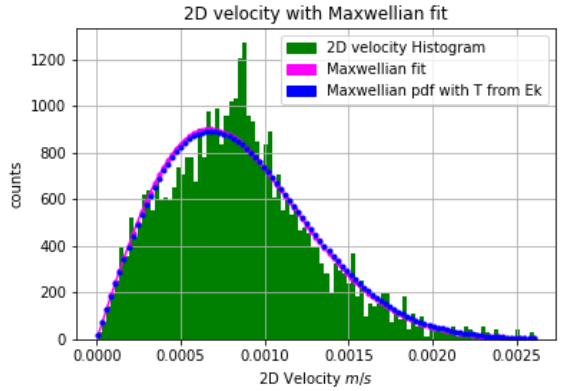

(a) *Maxwellian fit of the two-dimensional velocity distribution function*

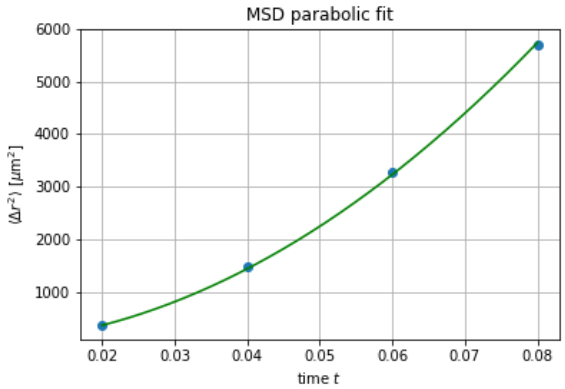

(b) *Parabolic fit of the first four points of the MSD*

Figure 5.25: Maxwellian fit of the two-dimensional velocity distribution function and parabolic fit of the first four points of the MSD that have been used in order to compute the results of Table 5.21.

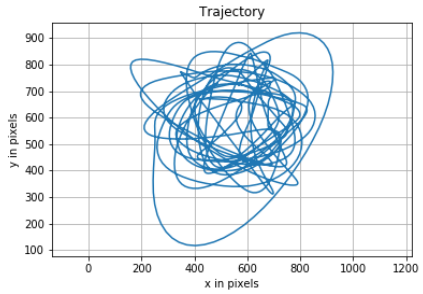

(a) *Observed trajectory for* **1,3 Pa** *of gas pressure: it can be described as a non-precise circle. The number of recorded frames for this case is 1363 instead of the usual 2726.*

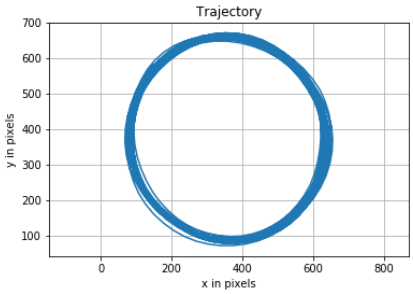

(b) *Observed trajectory for* **4,0 Pa** *of gas pressure: it can be described as a circle.*

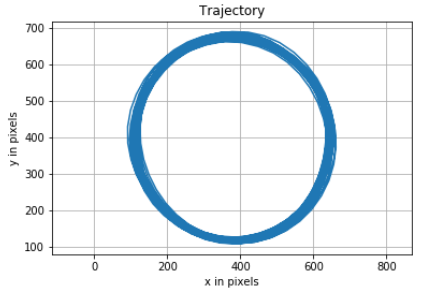

(c) *Observed trajectory for* **6,7 Pa** *of gas pressure: it can be described as a circle.*

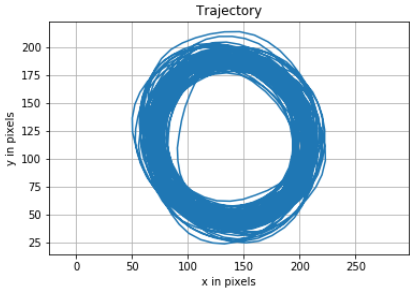

(d) *Observed trajectory for* **10,0 Pa** *of gas pressure: it can be described as a circle.*

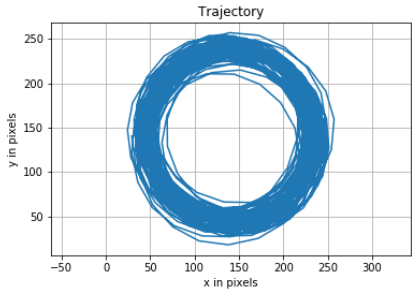

(e) *Observed trajectory for* **13,3 Pa** *of gas pressure: it can be described as a circle.*

Figure 5.26: Trajectories of one of the observed Janus particles at 99 mW of laser power (and 5 mW of RF power) changing the gas pressure. They are not shown in the same chronological order as they have been recorded during the experiment, but they are shown from the lower to the higher pressure value.

Table 5.22: Data about the observed Janus particle of figure 5.26. Laser power was 99 mW and RF power 5 W. r is the approximate trajectory radius in meters; f_{rot} is the rotational frequency in circles per second, which means Hz; v is the linear velocity and it has been calculated as $v = r f_{\mathrm{rot}}$. The results are not shown in chronological order, but for increasing pressure values.

Gas pressure	r	f_{rot}		v	
		x	y	x	y
(Pa)	(m)	(Hz)	(Hz)	($\mathrm{m\,s^{-1}}$)	($\mathrm{m\,s^{-1}}$)
1.3	$1{,}1 \times 10^{-3}$	$0.7 \pm 3{,}8 \times 10^{-4}$	$0.7 \pm 2{,}7 \times 10^{-4}$	$4{,}8 \times 10^{-4} \pm 1{,}4 \times 10^{-7}$	$5{,}0 \times 10^{-4} \pm 1{,}0 \times 10^{-7}$
4.0	$8{,}3 \times 10^{-4}$	$1.0 \pm 2{,}2 \times 10^{-5}$	$1.0 \pm 2{,}1 \times 10^{-5}$	$5{,}5 \times 10^{-4} \pm 6{,}1 \times 10^{-9}$	$5{,}6 \times 10^{-4} \pm 6{,}1 \times 10^{-9}$
6.7	$8{,}1 \times 10^{-4}$	$1.3 \pm 2{,}1 \times 10^{-5}$	$1.3 \pm 2{,}0 \times 10^{-5}$	$7{,}0 \times 10^{-4} \pm 5{,}5 \times 10^{-9}$	$7{,}1 \times 10^{-4} \pm 5{,}5 \times 10^{-9}$
10.0	$2{,}5 \times 10^{-4}$	$1.4 \pm 1{,}4 \times 10^{-4}$	$1.4 \pm 1{,}4 \times 10^{-4}$	$2{,}2 \times 10^{-4} \pm 1{,}1 \times 10^{-8}$	$2{,}5 \times 10^{-4} \pm 1{,}2 \times 10^{-8}$
13.3	$3{,}3 \times 10^{-4}$	$2.7 \pm 7{,}8 \times 10^{-5}$	$2.7 \pm 7{,}9 \times 10^{-5}$	$5{,}9 \times 10^{-4} \pm 8{,}6 \times 10^{-9}$	$6{,}1 \times 10^{-4} \pm 8{,}9 \times 10^{-9}$

Table 5.23: Kinetic temperature of the observed Janus particle of figure 5.26. Laser power was 99 mW and RF power 5 W. $T_{\mathrm{k,\ 2D}}$ is the two-dimensional kinetic temperature in K; $T_{\mathrm{k,\ 2D,\ nc}}$ is the two-dimensional kinetic temperature after subtracting the circular motion in K. Note that the more the circle is precise the lower is $T_{\mathrm{k,\ 2D,\ nc}}$ as the procedure of subtracting the circular motion is more effective obviously.

Gas pressure	$T_{\mathrm{k,\ 2D}}$	$T_{\mathrm{k,\ 2D,\ nc}}$
(Pa)	(K)	(K)
1.3	90715.0 ± 5438.7	40351.0 ± 3423.6
4.0	260356.1 ± 10294.9	819.6 ± 469.5
6.7	420048.5 ± 14261.5	787.4 ± 460.2
10.0	32823.8 ± 2265.7	10353.0 ± 1200.1
13.3	222846.3 ± 9309.5	1153.7 ± 557.2

Table 5.24: Data about the observed Janus particle of figure 5.29. Laser power was off and RF power 5 W. r is the approximate trajectory radius in meters; f_{rot} is the rotational frequency in circles per second, which means Hz; v is the linear velocity and it has been calculated as $v = r f_{\text{rot}}$. The results are not shown in chronological order, but for increasing pressure values.

Gas pressure	r	f_{rot}		v	
		x	y	x	y
(Pa)	(m)	(Hz)	(Hz)	($\mathrm{m\,s^{-1}}$)	($\mathrm{m\,s^{-1}}$)
4.0	$1{,}0 \times 10^{-4}$	$0.2 \pm 2{,}4 \times 10^{-4}$	$0.2 \pm 2{,}3 \times 10^{-4}$	$1{,}6 \times 10^{-5} \pm 8{,}0 \times 10^{-9}$	$1{,}8 \times 10^{-5} \pm 8{,}6 \times 10^{-9}$
6.7	$1{,}3 \times 10^{-4}$	$0.3 \pm 5{,}8 \times 10^{-5}$	$0.3 \pm 5{,}3 \times 10^{-5}$	$2{,}3 \times 10^{-5} \pm 2{,}6 \times 10^{-9}$	$2{,}1 \times 10^{-5} \pm 2{,}2 \times 10^{-9}$
10.0	$3{,}1 \times 10^{-4}$	$0.2 \pm 5{,}6 \times 10^{-5}$	$0.2 \pm 5{,}2 \times 10^{-5}$	$4{,}2 \times 10^{-5} \pm 5{,}8 \times 10^{-9}$	$4{,}0 \times 10^{-5} \pm 5{,}2 \times 10^{-9}$
13.3	$7{,}0 \times 10^{-4}$	$0.2 \pm 1{,}2 \times 10^{-4}$	$0.2 \pm 8{,}8 \times 10^{-5}$	$7{,}5 \times 10^{-5} \pm 2{,}7 \times 10^{-8}$	$7{,}8 \times 10^{-5} \pm 2{,}1 \times 10^{-8}$

Table 5.25: Kinetic temperature of the observed Janus particle of figure 5.29. Laser power was off and RF power 5 W. $T_{\text{k, 2D}}$ is the two-dimensional kinetic temperature in K; $T_{\text{k, 2D, nc}}$ is the two-dimensional kinetic temperature after subtracting the circular motion in K. Note that the more the circle is precise the lower is $T_{\text{k, 2D, nc}}$ as the procedure of subtracting the circular motion is more effective obviously. The values of the temperature for the case of 13,3 Pa are overestimated because of reasons related to the analysis.

Gas pressure	$T_{\text{k, 2D}}$	$T_{\text{k, 2D, nc}}$
(Pa)	(K)	(K)
4.0	664.4 ± 432.6	534.2 ± 378.9
6.7	1009.2 ± 378.7	744.2 ± 317.6
10.0	4212.3 ± 773.8	3135.2 ± 1200.1
13.3	25325.1 ± 2861.2	20730.9 ± 2580.2

almost perfect circular trajectory, in figure 5.28 the same results are shown for the second trajectory of figure 5.26 (case of 4 Pa).

The observed trajectories of the particle illuminated with 99 mW laser power are shown in figure 5.29 and some results are reported in Tables 5.24 and 5.25. Some trajectories have been tracked with `Trackpy` and not with `ImageJ` because with `ImageJ` I sometimes have had some problems in finding the particle positions in case of experiments performed with the torch instead of the laser.

In figure 5.30, the trend of the radius of the trajectories, of the rotation frequency and of the force (in arbitrary units) acting on the particles as functions of the gas pressure, in the cases of both laser on and off, is shown. The radius trend has already been commented. For what concerns the rotation frequency, it becomes larger with pressure when laser is on and it stays almost constant when laser is off. This means that the spinning frequency, which is equal to the rotation frequency according to the theory of Ref. [19], becomes

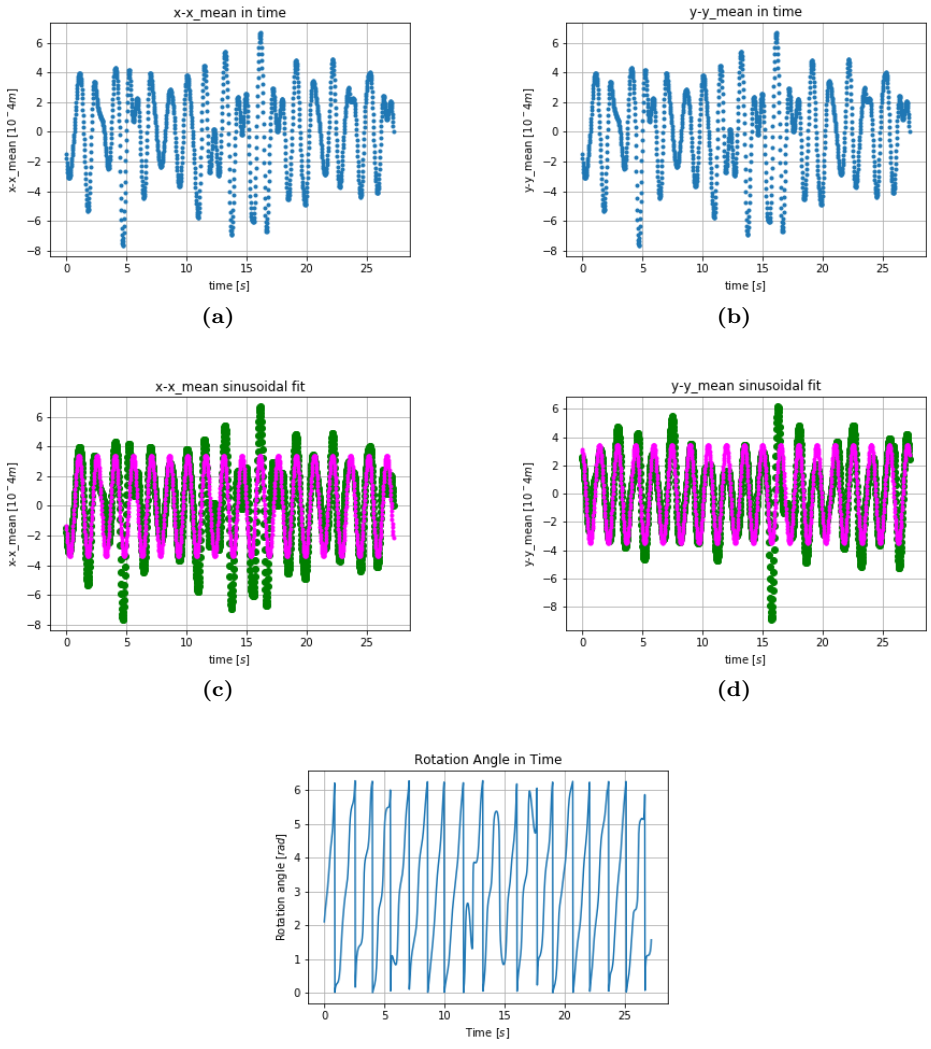

Figure 5.27: Details about the analysis for the case of 99 mW of laser power, 5 W of RF power and 1,3 Pa are shown. The trajectory is shown in image (a) of figure 5.26. The bigger circle the particle moves along at a certain point corresponds to the bigger amplitude in the difference between y and its mean at about 15,5 s.

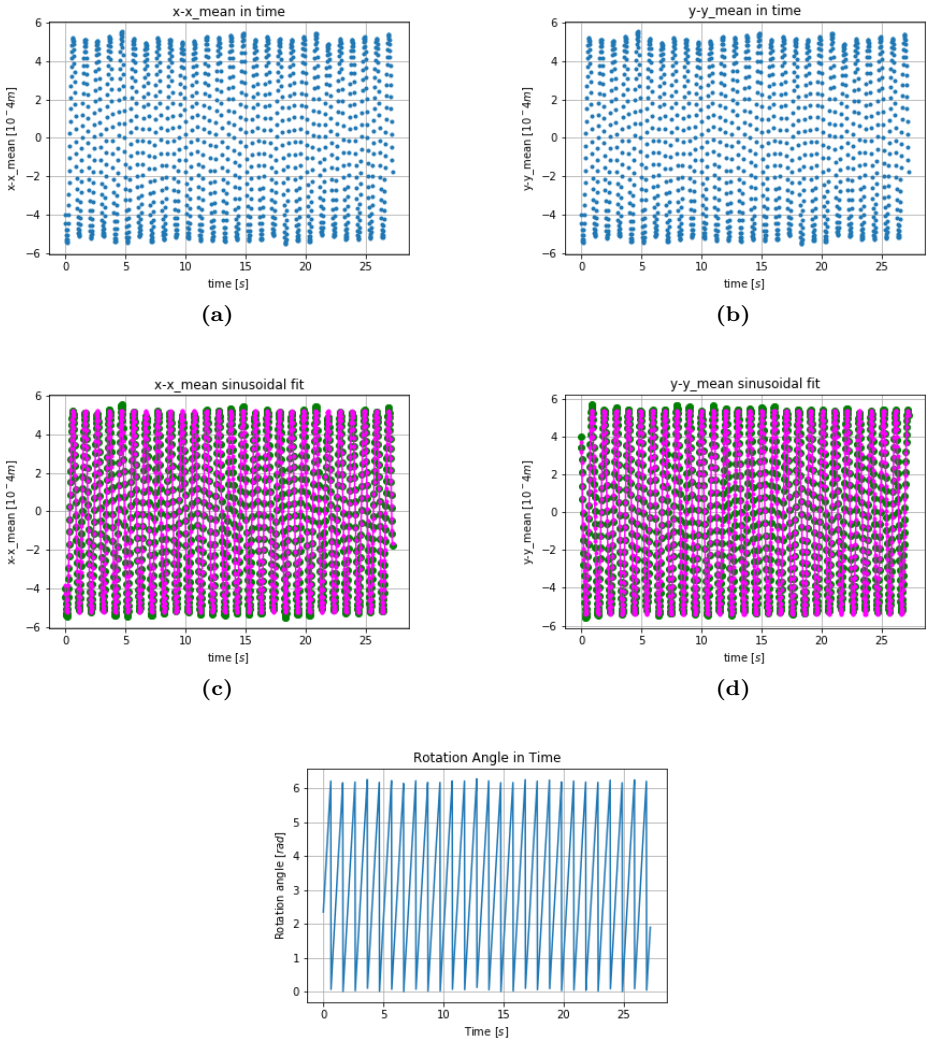

Figure 5.28: Details about the analysis for the case of 99 mW of laser power, 5 W of RF power and 4 Pa are shown. The trajectory is shown in image (b) of figure 5.26.

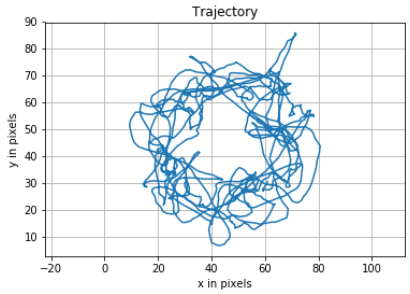

(a) *Observed trajectory for* **4,0 Pa** *of gas pressure: it can be described as a non-pure circle.*

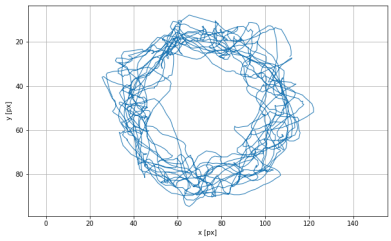

(b) *Observed trajectory for* **6,7 Pa** *of gas pressure: it can be described as a non-pure circle. It was computed with* `Trackpy` *because it was not possible with* `ImageJ`*.*

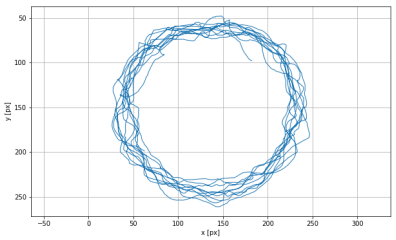

(c) *Observed trajectory for* **10,0 Pa** *of gas pressure: it can be described as a non-pure circle. It was computed with* `Trackpy` *because it was not possible with* `ImageJ`*.*

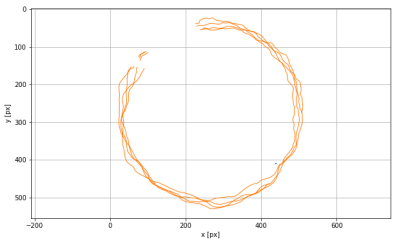

(d) *Observed trajectory for* **13,3 Pa** *of gas pressure: it can be described as a circle. It was computed with* `Trackpy` *because it was not possible with* `ImageJ`*.*

Figure 5.29: Trajectories of the observed Janus particles with laser power off (5 W is the applied RF power) changing the gas pressure. In this case, they are shown in the same chronological order as they have been recorded during the experiment.

larger with the neutrals number density only when laser is on. This actually means that the main cause of the spinning motion is probably the symmetry breaking due to the temperature gradient that originates on the Janus particle when laser is on.

The trend of the force acting on the particles of figure 5.30 has been traced in arbitrary units using the well known relation for circular trajectories $F_0 \propto r_c\omega$. In case of laser off, the force is becoming larger with gas pressure, as it should be for $F_{\Delta\alpha}$. In case of laser on, the trend of the force is not clear and it could be assumed for this reason that it is remaining about constant with pressure. As $F_{\Delta\alpha}$ and $F_{\Delta T}$ both depend linearly on pressure (see equations 3.10 and 3.33), then radiation pressure force is constant with pressure, that is is what should actually happen to it. The force is clearly stronger in case of laser on, as it has been predicted in equation 3.36. This is the proof that the two photophoretic mechanisms cannot be considered separately, but they always act together.

The force acting on the Janus particles is stronger for laser on than for laser off. This is in open contradiction with the results of section 5.4. But, already in that case, it was noticed that for large values of gas pressure, the behaviour with laser power changed, maybe because the two photophoretic forces vary differently with the pressure because of the coefficients. The results of the present section seem to be in contradiction even for what was said in section 5.4 regarding low gas pressure value. But the statistics of the experiments of the present section is small and it should be increased in order to obtain reliable data.

5.7 Results of the temporal-development experiments

Unfortunately, we cannot check with the optical microscope if the Pt layer is sputtered away from the Janus particle because of the plasma, so we do not have any proof of what happens to the Pt layer with time. It would be interesting to do this kind of study with an electron microscope or an optical one with a high enough resolution.

There is apparently no dependence on time for the behaviour of JP, neither for the main sample used nor for the old sample. However, a dependence on time was observed for the only two "heart-like" JP whose dependence on time was studied. It can be that the spinning frequency ν of the JP, that is also the propulsion frequency, changes in time for the reasons already explained. Changes in ν would lead to changes in ν/ω, that means changes in the shape of the trajectory and in its dimensions. However, this dependence is neither clear nor monotonic with respect to any of these parameters: rotational frequency, dimensions of the trajectory, shape of the trajectory and kinetic temperature.

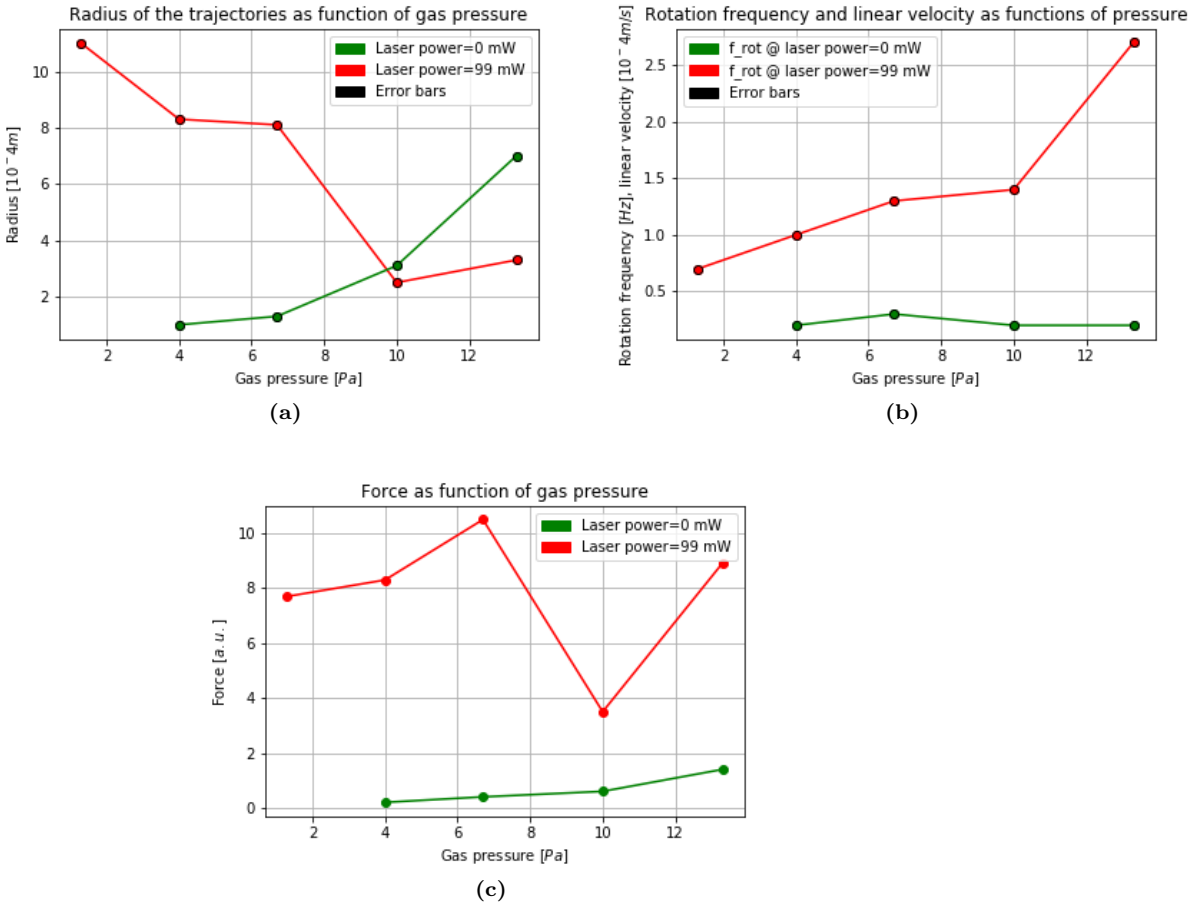

Figure 5.30: Parameters of the trajectories as functions of the gas pressure, in the cases of both laser off and on. The plotted values for f_{rot} are obtained as a mean between the values for x and y.

5.8 Dependence of MF particle behaviour on the laser power, RF power and the gas pressure

There is no dependence of MF particle behaviour on the laser power, RF power or the gas pressure for what concerns the shape of the trajectories. There is also no dependence of the kinetic temperature of the MF particle on RF power and on laser power. For what concerns the gas pressure, the lower it is the higher the kinetic temperature becomes. The reason of this is that gas viscosity, which is due to neutrals and which resists the particle motion, is made lower by lowering the gas pressure.

5.9 Experiments with an old sample of Janus particles

It has to be mentioned that the results shown in the present work have been obtained with a relatively new and fresh sample of Janus particle, which was about one year old at the time of the experiments. Moreover, before starting using this sample, a more than two-year-old one was used. The results from the old sample are most probably not reliable because of adsorption in time of water molecules from air on the surface of the Janus particles. In all of the several experiments performed with Janus particles from this sample, they moved along a random trajectory. The outcome of this observation is that it is important to use fresh samples of Janus particles in order to do experiments with them.

5.10 Janus particle spin

The calculated value of 4,3 Hz almost never corresponds to a resonance in the power spectrum of the particle image brightness. This does not automatically mean that the particle is not spinning, but it could be due to the fact that active matter is out of equilibrium or that other phenomena predominate. In fact, there are other contributions that most probably play a more significant role for what concerns particle brightness, i.e., an oscillation up and down of the particle which takes it more or less in the microscope's focus and also makes it become more or less well illuminated by the laser, the velocity of the particle that changes its shape in the recorded images and for this reason changes its brightness and so on. In particular, I observed the resonances in the power spectrum of the particle image brightness also for pure MF particles and they are again there and corresponding to similar frequency values.

However, Ref. [19] predicts that the frequency the active particle moves along its circular or "heart-like" trajectory with is equal to the spinning frequency of the particle. For this reason, in case of both non-perfect and perfect circular trajectories, when calculating the rotation frequency I am also calculating the spinning frequency of the particle. Actually, the values of f_{rot} shown in the present chapter are not that far from the value or 1,53 Hz

computed in section 3.2, especially for low values of gas pressure. The only unsolved problem is the following. If ω is the rotation and the spinning frequency and if ν is the propulsion frequency, considering that in my case ν should be equal to the propulsion frequency of the Janus particle, how is it possible that I have observed *looped limaçon*? It is predicted in fact in Ref. [19] that they correspond to the particle trajectory only when $\omega = 2\nu$ and this is a contradiction in my case. This remains an open question of my work. Maybe the propulsion mechanism depends on something else in time besides the mechanisms I discussed in section 3.3 or maybe for the case of undamped environment the theory of Ref. [19] should be modified.

Also, it has been found out that the probable cause of spinning is the symmetry breaking on the particle surface due to the generation of a temperature gradient in the presence of the laser light. In fact, image (b) of figure 5.30 shows that the spinning frequency becomes higher with pressure only when laser power is on. As collisions with neutrals make the particle spin, they only affect the spinning frequency when laser power is on, which means when a temperature gradient is generated on the particle surface.

Since the "circling" Janus particles have been the most commonly observed, then the conclusion is that usually Janus particles spin around axis b of figure 3.14. In fact, when the spinning axis is this one, the self-propulsion force is time-independent and the trajectories are circular. This leads to the conclusion that gravitational force plays a major role for what concerns the particle orientation: the platinum-covered side of the Janus particle is heavier and for this reason it tends to face downward.

Summary of chapter 5

The chief result of the experiments performed with single Janus particles in plasmas is that their peculiar property of spatial anisotropy makes them active also in a plasma environment. In fact, they perform trajectories that are not random, but circles, *epitrochoids*, particular kinds of *epitrochoids* called *limaçons* and *bilobed epicycloids*. Random trajectories were just seldom. As the environment used in the performed experiments is undamped, it is not possible to explain all the observed trajectories by the analytically and numerically predicted trajectories in the case of an overdamped environment. Some inconsistency between the results is, indeed, obvious: a comparison between the two of them can just be qualitative. The experiments with the confining ring shifted with respect to the centre of the lower electrode confirmed that the active motion of the Janus particles is due to the self-propulsion mechanisms that generate from the peculiar spatial anisotropy properties of the particles and has nothing to do with the other mechanisms listed in section 4.2.5. Considering the shapes of the trajectories performed, three different kinds of Janus particles can be distinguished: particles performing circular trajectories called "circling" Janus particles, particles performing both *limaçon*- and *bilobed epicycloid*-shaped trajectories called "heart-like" Janus particles (referring to the name given in literature to *cardiod*-shaped trajectories) and particles performing only random trajectories called "random" particles. It is important to note that these names have nothing to do with the shape of the particles themselves, but just with the shape of the trajectories they performed.

The results of the experiments where the RF power was varied suggest that the asymmetric ion drag force $F_{\text{asymm. ion drag}}$ is negligible. This result confirms the theoretical predictions in chapter 3 as the upper estimate of this force turned out to be the smallest value obtained among the ones which refer to the other possible forces acting as propulsion mechanisms on the Janus particle.

In concern with the results of the experiments where the laser power was varied, the three groups of Janus particles behaved differently. In the case of low gas pressure values, the relation that bonds the trajectory radius, the rotation frequency and the absolute value of the propulsion force acting on the particle, that is $F \propto r\omega$, suggests that the force acting on "circling" Janus particles becomes weaker for increasing laser power. As the

"photophoretic" force due to the difference in the accommodation coefficients of MF and platinum $F_{\Delta\alpha}$ turned out to be the only force acting when the laser is off, the action of the other two forces has the effect of making the net force acting on the particle weaker. This means that the alternating radiation pressure force F_{laser} and the photophoresis due to the temperature gradient that generates on the particle $F_{\Delta T}$, or at least one of the two forces, must have absolute values comparable to the one of $F_{\Delta\alpha}$ and opposite directions in relation to it. The first consequence is that, as the estimation of the absolute value of F_{laser} cannot be too wrong, the value of $F_{\Delta T}$ must have actually been underestimated considering the minimum possible ΔT that could generate on the particle surface and $F_{\Delta\alpha}$ must have been overestimated considering the maximum possible $\Delta\alpha$. Three hypotheses can be made.

- If the value of F_{laser} was close to the value of $F_{\Delta\alpha}$ and the value of $F_{\Delta T}$ was much smaller than either of them, as predicted in chapter 3, as F_{laser} surely pushes the platinum–cover face stronger, then the predicted direction of $F_{\Delta\alpha}$, which is from the platinum–cover face to the pure MF, would be wrong. Moreover, it is to be supposed that the MF accommodation coefficient is larger than the platinum one.

- If the values of $F_{\Delta\alpha}$ and $F_{\Delta T}$ were comparable and the value of F_{laser} was weaker, then this would imply that the direction of the two forces is opposite, so they could be either the way predicted in chapter 3 or the other way round.

- Otherwise, it is also possible that both F_{laser} and $F_{\Delta T}$ have values comparable to $F_{\Delta\alpha}$ and in this case the three of them would exhibit an interplay difficult to be predicted.

It should always be remembered that a better way to evaluate the action of the "photophoretic" mechanisms would be to consider them together, that would be possible only if reliable values of the temperatures of the two surfaces were present. In the case of high values of gas pressure, the net force shows a minimum that corresponds to intermediate laser power. As F_{laser} does not depend on gas pressure, it could be that, as both $F_{\Delta\alpha}$ and $F_{\Delta T}$ grow linearly with pressure, the multiplicative coefficients play a role and that $F_{\Delta T}$ grows a little bit faster than $F_{\Delta\alpha}$ with pressure. This would make it reasonable that now the two "photophoreses" are comparable for intermediate laser power and that $F_{\Delta T}$ plays a major role for strong laser power. The consequence of this is that the most likely conclusion of the ones listed above is that $F_{\Delta\alpha}$ and $F_{\Delta T}$ have comparable absolute values and opposite directions.

The "heart-like" Janus particles exhibit a cleaner and bigger shape of their trajectories as the laser power is increased. The force also seems to become larger with the laser power. The shape of their trajectories when the laser is off is always circular and never *limaçon*- and *bilobed epicycloid*–shaped. This is a clear sign that the laser light plays a major role in concern to the time-dependence of the propulsion forces. Moreover, this is another

proof of the negligibility of $F_{\text{asymm. ion drag}}$. "Random" Janus particles do not show any remarkable trend when laser power is varied.

In concern with the last important series of experiments where the gas pressure was varied, the results lead to interesting considerations. Only two "circling" particles were observed, one when laser was on and the other when laser was off. When the laser power is off, the net force acting on the particle seems to become bigger along with the gas pressure, that is exactly what should happen to $F_{\Delta\alpha}$. On the contrary, when the laser is on, the force seems to remain constant enough when the pressure was increased. This is actually what should happen as F_{laser} does not depend on gas pressure and as both $F_{\Delta\alpha}$ and $F_{\Delta T}$ grow linearly with it and tend to counteract each other. The result that is in open contraction with the results obtained in the series of experiments where the laser power was varied is that the force is stronger when the laser is on, whatever the pressure value is. Anyway, more statistics need to be collected in concern with this last series of experiments in order to get reliable conclusions.

The last consideration is about the particle spinning. As already mentioned, the propulsion frequency ν should be equal to the spinning frequency of the Janus particle. This frequency is in turn equal to the rotation frequency ω at which the trajectories are travelled. This would supposedly mean that ν is always equal to ω and this would just explain *cardioid*–shaped trajectories if a time-dependent self-propulsion force acts on the particle. Also, the "circular" trajectories are a result difficult to be explained because the particle should spin around the symmetry axis passing through the centres of the faces so that the propulsion force is time-independent. If the particle spins around the previously mentioned axis, then one side of the particle faces upwards and the other downwards. This would mean that no propulsion mechanisms act on the particle. The fact that some results are not clear could be due to the following considerations. First, the existing theory about single active particles confined in a harmonic potential well applies for the case of overdamped environments and, therefore, it is not appropriate to describe the details of what happens to them in an undamped environment. Then, "photophoretic" mechanisms have never been studied in detail in plasmas.

However, the spinning frequency of the particle, which is a very interesting result for complex plasma research community, is likely to be related to its rotation frequency, which can be easily calculated by a sinusoidal fit of the distance of the particle position from the centre of the trajectory.

Conclusions, open issues and perspectives

In my work, I demonstrated experimentally that the Janus particles used, which are 9,27(10) μm diameter melamine spheres half-covered with 10,0(1) nm of platinum, perform "active motion" in a complex plasma environment. I theorised the forces that could act as self-propulsion mechanisms in this environment and I discussed the reasons why some of them could depend on time. The experimental results that I obtained show that Janus particles spin in the plasma, most probably not always around the same symmetry axis. The spinning frequency of an active particle can be determined experimentally as it is equal to its rotational frequency, which is the frequency at which the particle performs its non-random trajectories. The so–called "heart-like" trajectories prove that the total propulsion force acting on the particles can vary over time. The four guessed forces acting as propulsion mechanisms are:

1. asymmetric ion drag force
2. alternating radiation pressure force
3. photophoresis due to a temperature gradient on the particle surface, that is an asymmetric neutral drag force due to a temperature difference
4. "photophoresis" due to different accommodation coefficients, that is an asymmetric neutral drag force due to different accommodation coefficients of MF and platinum.

The first has been demonstrated to be negligible compared to the others. The last two ones are likely to have comparable absolute values but probably opposite directions. The second one is possibly dominant for what concerns the time-dependence of the total acting force. These results prove that my evaluation of the temperature difference between the two faces is a big underestimation and that the evaluation of the difference in accommodation coefficients is an overestimation.

In concern with future developments of my research, from a theoretical point of view a lot of aspects should be deepened, i.e., what the motion of an active swimmer in an

undamped environment should be, how the "photophoretic" mechanisms in a plasma environment act (as the physics is much more complex than in common environments because of ions and electrons interacting with the particle), what the charge distribution on the surface of a Janus particle and the electric field generated by it are, what the actual temperature distribution on the Janus particle surface is (in both cases of laser illumination on and off), and so on. Calculating or measuring the accommodation coefficients of the two different materials in a weakly ionized plasma like the one used in this work is something else that should be done.

From an experimental point of view, apart from collecting more statistics about the experiments performed and obtaining more reliable data and conclusions about the experiments that I performed, observations of Janus particles before and after being dispersed in the plasma, with a microscope characterized by a high enough resolution to resolve the 10 nm of platinum should be done, in order to study an eventual sputtering of the Pt layer. If it came out that such a thin layer of metal does not survive long in plasma, even if I strongly doubt it, alternative more resistant materials to partially cover particle could be used, like Titanium, as it is done with polystyrene particles by the group of *Terahertz Technology Laboratory and Soft Matter Laboratory* in Moscow. Also alternative Janus particles and, in general, alternative active particles can be studied in order to compare them with the Janus particles used in my experiments and evaluate the differences in the behaviour. The Janus particles that will fit best this role, can be used in order to suspend groups of active particles and investigate the very interesting collective behaviours of active matter in such an interesting undamped environment like complex plasma one. If the ground-based experiments will come out to be interesting enough, some experiments in microgravity conditions could also be performed by the group, during a parabolic flight campaign or on the International Space Station (ISS).

Appendix A

Particle trajectory

Following there is the used code to print the particle positions in time and obtain a graph of the trajectories. "@" corresponds to a tabular key.

`data2` is a list of 1D arrays created to contain what comes out of ImageJ: in particular, for each frame `j data2[j][3]` is the particle position in the x-axis and `data2[j][4]` is its position in the y-axis. `fps` is number of frames per second taken by the camera and is always 50.`frames` is the number of recorded frames, which is usually 2627.

```
x=np.ones(frames)             #in pixel
y=np.ones(frames)             #in pixel
twoDpos=np.ones(frames)
#modulus of the vector of the 2D position in pixels
x_m=np.ones(frames)           #in meters
y_m=np.ones(frames)           #in meters
twoDpos_m=np.ones(frames)
#modulus of the vector of the 2D position in pixels
for j in range (frames):
@ x[j]=data2[j][3]
@ y[j]=data2[j][4]
@ twoDpos[j]=np.sqrt((x[j]**2)+(y[j]**2))
#scale is the conversion factor m/pixel, that is my case is 1.881E-6
@ x_m[j]=x[j]*scale
@ y_m[j]=y[j]*scale
@ twoDpos_m[j]=np.sqrt((x_m[j]**2)+(y_m[j]**2))

#tracking the particle's trajectory
plt.plot(x, y, '-')
#matplotlib.axes.Axes.set_aspect(1)
```

```
plt.axis('equal')
plt.title('Trajectory')
plt.ylabel('y in pixels')
plt.xlabel('x in pixels')
plt.grid()
plt.savefig('%s/Trajectory from ImageJ for %s frames' % (path, frames))
plt.show()
```

Appendix B

Fast Fourier transform of the particle positions

Following there is the used code to calculate the fft of the particle's positions.

`fps` is number of frames per second taken by the camera and is always 50.`frames` is the number of recorded frames, which is usually 2627 every time. "@" corresponds to a tabular key.

```
#calculating the 2D position fft
twoDpos_m_fft=np.fft.fft(twoDpos_m)

#calculating the fft absolute value
twoDpos_m_fft_abs=np.ones(len(twoDpos_m_fft))
for i in range(len(twoDpos_m_fft)):
@ twoDpos_m_fft_abs[i]=np.sqrt((twoDpos_m_fft[i].real**2)+(twoDpos_m_fft[i].imag**2))
twoDpos_m_fft_final=twoDpos_m_fft_abs*2/frames

#calculating the fft frequencies
t=np.linspace(0,frames-1,frames)/fps
freq=np.fft.fftfreq(frames, d=t[1]-t[0])

plt.plot(freq[1:], twoDpos_m_fft_final[1:], 'o-', color='red')
plt.xlim(xmin=0, xmax=fps/2)
plt.title('2D positions fft')
plt.ylabel('2D positions fft')
plt.xlabel('f $Hz$')
plt.grid()
plt.savefig('%s/2D positions fft' % path)
```

```
plt.show()
```

Appendix C

Fast Fourier transform of the particle brightness

Following there is the used code to graph the particle's brightness and to calculate its power spectrum through a fast Fourier transform.

In particular, `data2[j][2]` is the mean particle brightness, so its total brightness is calculated multiplying it by the particle's area, that is `data2[j][1]`. `fps` is number of frames per second taken by the camera and is always 50. `frames` is the number of recorded frames, which is usually 2627 every time.

```
mean_brightness=np.ones(frames)
particle_area=np.ones(frames)
total_brightness=np.ones(frames)
for j in range (frames):
mean_brightness[j]=data2[j][2]
particle_area[j]=data2[j][1]
total_brightness[j]=mean_brightness[j]*particle_area[j]
mean_mean_brightness=np.mean(mean_brightness)
std_mean_brightness=np.std(mean_brightness)
mean_total_brightness=np.mean(total_brightness)
std_total_brightness=np.std(total_brightness)
mean_particle_area=np.mean(particle_area)
std_particle_area=np.std(particle_area)
np.savetxt('%s/Mean Total Particle Brightness from ImageJ'%folder,...
 ...np.array([mean_total_brightness]))
np.savetxt('%s/Standard Dev. Total Particle Brightness from ImageJ'...
 ...%folder, np.array([std_total_brightness]))
np.savetxt('%s/Mean Particle Area from ImageJ'%folder,...
```

```
 ...np.array([mean_particle_area]))
np.savetxt('%s/Standard Dev. Particle Area from ImageJ'%folder,...
 ...np.array([std_particle_area]))

t=np.linspace(0,frames-1,frames)/fps

mean_total_brightness_array=np.linspace(mean_total_brightness, ...
... mean_total_brightness, len(t))
plt.plot(t, total_brightness, marker='.', color='yellow', linewidth=0.5)
plt.plot(t, mean_total_brightness_array, marker='.', color='black', ...
... linewidth=0.3)
plt.title('Particle brightness from ImageJ vs time')
plt.xlabel('time $s$')
plt.ylabel('Total Particle Brightness')
black = mpatches.Patch(color='black', label='mean brightness')
green = mpatches.Patch(color='yellow', label='brightness')
plt.legend(handles=[green, black])
plt.grid()
plt.savefig('%s/Particle brightness from ImageJ vs time' % path)
plt.show()

#calculating the total brightness fft
total_brightness_fft=np.fft.fft(total_brightness)
#np.savetxt('C:/Users/luon_fr/Documents/Francesca/Sin_fft' ,...
... np.array(brightness_fft))
print (len(total_brightness_fft))

#calculating the fft absolute value
total_brightness_fft_abs=np.ones(len(total_brightness_fft))

for i in range(len(total_brightness_fft)):
total_brightness_fft_abs[i]=np.sqrt((total_brightness_fft[i].real**2)+...
...(total_brightness_fft[i].imag**2))

total_brightness_fft_final=total_brightness_fft_abs*2/frames

#calculating the fft frequencies
freq=np.fft.fftfreq(frames, d=t[1]-t[0])
#inc=fps/frames
#freq=np.linspace(0, fps-inc, fps/inc)
```

```
#print len(freq)

plt.plot(freq[1:], total_brightness_fft_final[1:], 'o-', color='red')
plt.xlim(xmin=0, xmax=fps/2)
plt.title('total Brightness fft')
plt.ylabel('total Brightness fft')
plt.xlabel('f $Hz$')
plt.grid()
plt.savefig('%s/total Brightness fft' % path)
plt.show()
```

Appendix D

Iterative calculation of the temperatures of the two faces of Janus particles

Iterative code to compute T_1 and T_2 ("@" corresponds to a tabular key):

```
from numpy.polynomial import Polynomial as P
#import numpy as np

h_cond = 3.3E5
h_conv = 0.5
q_s = 3.2E2
alpha_2 = 0.4
T_amb = 296
e_1 = 0.075
e_2 = 0.95
s = 5.670373E-8


T_1=list()
T_1.append(T_amb)
T_2=list()
```

```
p0 = P([(-alpha_2*q_s - h_conv*T_amb - e_2*s*(T_amb)**4),...
... h_conv, 0, 0, (e_2*s)])
sol0 = p0.roots()

for i in range(len(sol0)):
if sol0[i].imag == 0 and sol0[i] > 0:
T_2.append(sol0[i].real)

diffT2 = 1
while diffT2==1:
@ pT2 = P([(-alpha_2*q_s - h_conv*T_amb - e_2*s*(T_amb)**4 - h_cond*T_1[-1]),...
... h_conv + h_cond, 0, 0, (e_2*s)])
@ solT2 = pT2.roots()
@ for i in range(len(solT2)):
@@ if solT2[i].imag == 0 and solT2[i] > 0:
@@@ T_2.append(solT2[i].real)
@ pT1 = P([(-h_cond*T_2[-1] - h_conv*T_amb - e_1*s*(T_amb)**4),...
... (h_cond + h_conv), 0, 0, (e_1*s)])
@ solT1 = pT1.roots()
@ for i in range(len(solT1)):
@@ if solT1[i].imag == 0 and solT1[i] > 0:
@@@ T_1.append(solT1[i].real)

@ if T_2[-1]<T_2[-2]:
@@ if T_2[-1]>(T_2[-2]-0.0001):
@@@ diffT2 = 0
@ else:
@@ if T_2[-1]<(T_2[-2]+0.0001):
@@@ diffT2 = 0

print(T_2[-1])
print(T_1[-1])


#with the laser off
q_s=0

T_1_off=list()
T_1_off.append(T_amb)
T_2_off=list()
```

```
p0_off = P([(-alpha_2*q_s - h_conv*T_amb - e_2*s*(T_amb)**4),...
... h_conv, 0, 0, (e_2*s)])
sol0_off = p0_off.roots()

for i in range(len(sol0_off)):
@ if sol0_off[i].imag == 0 and sol0_off[i] > 0:
@@ T_2_off.append(sol0_off[i].real)

diffT2_off = 1
while diffT2_off==1:
@ pT2_off = P([(-alpha_2*q_s - h_conv*T_amb - e_2*s*(T_amb)**4 - h_cond*T_1_off[-1]), h_co
@ solT2_off = pT2_off.roots()
@ for i in range(len(solT2_off)):
@@ if solT2_off[i].imag == 0 and solT2_off[i] > 0:
@@@ T_2_off.append(solT2_off[i].real)
@ pT1_off = P([(-h_cond*T_2_off[-1] - h_conv*T_amb - e_1*s*(T_amb)**4), (h_cond + h_conv),
@ solT1_off = pT1_off.roots()
@ for i in range(len(solT1_off)):
@@ if solT1_off[i].imag == 0 and solT1_off[i] > 0:
@@@ T_1_off.append(solT1_off[i].real)

@ if T_2_off[-1]<T_2_off[-2]:
@@ if T_2_off[-1]>(T_2_off[-2]-0.0001):
@@@ diffT2_off = 0
@ else:
@@ if T_2_off[-1]<(T_2_off[-2]+0.0001):
@@@ diffT2_off = 0

print(T_2_off[-1])
print(T_1_off[-1])
```

Bibliography

[1] C. R. Du, V. Nosenko, H. M. Thomas, A. Müller, A. M. Lipaev, V. I. Molotkov, V. E. Fortov, A. V. Ivlev, "Photophoretic force on microparticles in complex plasmas", New J. Phys. **19** (2017) 073015

[2] V. Nosenko, A. V. Ivlev, G. E. Morfill, "Laser-induced rocket force on a microparticle in a complex (dusty) plasma", Physics of Plasmas **17**, 123705 (2010)

[3] V. E. Fortov, A. V. Ivlev, S. A. Khrapak, A. G. Khrapak, G. E. Morfill, "Complex (dusty) plasmas: Current status, open issues, perspectives", Physics Reports **421** (2005) 1-103

[4] S. A. Khrapak, A. V. Ivlev, G. E. Morfill, H. M. Thomas, "Ion drag force in complex plasmas", Physical Review **E 66**, 046414 (2002)

[5] C. Bechinger, R. Di Leonardo, H. Löwen, C. Reichhardt, G. Volpe, G. Volpe, "Active Particles in Complex and Crowded Environments", Rev. Mod. Phys. **88**, 045006 (2016)

[6] H. Horvath, "Photophoresis - a Forgotten Force??", Powder and Particle Journal No. 31 (2014)

[7] A. V. Ivlev, A. G. Khrapak, S. A. Khrapak, B. M. Annaratone, G. Morfill, K. Yoshino, "Rodlike particles in gas discharge plasmas: Theoretical model", Physical Review **E 68**, 026403 (2003)

[8] A. V. Ivlev, G. Morfill, V. E. Fortov, "Potential of a dielectric particle in a flow of a collisionless plasma", Physics of plasmas, Volume 6, number 5 (1999)

[9] B. Liu, J. Goree, V. Nosenko, L. Boufendi, "Radiation pressure and gas drag forces on a melamine-formaldehyde microsphere in a dusty plasma", Physics of plasmas **10**, 9 (2003)

[10] H. Maurer, R. Basner, H. Kersten, "Measuring the temperature of microparticles in plasmas", Review of Scientific Instruments **79**, 093508 (2008)

[11] J. E. Daugherty and D. B. Graves, "Particulate temperature in radio frequency glow discharges" J. Vac. Sci. Technol. **A 11**, 1126 (1993)

[12] G. Swinkels, “Optical studies of micron-sized particles immersed in a plasma,” Ph.D. thesis, TU Eindhoven, (1999)

[13] G. Swinkels, H. Kersten, H. Deutsch, and G. M. W. Kroesen, "Measuring the temperature of microparticles in plasmas" J. Appl. Phys. **88**, 1747 (2000)

[14] J. H. Leck, "Pressure measurement in vacuum systems"

[15] "A Heat Transfer Textbook", fourth edition, John H. Lienhard IV and John H. Lienhard V

[16] Handbook of Chemistry and Physics, Chemical Rubber Publishing Co., Cleveland, Ohio, DMIC Report 177, Battelle Memorial Institute, Thermal Radiation Properties Survey, Honeywell Research Center

[17] Bruce E. Poling, John M. Prausnitz, John P. O’Connell, "The properties of gas and liquids", section 10.2

[18] E. B. Smith, "The intermolecular pair-potential energy functions of the inert gases", Physica **73** (1974) 211-225

[19] S. Jahanshahi, H. Löwen, B. ten Hagen, "Brownian motion of a circle swimmer in a harmonic trap", Phys. Rev. **E 95**, 022606 (2017)

[20] C. A. Knapek et al., "Kinetic Characterization of Strongly Coupled Systems", Phys. Rev. Lett. **98**, 015001 (2007)

[21] R. Quinn and J. Goree, "Single-particle Langevin model of particle temperature in dusty plasmas", Phys. Rev. E **61**, 3033 (2000)

[22] C. Y. Soong, W. K. Li, C. H. Liu, and P. Y. Tzeng, "Theoretical analysis for photophoresis of a microscale hydrophobic particle in liquids", Opt. Express **18**, 2168 (2010)

[23] Kunststofftaschenbuch, 28. Ausg; Carl Hanser Verlag München Wien, 2001, p. 670

[24] https://www.makeitfrom.com/material-properties/Melamine-Formaldehyde-MF

[25] https://microparticles.de/en/eigenschaften

[26] "RF magnetron sputtering of thick platinum coatings on glass microspheres", Thin Solid Films, vol. 72, Issue 2 (1980), p. 373-378

[27] J. Kong, K. Qiao, L. S. Matthews, T. W. Hyde, "Temperature measurement of a dust particle in a RF plasma GEC reference cell", J. Plasma Phys. (2016), vol. 82, 905820505

[28] Einstein, A. (1905) "Uber die von der molekularkinetischen Theorie der Warme geforderte Bewegung von in ruhenden Flussigkeiten suspendierten Teilchen". Ann. Phys. (Berlin) **322**, 549–560

[29] G.E. Uhlenbeck and L.S. Ornstein, Phys. Rev. **36**, 823 (1930)

[30] M.C. Wang and G.E. Uhlenbeck, Rev. Mod. Phys. **17**, 323 (1945)

[31] github.com/soft-matter/trackpy

[32] V. Mancois, B. Marcos, P. Viot, D. Wilkowski, "Two-temperature Brownian dynamics of a particle in a confining potential", Physical Review J. **E 97**, 052121 (2018)

[33] M. Rubin-Zuzic, V. Nosenko, S. Zhdanov, A. Ivlev, H. Thomas, S. Khrapak, L. Couedel, "Single Particle Dynamics in a Radio-Frequency Produced Plasma Sheath", AIP Conference Proceedings **1925**, 020023 (2018)

[34] M. Chaudhuri, V. Nosenko, C. Knapek, U. Konopka, A. V. Ivlev, H. M. Thomas, G. E. Morfill, "Direct experimental observation of binary agglomerates in complex plasmas", Applied Physics Letters **100**, 264101 (2012)

[35] M. I. Mendivil Palma, B. Krishnan, G. A. Castillo Rodriguez, T. K. Das Roy, D. Avellaneda, S. Shaji, "Synthesis and Properties of Platinum Nanoparticles by Pulsed Laser Ablation in Liquid", Journal of Nanomaterials, vol. 2016, 9651637

[36] Rajathi, Fatimson, "Phytofabrication of nano-crystalline platinum particles by leaves of cerbera manghas and its antibacterial efficacy", International Journal of Pharma and Bio Sciences **5** (2014), 619-628